VIRAL HEPATITIS: PATHOPHYSIOLOGY, PREVENTION, AND CONTROL

EDITED BY: Milan Surjit, Cheng Kao and C. T. Ranjith-Kumar
PUBLISHED IN: Frontiers in Cellular and Infection Microbiology

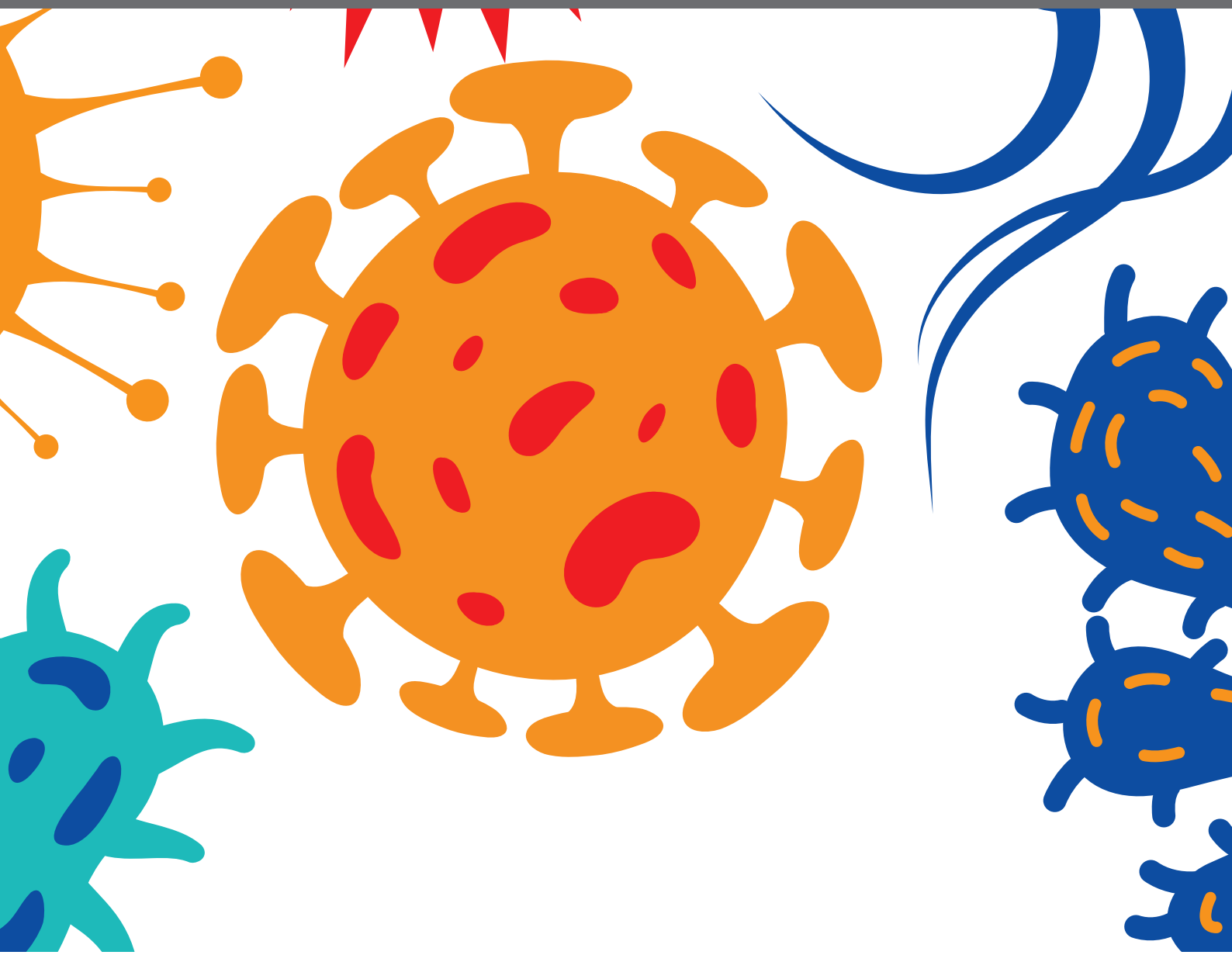

frontiers Research Topics

ISSN 1664-8714
ISBN 978-2-88971-495-7
DOI 10.3389/978-2-88971-495-7

About Frontiers

Frontiers is more than just an open-access publisher of scholarly articles: it is a pioneering approach to the world of academia, radically improving the way scholarly research is managed. The grand vision of Frontiers is a world where all people have an equal opportunity to seek, share and generate knowledge. Frontiers provides immediate and permanent online open access to all its publications, but this alone is not enough to realize our grand goals.

Frontiers Journal Series

The Frontiers Journal Series is a multi-tier and interdisciplinary set of open-access, online journals, promising a paradigm shift from the current review, selection and dissemination processes in academic publishing. All Frontiers journals are driven by researchers for researchers; therefore, they constitute a service to the scholarly community. At the same time, the Frontiers Journal Series operates on a revolutionary invention, the tiered publishing system, initially addressing specific communities of scholars, and gradually climbing up to broader public understanding, thus serving the interests of the lay society, too.

Dedication to Quality

Each Frontiers article is a landmark of the highest quality, thanks to genuinely collaborative interactions between authors and review editors, who include some of the world's best academicians. Research must be certified by peers before entering a stream of knowledge that may eventually reach the public - and shape society; therefore, Frontiers only applies the most rigorous and unbiased reviews.
Frontiers revolutionizes research publishing by freely delivering the most outstanding research, evaluated with no bias from both the academic and social point of view. By applying the most advanced information technologies, Frontiers is catapulting scholarly publishing into a new generation.

What are Frontiers Research Topics?

Frontiers Research Topics are very popular trademarks of the Frontiers Journals Series: they are collections of at least ten articles, all centered on a particular subject. With their unique mix of varied contributions from Original Research to Review Articles, Frontiers Research Topics unify the most influential researchers, the latest key findings and historical advances in a hot research area! Find out more on how to host your own Frontiers Research Topic or contribute to one as an author by contacting the Frontiers Editorial Office: frontiersin.org/about/contact

VIRAL HEPATITIS: PATHOPHYSIOLOGY, PREVENTION, AND CONTROL

Topic Editors:
Milan Surjit, Translational Health Science and Technology Institute (THSTI), India
Cheng Kao, Indiana University Bloomington, United States
C. T. Ranjith-Kumar, Guru Gobind Singh Indraprastha University, India

Citation: Surjit, M., Kao, C., Ranjith-Kumar, C. T., eds. (2021).
Viral Hepatitis: Pathophysiology, Prevention, and Control.
Lausanne: Frontiers Media SA. doi: 10.3389/978-2-88971-495-7

Table of Contents

frontiers in Cellular and Infection Microbiology

EDITORIAL
published: 26 August 2021
doi: 10.3389/fcimb.2021.633580

Editorial: Viral Hepatitis: Pathophysiology, Prevention, and Control

Cheng Kao[1]*, *Milan Surjit*[2]* and *C. T. Ranjith-Kumar*[3]*

[1] Molecular and Cellular Biochemistry, Indiana University, Bloomington, IN, United States, [2] Vaccine and Infectious Disease Research Center, Translational Health Science and Technology Institute (THSTI), Faridabad, India, [3] University School of Biotechnology, Guru Gobind Singh Indraprastha University, New Delhi, India

Keywords: viral hepatitis, HAV, HBV, HCV, HDV, HEV

Editorial on the Research Topic

Viral Hepatitis: Pathophysiology, Prevention, and Control

Viral hepatitis, characterized by liver inflammation and damage, is among the leading human global health threats (World Health Organization, 2012). Billions of people worldwide have been infected with hepatitis viruses. Millions worldwide are living with viral hepatitis and over 1.4 million deaths occur annually as a result of liver cirrhosis and cancer (World Health Organization, 2016). Notably, many infected individuals are unaware of their infection and can transmit the virus to others.

The majority of viral hepatitis, alphabetically referred to as Types A, B, C, D, and E, are caused by five different viruses. In addition, human adenoviruses are also known to cause hepatitis in immunocompromised individuals. These viruses are from distinct taxonomic grouping, have different infectivity, replication strategies, reservoirs, and pathogenesis. In turn, the course of the disease, epidemiology, prevention and treatment could differ.

The enveloped hepatitis B virus (HBV) and hepatitis C virus (HCV) cause both acute and chronic liver disease. Together HBV and HCV account for ~ 90% of the fatalities. HCV, a member of the *Flaviviridae* family of positive-strand RNA virus, infects through exposures to virus-containing blood or body fluids that contain blood. HBV is a member of the *Hepadnaviridae* family with a reverse-transcribed partially double-stranded genome. It infects through puncture of the skin or mucosal contact with infectious blood or body fluids. Hepatitis D virus (HDV) contains a circular single-stranded negative-sense RNA genome and it co-infects people along with hepatitis B or infect people who are already chronically infected by HBV. The envelope of HDV contains the HBV envelope proteins and it uses the same cellular receptor for entry as HBV (Yan et al., 2012). HDV and HBV co-infection can speed up liver disease progression.

Hepatitis A virus (HAV) and hepatitis E virus (HEV) from feces are nonenveloped viruses. Interestingly, HEV from blood contain membrane from exosomes and are classified as quasi-enveloped (Nagashima et al., 2017). Both viruses spread through close contact with an infected individual or through ingestion of virus-contaminated food or drink. HAV and HEV belong to the family of *Picronaviridae* and *Hepeviridae*, respectively, and both possess single-stranded positive-sense RNA genomes (Aggarwal, 2013; Lemon et al., 2017). It is important to note that HEV also infects a number of animals that serve as reservoirs and ingestion of undercooked meats can lead to transmission (Doceul et al., 2016). HAV and HEV typically lead to self-limiting diseases, although the illness could last for a few months. In a small percentage of people, especially immunocompromised individuals, specific genotypes of HEV can cause chronic infection

OPEN ACCESS

Edited and reviewed by:
Curtis Brandt,
University of Wisconsin-Madison,
United States

***Correspondence:**
Cheng Kao
ckao@indiana.edu
Milan Surjit
milan@thsti.res.in
C. T. Ranjith-Kumar
ctrkumar@ipu.ac.in

Specialty section:
This article was submitted to Virus and Host, a section of the journal Frontiers in Cellular and Infection Microbiology

Received: *25 November 2020*
Accepted: *09 July 2021*
Published: *26 August 2021*

Citation:
Kao C, Surjit M and Ranjith-Kumar CT (2021) Editorial: Viral Hepatitis: Pathophysiology, Prevention, and Control. Front. Cell. Infect. Microbiol. 11:633580. doi: 10.3389/fcimb.2021.633580

(Hoofnagle et al., 2012). Severe acute infections can also lead to a small percentage of fatalities, and fatalities could be higher in pregnant women (Khuroo and Kamili, 2003).

Significant progress to prevent infection by hepatitis viruses has been made. Highly effective and safe prophylactic vaccines are available for hepatitis A and B. For hepatitis B, vaccination of newborns weighing over 2 kg is recommended (Schillie et al., 2018). Proper vaccination will also produce essentially life-long immunity (Loader et al., 2019). Preventing HBV infection will also protect against HDV infection. For chronically infected hepatitis B patients, the vaccine will not cure the infection, but family members and associates who receive the vaccine can be protected from infection. A recombinant vaccine against HEV is available in China (Zhu et al., 2010). A vaccine is not available for hepatitis C. Prevention of infection should focus on improved education, hygiene, improving infrastructure, and healthcare practices.

It is important to have therapies for viral hepatitis. Thus far, therapy development have primarily focused on hepatitis B and C. HBV can now be controlled with direct-acting antivirals (DAAs), although the virus cannot be effectively eliminated. Additional therapies with multiple modalities that can achieve functional cures, the sustained loss of the HBV surface antigen, are actively pursued by the biotech and pharma industry (Lok et al., 2017; Tang et al., 2017). Treatment for hepatitis C has shifted from the use of immunomodulators and the general viral inhibitor ribavirin to molecules that target the viral replication proteins (Scheel and Rice, 2013). Several combinations of DAAs can effectively elimination pan-genotypic HCV with very low rate of viral relapse (Zoratti et al.,). The general recommendation for individuals infected with HAV is to rest and avoid stressors that can exacerbate symptoms. As discussed above, there is more urgent need to treat HEV infection. Currently, recombinant interferon and ribavirin are available, but effective DAAs remain to be identified (Netzler et al.,).

This Research Topic contains both reviews and original articles that deal with a range of topics on viral hepatitis. Despite the significant advances made in Hepatitis B research, HBV continues to be a serious threat to public health worldwide. In their review, Steinmann et al. put hepatitis B into a historical context and the lessons on proper formulation of vaccines. The authors emphasized on the high heat tolerance of HBV and suggested the importance of proper washing and disinfection to minimize HBV contamination and overall safety. The entry of HBV into host cells is not completely understood and is an area that requires more attention. Though sodium-taurocholate cotransporting polypeptide (NTCP) was shown to be a functional receptor for HBV, other molecules are reported to aid in HBV infection. To better understand HBV infectivity, Hu et al. documented that E-cadherin, an adhesion molecule that is abundant in epithelial tissue, can interact with the HBV receptor to affect its localization in cells and thus impact HBV entry. Interestingly, E-cadherin binds only to the glycosylated form of NTCP, which is important for it to act as the HBV receptor, and thus preferentially regulates the membrane localization of glycosylated NTCP.

Three articles dealt with viral pathogenesis. Liu et al. used transcriptome analysis to demonstrate that the HCV Core protein expressed from a chimeric virus can induce interleukin-32 expression. Use of specific inhibitors in their study pointed to the involvement of PI3K/AKT pathway in IL32 induction. Authors suggested that the HCV core protein dependent IL32 expression leads to the elevated inflammation associated with severe hepatitis. One of the peculiar disease manifestations of HEV is its involvement in neurological disorders. Not much is known about how HEV induces neurological complications. Tian et al. showed that HEV could cause mitochondrial-associated apoptosis in cultured human brain cells and in the brains of HEV-infected gerbils. This further induced the production of high amounts of pro-inflammatory cytokines possibly explaining the observed extrahepatic injuries associated with HEV infection. In the review by Sehgal et al., the link between gut microbiota and the severity of viral hepatitis was examined. The authors focused on the role of bacterial pathogen-associated molecular patterns in activating innate immune receptors resulting in the NFκB signaling in hepatitis B and C dependent hepatitis. Fecal microbiota transplant could be an alternative method of treatment and management for viral hepatitis.

Four articles deal with therapeutic development and possible therapeutic molecules. Khan et al. reviewed the diverse HCV replicons that were instrumental to the development of HCV drugs and threw light on drug resistance. The replicons for all the major HCV genotypes, including subgenomic and full-length replicons, and their importance in HCV drug discovery are discussed. For HEV, a promising drug target is the protease. HEV encoded protease was suggested to be a papain-like cysteine protease as well as chymotrypsin like protease. In their work, Saraswat et al. showed that the HEV protease was able to process the ORF1 polyprotein. Furthermore, the authors used biochemical assays and in silico modeling to show that the HEV protease is indeed a papain-like cysteine protease. Also in this Research Topic, the modulation of polyamine synthesis as a possible antiviral strategy was investigated. Polyamines are known to play a role in the replication of many RNA and DNA viruses. Mao et al. showed that polyamines help in HBV replication and an inhibitor of polyamine synthesis can inhibit HBV by increasing the proteasome-mediated degradation of the Core protein. Finally, in this Research Topic, Wang et al. focused on another virus whose infection can cause hepatitis, the human adenovirus. They developed a mouse monoclonal antibody against one of the major capsid proteins of human adenovirus (HAdV-7) and showed that this antibody has a potent neutralizing activity.

The original articles and reviews presented in this Research Topic showcase the work of diverse group of researchers from different parts of the world on viral hepatitis. The knowledge provided will contribute to the development of interference strategies and treatment for viral hepatitis.

C. Cheng Kao
Milan Surjit
C. T. Ranjith-Kumar

AUTHOR CONTRIBUTIONS

CK, MS and CR-K were the topic editors of this Research Topic and co-wrote the editorial. All the authors contributed to the article and approved the submitted version.

REFERENCES

Aggarwal, R. (2013). Hepatitis E: Epidemiology and Natural History. *J. Clin. Exp. Hepatol.* 3, 125. doi: 10.1016/j.jceh.2013.05.010

Doceul, V., Bagdassarian, E., Demange, A., and Pavio, N. (2016). Zoonatic Hepatitis E Virus: Classification, Animal Reservoirs and Transmission Routes. *Viruses* 8 (10), 270. doi: 10.3390/v8100270

Hoofnagle, J. H., Nelson, K. E., and Purcells, R. H. (2012). Hepatitis E. *N. Engl. J. Med.* 367, 1244. doi: 10.1056/NEJMra1204512

Khuroo, M. S., and Kamili, S. (2003). Aetiology, Clinical Course and Outcome of Sporadic Acute Viral Hepatitis in Pregnancy. *J. Viral Hepat.* 10, 61. doi: 10.1046/j.1365-2893.2003.00398.x

Lemon, S. M., Ott, J., Damme, V., and Shouval, D. (2017). Type A Hepatitis: A Summary and Update on the Molecular Virology, Epidemiology, Pathogenesis and Prevention. *J. Hepat.* 68, 167. doi: 10.1016/j.jhep.2017.08.034

Loader, M., Moravek, R., Witowshi, S., and Driscoll, L. M. (2019). A Clinical Review of Viral Hepatitis. *J. Am. Acad. Physic. Assit.* 32, 15. doi: 10.1097/01.JAA.0000586300.88300.84

Lok, A. S., Zoulim, F., Dusheiko, G., and Gheny, M. (2017). Hepatitis B Cure: From Discovery to Regulatory Approval. *J. Hepatol.* 67, 847. doi: 10.1016/j.jhep.2017.05.008

Nagashima, S., Takahashi, M., Kobayashi, T., Nishiyam, T. T., Nishiyama, T., et al. (2017). Characterization of the Quasi-Enveloped Hepatitis E Virus Particles Released by the Cellular Exosomal Pathway. *J. Virol.* 22, e00822–e00817. doi: 10.1128/JVI.00822-17

Netzler, N. E., Tuipulotu, D. E., Vasudevan, S. G., Mackenzie, JM, and White, P. A. (2019). Antiviral Candidates for Treating Hepatitis E Virus Infection. *Antimicrob. Agents Chemotherap.* 63, e00003–e00019. doi: 10.1128/AAC.00003-19

Scheel, T. K., and Rice, C. M. (2013). Understanding the Hepatitis C Virus Life Cycle Paves the Way for Highly Effective Therapies. *Nat. Med.* 19, 837. doi: 10.1038/nm.3248

Schillie, S., Vellozzi, C., Reingold, A., Harris, A., Haber, P., et al. (2018). Prevention of Hepatitis B Virus Infection in the United States: Recommendations of the Advisory Committee on Immunization and Practices. *Morbidity Mortality Wkly. Rep.* 67, 1. doi: 10.15585/mmwr.rr6701a1

Tang, L., Zhao, Q., Wu, S., Cheng, J., and Guo, J.-T. (2017). The Current Status and Future Directions for Hepatitis B Antiviral Drug Discovery. *Expert Opin. Drug Disc.* 12, 5. doi: 10.1080/17460441.2017.1255195

World Health Organization (2012). *Prevention and Control of Viral Hepatitis Infection: Framework for Global Action*. World Health Organization. Available at: https://apps.who.int/iris/handle/10665/130012.

World Health Organization (2016). *Combating Hepatitis B and C to Reach Elimination by 2030. Advocacy Brief*. World Health Organization. Available at: https://apps.who.int/iris/handle/10665/206453.

Yan, H., Zhong, G., Xu, G., He, W., Jing, Z., et al. (2012). Sodium Cholate Co-Transporting Polypeptide Is a Functional Receptor for Human Hepatitis B and D Virus. *eLife* 1, e00049. doi: 10.7554/eLife.00049

Zhu, F.-C., Zhang, J., Zhang, X.-F., Zhou, C., Want, Z.-Z., et al. (2010). Efficacy and Safety of a Recombinant Hepatitis E Vaccine in Healthy Adults: A Large-Scale, Randomized, Double-Blind Placebo-Controlled, Phase 3 Trial. *Lancet* 376, 895. doi: 10.1016/S0140-6736(10)61030-6

Zoratti, M. J., Siddiqua, A., Morassut, R. E., Zeraatkar, D., Chou, R., van Holten, J., et al. Pangenotypic Direct Acting Antivirals for the Treatment of Hepatitis C Virus Infection: A Systematic Literature Review. *EClin. Med.* 18, 100237. doi: 10.1016/j.eclinm.2019.12.007

Conflict of Interest: The authors declare that the research was conducted in the absence of any commercial or financial relationships that could be construed as a potential conflict of interest.

frontiers in Cellular and Infection Microbiology

ORIGINAL RESEARCH
published: 04 December 2019
doi: 10.3389/fcimb.2019.00417

A Murine Monoclonal Antibody With Potent Neutralization Ability Against Human Adenovirus 7

*Rong Wang†, Jiansheng Lu†, Quan Zhou, Lei Chen, Ying Huang, Yunzhou Yu and Zhixin Yang**

Laboratory of Protein Engineering, Beijing Institute of Biotechnology, Beijing, China

B1-type human adenoviruses (HAdVs) HAdV-3, HAdV-7, and HAdV-55 have caused epidemics in North America, Asia, and Europe. However, to date, no adenovirus vaccines or antiviral drugs have been approved for general use. In the present work, a scFv-phage immune library was constructed and mouse monoclonal antibody (MMAb) 10G12 was obtained through selection. 10G12 is specific for HAdV-7 and binds the hexon loop1 and loop2 (LP12), resulting in strong neutralization activity against HAdV-7. Additionally, it is stable in serum and buffer at various pH values. The findings provide insight into adenovirus and antibody responses and may facilitate the design and development of adenovirus vaccines and antiviral drugs.

Keywords: human adenovirus type 7 (HAdV-7), mouse monoclonal antibody (MMAb), immune library, neutralizing antibody, antiviral drugs

OPEN ACCESS

Edited by:
Milan Surjit,
Translational Health Science and Technology Institute (THSTI), India

Reviewed by:
Santosh Dhakal,
Johns Hopkins University, United States
Yucel Aydin,
Tulane University, United States

***Correspondence:**
Zhixin Yang
yy_xiao@126.com

†These authors have contributed equally to this work

Specialty section:
This article was submitted to Virus and Host, a section of the journal Frontiers in Cellular and Infection Microbiology

Received: *17 August 2019*
Accepted: *21 November 2019*
Published: *04 December 2019*

Citation:
Wang R, Lu J, Zhou Q, Chen L, Huang Y, Yu Y and Yang Z (2019) A Murine Monoclonal Antibody With Potent Neutralization Ability Against Human Adenovirus 7. Front. Cell. Infect. Microbiol. 9:417. doi: 10.3389/fcimb.2019.00417

INTRODUCTION

Human adenoviruses (HAdVs), non-enveloped, icosahedral, double-stranded DNA viruses spanning > 85 genotypes, are classified into seven species (A–G) (Yoshitomi et al., 2017). HAdV infection is characterized by a broad spectrum of disease symptoms in humans, including sore throat, pneumonia, fever, and acute otitis media, with most cases involving gastrointestinal symptoms that vary with infection genotype (Arnold et al., 2010; Kunz and Ottolini, 2010). Symptoms are generally mild and self-limiting in immune-competent adults, but outbreaks of acute respiratory diseases (ARDs), such as community-acquired pneumonia (CAP), can occur in newborns, school students, and military recruits (Tan et al., 2016). B1 type adenoviruses HAdV-3, HAdV-7, and HAdV-55 are responsible for most epidemics in North America, Asia, and Europe (Choi et al., 2005; Zhang et al., 2006; James et al., 2007; Selvaraju et al., 2011; Tang et al., 2011; Gopalkrishna et al., 2016). To date, no vaccines for the general population available for HAdVs, and only vaccines against HAdV types 4 and 7 have been developed for the USA military (Russell et al., 2006; Kajon et al., 2015). Additionally, no antiviral drugs or efficient antiviral therapies have been approved for treating HAdVs (Echavarría, 2008).

Immune reconstitution plays a critical role in controlling AdV infection, and serotype-specific neutralizing monoclonal antibodies (MAbs) correlate with clearance of AdV (Heemskerk et al., 2005; Echavarría, 2008). The adenovirus capsid is formed from three major proteins (hexon, penton base, and fiber) and four minor proteins (IIIa, VI, VIII, and IX). Hexon, the most abundant capsid protein, recruits cytoplasmic dynein, a crucial component for transporting viral capsids along microtubules (Scherer and Vallee, 2015). Hexon is also an important antigen for neutralizing antibodies against HAdV-3, -5, -7, -14, and -55 (Sumida et al., 2005; Tian et al., 2011; Yu et al., 2013; Su et al., 2016). Type-specific neutralization epitopes on hexon proteins of many adenoviruses

are primarily located in seven hypervariable regions (Rux et al., 2003; Pichla-Gollon et al., 2007; Yuan et al., 2009; Bradley et al., 2012; Qiu et al., 2012; Tian et al., 2018b). Hexon stimulates type-specific neutralizing Abs (NAbs), whereas fiber induces Abs with cross-neutralizing activity against HAdV-14 and HAdV-55 (Feng et al., 2018). However, to date, only a few neutralization epitopes on the HAdV fiber knob region have been identified.

In the present study, scFv 10G12 was screened from an scFv-phage antibody immune library and subcloned to generate an MMAb. We identified MMAb 10G12 as a potent antibody that effectively targets HAdV-7 *in vitro* at low concentrations by binding to hexon loop1 and loop2 (LP12). MMAb 10G12 displayed good stability in serum and phosphate buffer (PB) at different pH values.

MATERIALS AND METHODS

Cell Lines and Viruses

HEK293F and A549 cells (ATCC, USA) were cultured in Dulbecco's modified Eagle's medium (DMEM) containing 10% fetal bovine serum (FBS) (Excell, China). FreeStyle^{TM} 293-F cells (Invitrogen, USA) were cultured in FreeStyle^{TM} 293 Expression Medium (12338; Gibco, USA). Cells were incubated at 37°C in a 5% CO_2 atmosphere. The HAdV-7 GZ6965 strain (human/CHN/GZ6965/2001) used herein was obtained as described previously (Qiu et al., 2012) and maintained in our laboratory. The HAdV-55 strain was isolated from a patient and kindly provided by Prof. Hongbin Song (Center for Disease Control and Prevention of Chinese PLA, Beijing, China). HAdV-7 and HAdV-55 were propagated in HEK293-F cells grown in DMEM containing 2% FBS. When 75–95% of cells exhibited typical cytopathic effects (CPEs) consistent with HAdV infection, the cell suspension was frozen at −80°C and thawed three times, centrifuged at 4,000 g for 5 min, and the supernatant was inactivated and purified using standard CsCl gradient centrifugation (Wu et al., 2002). The obtained virus particles were aliquoted and stored at −80°C.

Construction and Selection of scFv-phage Antibody Immune Libraries

Preparation and characterization of the scFv-phage display library was subsequently performed. Female BALB/c mice at 6–8 weeks old were immunized with inactivated HAdV-7. Pre-immune sera were collected from mouse tails and used as negative controls. A 100 μg sample of inactivated HAdV-7 emulsified in Freund's complete adjuvant (Sigma, USA) was intraperitoneally injected, followed by four boosters of the same dose at 2-week intervals. Spleens were harvested 3 days after the final booster, and total RNA was isolated from spleen cells and was reverse transcribed into cDNA (K1621, Thermo Scientific, USA). Primers for reverse-transcription were PmCGR (TGCATTTGAACTCCTTGCC) and PmCKR (CCATCAATCTTCCACTTGAC). Full-length variable light (V_L) and variable heavy (V_H) chain genes were amplified by overlay-extended PCR and the scFv fragment was cloned into phage display vector pADSCFV-S. Competent *Escherichia coli* HST08 Blue cells were transformed with the ligation mixture by electroporation. Transformed cells were titrated on agar plates to determine the library size, and colony PCR was performed on a selection of colonies to determine the presence of DNA inserts in the vector. Harvested cells samples harboring the final scFv antibody gene library were combined, aliquoted, and stored at −80°C.

Purified HAdV-7 (300 ng, 100 μl) in PBS was incubated in a microtiter plate well overnight at 4°C, then blocked with 3% BSA in TBS (50 mM Tris-HCl pH 7.5, 150 mM NaCl) for 2 h at 37°C. A 100 μl sample of phage library at 1.9×10^7 plaque-forming units (pfu) per ml was added and incubated for an additional 2 h at 37°C after a washing step. After washing, wells with TBST (TBS containing 0.05% Tween-20), bound phage was eluted with 120 μl 0.1 M glycine-HCl (pH 2.2) and neutralized with 15 μl 1 M Tris-HCl (pH 9.0). After eluting, phage was amplified by infecting *E. coli* XL1-Blue cells, and four rounds of panning were carried out. Positively selected phages were amplified and resulting scFv was subjected to DNA sequence.

MMAb Generation of scFv

PCR was performed to amplify the full-length variable light (V_L) and variable heavy (V_H) chain genes of positively selected phages. PCR products were digested with restriction endonucleases *Sal* I and *Age* I, then cloned separately into pMABG1 and pMABKa vectors containing a mouse immunoglobulin constant gene. Recombinant antibodies were obtained as IgG1 molecules, regardless of their original isotype. FreeStyle 293-F cells were transfected with equal quantities of plasmids encoding heavy and light chains using a FectoPRO transfection kit (116-001, Polyplus-Transfection, French) for antibody expression. At 4 days after transfection, antibody-containing supernatants were harvested, and antibodies were purified using HiTrap MabSelect Xtra (28-4082-60, GE Healthcare, USA).

Expression and Purification of Loop1 and Loop2 (LP12) and Fiber

Viral DNA was extracted from A549 cells infected with HAdV-7 or HAdV-55 using DNAVzol (Vigorous, Beijing, China) following the manufacturer's instructions. Genes encoding the hexon LP12 fragment and fiber were amplified by PCR and inserted into the pTIG-TRX vector. Primers used for PCR are listed in **Table 1** (7LP12, LP12 of HAdV-7; 55LP12, LP12 of HAdV-55; 7Fiber, Fiber of HAdV-7; 55Fiber, Fiber of HAdV-55). The pTIG-TRX-LP12 plasmid was transformed into *E. coli* BL21 (DE3) cells (TransGen, Beijing, China) for expression of His-tagged fusion protein. Transformed cells were cultured in Luria-Bertani medium containing ampicillin at 37°C, and recombinant expression was induced with 0.6 mM isopropyl b-D-thiogalactoside (IPTG) when the absorbance at 600 nm (OD600) reached 0.4–0.6. After reducing the temperature from 37°C to 16°C, cells were cultured for a further 16 h. Bacteria were lysed by ultrasonic treatment, and recombinant protein was purified by Ni-agarose resin.

ELISA Assay

Wells of ELISA assay plates (9018, Costar, USA) were coated with 200 ng antigen and incubated overnight at 4°C. Wells were

TABLE 1 | Sequences of primers used for PCR.

Primer name	Primer sequences (5′-3′)
7LP12-F	AGGAATTCTAATGGGATCCCACCACCATCATCATCATACATCT CAGTGGATAGTTACA
7LP12-R	GTGCTCGAGCTCGAGCTATTAATTGTCCATTGGGTCAAG
55LP12-F	AGGAATTCTAATGGGATCCCACCACCATCATCATCATAGTTTC AAACCCTATTCTGGTAC
55LP12-R	GTGCTCGAGCTCGAGCTATTACCGCCCGTTCATGTAGTCGTA
7Fiber-F	AGGAATTCTAATGGGATCCCACCACCATCATCATCATACCAAG AGAGTCCGGCTCA
7Fiber-R	GGTGCTCGAGTCATTAGTCGTCTTCTCTGATGTA
55Fiber-F	AGGAATTCTAATGGGATCCCACCACCATCATCATCATACCAA GAGAGTCCGGCTCAGT
55Fiber-R	GGTGCTCGAGTCATTAGTCGTCTTCTCTGATGTAG

then blocked with 200 μl of 5% (w/v) skimmed milk-PBS for 2 h at 37°C, and 200 μl of antibody was added and incubated for 2 h at 37°C. Plates were washed three times with PBS-Tween (0.1% v/v), and goat anti-mouse horseradish peroxidase (HRP)-conjugated IgG antibody (1:5,000, v/v) was added and incubated for 1 h at 37°C. Finally, three rounds of washing with PBS-Tween were carried out, and detection at 492 and 630 nm was performed using OPD chromogen substrate.

To examine whether MMAb 10G12 was specific for HAdV-7, inactivated HAdV-7 and HAdV-55 were used as antigens, and inactivated influenza virus H3N2 (A/swine/Colorado/1/77) (Karasin et al., 2000) and a synthetic polypeptide antigen of foot-and-mouth disease virus (FMDV) (ETQVQRRQHTDVSFILDRFVKVTPKDQINALDLMQTPAH TEPGSRVTNVRGDLQVLAQKAARTLPPGSRHKQKIVAPVK QLL) served as negative controls. The MMAb antibody 10G12 was used at a concentration of 7.5 μg/mL. To examine the affinity of MMAb 10G12 for HAdV-7, inactivated HAdV-7 was used as antigen, and the MMAb 10G12 antibody was 2-fold serially diluted from an initial concentration of 80 μg/mL to 19.07 pg/mL. To identify which epitope MMAb 10G12 binds, fiber, and the hexon LP12 from HAdV-7 and HAdV-55 were used as antigens, and MMAb 10G12 antibody employed at 7.5 μg/mL.

Virus Neutralization Test

For *in vitro* adenovirus neutralization experiments, 100 μl of A549 cells (3×10^5 cells/ml) were seeded in each well of 96-well plates incubated overnight at 37°C in a 5% CO_2 atmosphere. Purified 10G12 was serially diluted 2-fold from 25 to 0.1 μg/ml in DMEM, and 50 μl aliquots of each dilution were mixed with 50 μl HAdV-7 or HAdV-55 with 100$TCID_{50}$. Anti-DENV1 (Lu et al., 2018) and anti-EGFR (CN102993305B) antibodies served as negative controls. Antibody-virus mixtures were incubated at 37°C for 1 h, transferred to 96-well plates containing 85–95% confluent A549 cell monolayers, and cultured in DMEM without Phenol Red or serum for 72 h. Infected cells were observed under a microscope and the number of holes in cells with lesions was counted.

To test the ability of MMAb to rescue HAdVs infection, 100 μl of A549 cells (3×10^5 cells/ml) were seeded in each well of 96-well plates and incubated overnight at 37°C in a 5% CO_2 atmosphere. Next, 100 μl samples of HAdV-7 or HAdV-55 with 100$TCID_{50}$ were added to 96-well plates containing 85–95% confluent A549 cell monolayers and incubated at 37°C for 1 h. Purified 10G12 was serially diluted 2-fold from 25 to 0.1 μg/ml in DMEM without Phenol Red and serum, and 100 μl aliquots of each dilution were added to 96-well plates and incubated for 1 week at 37°C. Anti-DENV1 and anti-EGFR antibodies served as negative controls. Infected cells were observed under a microscope and the number of holes in cells with lesions was counted.

MMAb Stability Analysis

To test the stability of MMAb in serum, purified 10G12 was diluted in fetal bovine serum (FBS, Excell) to 25 μg/ml and incubated for 3, 7, or 10 days at 37°C. ELISA assays were then performed to detect whether samples still efficiently recognized HAdV-7.

To test the MMAb stability in PB at different pH values, purified 10G12 was diluted in PB at pH 6.0, 6.5, 7.0, 7.5, and 8.0, and incubated at 37°C for 5 or 8 days. ELISA assays were then performed to detect whether samples still efficiently recognized HAdV-7.

Western Blotting Assay

Purified antigens were quantified using a NanoDrop One^c instrument (Thermo, USA). A 7.5 μg sample of reduced protein was separated by SDS-PAGE and subsequently transferred to a polyvinylidene fluoride (PVDF) membrane. Primary antibody 10G12 (1 mg/mL) was diluted 1:1,000, and secondary antibody HRP-goat anti-mouse immunoglobulin G (IgG) (ZSGB-BIO) was diluted 1:5,000. Signals were detected using Western HPR Substrate Peroxide solution (Millipore).

Statistical Analysis

All experiments were repeated at least three times, except for the stability assay. Data are presented as means ± standard deviation (SD). Statistical significance was determined using GraphPad Prism 5.0 software. An affinity graph was plotted, and EC_{50} values were determined using GraphPad Prism 5.0 software, too. The significance of differences in protective effects compared with controls was evaluated using two-tailed Student's *t*-tests, and *p*-values < 0.05 were considered statistically significant.

RESULTS

Construction and Selection of scFv-phage Antibody Immune Libraries

Female BALB/c mice at 6–8 weeks old were immunized with inactivated HAdV-7, and spleens were harvested for RNA extraction after four booster injections. Genes encoding V_L and V_H chains were amplified by PCR, and DNA fragments of the expected size (350 bp) were obtained. Overlay-extended PCR was performed to generate scFv DNA fragments of ∼750 bp, which were then cloned into the phage vector pADSCFV-S. The final

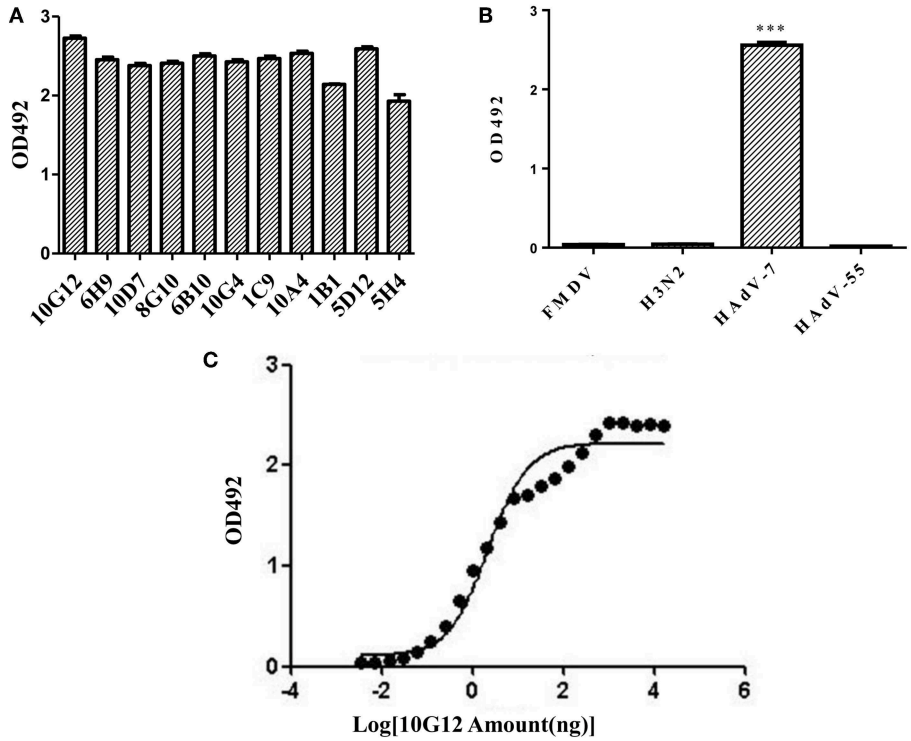

FIGURE 1 | Identification of mouse monoclonal antibodies (MMAbs) against HAdV-7. **(A)** Screening of scFv-displaying phage by ELISA. After three round of panning, 11 positive clones were identified that recognized HAdV-7. **(B)** ELISA analysis of binding between MMAb 10G12 and various antigens. The synthetic polypeptide antigen of foot-and-mouth disease virus (FMDV) and influenza A virus H3N2 (A/swine/Colorado/1/77) served as negative controls. HAdV-55 was tested for potential cross-reactivity. Results are presented as means ± SD from three independent experiments (***$p < 0.001$ vs. negative controls calculated by *t*-tests). **(C)** Affinity curve of the ELISA results for binding between HAdV-7 and serially diluted MMAb 10G12. ELISA assays were performed with 200 ng of inactivated HAdV-7 per well. MMAb 10G12 was serially diluted from an initial concentration of 80 μg/mL.

scFv antibody gene library consisted of 1.9×10^7 independent clones, with 80% correctness.

In total, 11 positive clones were identified from samples after the third round of panning against HAdV-7, and their ability to interact with HAdV-7 is shown in **Figure 1A**. These phagemids were extracted and each insert was sequenced. The results revealed five unique full-size scFv sequences among the 11 clones (10G12, 6H9, 10D7, 8G10, 6B10, 10G4, and 1C9 shared the same sequence; 5H4 had the wrong sequence). V_H and V_L of 10G12, 10A4, 1B1, and 5D12 were recloned into pMABG1 or pMABKa to generate murine IgG1 molecules. Although these four antibodies were specific to HAdV-7, 10A4, 1B1, and 5D12 did not exhibit neutralizing activity (data not shown). Thus, subsequent experiments only characterized 10G12.

MMAb 10G12 Is Specific for HAdV-7

To examine whether MMAb 10G12 is specific for HAdV-7, an ELISA assay was performed. Since positive clones bound to various unrelated viruses in the previous selection of the scFv-phage antibody library, two unrelated antigens (influenza virus H3N2 and the synthetic polypeptide antigen of FMDV) were included as negative controls. Additionally, since there are more than 85 HAdV genotypes, HAdV-55 was tested for potential cross-reactivity with MMAb 10G12. As shown in **Figure 1B**, MMAb 10G12 bound to inactivated HAdV-7, but not to inactivated influenza virus H3N2, the synthetic polypeptide antigen of FMDV, or HAdV-55. Furthermore, ELISA assay was performed to test the affinity of MMAb 10G12 for HAdV-7. Based on the absorbance at 492 nm, and affinity graph was plotted using GraphPad Prism 5.0 software (**Figure 1C**). The resulting EC_{50} values indicated that the affinity between MMAb and HAdV-7 was 0.14 nM.

In vitro Neutralizing Activity and Therapeutic Effects of MMAb 10G12

To examine the neutralization potential of MMAb 10G12, *in vitro* adenovirus neutralization experiments were performed using A549 cells. Purified 10G12 was serially diluted 2-fold from 25 to 0.1 μg/ml in DMEM, and 50 μl aliquots of each dilution were mixed with 50 μl HAdV-7 or HAdV-55 with $100TCID_{50}$. The antibody-virus mixtures were transferred to A549 cells, and every dilution included eight replicates. After 72 h, infected cells were observed under the microscope, and wells containing surviving cells were counted. Two antibodies (anti-DENV and anti-EGFR) served as negative controls. As shown in **Table 2**, 50 μl aliquots of 10G12 with 0.4 μg/ml could neutralize 100% of 50 μl HAdV-7 with $100TCID_{50}$, and all cells at this dilution

TABLE 2 | *In vitro* neutralization activity of MMAb 10G12 (surviving cell holes/total).

Virus	Antibody	Antibody concentration (μg/ml)								
		25	12.5	6.25	3.2	1.6	0.8	0.4	0.2	0.1
No	10G12	8/8	8/8	8/8	8/8	8/8	8/8	8/8	8/8	8/8
HAdV-7	Anti-DENV1	2/8	0/8	0/8	0/8	0/8	0/8	0/8	0/8	0/8
HAdV-7	Anti-EGFR	0/8	0/8	0/8	0/8	0/8	0/8	0/8	0/8	0/8
HAdV-7	No	0/8	0/8	0/8	0/8	0/8	0/8	0/8	0/8	0/8
HAdV-7	10G12	8/8	8/8	8/8	8/8	8/8	8/8	8/8	4/8	0/8
HAdV-55	10G12	0/8	0/8	0/8	0/8	0/8	0/8	0/8	0/8	0/8

TABLE 3 | *In vitro* therapeutic effects of MMAb 10G12 (surviving cell holes/total).

Virus	Antibody	Antibody concentration (μg/ml)								
		25	12.5	6.25	3.2	1.6	0.8	0.4	0.2	0.1
No	10G12	8/8	8/8	8/8	8/8	8/8	8/8	8/8	8/8	8/8
HAdV-7	Anti-DENV1	0/8	0/8	0/8	0/8	0/8	0/8	0/8	0/8	0/8
HAdV-7	Anti-EGFR	0/8	0/8	0/8	0/8	0/8	0/8	0/8	0/8	0/8
HAdV-7	No	0/8	0/8	0/8	0/8	0/8	0/8	0/8	0/8	0/8
HAdV-7	10G12	8/8	8/8	8/8	8/8	6/8	2/8	0/8	0/8	0/8
HAdV-55	10G12	0/8	0/8	0/8	0/8	0/8	0/8	0/8	0/8	0/8

had no lesions. Even 50 μl aliquots of 10G12 with 0.2 μg/ml could neutralize 50% of 50 μl HAdV-7 with 100$TCID_{50}$, but cells at this dilution had partial lesions. Furthermore, even 10G12 at 25 μg/ml was unable to neutralize HAdV-55 with 100$TCID_{50}$. These findings indicate that MMAb 10G12 exhibited strong neutralization activity against HAdV-7 and poor cross-reactivity with HAdV-55.

Next, the ability of MMAb 10G12 to rescue HAdVs infection was investigated to explore potential therapeutic effects. HAdV-7 or HAdV-55 with 100$TCID_{50}$ were added to 96-well plates containing 85–95% confluent monolayers of A549 cells and incubated at 37°C for 1 h. Purified 10G12 was then serially diluted 2-fold from 25 to 0.1 μg/ml, added to infected A549 cells and incubated for 1 week at 37°C. Anti-DENV1 and anti-EGFR antibodies served as negative controls. Infected cells were observed under a microscope and the number of holes in cells with lesions was counted. As shown in **Table 3**, even at 1 h after infection, 3.2 μg/ml 10G12 could rescue 100% of cells infected with 100$TCID_{50}$ HAdV-7, and none of the cells at this dilution displayed lesions. Even 0.8 μg/ml 10G12 could protect 25% of cells infected with 100$TCID_{50}$ HAdV-7. Furthermore, even 25 μg/ml 10G12 was unable to rescue A549 cells infected with 100$TCID_{50}$ HAdV-55. These findings indicate that MMAb 10G12 exhibited potent therapeutic effects against HAdV-7.

MMAb 10G12 Is Stable in Serum and PB at Different pH Values

To test MMAb stability in serum, purified 10G12 was diluted in FBS to 25 μg/ml and incubated in 37°C for 3, 7, and 10 days. ELISA assays were then performed to detect whether samples still efficiently recognized HAdV-7. As shown in **Figure 2A**, compared with day 0, the binding activity of samples diluted in FBS after 3, 7, and 10 days decreased by a statistically significant amount. However, even after 10 days of incubation at 37°C, the binding activity was only decreased 20%. Additionally, from day 3 to 10, the binding activity did not decrease with increasing incubation duration. Differences between fetal bovine serum and the mouse monoclonal antibody may explain this decrease in binding activity. The results indicate that MMAb 10G12 was relatively stable in serum.

To test the MMAb stability in PB at different pH values, purified 10G12 was diluted in PB at pH 6.0, 6.5, 7.0, 7.5, and 8.0, and incubated at 37°C for 5 or 8 days. ELISA assays were then performed to detect whether samples still efficiently recognized HAdV-7. As shown in **Figure 2B**, samples diluted in PB at pH 6.0, 6.5, 7.0, 7.5, and 8.0 after 8 days of incubation still had the same binding activity as those before incubation. These results indicate that MMAb 10G12 is stable in serum and PB at different pH values.

MMAb 10G12 Binds Hexon Loop1 and Loop2

Hexon is an important antigen of neutralizing antibodies, and fiber also has a few neutralization epitopes. To determine to which epitope MMAb 10G12 binds, fragments comprising loop1 and loop2 (LP12) of hexon and fiber from HAdV-7 and HAdV-55 were amplified by PCR and subcloned into pTIG-TRX. Recombinant proteins were expressed and purified (**Figure 3A**), and the results of western blotting showed that MMAb 10G12 bound LP12 of HAdV-7 but not HAdV-55 or fiber (**Figure 3B**). When using reduced protein samples for SDS-PAGE, 10G12 should bind the linear epitopes of 7LP12. Thus, ELISA assay plates were coated with LP12 or fiber from HAdV-7 and HAdV-55 at 200 ng per well, and the affinity for MMAb 10G12 was measured. As shown in **Figure 3C**, MMAb 10G12 bound LP12 of HAdV-7 but not fiber, consistent with the results of western blotting in **Figure 3B**. However, the ELISA result showed that 10G12 bound LP12 of HAdV-55 with weaker affinity than HAdV-7. Combined with the western blotting results in **Figure 3B**, this indicates that 10G12 might bind some spatial epitopes of 55LP12. However, 10G12 did not neutralize HAdV-55 (**Table 2**), suggesting that these might be non-neutralizing spatial epitopes. In summary, MMAb 10G12 clearly bound the hexon LP12 region.

DISCUSSION

In this study, we identified antibody MMAb 10G12 that binds specifically to HAdV-7 through the hexon LP12 region. MMAb 10G12 exhibited strong neutralization activity against HAdV-7 and was stable in serum and PB at different pH values.

Despite more than 85 genotypes have been identified for HAdVs, few neutralizing antibodies have been reported. Tian et al. (2018a) reported that the recombinant trimeric HAdV-11 fiber knob region is responsible for cross-neutralizing antibody responses against HAdV-11, -7, -14p1, and -55 in mice. Three neutralizing MAbs, 6A7, 3F11, and 3D8, were

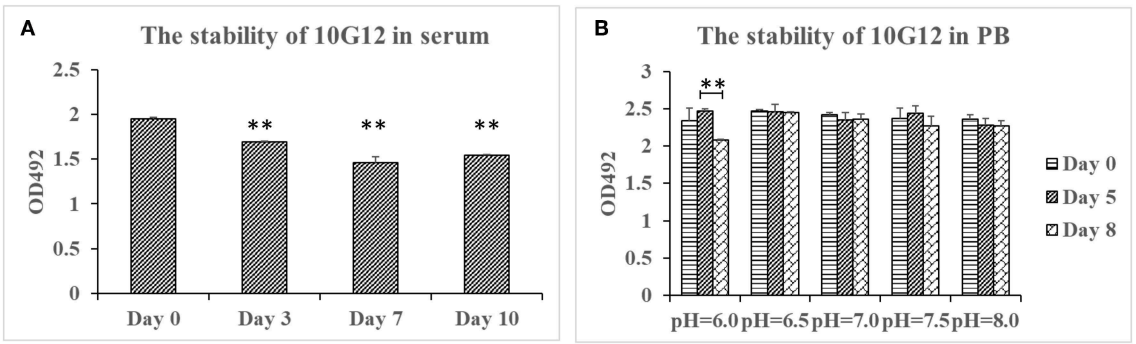

FIGURE 2 | Stability of 10G12 in serum and PB at different pH values. **(A)** ELISA analysis of the binding between HAdV-7 and MMAb 10G12 in serum. Purified 10G12 was diluted in fetal bovine serum to 25 μg/ml and incubated at 37°C for 3, 7, and 10 days. ELISA assays were performed with 200 ng of inactivated HAdV-7 per well. **(B)** ELISA analysis of binding between HAdV-7 and MMAb 10G12 in PB at different pH values. Purified 10G12 was diluted in PB at pH 6.0, 6.5, 7.0, 7.5, and 8.0 and incubated at 37°C for day 5 and 8. ELISA assays were performed with 200 ng inactivated HAdV-7 per well. Data were obtained from two separate experiments, and results are presented as means ± SD (**$p < 0.01$ vs. day 0 values calculated by *t*-test).

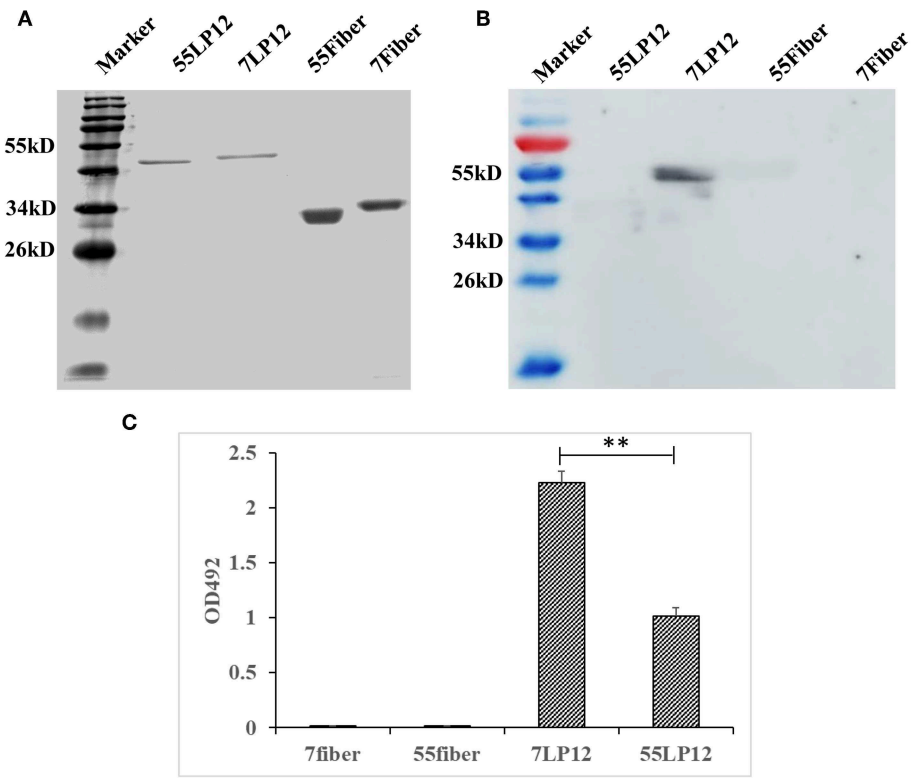

FIGURE 3 | Binding of MMAb 10G12 to loops 1 and 2 (LP12) of hexon. **(A)** Reducing polyacrylamide gel electrophoresis analysis of purified antigens. A 5 μg sample of reduced Fiber and LP12 of HAdV-7 and HAdV-55 was separated by SDS-PAGE and subsequently stained with Coomassie Brilliant Blue. **(B)** Western blotting analysis of binding between 10G12 and various antigens. A 7.5 μg sample of reduced Fiber and LP12 of HAdV-7 and HAdV-55 was separated by SDS-PAGE and subsequently transferred to a PVDF membrane. Primary antibody 10G12 (1 mg/mL) was diluted 1:1,000, and secondary antibody HRP-goat anti-mouse IgG was diluted 1:5,000. Signals were detected using Western HPR Substrate Peroxide solution. **(C)** ELISA analysis of binding between 10G12 and various antigens. Data were obtained from three separate experiments, and results are presented as means ± SD (**$p < 0.05$ between 7LP12 and 55LP12, calculated by *t*-tests).

obtained via mouse hybridoma fusion, of which 3F11 and 3D8 cross-neutralized HAdV-11,-7, and -55, but not HAdV-14p1 (Tian et al., 2018a). Feng et al. (2018) previously demonstrated that a fiber-specific antibody in sera contributed to cross-neutralizing activity against HAdV-14 and HAdV-55. However, HAdV-55 is a recombinant chimera of HAdV-11 and -14 that contains the fiber gene from HAdV-14. Our current study shows that 10G12 does not neutralize HAdV-55, and

has poor cross-reactivity, probably through interaction with non-neutralizing epitopes.

MMAb 10G12 is a murine neutralizing antibody like 6A7, 3F11, and 3D8 (Tian et al., 2018a). Monoclonal antibodies of mouse origin can induce human anti-mouse antibody (HAMA) responses, which restricts the use of MMAb in humans (Hertel et al., 1990). The first MMAb, Muromonab, has been on the market since 1992, and humanized antibodies based on murine MAb are increasingly being developed (Makulska-Nowak, 1993). In future work, MMAb 10G12 may be further humanized for therapeutic use.

In this study, we expressed and purified the recombinant LP12 hexon region. ELISA assay plates were coated with 200 ng of inactivated HAdV-7 or LP12 per well, and the affinity for MMAb remained the same (**Figures 1B**, **3C**). This indicates that LP12 is present in the main neutralization epitopes of HAdV-7. Previous studies confirmed that hexon protein, the most abundant capsid protein, is the predominant target of neutralizing antibodies (NAbs) recognizing HAdV-3, -5, -7, -14, and -55 (Sumida et al., 2005; Tian et al., 2011; Bradley et al., 2012; Yu et al., 2013; Su et al., 2016; Feng et al., 2018). Additionally, the affinity results indicate that LP12 could substitute for inactivated HAdV-7 in initial screening and testing.

In summary, MMAb 10G12 was specific for HAdV-7 and displayed good stability. In future work, we will explore whether MMAb 10G12 can provide protection against HAdV-7 *in vivo*, and if so, MMAb may be further humanized for use as a therapeutic agent.

DATA AVAILABILITY STATEMENT

The data used to support the findings of this study are available from the corresponding author upon request.

ETHICS STATEMENT

The animal study was reviewed and approved by Academy of Military Medical Sciences (AMMS; ID: SYXK2012–05).

AUTHOR CONTRIBUTIONS

JL and ZY conceived this study. YH, YY, and ZY carried out experiments. RW, YH, LC, and QZ performed data analysis. RW and ZY drafted, wrote, edited, and reviewed the manuscript. ZY acquired funding. JL and QZ provided resources. RW, YH, YY and ZY supervised the work.

FUNDING

This work was supported by 2015ZX09J15105-003-003.

ACKNOWLEDGMENTS

The authors thank Prof. Hongbin Song (Center for Disease Control and Prevention of Chinese PLA, Beijing, China) for kindly providing the HAdV-55.

REFERENCES

Arnold, J., Jánoska, M., Kajon, A. E., Metzgar, D., Hudson, N. R., Torres, S., et al. (2010). Genomic characterization of human adenovirus 36, a putative obesity agent. *Virus Res.* 149, 152–161. doi: 10.1016/j.virusres.2010.01.011

Bradley, R. R., Maxfield, L. F., Lynch, D. M., Iampietro, M. J., Borducchi, E. N., and Barouch, D. H. (2012). Adenovirus serotype 5-specific neutralizing antibodies target multiple hexon hypervariable regions. *J. Virol.* 86, 1267–1272. doi: 10.1128/JVI.06165-11

Choi, E. H., Kim, H. S., Eun, B. W., Kim, B. I., Choi, J. Y., Lee, H. J., et al. (2005). Adenovirus type 7 peptide diversity during outbreak, Korea, 1995-2000. *Emerg. Infect. Dis.* 11, 649–654. doi: 10.3201/eid1105.041211

Echavarría, M. (2008). Adenoviruses in immunocompromised hosts. *Clin. Microbiol. Rev.* 21, 704–715. doi: 10.1128/CMR.00052-07

Feng, Y., Sun, X., Ye, X., Feng, Y., Wang, J., Zheng, X., et al. (2018). Hexon and fiber of adenovirus type 14 and 55 are major targets of neutralizing antibody but only fiber-specific antibody contributes to cross-neutralizing activity. *Virology* 518, 272–283. doi: 10.1016/j.virol.2018.03.002

Gopalkrishna, V., Ganorkar, N. N., and Patil, P. R. (2016). Identification and molecular characterization of adenovirus types (HAdV-8, HAdV-37, HAdV-4, HAdV-3) in an epidemic of keratoconjunctivitis occurred in Pune, Maharashtra, Western India. *J. Med. Virol.* 88, 2100–2105. doi: 10.1002/jmv.24565

Heemskerk, B., Lankester, A. C., van Vreeswijk, T., Beersma, M. F., Claas, E. C., Veltrop-Duits, L. A., et al. (2005). Immune reconstitution and clearance of human adenovirus viremia in pediatric stem-cell recipients. *J. Infect. Dis.* 191, 520–530. doi: 10.1086/427513

Hertel, A., Baum, R. P., Auerbach, B., Herrmann, A., and Hör, G. (1990). The clinical relevance of human anti-mouse-antibody (HAMA) in immunoscintigraphy. *Nuklearmedizin* 29, 221–227. doi: 10.1055/s-0038-1629535

James, L., Vernon, M. O., Jones, R. C., Stewart, A., Lu, X., Zollar, L. M., et al. (2007). Outbreak of human adenovirus type 3 infection in a pediatric long-term care facility–Illinois, 2005. *Clin. Infect. Dis.* 45, 416–420. doi: 10.1086/519938

Kajon, A. E., Hang, J., Hawksworth, A., Metzgar, D., Hage, E., Hansen, C. J., et al. (2015). Molecular epidemiology of adenovirus type 21 respiratory strains isolated from US military trainees (1996-2014). *J. Infect. Dis.* 212, 871–880. doi: 10.1093/infdis/jiv141

Karasin, A. I., Schutten, M. M., Cooper, L. A., Smith, C. B., Subbarao, K., Anderson, G. A., et al. (2000). Genetic characterization of H3N2 influenza viruses isolated from pigs in North America, 1977-1999: evidence for wholly human and reassortant virus genotypes. *Virus Res.* 68, 71–85. doi: 10.1016/S0168-1702, 00154-4

Kunz, A. N., and Ottolini, M. (2010). The role of adenovirus in respiratory tract infections. *Curr. Infect. Dis. Rep.* 12, 81–87. doi: 10.1007/s11908-010-0084-5

Lu, J., Wang, R., Xia, B., Yu, Y., Zhou, X., Yang, Z., et al. (2018). Potent neutralization ability of a human monoclonal antibody against serotype 1 *Dengue virus*. *Front. Microbiol.* 9:1214. doi: 10.3389/fmicb.2018.01214

Makulska-Nowak, E. (1993). Muromonab CD3–the first monoclonal antibody used in humans. *Pol. Tyg. Lek.* 48, 857–859.

Pichla-Gollon, S. L., Drinker, M., Zhou, X., Xue, F., Rux, J. J., Gao, G. P., et al. (2007). Structure-based identification of a major neutralizing site in an adenovirus hexon. *J. Virol.* 81, 1680–1689. doi: 10.1128/JVI.02023-06

Qiu, H., Li, X., Tian, X., Zhou, Z., Xing, K., Li, H., et al. (2012). Serotype-specific neutralizing antibody epitopes of human adenovirus type 3 (HAdV-3) and HAdV-7 reside in multiple hexon hypervariable regions. *J. Virol.* 86, 7964–7975. doi: 10.1128/JVI.07076-11

Russell, K. L., Hawksworth, A. W., Ryan, M. A., Strickler, J., Irvine, M., Hansen, C. J., et al. (2006). Vaccine-preventable adenoviral respiratory illness in US military recruits, 1999-2004. *Vaccine* 24, 2835–2842. doi: 10.1016/j.vaccine.2005.12.062

Rux, J. J., Kuser, P. R., and Burnett, R. M. (2003). Structural and phylogenetic analysis of adenovirus hexons by use of high-resolution x-ray crystallographic, molecular modeling, and sequence-based methods. *J. Virol.* 77, 9553–9566. doi: 10.1128/JVI.77.17.9553-9566.2003

Scherer, J., and Vallee, R. B. (2015). Conformational changes in the adenovirus hexon subunit responsible for regulating cytoplasmic dynein recruitment. *J. Virol.* 89, 1013–1023. doi: 10.1128/JVI.02889-14

Selvaraju, S. B., Kovac, M., Dickson, L. M., Kajon, A. E., and Selvarangan, R. (2011). Molecular epidemiology and clinical presentation of human adenovirus infections in Kansas City children. *J. Clin. Virol.* 51, 126–131. doi: 10.1016/j.jcv.2011.02.014

Su, X., Tian, X., Jiang, Z., Ma, Q., Liu, Q., Lu, X., et al. (2016). Human adenovirus serotype 3 vector packaged by a rare serotype 14 hexon. *PLoS ONE* 11:e0156984. doi: 10.1371/journal.pone.0156984

Sumida, S. M., Truitt, D. M., Lemckert, A. A., Vogels, R., Custers, J. H., Addo, M. M., et al. (2005). Neutralizing antibodies to adenovirus serotype 5 vaccine vectors are directed primarily against the adenovirus hexon protein. *J. Immunol.* 174, 7179–7185. doi: 10.4049/jimmunol.174.11.7179

Tan, D., Zhu, H., Fu, Y., Tong, F., Yao, D., Walline, J., et al. (2016). Severe community-acquired pneumonia caused by human adenovirus in immunocompetent adults: a multicenter case series. *PLoS ONE* 11:e0151199. doi: 10.1371/journal.pone.0151199

Tang, L., Wang, L., Tan, X., and Xu, W. (2011). Adenovirus serotype 7 associated with a severe lower respiratory tract disease outbreak in infants in shaanxi province, China. *Virol. J.* 8:23. doi: 10.1186/1743-422X-8-23

Tian, X., Fan, Y., Liu, Z., Zhang, L., Liao, J., Zhou, Z., et al. (2018a). Broadly neutralizing monoclonal antibodies against human adenovirus types 55, 14p, 7, and 11 generated with recombinant type 11 fiber knob. *Emerg. Microbes Infect.* 7:206. doi: 10.1038/s41426-018-0197-8

Tian, X., Qiu, H., Zhou, Z., Wang, S., Fan, Y., Li, X., et al. (2018b). Identification of a critical and conformational neutralizing epitope in human adenovirus Type 4 hexon. *J. Virol.* 92:e01643-17. doi: 10.1128/JVI.01643-17

Tian, X., Su, X., Li, H., Li, X., Zhou, Z., Liu, W., et al. (2011). Construction and characterization of human adenovirus serotype 3 packaged by serotype 7 hexon. *Virus Res.* 160, 214–220. doi: 10.1016/j.virusres.2011.06.017

Wu, H., Dmitriev, I., Kashentseva, E., Seki, T., Wang, M., and Curiel, D. T. (2002). Construction and characterization of adenovirus serotype 5 packaged by serotype 3 hexon. *J. Virol.* 76, 12775–12782. doi: 10.1128/JVI.76.24.12775-12782.2002

Yoshitomi, H., Sera, N., Gonzalez, G., Hanaoka, N., and Fujimoto, T. (2017). First isolation of a new type of human adenovirus (genotype 79), species human mastadenovirus B (B2) from sewage water in Japan. *J. Med. Virol.* 89, 1192–1200. doi: 10.1002/jmv.24749

Yu, B., Dong, J., Wang, C., Zhan, Y., Zhang, H., Wu, J., et al. (2013). Characteristics of neutralizing antibodies to adenovirus capsid proteins in human and animal sera. *Virology* 437, 118–123. doi: 10.1016/j.virol.2012.12.014

Yuan, X., Qu, Z., Wu, X., Wang, Y., Liu, L., Wei, F., et al. (2009). Molecular modeling and epitopes mapping of human adenovirus type 3 hexon protein. *Vaccine* 27, 5103–5110. doi: 10.1016/j.vaccine.2009.06.041

Zhang, Q., Su, X., Gong, S., Zeng, Q., Zhu, B., Wu, Z., et al. (2006). Comparative genomic analysis of two strains of human adenovirus type 3 isolated from children with acute respiratory infection in southern China. *J Gen. Virol.* 87, 1531–1541. doi: 10.1099/vir.0.81515-0

Conflict of Interest: The authors declare that the research was conducted in the absence of any commercial or financial relationships that could be construed as a potential conflict of interest.

frontiers in Cellular and Infection Microbiology

ORIGINAL RESEARCH
published: 20 December 2019
doi: 10.3389/fcimb.2019.00433

Hepatitis E Virus Induces Brain Injury Probably Associated With Mitochondrial Apoptosis

Jijing Tian[1†], *Ruihan Shi*[1,2†], *Peng Xiao*[1], *Tianlong Liu*[1], *Ruiping She*[1*], *Qiaoxing Wu*[1], *Junqing An*[1], *Wenzhuo Hao*[1] *and MajidHussain Soomro*[1]

[1] *Laboratory of Animal Pathology and Public Health, Key Laboratory of Zoonosis of Ministry of Agriculture, College of Veterinary Medicine, China Agricultural University, Beijing, China,* [2] *Institute of Animal Husbandry and Veterinary Medicine, Beijing Academy of Agriculture and Forestry Sciences, Beijing, China*

Hepatitis E virus (HEV) infection has been associated with extrahepatic manifestations, particularly neurological disorders. Although it has been reported that HEV infection induced hepatocyte apoptosis associated with mitochondria injury, activation of mitochondrial apoptotic pathway in the central nervous system during HEV infection was not clearly understood. In this study, the induction of mitochondrial apoptosis-associated proteins and pro-inflammatory cytokines were detected in HEV infected Mongolian gerbil model and primary human brain microvascular endothelial cells (HBMVECs). Mitochondrial exhibited fragments with loss of cristae and matrix in HEV infected brain tissue by transmission electron microscope (TEM). *In vitro* studies showed that expression of NADPH oxidase 4 (NOX4) was significantly increased in HEV infected HBMVECs ($p < 0.05$), while ATP5A1 was significantly decreased ($p < 0.01$). Expressions of pro-apoptotic proteins were further evaluated. Bax was significantly increased in both HEV infected brain tissues and HBMVECs ($p < 0.01$). *In vivo* studies showed that caspase-9 and caspase-3 were activated after HEV inoculation ($p < 0.01$), associated with PCNA overexpression as response to apoptosis. Cytokines were measured to evaluate tissue inflammatory levels. Results showed that the release of TNFα and IL-1β were significantly increased after HEV infection ($p < 0.01$), which might be attributed to microglia activation characterized by high level of IBA1 expression ($p < 0.01$). Taken together, these data support that HEV infection induces high levels of pro-inflammatory cytokines, associated with mitochondria-mediated apoptosis. The results provide new insight into mechanisms of extra-hepatic injury of HEV infection, especially in the central nervous system.

Keywords: Hepatitis E virus, mitochondrial apoptosis, neuroinflammation, mongolian gerbils, human brain microvascular endothelial cells

OPEN ACCESS

Edited by:
Milan Surjit,
Translational Health Science and Technology Institute (THSTI), India

Reviewed by:
Asuka Nanbo,
Nagasaki University, Japan
Logan Banadyga,
National Microbiology Laboratory, Canada

***Correspondence:**
Ruiping She
sheruiping@126.com

[†]These authors have contributed equally to this work

Specialty section:
This article was submitted to Virus and Host, a section of the journal Frontiers in Cellular and Infection Microbiology

Received: *25 August 2019*
Accepted: *04 December 2019*
Published: *20 December 2019*

Citation:
Tian J, Shi R, Xiao P, Liu T, She R, Wu Q, An J, Hao W and Soomro M (2019) Hepatitis E Virus Induces Brain Injury Probably Associated With Mitochondrial Apoptosis. Front. Cell. Infect. Microbiol. 9:433. doi: 10.3389/fcimb.2019.00433

INTRODUCTION

Globally, there were an estimated 20 million people infected by the Hepatitis E virus (HEV) in the year of 2018 (Montpellier et al., 2018). HEV is a small non-enveloped virus with a 7.2 kb plus-strand single-stranded RNA genome and up to 8 genotypes were reported (Wang et al., 2019). Except for humans, genotypes 3 and/or 4 were observed in several domestic animals, including swine, deer,

and rabbits (Kenney and Meng, 2019). Evidence for transmission of HEV-3 and HEV-4 between humans and animals has been reviewed, including waterborne transmission by accidental fecal contamination of drinking water, zoonotic transmission such as contact with infected animals or consumption of contaminated food products, and iatrogenic transmission through infected blood and blood products (Kamar et al., 2017). Though infection with HEV usually causes an acute, self-limiting form of liver inflammation, it is worth noting that extrahepatic injury of HEV, including renal diseases, reproductive system disorders, as well as pancreatitis, and a variety of neurological disorders such as Guillain-Barré syndrome, neuralgic amyotrophy, meningoencephalitis, and peripheral neuropathy, which were reported (Pischke et al., 2017; Soomro et al., 2017; Kenney and Meng, 2019; Tian et al., 2019). Since HEV infection is commonly asymptomatic or unrecognized, HEV associated extrahepatic manifestations are frequently unscreened in clinical diagnosis. Thus, it is important to understand the mechanism underlying HEV infection, especially neurological injury during infection. Mitochondria-mediated apoptosis was involved in many viral diseases. It has been reported that the release of cytochrome c was increased in BHK-21 cells infected with bovine ephemeral fever virus (BEFV) and activation of caspase-9, as well as the downstream effector caspase-3, were further detected (Lin et al., 2009). In gerbil model of HEV infection, mitochondrial damages such as mitochondria swelling, devoid of mitochondrial cristae were observed in hepatocytes via transmission electron microscope (TEM) (Yang et al., 2018). In Yang's study, up-regulation of mitochondria-mediated apoptosis regulating proteins, Bax and Bcl-2, in HEV-infected gerbils, as well as induction of activated caspase-9 and caspase-3 were observed.

Mitochondria dysfunction was reported in lots of central nervous system diseases. It has been reported that mitochondrial production of reactive oxygen species (ROS) was increased in Parkinson's disease (PD), and pro-apoptotic pathways were also activated with following activation of caspase-9, caspase-3 and Bax, which were crucial factors in mitochondria-mediated apoptosis pathway (Bose and Beal, 2016). Venezuelan equine encephalitis virus (VEEV) infection in murine brain microglial cells showed that VEEV inoculation increased cellular apoptosis, with accumulation of ROS and a marked increase of inflammatory cytokines, such as IFN-γ, IL-1α, and IL-1β (Keck et al., 2018). Thus, mitochondria play critical roles during the process of central nervous system injuries.

Previously, it was demonstrated that dysfunction of the blood-brain barrier (BBB) especially tight junction proteins contributed to the brain injury in HEV infection. However, in HEV induced brain injury, whether mitochondria-mediated apoptosis was activated or not has not been elucidated. In this study, morphological changes of mitochondria in HEV-infected gerbil brain tissues were observed by TEM. We further detected the expression of proteins that involved in mitochondria injury and significant alteration of NOX4, ATP5A1, and Bax were observed, indicating that HEV infection might facilitate pro-apoptotic signaling activation in brain tissues. Thus, caspase-9 and caspase-3 which were key effectors of mitochondrial apoptosis were examined. Both caspase-9 and caspase-3 induction were observed in cells and brain tissues that were infected with HEV. We have reported that HEV infection triggered the proliferation of microglial cells in gerbils and rabbits infected with HEV (Shi et al., 2016; Tian et al., 2019). IBA, a marker of microglial cells, was highly expressed in HEV infected brain tissues, which indicated HEV infection-induced inflammation of the brain tissues. Our study further confirmed that inflammatory cytokines such as TNFα and IL-1β were significantly induced in HEV infected brain tissues. Hence, we hypothesized that HEV induced brain tissue inflammation further promoted progress of mitochondria injury and mitochondria-mediated apoptosis. These findings provide new insights into further understanding mechanisms of extra-hepatic injury of HEV, especially the central nervous system.

MATERIALS AND METHODS

Virus, Inoculation, and Animals

The HEV strain (CHN-HB-HD-L2, GenBank accession number KM024042) was derived from a swine liver. Shortly, the liver tissue was homogenized in 0.9% NaCl and spin down (12,000 rpm, 4°C) for 20 min. Then the supernatant was collected and filtered by a 0.22 um filter and the HEV load was tested by qPCR with a titer of 6.57×10^5 genome equivalents (GE) per uL. The viral stock was stored at −86°C prior to inoculation.

72 SPF (specific-pathogen-free) male Mongolian gerbils, purchased from the Department of Experimental Animal Sciences of Capital Medical University (Beijing, China), with body weights about 50–60g were randomly assigned to 2 groups (mock group and HEV infectious group) and accommodated in separate isolators in an air-conditioned room maintained at 21–24°C with a cycle of 12 h of light and 12 h of dark for 1 week preceding the *in vivo* experiment, and feed and water were provided *ad libitum.* Gerbils in the infected group were intraperitoneally inoculated with 0.1 mL (6.57×10^7 GE) of prepared viral homogenate, while gerbils in the mock group were injected with the same dose of HEV-negative swine liver homogenates.

Sampling

Gerbils were sacrificed at 0, 7, 14, 21, 28, 42, and 56 day postinoculation (dpi). Brain and spinal cord samples were collected rapidly after euthanasia and stored at −86°C or fixed in neutral 4% paraformaldehyde or 2.5% (v/v) glutaraldehyde-polyoxymethylene solution for further study.

The levels of serum alanine aminotransferase (ALT), aspartate aminotransferase (AST), total bilirubin (T-BIL) (Yang et al., 2015) and pathological changes of the central nervous system (CNS) induced by HEV infection were examined previously (Shi et al., 2016). Positive and negative stand of HEV RNA in CNS have been tested by PCR as shown before (Shi et al., 2016). Tissues used in the present study derived from the same animals in previous research (Yang et al., 2015; Shi et al., 2016). HEV RNA-positive brain samples accompanying significant changes on liver function index collected on 14, 21, and 28 dpi were chosen for further study.

All animal protocols were approved by the Animal Care and Use Committee of China Agricultural University and were performed humanely for the alleviation of suffering.

TUNEL Assay

TUNEL staining for apoptotic cells in the histological sections was performed using *in situ* BrdU-Red DNA fragmentation (TUNEL) Assay Kit (ab66110, Abcam) and slides were counterstained with DAPI. The images were analyzed with fluorescent microscopy. Quantification of positive signals was performed by examining number of positive cells in five randomly selected fields of each brain section.

Immunohistochemistry Assays

The brain tissues were dehydrated and embedded in paraffin wax, and serial paraffin sections (4 μm) were obtained for immunohistochemical analysis. Immunohistochemical staining was performed using a commercial kit, according to the manufacturer's instructions (ZSGB-BIO, Beijing, China). Primary antibodies used in this study were anti-Bax (1:500, BA0315), anti-Bcl-2 (1:200, BA0412) and anti-active caspase-3 (1:300, BA3968), anti-active caspase-9 (1:300, BA0690), anti-TNF-α (1:300, BA0130), obtained from Boster, Co., Ltd., Beijing, China. Anti-IBA1 (1:500, PB0517), anti-PCNA (1:300, BS-2007R), anti-VIP (1:300, BS0077R), anti-IL-1β (1:300, BS20449R), and anti-Substance P (1:500, BS0065R) were purchased from Bioss, Co., Ltd., Beijing, China. Shortly, the sections were immersed in three consecutive 5-min xylene washes to remove paraffin and were subsequently hydrated with five consecutive ethanol washes in descending order of concentration: 100, 95, 80, 70%, and deionized water. Then, the sections were incubated with primary antibodies, respectively. The sections were executed in a moist chamber, and this procedure has been exclusively described by Ding et al. (Ding et al., 2011). The slides were finally visualized using a light microscope (LM, BX51, Olympus Co., Japan). The positive signal with brown or yellow granular mass was finally measured via the Motic Med 6.0 CMIAS Image Analysis System (Motic China Group Co., Ltd., China). The area density that represented the positive staining intensity was calculated as the ratio between the stained area and the total analyzed field. For quantitation of PCNA positive signal, positive cells in each high power field were counted. At least 5 high power fields in each slide were used for the semi-quantitative test.

Transmission Electron Microscope (TEM)

For transmission electron microscopy, the brain samples were cut into pieces (1 × 1× 1 mm) and fixed in 2.5% (v/v) glutaraldehyde-polyoxymethylene solution overnight at 4°C. The tissues were then washed and postfixed in 2% osmium tetroxide for 1 h at 4°C and embedded in Araldite CY212 after dehydration in ascending grades of ethanol. Ultrathin sections (50–60 nm) were cut and stained with alkaline and lead citrate uranyl acetate. The sections were examined under a JEM 1230 transmission electron microscope (JEOL, Ltd, Japan).

Cell Culture

Primary human brain microvascular endothelial cells (HBMVECs) (BK-PM-010) were purchased from a company (Biopike Technology Company Ltd., Beijing, China) and cultured as described previously (Renou et al., 2014). Shortly, cells were inoculated with HEV (300 multiplicity of infection) and collected in 48 h for western blotting. HEV-negative homogenate served as control.

Western Blotting

The protein concentration from HEV RNA inoculated cells and controls were determined with the BCA protein assay kit (Thermo Fisher Scientific, Waltham, MA, USA) and 20 μg of protein was separated by SDS-PAGE. The blots were incubated with anti-NOX4 (1:600), ATP5A1 (1:500), Bax (1:800), Bcl-2 (1:800), Caspase-9 (1:500), Caspase-3 (1:500) were purchased from Boster Biological Technology Co., Ltd. (China), Beijing Bioss Biological Technology Co., Ltd. (China) or ABclonal Biotechnology Co., Ltd (US), and β-actin (1:2000) purchased from Cell Signaling Technology (CST) (US), served as internal control, for 16 h at 4°C. The membranes were then incubated with the secondary antibodies conjugated with horseradish peroxidase (Santa Cruz Biotechnology) and developed by enhanced chemiluminescence (Thermo Scientific). The images were analyzed with ImageJ (NIH, Bethesda, MD, USA) Gray value was analyzed with ImageJ (NIH, Bethesda, MD, USA) to quantitatively analyze the expression levels of targeted proteins according to the level of exposure gray (resolution). Data were finally normalized to the expression of anti-β-actin.

Quantitative and Statistical Analysis

The data represents 3 experiments analyses by one-way analysis of variance (ANOVA) or Dunnett's test using GraphPad Prism 5 (GraphPad Software). The results are expressed as the mean ± SEM. Differences are considered to be statistically significant, with $^{*}p < 0.05$ and $^{**}p < 0.01$ compared with the mock group.

RESULTS

HEV Infection Induced Mitochondrial Dysfunction

To investigate the function of mitochondria in the process of HEV infection, primary human brain microvascular endothelial cells (HBMVECs) were infected with HEV. After 48 h inoculation, high levels of NOX4 were detected in HEV infected cells ($p < 0.05$) (**Figure 1A**), while ATP5A1 was significantly decreased in HEV infected cells ($p < 0.01$) (**Figure 1B**). To further detect effects of HEV infection on mitochondria morphological changes, HEV infected brain and spinal cord tissues were examined under transmission electron microscope (TEM) and fragmented mitochondria with loss of cristae and matrix in HEV infected gerbil brain tissues was observed (**Figures 1F–H**). Occasionally, after HEV infection, mild distended cisternal space of the rough endoplasmic reticulum was presented in neuron

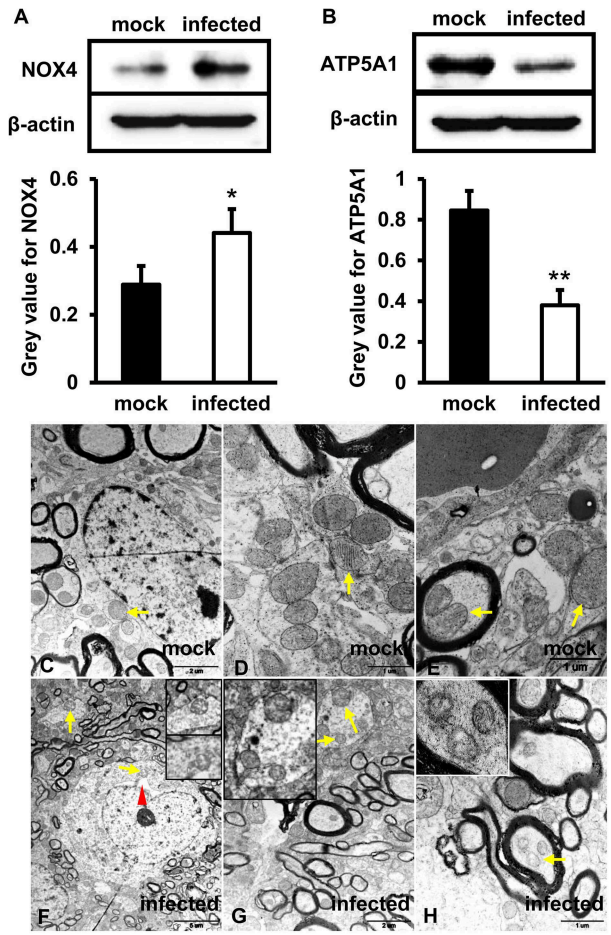

FIGURE 1 | Mitochondrial dysfunction was related to an increased level of NOX4 and decreased expression of ATP5A1 in HEV infected brain tissues. **(A,B)** *in vitro*, HBMVECs were inoculated with 300 MOI HEV for 48 h for western blot, and HEV-negative homogenate served as control. Data showed that expression of NOX4 in HBMVECs treated with HEV for 48 h was significantly increased compared with mock group ($^{*}p < 0.05$). Meanwhile, ATP5A1 was detected significantly attenuated in HEV inoculated cells ($^{**}p < 0.01$). **(C-H)** *In vivo*, brain and spinal cord tissues that detected for HEV-RNA positive were selected for ultrastructural study. **(C–E)** Mitochondria were observed with clear cristae folded by the inner membrane in brain tissue of mock group. **(F–H)** Mitochondria with loss of cristae were found in tissues of HEV infected animals (arrows). The rough endoplasmic reticulum of neuron cells was also observed with mild distended cisternal space in HEV infected tissues (arrowhead). For western blot, gray value was analyzed with ImageJ to quantitatively analyze the expression levels of targeted proteins according to the level of exposure gray (resolution). Data were finally normalized to the expression of anti-β-actin.

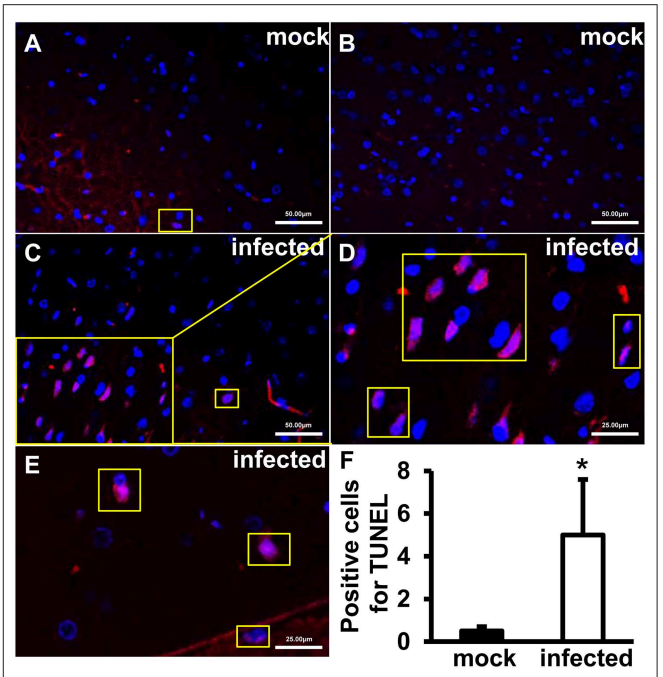

FIGURE 2 | TUNEL-positive cells increased after HEV infection. TUNEL staining of the HEV-RNA positive brain tissues collected on 14, 21, and 28 dpi was performed using *in situ* BrdU-Red DNA Fragmentation (TUNEL) Assay Kit and slides were counterstained with DAPI (Blue). TUNEL-positive signals merged with DAPI were shown as purple. **(A,B)** Few positive signals were detected in animals of mock group. **(C–E)** Positive signals were exhibited in infected brain sections. The high magnification images **(D,E)** depicted granular masses of positive signals at nucleus of the apoptotic cells. **(F)** TUNEL-positive cells were significantly increased in HEV-infected gerbil brain tissues ($^{*}p < 0.05$).

cells (**Figure 1F**). In normal brain tissue, mitochondria with intact membrane and visible cristae were showed (**Figures 1C–E**).

Increased TUNEL-Positive Signals Were Detected in HEV Infected Gerbils Brain Tissue

To explore roles of HEV infection on cell apoptosis, apoptotic cells were detected using TUNEL Assay Kit. The positive signals were mainly located in nucleus of cells in the brain. Few positive cells were detected in uninfected tissues (**Figures 2A,B**). More positive signals were observed in infected animals and high magnification images depicted granular masses of positive signals at nucleus of the apoptotic cells (**Figures 2C–E**). Further analysis showed that the apoptotic cells were significantly increased in HEV-infected brain tissues compared with uninfected animals ($p < 0.05$) (**Figure 2F**).

Bax and Bcl-2 Expression Levels Increased in HEV Infected Gerbils Brain Tissue

To test whether mitochondria-mediated apoptosis was activated by HEV challenge in brain tissues, Bax and Bcl-2 were detected. IHC study showed that positive signal of Bax protein in the brain tissue of HEV infected gerbils was mainly distributed in neurons and a small number of glial cells, and significantly upregulated following HEV infection (**Figure 3B**), compared with mock group (**Figure 3A**) ($p < 0.05$). Bcl-2 was expressed in few neurons in both HEV infected gerbils and uninfected animals, and expression level was not significantly changed (**Figures 3C,D**). Western blot also showed that expression of Bcl-2 was not significantly induced after HEV infection, while Bax

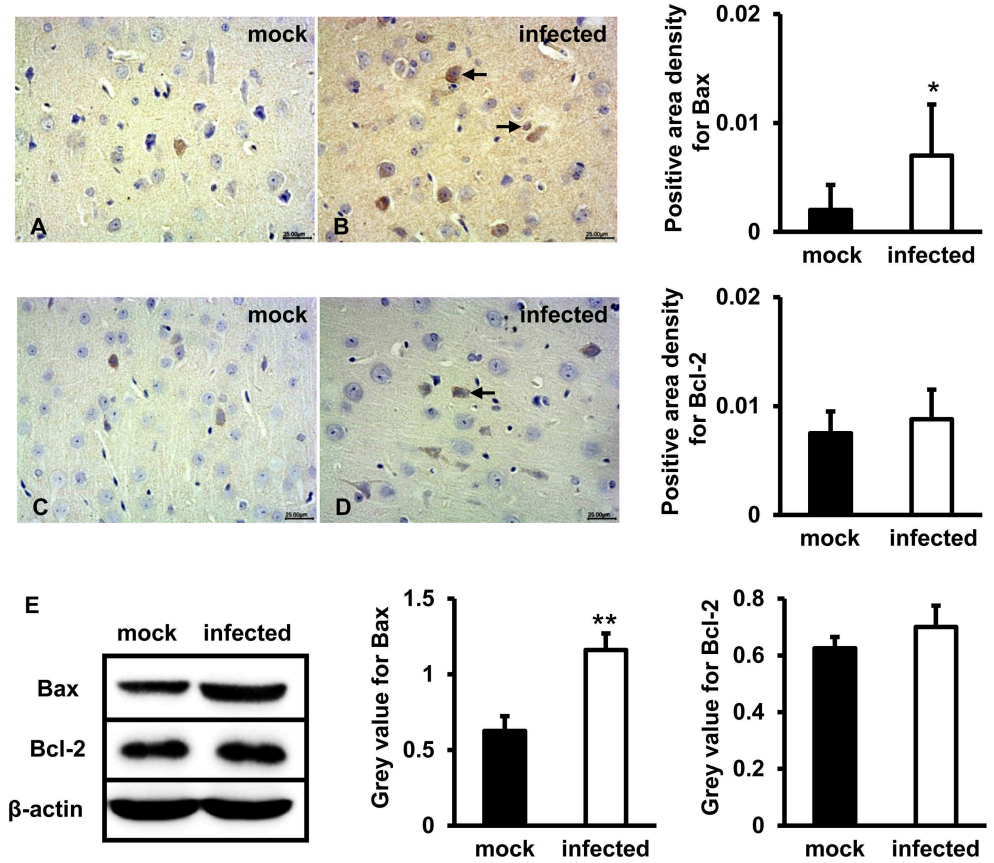

FIGURE 3 | Pro-apoptotic protein Bax but not Bcl-2 was upregulated following HEV infection. **(A–D)** HEV-RNA positive brain tissues collected on 14, 21, and 28 dpi were used for the immunohistochemistry study of Bax (rabbit polyclonal IgG) and Bcl-2(rabbit polyclonal IgG). Goat anti-rabbit IgG was chosen as secondary antibody. The positive signal was measured via the Motic Med 6.0 CMIAS Image Analysis System. Data showed that Bax was mainly distributed in cytosol of neuron cells, vascular endothelial cells and few microglial cells of HEV infection tissues with increased amount compared with mock group (*$p < 0.05$). Bcl-2 was detected in few neurons and vascular endothelial cells in both groups. **(E)** For western blot, HBMVECs were inoculated with 300 MOI HEV for 48 h and HEV-negative homogenate served as control. Data showed that expression level of Bax was significantly higher in HBMVECs inoculated with HEV (**$p < 0.01$), but induction of Bcl-2 was not significant. For western blot, gray value was analyzed with ImageJ to quantitatively analyze the expression levels of targeted proteins according to the level of exposure gray (resolution). Data were finally normalized to the expression of anti-β-actin.

protein was significantly increased in HBMVECs infected with HEV ($p < 0.01$) (**Figure 3E**).

Caspase-9, Caspase-3, and PCNA Expression Levels Significantly Increased in HEV Infected Gerbils Brain Tissue

To further figure out whether caspase-9 and caspase-3 were involved in this process, protein location, and expression levels were examined by both IHC and western blot. IHC showed that positive signals of activated caspase-9 and caspase-3 were distributed in few neurons and vascular endothelial cells in brain tissue of mock animals (**Figures 4A,C**) and more positive cells were detected in HEV infected tissue (**Figures 4B,D**). Western blot showed that high levels of activated caspase-9 and caspase-3 in HBMVECs infected with HEV ($p < 0.01$) (**Figures 4E,F**). In HEV infected animal brain tissues, PCNA positive cells were mainly distributed in glial cells and vascular endothelial cells and were significantly increased ($p < 0.01$) compared with normal brain tissues (**Figures 4G,H**).

SP and VIP Expression Induced in HEV Infected Gerbils Brain Tissue

To detect immunoregulatory response to HEV infection in brain tissues, SP and VIP were examined by IHC. The results showed that a positive signal of SP was distributed in the cytoplasm of some large oval and conical neurons of the gray matter of the brain in both uninfected and infected animals (**Figures 5A,B**). Expression of VIP was observed in vascular endothelial cells, astrocytes, and oligodendrocytes in white matter of the brain tissue in both groups (**Figures 5C,D**). Quantitative analysis of positive areas density of SP and VIP showed that expression levels of both proteins were significantly increased in HEV infected animals ($p < 0.01$, $p < 0.05$) (**Figure 5**).

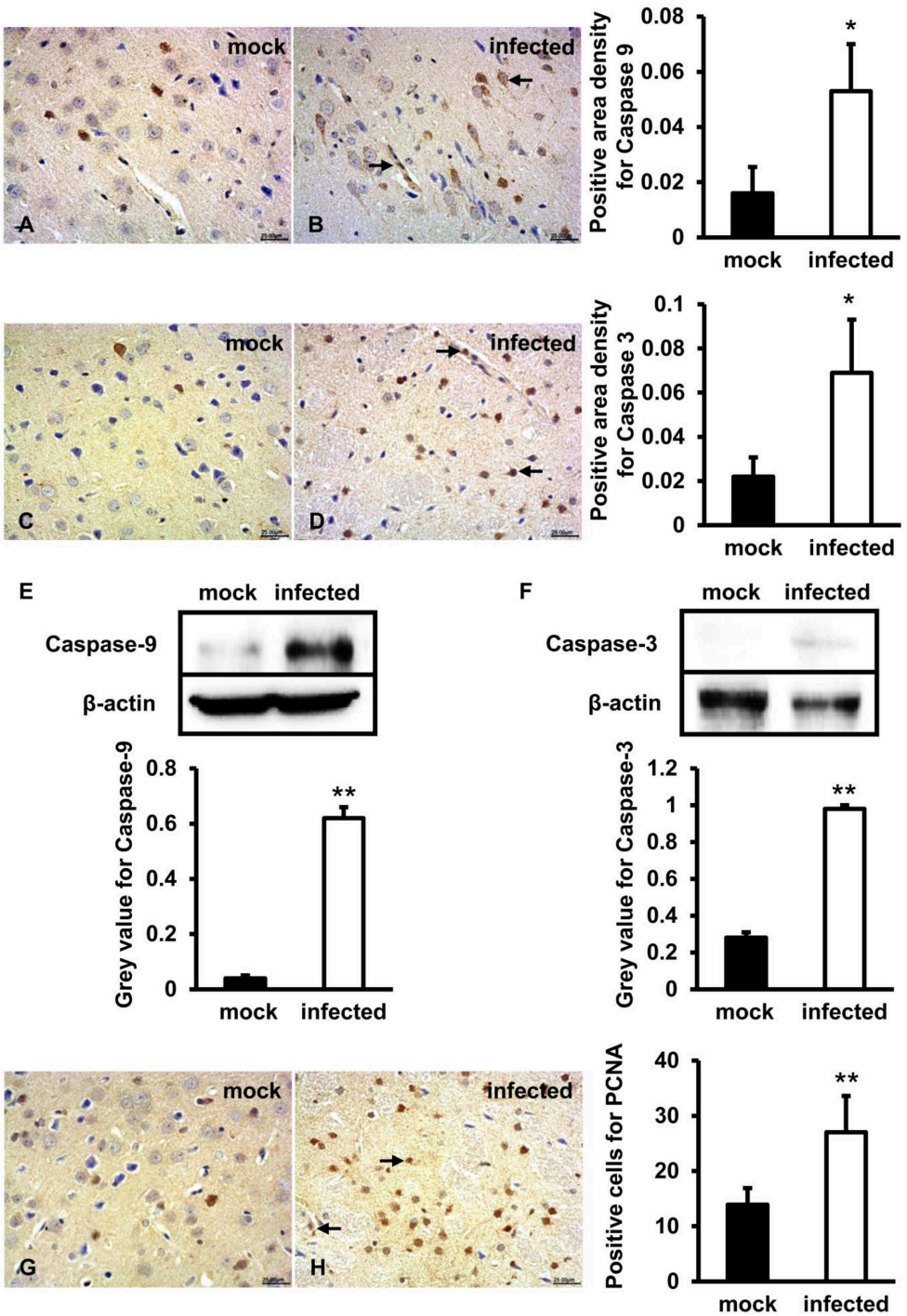

FIGURE 4 | Mitochondrial apoptotic signaling was activated during HEV infection. HEV-RNA positive brain tissues collected on 14, 21, and 28 dpi were used for the immunohistochemistry study of caspase-9 (rabbit polyclonal IgG), caspase-3 (rabbit polyclonal IgG) and PCNA (rabbit polyclonal IgG). Goat anti-rabbit IgG was chosen as secondary antibody. The positive signal was measured via the Motic Med 6.0 CMIAS Image Analysis System. **(A–D)** Immunohistochemistry study showed that expression levels of activated caspase-9 and caspase-3 were expressed in neuronal cells and vascular endothelial cells of the brain tissue, with higher amount in HEV infected animals compared with mock animals (*$p < 0.05$). **(E,F)** For western blot, HBMVECs were inoculated with 300 MOI HEV for 48 h and HEV-negative homogenate served as control. Data showed that expression levels of cleaved caspase-9 and caspase-3 were significantly increased in HBMVECs infected with HEV compared with mock group (**$p < 0.01$). **(G,H)** Positive signal of PCNA was detected in glial cells and vascular endothelial cells, with significantly higher level in HEV infected brain sections compared with mock group (**$p < 0.01$). For western blot, gray value was analyzed with ImageJ to quantitatively analyze the expression levels of targeted proteins according to the level of exposure gray (resolution). Data were finally normalized to the expression of anti-β-actin.

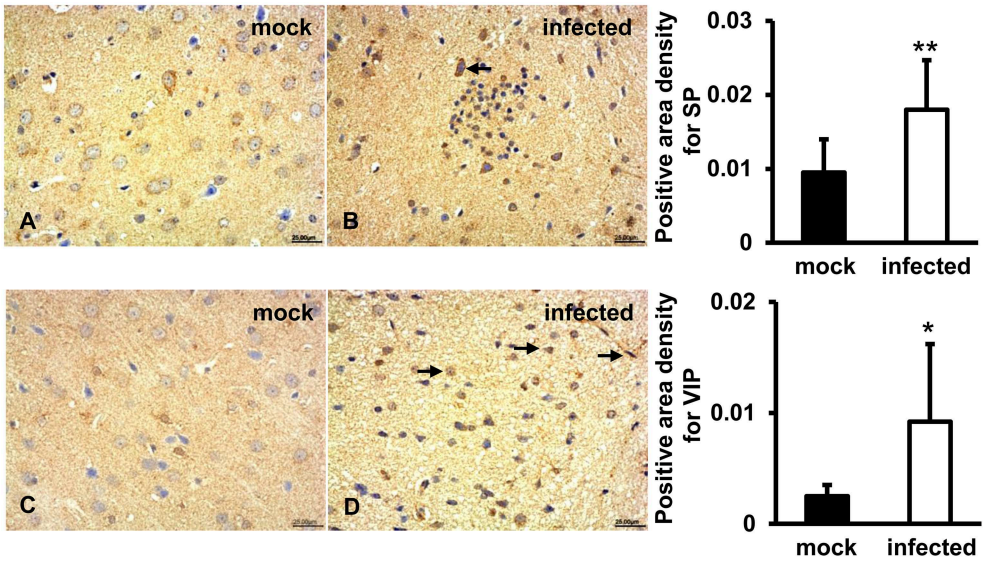

FIGURE 5 | Immunoregulation of the brain tissue during HEV infection. HEV-RNA positive brain tissues collected on 14, 21, and 28 dpi were used for immunohistochemistry study of SP (rabbit polyclonal IgG) and VIP (rabbit polyclonal IgG). Goat anti-rabbit IgG was chosen as secondary antibody. The positive signal was measured via the Motic Med 6.0 CMIAS Image Analysis System. **(A,B)** A positive signal of SP was found in the cytoplasm of neuronal cells of brain tissue in both groups and was significantly induced in HEV infected animals compared with animals from mock group (**$p < 0.01$). **(C,D)** Expression of VIP was observed in vascular endothelial cells, astrocytes and oligodendrocytes in both groups, with significantly increased levels in HEV infected tissues compared with tissues from mock group (*$p < 0.05$).

TNFα, IL-1β, IBA1 Expression Levels Induced in HEV Infected Gerbil Brain Tissues

In order to evaluate the activation of microglial cells and associated inflammatory response, TNFα, IL-1β, and IBA1 were detected by IHC. The results showed that a positive signal of TNFα was observed in few microglia and astrocytes in gerbil brain of the mock group (**Figure 6A**). In HEV infected animals, TNFα was diffusely distributed in a large number of microglia and astrocytes, as well as a few pyramidal neurons (**Figure 6B**). Expression of secretory IL-1β protein was detected in microglia, astrocytes and few neuronal cytoplasms in gerbil brain of the mock group (**Figure 6C**), while in HEV infected gerbils it was diffusely distributed in a large amount of microglia, astrocytes and neuron cells (**Figure 6D**). A positive signal of IBA1 was observed in microglial cells in brain tissue of both groups (**Figures 6E,F**). Quantitative analysis of positive areas density or number of positive cells of TNFα, IL1β, and IBA1 showed that expression levels of all proteins were significantly increased in HEV infected animals ($p < 0.01$) (**Figure 6**).

DISCUSSION

Our previous study showed that HEV infection could cause mitochondria damages, especially in the endothelial cells of the brain tissue. Moreover, HEV infection in the brain tissues disrupted the blood-brain barrier (BBB), especially the tight junction protein expression in endothelial cells (Shi et al., 2016; Tian et al., 2019). In the present study, primary human brain microvascular endothelial cells (HBMVCs) were chosen to further investigate the roles of mitochondria-mediated apoptotic signaling during HEV infection.

Mitochondria play a pivotal role in cellular energy-generating processes and are sensitive to cellular stress, which might further initiate programmed cell death. Both NOX4 and ATP5A1 are critical factors involved in mitochondria function and alteration of their expression levels reflected changes of mitochondria function. It has been documented that a large number of reactive oxygen species (ROS) produced by overexpression of NOX4, leading to oxidative stress in brain tissue, with further increasing the permeability of BBB and inducing neuronal apoptosis (Bedard and Krause, 2007). In our experiment, the expression of NOX4 in HBMVCs inoculated with HEV was higher than that in mock groups by western-blot assay, indicating that HEV infection up-regulated the expression of NOX4 in HBMVCs, which might lead to ROS accumulation in cells and increasing tendency to apoptosis. The study has shown that mutation of ATP5A1 gene led to fatal mitochondrial encephalopathy in newborns, which proved the importance of ATP5A1 in mitochondrial maintenance (Jonckheere et al., 2013). Our experiment demonstrated that the expression of ATP5A1 in HBMVCs infected with HEV was lower than that in the mock group by immunoblotting, indicating that HEV infection may induce mitochondrial damage and trigger ATP synthase dysfunction.

Apoptosis, a physiological process of cell death, is a form of programmed cell death (PCD) that occurs in cells during every minute of life. It can be induced through the activation

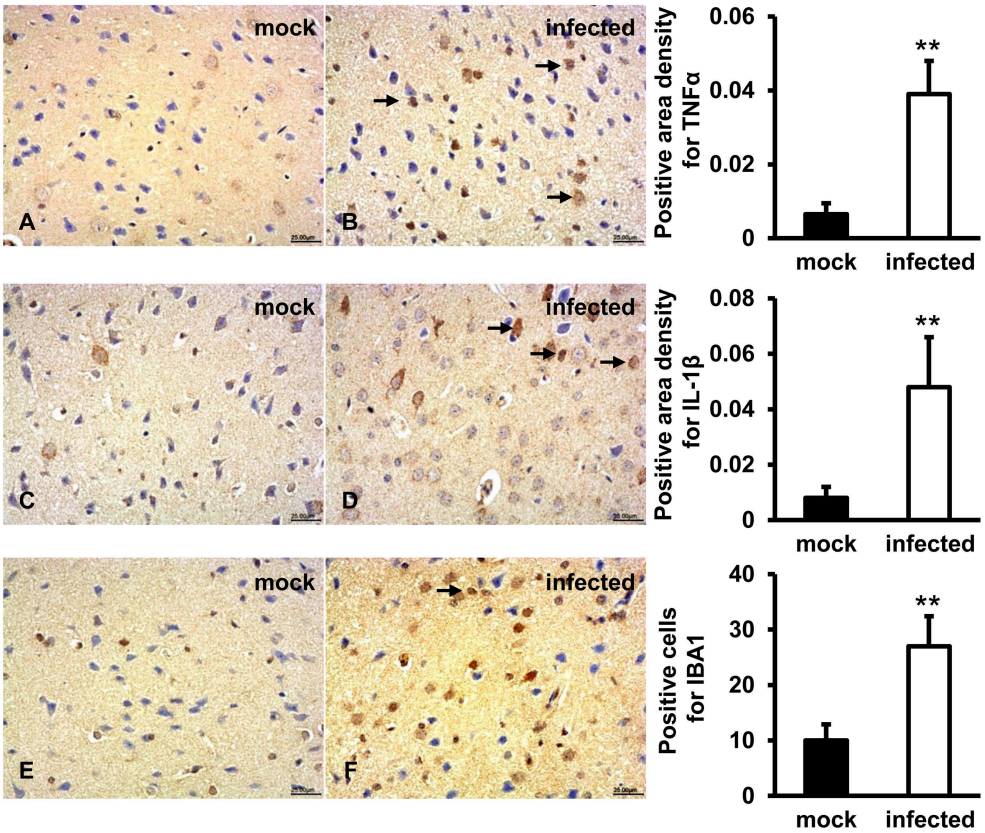

FIGURE 6 | Increased pro-inflammatory responses were examined in HEV infected animal brain tissues. HEV-RNA positive brain tissues collected on 14, 21, and 28 dpi were used for immunohistochemistry study of TNFα (rabbit polyclonal IgG), IL-1β (rabbit polyclonal IgG), and IBA1 (rabbit polyclonal IgG). Goat anti-rabbit IgG was chosen as secondary antibody. The positive signal was measured via the Motic Med 6.0 CMIAS Image Analysis System. **(A,B)** Positive signal of TNFα was diffusely observed in a large number of microglial cells, astrocytes and few pyramidal neurons in HEV infected animal brain tissues, and expression level was significantly induced compared with mock group (**$p < 0.01$). **(C,D)** The expression level of activated IL-1β was found in microglia, astrocytes, and few neuronal cytoplasms and was significantly increased in HEV infected brain sections compared with tissues from mock group (**$p < 0.01$). **(E,F)** Positive expression of IBA1 was detected in microglial cells with significantly elevated levels in brain tissues infected with HEV compared with mock group (**$p < 0.01$).

of the death receptor or the mitochondrial apoptotic pathways. Mitochondria mediated apoptosis, also known as the intrinsic apoptotic pathway, is thought to be the central intracellular pathway involved in the majority of apoptosis in mammalian cells (Khosravi-Far and Esposti, 2004). TUNEL assay was known to detect apoptotic cells undergoing extensive DNA degradation (Kyrylkova et al., 2012). The morphology changes of mitochondria are critically important in apoptosis (Burke, 2017). Many death signals converge on mitochondria to activate Bak and Bax, which results in the permeabilization of the outer mitochondrial membrane and the release of pro-apoptotic factors into the cytosol and further activates caspase-9 and the apoptotic effector caspases (Alirol and Martinou, 2006; Lopez and Tait, 2015). The steady state of pro-survival Bcl-2 members could also be destroyed after the activation of Bak and Bax (McArthur et al., 2018). The previous study has shown that HEV infection led to mitochondria-mediated apoptosis of hepatocytes, such as induction of Bax, Bcl-2, caspase-9, and caspase-3 (Yang et al., 2018). In our study, increased TUNEL-positive signals were observed in infected brain tissues. Further study showed that mitochondria-mediated apoptosis was induced by HEV infection in brain tissues, including induction of pro-apoptotic protein Bax and cleaved caspase-9 and caspase-3. But expression of Bcl-2 was not significantly changed in brain tissues infected with HEV. It might be a possible reason that BBB acts effectively to protect the brain from HEV infection, while hepatic blood flow directly comes from other organs. In this condition, hepatocytes are exposed to HEV that trigger hepatocytes injury. Additionally, we observed overexpression of PCNA in brain tissue of infected HEV gerbils. It is known that neuronal cells have a high degree of differentiation and weak proliferative capacity and overexpression of PCNA in cells with weak proliferative capacity is a manifestation of DNA repair process, indicating that PCNA expression in HEV-infected brain tissues may be involved in DNA repair in responding to apoptosis. Together, HEV infection caused mitochondrial dysfunction and activation of mitochondrial apoptotic pathway. Previously, it has been reported that apoptosis involved in neuronal cell death in many of the neurological disorders, such as Alzheimer's disease

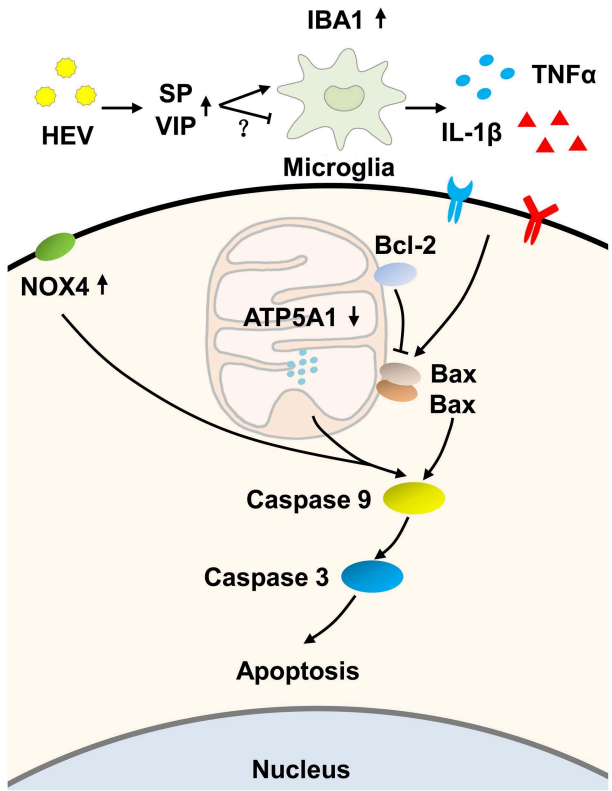

FIGURE 7 | Hypothesized pathway of mitochondrial apoptosis activation induced by HEV infection. HEV entry to the brain tissue promoted the release of Substance P (SP) to activate microglial cells, while increased production of vasoactive intestinal peptide (VIP) negatively regulated activation of microglial cells as a compensatory response. Activated microglial cells produced more inflammatory cytokines such as TNFα and IL-1β. The release of TNFα and IL-1β further initiated mitochondrial apoptotic pathway. During the process, pro-apoptotic protein Bax induced ruptures of the outer membranes altered mitochondrial membrane permeability and further induced activation of caspase-9. Up-regulated expression of NOX4 and down-regulated expression of ATP5A1 also contributed to activation of caspase-9 and caspase-3 cascade and ultimately induced mitochondria-mediated apoptosis, which might be a potential way to eliminate virus but on the other hand caused neurological disorders.

and Parkinson's disease (Honig and Rosenberg, 2000). In our study, mitochondrial apoptosis might contribute to HEV induced brain injury, which might be correlated with HEV induced neurological disorders.

It has been reported that expression of substance P (SP) and vasoactive intestinal peptide (VIP) was associated with tissue injury or tissue repair, especially in inflammatory responses (Delgado et al., 2001; O'Connor et al., 2004). SP is widely distributed in the nervous system where it exerts its biological and immunological activity via high-affinity neurokinin 1 receptor (Suvas, 2017). It was shown that increased levels of SP were detected in the serum of HIV infected patients and simian immunodeficiency virus-infected rhesus macaques, and viral levels were correlated with the amount of SP released by immune cells (Johnson et al., 2016). VIP was reported to have protective effects on the focal ischemia of the brain and be a potential therapeutics for experimental autoimmune encephalomyelitis (EAE) (Deng and Jin, 2017). In our study, both induced high levels of SP and VIP were observed in HEV inoculated animals, revealing the critical immunoregulatory function of SP and VIP in HEV induced brain injury.

It has been documented that mitochondrial dysfunctions can result from abnormalities in immuno-inflammatory pathways involving elevated pro-inflammatory cytokines (Morris and Maes, 2014). TNFα was considered to play a role in hepatocytes apoptosis and liver injury and further triggered Bax activation and cleavage of caspase-9 and caspase-3 in acute liver failure (ALF) (Xu et al., 2018). Maturation of IL-1β facilitated a decrease of mitochondrial oxygen consumption, loss of mitochondrial membrane potential, depletion of ATP synthesis (Morris and Maes, 2014). Additionally, TNFα and IL-1β were reported to disturb mitochondrial function in human chondrocytes by inducing mitochondrial DNA damage, decreasing energy production and mitochondrial transcription, which correlated with the induction of apoptosis (Kim et al., 2010). In our study, increased levels of TNFα and IL-1β were detected in HEV infected brain tissues. In responding to internal or external stimuli, TNFα and IL-1β could be produced by microglia of the central nervous system. The previous study has shown that Japanese encephalitis virus infection of the central nervous tissue caused the proliferation of microglia and astrocytes, which further triggered neuroinflammatory responses (Chen et al., 2011). This work also showed that expression level of ionized calcium-binding adapter molecule 1 (IBA1), which was an activated microglial marker, was significantly increased in HEV infected animal brain sections. Combined with our previous data (Shi et al., 2016), the present results indicated that induction of the pro-inflammatory cytokines might result from proliferation of microglial cells in infected gerbils and activation and proliferation of microglial cells further contribute to damage of brain tissue in infected gerbils.

In conclusion, we hypothesized that HEV infection activated the mitochondrial apoptosis of the brain tissue, according to our examination including increased TUNEL-positive signals and expression levels of Bax, cleaved caspase-9 and caspase-3. The up-regulation of PCNA might be a compensatory response to repair injured tissue. Furthermore, an increased amount of pro-inflammatory cytokines was supposed to correlate with the induction of mitochondrial apoptosis during HEV infection (**Figure 7**). These data present perspectives on pathogenesis of HEV induced injury of the central nervous system. More attention must be paid to the intensive study of inflammatory injury and mechanisms controlling apoptosis during HEV infection.

DATA AVAILABILITY STATEMENT

All datasets generated for this study are included in the article/supplementary material.

ETHICS STATEMENT

The animal study was reviewed and approved by Animal Care and Use Committee of China Agricultural University.

AUTHOR CONTRIBUTIONS

JT, RShi, and RShe performed the study concept and design. RShi, PX, TL, QW, and JA performed the laboratory work and data analysis. WH and MS performed the analysis and interpretation of data. JT and RShi wrote the paper. All of the authors read and approved the final article.

FUNDING

This study was supported by the National Natural Science Foundation of China (Grant nos. 31472165, 31802162, 31272515) and Innovative Project of Young Teachers of China Agricultural University (Grant nos. 2018QC015 and 2019TC004).

ACKNOWLEDGMENTS

We would like to thank Dr. Heng Li and all colleagues from our lab for their critical comments on this paper. Dr. Heng Li and Jie Qiao provided valuable suggestions during the language editing.

REFERENCES

Alirol, E., and Martinou, J. C. (2006). Mitochondria and cancer: is there a morphological connection? *Oncogene* 25, 4706–4716. doi: 10.1038/sj.onc.1209600

Bedard, K., and Krause, K. H. (2007). The NOX family of ROS-generating NADPH oxidases: physiology and pathophysiology. *Physiol. Rev.* 87, 245–313. doi: 10.1152/physrev.00044.2005

Bose, A., and Beal, M. F. (2016). Mitochondrial dysfunction in parkinson's disease. *J. Neurochem.* 139 (Suppl. 1), 216–231. doi: 10.1111/jnc.13731

Burke, P. J. (2017). Mitochondria, bioenergetics and apoptosis in cancer. *Trends Cancer* 3, 857–870. doi: 10.1016/j.trecan.2017.10.006

Chen, C. J., Ou, Y. C., Chang, C. Y., Pan, H. C., Liao, S. L., Raung, S. L., et al. (2011). TNF-alpha and IL-1beta mediate Japanese encephalitis virus-induced RANTES gene expression in astrocytes. *Neurochem. Int.* 58, 234–242. doi: 10.1016/j.neuint.2010.12.009

Delgado, M., Abad, C., Martinez, C., Leceta, J., and Gomariz, R. P. (2001). Vasoactive intestinal peptide prevents experimental arthritis by downregulating both autoimmune and inflammatory components of the disease. *Nat. Med.* 7, 563–568. doi: 10.1038/87887

Deng, G., and Jin, L. (2017). The effects of vasoactive intestinal peptide in neurodegenerative disorders. *Neurol. Res.* 39, 65–72. doi: 10.1080/01616412.2016.1250458

Ding, Y., Zou, J., Li, Z., Tian, J., Abdelalim, S., Du, F., et al. (2011). Study of histopathological and molecular changes of rat kidney under simulated weightlessness and resistance training protective effect. *PLoS ONE* 6:e20008. doi: 10.1371/journal.pone.0020008

Honig, L. S., and Rosenberg, R. N. (2000). Apoptosis and neurologic disease. *Am. J. Med.* 108, 317–330. doi: 10.1016/s0002-9343(00)00291-6

Johnson, M. B., Young, A. D., and Marriott, I. (2016). The therapeutic potential of targeting substance P/NK-1R interactions in inflammatory CNS disorders. *Front. Cell. Neurosci.* 10:296. doi: 10.3389/fncel.2016.00296

Jonckheere, A. I., Renkema, G. H., Bras, M., van den Heuvel, L. P., Hoischen, A., Gilissen, C., et al. (2013). A complex V ATP5A1 defect causes fatal neonatal mitochondrial encephalopathy. *Brain* 136, 1544–1554. doi: 10.1093/brain/awt086

Kamar, N., Izopet, J., Pavio, N., Aggarwal, R., Labrique, A., Wedemeyer, H., et al. (2017). Hepatitis E virus infection. *Nat. Rev. Dis. Primers* 3:17086. doi: 10.1038/nrdp.2017.86

Keck, F., Khan, D., Roberts, B., Agrawal, N., Bhalla, N., and Narayanan, A. (2018). Mitochondrial-directed antioxidant reduces microglial-induced inflammation in murine *in vitro* model of TC-83 infection. *Viruses* 10:606. doi: 10.3390/v10110606

Kenney, S. P., and Meng, X. J. (2019). Hepatitis E virus: animal models and zoonosis. *Annu. Rev. Anim. Biosci.* 7, 427–448. doi: 10.1146/annurev-animal-020518-115117

Khosravi-Far, R., and Esposti, M. D. (2004). Death receptor signals to mitochondria. *Cancer Biol. Ther.* 3, 1051–1057. doi: 10.4161/cbt.3.11.1173

Kim, J., Xu, M., Xo, R., Mates, A., Wilson, G. L., Pearsall, A. W., et al. (2010). Mitochondrial DNA damage is involved in apoptosis caused by pro-inflammatory cytokines in human OA chondrocytes. *Osteoarthr. Cartil.* 18, 424–432. doi: 10.1016/j.joca.2009.09.008

Kyrylkova, K., Kyryachenko, S., Leid, M., and Kioussi, C. (2012). Detection of apoptosis by TUNEL assay. *Methods Mol. Biol.* 887, 41–47. doi: 10.1007/978-1-61779-860-3_5

Lin, C. H., Shih, W. L., Lin, F. L., Hsieh, Y. C., Kuo, Y. R., Liao, M. H., et al. (2009). Bovine ephemeral fever virus-induced apoptosis requires virus gene expression and activation of fas and mitochondrial signaling pathway. *Apoptosis* 14, 864–877. doi: 10.1007/s10495-009-0371-5

Lopez, J., and Tait, S. W. (2015). Mitochondrial apoptosis: killing cancer using the enemy within. *Br. J. Cancer* 112, 957–962. doi: 10.1038/bjc.2015.85

McArthur, K., Whitehead, L. W., Heddleston, J. M., Li, L., Padman, B. S., Oorschot, V., et al. (2018). BAK/BAX macropores facilitate mitochondrial herniation and mtDNA efflux during apoptosis. *Science* 359:eaao6047. doi: 10.1126/science.aao6047

Montpellier, C., Wychowski, C., Sayed, I. M., Meunier, J. C., Saliou, J. M., Ankavay, M., et al. (2018). Hepatitis E virus lifecycle and identification of 3 forms of the ORF2 capsid protein. *Gastroenterology* 154, 211–223. e218. doi: 10.1053/j.gastro.2017.09.020

Morris, G., and Maes, M. (2014). Mitochondrial dysfunctions in myalgic encephalomyelitis/chronic fatigue syndrome explained by activated immuno-inflammatory, oxidative and nitrosative stress pathways. *Metab. Brain Dis.* 29, 19–36. doi: 10.1007/s11011-013-9435-x

O'Connor, T. M., O'Connell, J., O'Brien, D. I., Goode, T., Bredin, C. P., and Shanahan, F. (2004). The role of substance P in inflammatory disease. *J. Cell. Physiol.* 201, 167–180. doi: 10.1002/jcp.20061

Pischke, S., Hartl, J., Pas, S. D., Lohse, A. W., Jacobs, B. C., and Van der Eijk, A. A. (2017). Hepatitis E virus: infection beyond the liver? *J. Hepatol.* 66, 1082–1095. doi: 10.1016/j.jhep.2016.11.016

Renou, C., Gobert, V., Locher, C., Moumen, A., Timbely, O., Savary, J., et al. (2014). Prospective study of hepatitis E virus infection among pregnant women in France. *Virol. J.* 11:68. doi: 10.1186/1743-422X-11-68

Shi, R., Soomro, M. H., She, R., Yang, Y., Wang, T., Wu, Q., et al. (2016). Evidence of hepatitis E virus breaking through the blood-brain barrier and replicating in the central nervous system. *J. Viral Hepat.* 23, 930–939. doi: 10.1111/jvh.12557

Soomro, M. H., Shi, R., She, R., Yang, Y., Wang, T., Wu, Q., et al. (2017). Molecular and structural changes related to hepatitis E virus antigen and its expression in testis inducing apoptosis in Mongolian gerbil model. *J. Viral Hepat.* 24, 696–707. doi: 10.1111/jvh.12690

Suvas, S. (2017). Role of substance P neuropeptide in inflammation, wound healing, and tissue homeostasis. *J. Immunol.* 199, 1543–1552. doi: 10.4049/jimmunol.1601751

Tian, J., Shi, R., Liu, T., She, R., Wu, Q., An, J., et al. (2019). Brain infection by hepatitis E virus probably via damage of the blood-brain barrier due to alterations of tight junction proteins. *Front. Cell. Infect. Microbiol.* 9:52. doi: 10.3389/fcimb.2019.00052

Wang, L., Teng, J. L. L., Lau, S. K. P., Sridhar, S., Fu, H., Gong, W., et al. (2019). Transmission of a novel genotype of hepatitis E virus from bactrian camels to cynomolgus macaques. *J. Virol.* 93, e02014–e02018. doi: 10.1128/JVI.02014-18

Xu, L., Zheng, X., Wang, Y., Fan, Q., Zhang, M., Li, R., et al. (2018). Berberine protects acute liver failure in mice through inhibiting inflammation and mitochondria-dependent apoptosis. *Eur. J. Pharmacol.* 819, 161–168. doi: 10.1016/j.ejphar.2017.11.013

Yang, Y., Shi, R., She, R., Soomro, M. H., Mao, J., Du, F., et al. (2015). Effect of swine hepatitis E virus on the livers of experimentally infected Mongolian gerbils by swine hepatitis E virus. *Virus Res.* 208, 171–179. doi: 10.1016/j.virusres.2015.06.007

Yang, Y., Shi, R., Soomro, M. H., Hu, F., Du, F., and She, R. (2018). Hepatitis E virus induces hepatocyte apoptosis via mitochondrial pathway in Mongolian gerbils. *Front. Microbiol.* 9:460. doi: 10.3389/fmicb.2018.00460

Conflict of Interest: The authors declare that the research was conducted in the absence of any commercial or financial relationships that could be construed as a potential conflict of interest.

frontiers in Cellular and Infection Microbiology

ORIGINAL RESEARCH
published: 23 January 2020
doi: 10.3389/fcimb.2019.00478

Hepatitis E Virus Cysteine Protease Has Papain Like Properties Validated by *in silico* Modeling and Cell-Free Inhibition Assays

*Shweta Saraswat, Meenakshi Chaudhary and Deepak Sehgal**

Virology Lab, Department of Life Sciences, Shiv Nadar University, Greater Noida, India

OPEN ACCESS

Edited by:
Milan Surjit, Translational Health Science and Technology Institute (THSTI), India

Reviewed by:
Khalid Parvez, King Saud University, Saudi Arabia
Zhuoming Liu, Harvard Medical School, United States
Baibaswata Nayak, All India Institute of Medical Sciences, India

***Correspondence:**
Deepak Sehgal
deepak.sehgal@snu.edu.in

Specialty section:
This article was submitted to Virus and Host, a section of the journal Frontiers in Cellular and Infection Microbiology

Received: *30 September 2019*
Accepted: *27 December 2019*
Published: *23 January 2020*

Citation:
Saraswat S, Chaudhary M and Sehgal D (2020) Hepatitis E Virus Cysteine Protease Has Papain Like Properties Validated by in silico Modeling and Cell-Free Inhibition Assays. Front. Cell. Infect. Microbiol. 9:478. doi: 10.3389/fcimb.2019.00478

Hepatitis E virus (HEV) has emerged as a global health concern during the last decade. In spite of a high mortality rate in pregnant women with fulminant hepatitis, no antiviral drugs or licensed vaccine is available in India. HEV-protease is a pivotal enzyme responsible for ORF1 polyprotein processing leading to cleavage of the non-structural enzymes involved in virus replication. HEV-protease region encoding 432–592 amino acids of Genotype-1 was amplified, expressed in Sf21 cells and purified in its native form. The recombinant enzyme was biochemically characterized using SDS-PAGE, Western blotting and Immunofluorescence. The enzyme activity and the inhibition studies were conducted using Zymography, FTC-casein based protease assay and ORF1 polyprotein digestion. To conduct ORF1 digestion assay, the polyprotein, natural substrate of HEV-protease, was expressed in *E. coli* and purified. Cleavage of 186 kDa ORF1 polyprotein by the recombinant HEV-protease lead to appearance of non-structural proteins viz. Methyltransferase, Protease, Helicase and RNA dependent RNA polymerase which were confirmed through immunoblotting using antibodies generated against specific epitopes of the enzymes. FTC-casein substrate was used for kinetic studies to determine Km and Vmax of the enzyme and also the effect of different metal ions and other protease inhibitors. A 95% inhibition was observed with E-64 which was validated through *in silico* analysis. The correlation coefficient between inhibition and docking score of Inhibitors was found to have a significant value of $r^2 = 0.75$. The predicted 3D model showed two domain architecture structures similar to Papain like cysteine protease though they differed in arrangements of alpha helices and beta sheets. Hence, we propose that HEV-protease has characteristics of "Papain-like cysteine protease," as determined through structural homology, active site residues and class-specific inhibition. However, conclusive nature of the enzyme remains to be established.

Keywords: HEV-protease, papain like enzyme, baculovirus expression system, *in silico* modeling, biochemical characterization

INTRODUCTION

Hepatitis E virus (HEV) is one of the most important viruses responsible for water born epidemics (Kamar et al., 2014). It is primarily transmitted through the faeco-oral contaminated drinking water. HEV was discovered in 1983 in an outbreak of unexplained hepatitis in Soviet soldiers in Afghanistan. Although, HEV is more prevalent in developing countries due to poor sanitation and water supplies (Cao and Meng, 2012) however, cases of HEV infection in industrialized countries like Europe, USA and Japan are becoming more common (Minuk et al., 2007; Bendall et al., 2008; Mushahwar, 2008). HEV causes self-limiting acute infection in approximately 20 million people annually, with a global mortality rate of 3% (Jameel, 1999; Nan and Zhang, 2016). This mortality rate remarkably increases up to 30% in the infected pregnant women in their third trimester due to fulminant liver failure (Navaneethan et al., 2008; Aggarwal and Naik, 2009). Infection with HEV represents an important global public health problem due to significant morbidity and mortality (Gupta and Agarwala, 2018). Currently a vaccine has been developed but licensed only in China, thus there is no vaccine or therapeutics available against HEV infection elsewhere. Also, there is no accepted treatment for HEV but the treatments of both interferon and/or ribavirin as a combinatorial therapy have been used successfully to treat chronic HEV infection (Kamar et al., 2014), though it has some side effects.

Genetically, HEV genome is a non-enveloped single-stranded positive sense RNA of ∼7.2 kb long and contains three partially overlapping open reading frames ORF1, ORF2, and ORF3 (Tam et al., 1991; Tsarev et al., 1992; Ahmad et al., 2011). HEV ORF3 translates into a small phospho-protein that modulates some of the host-regulatory functions including establishment of infection and virion egress (Graff et al., 2005; Chandra et al., 2008; Yamada et al., 2009). ORF2 forms a 660 amino acid (72 kDa) protein and its processed form constitutes the viral capsid. ORF1 is the largest ORF, 5,109 bases long and translated into 1,693 amino acids, which encode the non-structural polyprotein of ∼186 kDa, essential for viral replication (Ansari et al., 2000). Computational analysis of ORF1 has identified seven putative domains (Koonin et al., 1992). These include an active methyltransferase domain (Met), Y domain (Y) (Parvez, 2017), papain-like cysteine protease (PCP) (Parvez, 2013; Paliwal et al., 2014), a proline -rich region that contains a hypervariable region (H), X -domain (X), helicase (Hel), and an RNA dependent RNA polymerase (RdRP) From N- to C-terminal (Koonin et al., 1992; Parvez, 2017). Except PCP and Y domain, all other putative domains have been partially characterized and their functions have been predicted bioinformatically and some of them even experimentally (Agrawal et al., 2001; Magden et al., 2001; Karpe and Lole, 2010a,b). A recent report has identified an additional ORF4 in genotype-1 HEV, which is presumed to play an essential role in viral replication (Nair et al., 2016).

Various attempts have been made to study ORF1 processing and validate proteolytic activity of the PCP domain but not much success has been achieved. Expression of ORF1 in cell free system and the bacteria showed a 186 kDa polyprotein (Ansari et al., 2000) while the same construct, expressed using vaccinia virus showed two fragments of 107 kDa and 78 kDa in HepG2 cell (Ropp et al., 2000). In another study, transfection of infectious HEV RNA into HepG2 cells showed processed ORF1 fragments, of 35, 38, and 36 kDa using anti-MetT, anti-Hel and anti-RdRp antibodies, respectively (Panda et al., 2000). Similarly expression of ORF1 using baculovirus system showed processing of ORF1 as eight fragments that was inhibited by cell permeable cysteine protease inhibitor (E-64d) (Sehgal et al., 2006) but this could not be concluded whether the ORF1 processing was due to HEV-protease or an host-encoded protease. In recent report the role of host factor Xa and thrombin was postulated to initiate the HEV ORF1 processing but it still needs further validation (Kanade et al., 2018). Recently, mutation in conserved cysteine and histidine residues in the putative protease inhibits its proteolytic activity indicating its role in ORF1 processing and viral replication (Paliwal et al., 2014).

The HEV-protease has been reported to act as papain-like cysteine proteases with conserved catalytic dyad (Cys and His) (Koonin et al., 1992; Parvez and Khan, 2014), but it was also reported as a chymotrypsin like protease in another study (Paliwal et al., 2014).The main goal of our study has been to validate the nature of HEV-protease and established its role in the polyprotein processing. Since, other viral proteases have been identified as a potent antiviral target in literature (Lv et al., 2015) hence, HEV-prorease was thought to be a putative inhibitor for HEV replication. Therefore, we report the expression of a soluble, catalytically active recombinant HEV protease using baculovirus system. Further, we developed highly sensitive and reliable cell free assays to screen the cysteine protease activity. Also a 3D model of the HEV protease was generated to identify possible active sites and the residues responsible for binding of inhibitors. We considered the HEV-protease to be a Papain like cysteine protease. Collectively, this study significantly advances our understanding of the structure and function of HEV protease.

RESULT

Generation of Recombinant Baculovirus Containing HEV-Protease

A 482 bp segment encoding HEV-protease was amplified using pSK-HEV-2 clone as template by PCR (**Figure 1A**). The purified HEV-protease amplicon was cloned in pFastBac/CT-TOPO vector in frame with 6xHis at C-terminal, under polyhedrin (PH) promoter (**Figure 1B**). Screening of selected clones by PCR using gene specific primers confirmed integration of desired sequence (**Figure 1C**). Further, DNA sequencing confirmed the clone in correct reading frame with 100% similarity to the PCP sequences of the genotype-1 of HEV (**Supplementary Figure 1**, **Data Sheets 2**, **3**). Transformation of pFastBac-PCP in DH10Bac cells resulted in the formation of recombinant bacmid carrying HEV-protease sequence under the PH promoter and the recombination was confirmed through PCR (**Figure 1D**). Hence, a recombinant baculovirus containing the HEV-protease expression cassette was formed by transfecting

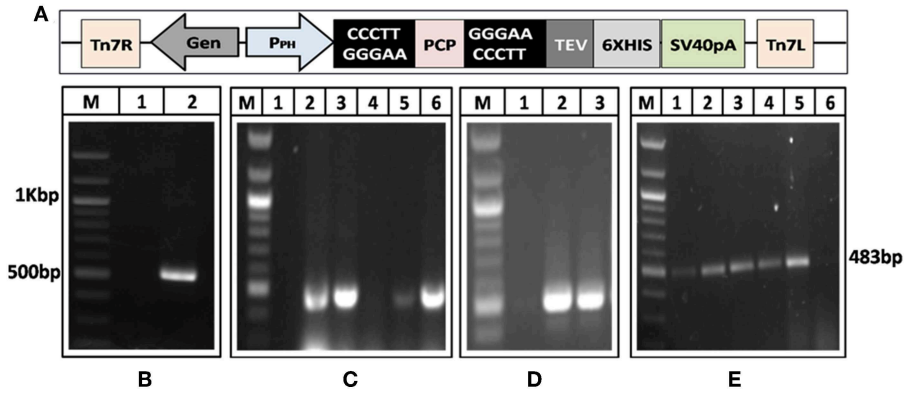

FIGURE 1 | Generation of recombinant baculovirus to express HEV-protease. **(A)** Amplification of HEV-protease gene from pSK-HEV2 plasmid; lane M, 100 bp DNA ladder, lane 1, negative control (non-template control); lane 2, PCR amplified HEV-protease fragment. **(B)** Vector map of recombinant pFastBac-PCP showing integration of PCP gene under PH promoter. **(C)** Colony PCR of DH5α transformants to identify clones having PfastBac-PCP construct; lane M, marker, lane 1 negative control, lane 2–5 amplification from different colonies obtained after transformation of PfastBac-PCP construct in DH5α cells, lane 6, Positive control (amplified product of pSK-HEV2 plasmid). **(D)** Analysis of recombinat bacmid DNA by PCR; lane M, marker, 1, negative control (amplification without template), lane 2, amplification from recombinant bacmid containing HEV-protease, lane 3, Positive control (amplified product of pSK-HEV2 plasmid), **(E)** Production of recombinant baculovirus in transfected Sf21 cells; lane M, marker, lane 1–4, amplification from recombinant baculovirus infected Sf21 cells. lane 5, Positive control (PCR amplification from pSK-HEV2 plasmid); lane 6, Amplification from uninfected Sf21 cells.

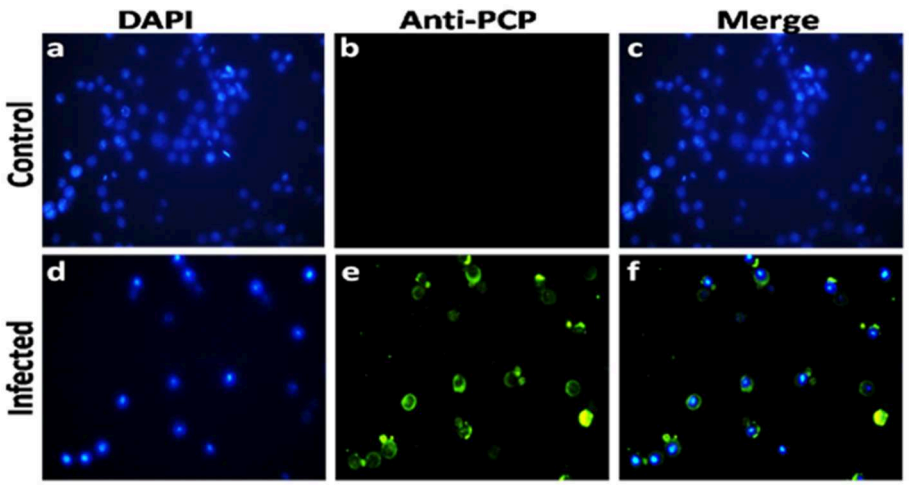

FIGURE 2 | Immunofluorescence analysis of HEV-protease expression in Sf-21 cells. **(a,d)** represent the DAPI-stained uninfected and infected sf21 cells; **(b,e)** represent immunoflorescence of uninfected and infected Sf21 cells after staining with HEV-protease epitope specific primary antibody and goat anti-rabbit IgG-Alexa Fluor 488 secondary antibody; **(c,f)** shows composite image of DAPI- and Alexa Fluor 488-stained uninfected and infected Sf21cells.

the recombinant bacmid into Sf21 insect cells. Transfection leads to cell enlargement, granulation, and vacuole formation after 72 h. Integration of HEV-protease was confirmed by PCR from baculovirus genomic (**Figure 1E**).

Confirmation of HEV-Protease Expression

In order to confirm the expression of HEV-protease in infected Sf21 cells, an indirect immunofluorescence assay was performed using HEV-protease epitope specific antibody. The Baculovirus-infected Sf21 cells produced fluorescence after staining with HEV-protease antibody (**Table 1**, **Figure 2**).

Expression and Purification of HEV-Protease

The highest expression of HEV-protease was obtained at 27°C at 10 MOI after 48 h of infection. SDS-PAGE analysis showed expression of ∼18 kDa HEV-protease on SDS-PAGE (**Figure 3A**) which was confirmed by immunoblotting using anti HEV-protease antibody (**Figure 3B**). The expressed protein was solubilized using 1% CHAPS and 10% DMSO. Purification was performed by Ni^{2+}-NTA affinity chromatography under native conditions. The eluted protein was >95% pure by gel analysis (**Figure 3C**).

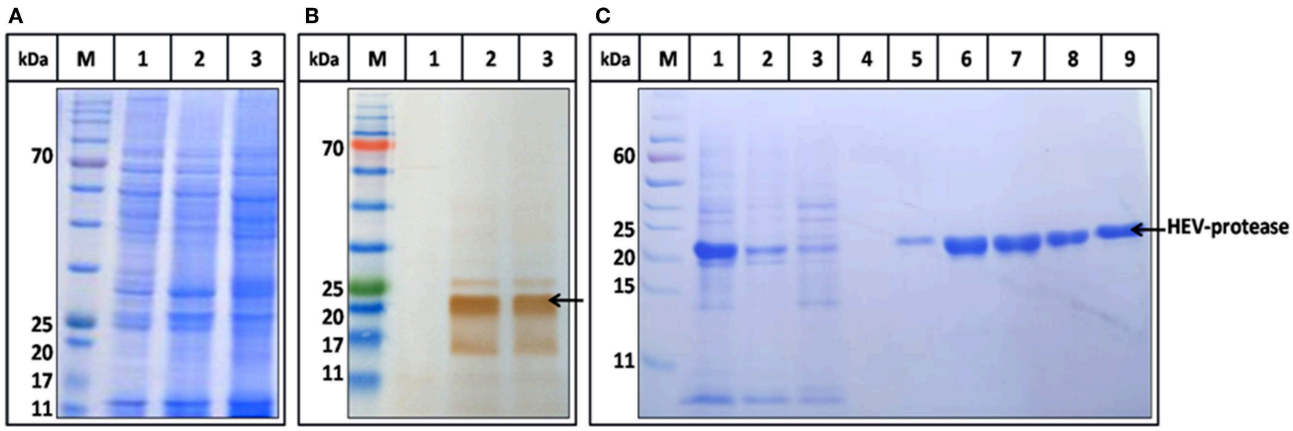

FIGURE 3 | Expression and Purification profile of HEV-protease. Highest expression level was seen at 48 h of post infection at 10 MOI. **(A)** SDS-PAGE and coomassie blue staining of Sf21 expressed HEV-protease. **(B)** Western blot analysis of HEV-protease by HEV PCP antibody; lane M marker, lane 1 cell lysate of uninfected Sf21 cells, lane 2 and 3, cell lysate of infected Sf21 cells after 48 and 72 h of post infection. **(C)** SDS-PAGE and coomassie blue staining of Ni-NTA chromatography fractions: lane M, marker; lane 1, solubilized protein; lane 2, Flow through; lane 3,4, Wash fractions; lane 5–9, Elution Fractions.

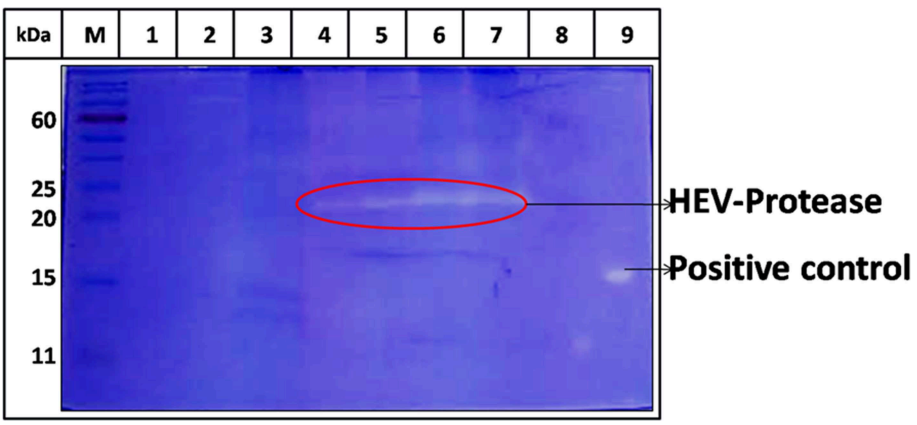

FIGURE 4 | Zymography of HEV protease using gelatin as a substrate. Purified HEV-protease was loaded in the wells for determining cleavage of gelatin; lane M, protein ladder, lanes 1 and 2 were loaded with 10 and 20 μl of solubilization buffer to eliminate any contaminating protease activity, lane 3 was loaded with 20 μl cell sup of uninfected Sf21 cells, lane 4–7 were loaded with increased quantity of HEV-protease (5,10,15, and 20 ng, respectively), lane 8 was left blank, and lane 9 was loaded with 5 ng of trypsin as a positive control. The cleavage of gelatin confirmed the protease activity. There was no digestion of gelatin in the negative control lane, indicating the absence of any non-specific protease activity.

Substrate Specific Catalytic Activity of HEV Protease

The activity of purified HEV-protease was determined by negative staining using native gelatin zymography. Gelatin is a non-specific substrate for protease and forms a clear zone on zymography assay due to its digestion. Increasing quantity of HEV-protease (5, 10, 15, and 20 ng) resulted with increased intensity of clear zone due to digestion of gelatin (**Figure 4,** lane 4–7). Digestion of gelatin was not seen in negative control (**Figure 4**, lane 2,3), indicating specificity of the assay.

Further, protease activity was confirmed by digestion assay using ORF1 as a substrate. ORF1 has been reported to cleave in putative domains of MeT, PCP, Hel, and RdRp (Sehgal et al., 2006). For the first time we showed digestion of ORF1 polyprotein into smaller fragments. After digestion, 186 kDa polyprotein breaks in to 110 and 85 kDa products which further breaks into smaller product of 55, 37, 27, and 18 kDa (**Figure 5**, lane 3–5). No autolysis has been seen in full length ORF1 even after 24 h of incubation at 37°C (**Figure 5A**, lane 2) validating the specificity of proteolysis of ORF1 by HEV-protease in digestion assay. To confirm the processing of ORF1, digested samples were immunoblotted using anti-MeT, anti-protease, anti-RdRp and anti-Hel antibodies (**Table 1**). Approximately 35, 20, 55, and 27 kDa size of bands were visualized with anti-Met, anti-protease, anti-RdRp and anti-Hel antibodies corresponding to the size of putative domain of methyletransferase (**Figure 5B**, lane 3–5), protease (**Figure 5C**, lane 3–5), RdRp (**Figure 5D**, lane

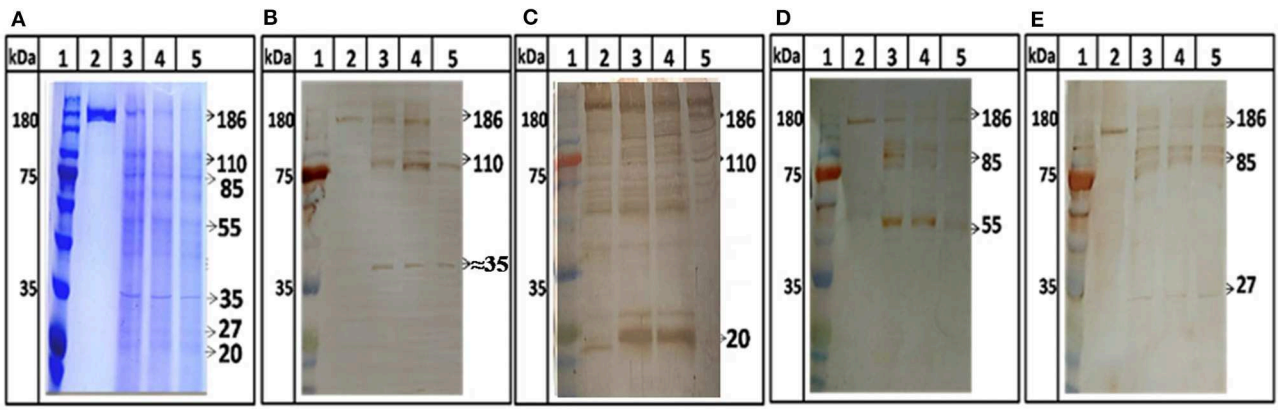

FIGURE 5 | ORF1 digestion by HEV Protease. Full length ORF1 protein of HEV was purified and used as the natural substrate of HEV-protease. The ORF1 protein was digested with HEV-protease and fractionated on SDS-PAGE. Western blot was performed using antibodies generated against other domains of ORF1 polyprotein. **(A)** SDS-PAGE and coomassie blue staining of digested ORF1 using protease. lane 1, Marker; lane 2, Undigested ORF1; lane 3–5, digested ORF1 after 1, 3, and 5 h digestion. **(B)** western blot analysis using anti-Met antibodies, the Met was seen as the digested product of ORF1 (**B,** lane 3–5). Similarly, the blots were probed with protease, RdRp and helicase antibodies **(C–E)**. Lane 2 represents undigested ORF1 while lane 3–5 represents the ORF1 digestion at different time points (1, 3, and 5 h respectively). The figure clearly showed 186 kDa ORF1 and the Met, RdRp and Hel as proteolytic fragment of ORF1.

3–5), and Helicase (**Figure 5E**, lane 3–5). This suggests the role of HEV-protease in cleavage of ORF1 polyprotein.

Enzyme Kinetics

Next, FTC-casein was used as a substrate to determine the activity of HEV protease. The cleavage of FTC-casein results TCA-soluble, FTC-peptides in the presence of active protease. Protease activity was quantified by measuring absorbance at 492 nm. As seen in **Figure 6A** significant protease activity could be detected as compared to the mock reaction. Protease activity was proportional to the quantity of the substrate. Signal saturation was obtained at 9 h (**Figure 6B**). Further experiments were carried out to estimate kinetic parameters of HEV protease using the above conditions Reaction velocity V_0 (mM/h) was found to be different for each substrate concentration S (mM). Accordingly, different V_0 and S the Lineweaver-Burk graph was plotted against 1/V and 1/S to calculate Km and Vmax. Through the slope and the interception of the plot of 1/V vs. 1/S, the exact values of Km and Vmax were determined to be 0.054 mM and 0.77 mM/h, respectively (**Figures 6C,D**).

Optimization of Reaction Conditions of Protease Activity

Buffer and assay conditions were optimized to find activity at pH 4–7.8. Higher pH impaired the protease activity significantly in comparison to lower pH (**Figure 7A**). The optimal temperature for protease activity was found to be 37–48°C (**Figure 7B**). The effect of glycerol (anti-chemotropic agent) was also observed. At 10–20% glycerol concentration, slight increase in protease activity was seen. However, further increase in glycerol concentration resulted in the decrease of protease activity (**Figure 7C**). The results with different Na+ concentrations indicated that the optimal concentration was around 50–150 mM and that the enzyme is relatively insensitive to Na^+ (**Figure 7D**) Analysis of the effect of different divalent cations like Ca^{2+}, Cu^{2+}, Mg^{2+}, Mn^{2+}, Ni^{2+}, Zn^{2+}, Fe^{2+}, and Pb^{2+} on the activity of HEV protease revealed that Ca^{2+}, Mg^{2+}, Pb^{2+}, and Fe^{2+} had no effect, however, Zn^{2+} ($p = 0.0001$), Ni^{2+}, Pb^{2+} ($p = 0.01$) and Mn^{2+}($p = 0.001$) significantly decreased the protease activity (**Figure 7E**).

Analysis of the Effect of Protease Inhibitors

The effect of different protease inhibitors was tested using FTC-casein protease assay in the presence of inhibitors. The enzyme was completely resistant to serine proteases inhibitors (PMSF, AEBSF, aprotinin), aspartic proteases (pepstatin), amino-peptidases (bestatin), metallo-endoproteases (phosphoramidon). The enzyme was moderately inhibited by cysteine protease inhibitors (antipain, leupeptin, ALLN, chymostatin, and E-64) (**Figure 8A**). Minimum relative protease activity seen with E-64 suggested it to be a papain like cysteine protease. Further, activity of HEV protease on ORF1 digestion was tested in the presence of twelve different protease inhibitors in independent reactions (**Figure 8B**). It was observed that HEV protease was strongly inhibited by E-64 (99%) and chymostatin (98%). Moderate inhibition was seen with leupeptin, ALLN and antipain whereby no inhibition was observed with phosphoramidon, PMSF, AEBSF, aprotinin, pepstatin (**Figure 8B**).

In silico Analysis of HEV-Protease

To further know the active site residue involved in the interaction between HEV-protease with inhibitors, its 3D structure has been modeled which also showed the nature of the HEV-protease. The predicted model showed two domains architecture, N-terminal helix and C-terminal β-sheet domain similar to papain-like cysteine proteases (Verma et al., 2016) but differ in arrangement of secondary structure elements. An active site

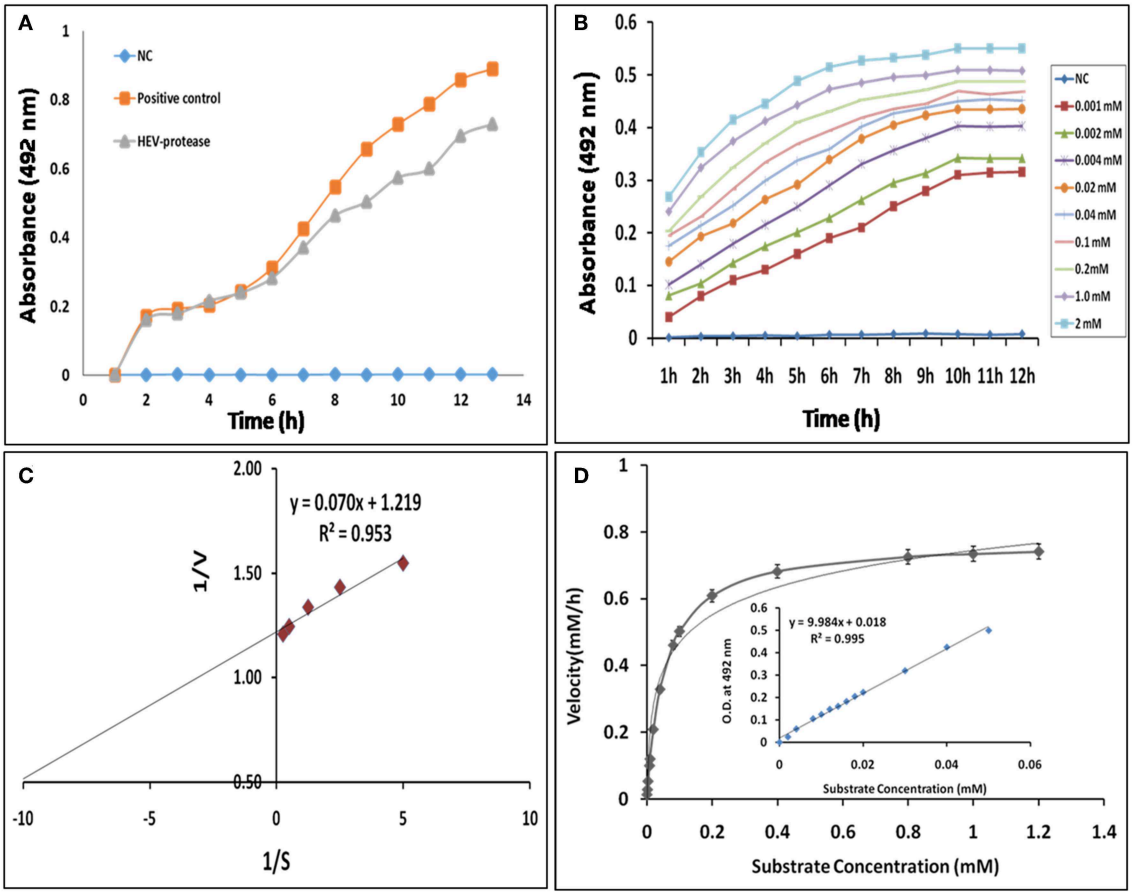

FIGURE 6 | Enzyme kinetics of HEV protease: **(A)** FTC-casein based protease assay was developed for the determination of HEV protease activity. A negative control (NC) reaction was performed without enzyme, which did not show any change in the absorbance. **(B)** Real-time profile of proteolytic assay with increasing substrate concentrations, ranging from 0.01 to 2 mM, using 1 μM protease was performed and the absorbance measured at different time points every 1 h till 12 h till increase in absorbance was observed. Background absorbance (NC) was subtracted for clarity for comparison. **(C)** Lineweaver–Burk plot and regression equation plotted to determine km and Vmax of HEV-protease. **(D)** Reaction velocity (mM/h) calculated with the help of standard curve and plotted over different range of substrate concentration (means of three independent experiments performed in triplicate).

(catalytic pocket) for substrate binding was present between two domains. The residues present in the predicted active site cleft were Gln479, Thr482, Cys483, Val507, Asp508, Leu582, Pro509, Ile561, Glu588, Arg589, His590, Asn591, Leu592, Met474, Lys457, Leu476, Phe575, and Gly478. A "Cysteine(Cys)-Histidine(His)-Asparagine(Asn)" catalytic triads has also been seen between N-terminal helical domain and a C-terminal β-sheet domain.Cys483-His590-Asn591 residues were found to be involved in this catalytic triad, which is the main characteristic of the "papain" family. One Di-sulfide bond observed between Cys434 and Cys481 necessary for stability and the proper folding of the protein. Residues present in CTC motif (Cys481 and Cys483) and CHC motif (Cys457 and Cys 459) may be involved in zinc metal ion coordination and catalysis (**Figure 9A**). It is reported that the Zn binding site present on the opposite side of active site (Herold et al., 1999), which even validated by crystal structure of hepatitis C virus NS3 proteases (Stempniak et al., 1997; Barbato et al., 1999; Arasappan et al., 2005) picornavirus 2A (Yu and Lloyd, 1992) PL1pro of HCoV-229E (Ziebuhr et al., 2007), p150 of RUBV (Zhou et al., 2007), and Lpro of FMDV (Guarne et al., 2000). The diagrammatic representation indicates presence of CHC motif, opposite to the predicted active site, could be zinc binding site of HEV-protease (**Figure 9**).

Docking Study of Inhibitors for the Validation of HEV PCP Model

The inhibition efficiency of all the inhibitors used in protease assay was also proved by docking studies to know the interaction between inhibitors and predicted active site residues of HEV-protease. Results summarized in **Table 2** showed that most of the active compounds had good agreement between the docking score and experimental results ($r^2 \approx 0.75$). It suggests that the parameters of docking simulations and quality of structural model are good in reproducing experimental course of these compounds in the modeled HEV PCP. The observed difference among E64 docking scores and interacting residues may be due to difference in binding affinity of different

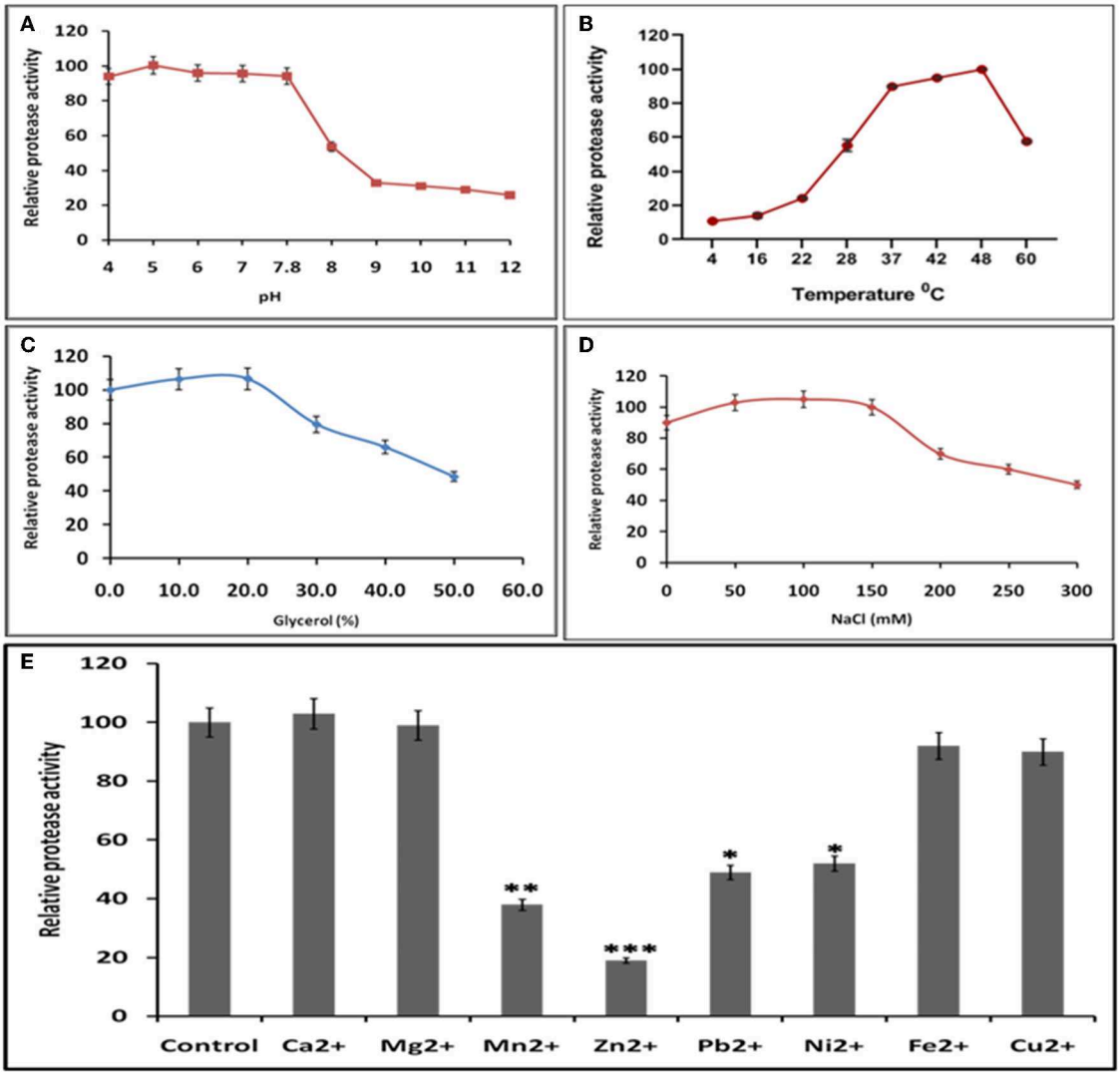

FIGURE 7 | Optimal reaction conditions for the protease activity of HEV-protease **(A)** Effects of pH on protease activity. HEV protease and substrate were incubated with various buffers of pH ranging from 4 to 12. The relative activity was calculated at different pH at pH 7.8 as 100%. **(B)** Effects of temperature (4–60°C), the relative activity was calculated by taking activity at 37°C as 100%. **(C)** Effect of glycerol and **(D)** NaCl concentration on protease activity. HEV protease and substrate were incubated in a buffer of 50 mM Tris (pH 7.8) containing the indicated concentrations (0, 50, 100, 150, 200, 250, and 300 mM) of NaCl. **(E)** Effects of various divalent cations (2 mM) on protease activity (*$p < 0.01$, **$p < 0.001$, ***$p < 0.0001$) with respect to control.

inhibitors as observed in inhibitory efficiency. Four inhibitors (E64, Chymostatin, Leupeptin, and ALLN) showed good ligand–receptor interactions that correlated better with the enzyme inhibition activity of recombinant HEV PCP protein with Glide docking (**Table 2**). Docking result shows that cysteine protease inhibitors E64, Chymostatin, Leupeptin, and ALLN (docking score −6, −5.1, −5.8, −4.3 respectively) have strong binding affinity. Result of E64 docking shows that strong H-bond interactions formed with backbone oxygen of Leu477and Lys475 and side chain OE2 atom of Glu 586 and nine hydrophobic interactions observed with Met474, Gln479, Cys483, Ala513, Val507, Ile561, His590, Asn591, Leu592, Arg589, Leu581, residues (**Table 3**). All inhibitors bound to the HEV PCP active site in a manner similar to the inhibitor E64 (**Figure 10**). In Chymostatin five H-bond interactions formed, two with backbone oxygen of Met474 and Leu477 and one nitrogen atom of Asn591, whereas two side chain H-bond interactions were observed with oxygen atom of Glu479 and Thr482 and eight hydrophobic interactions were observed with Val507, His590, Leu592, Phe576, Glu586, Leu581, Glu583, Leu535 residues. Leupeptin had an H-bond with backbone oxygen of Asn591 and twelve hydrophobic interactions observed with Gln479, Met474, Thr482, Ala513, Val507, Ile517, Ile561, Phe576, His590, Leu592, Arg589, Leu581 residues. Inhibitor ALLN showed two side chain

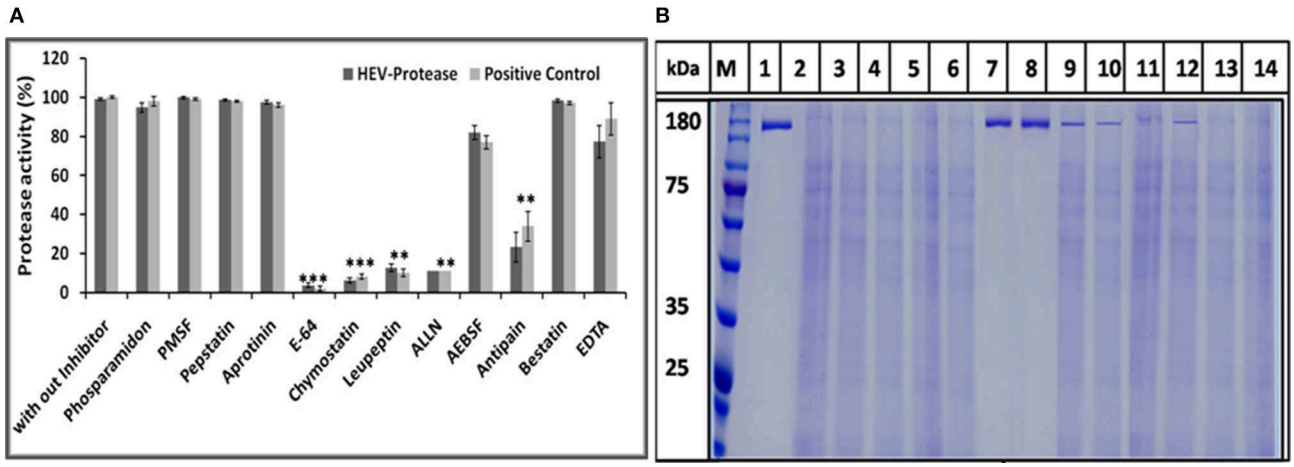

FIGURE 8 | Inhibition assay: **(A)** Effects of different protease inhibitors on protease activity. The FTC-casein based protease assay was performed in presence of various inhibitors. The relative protease activity was determined by taking protease activity as 100% without inhibitor. The standard errors of the means of results from three independent experiments have been seen. The asterisk indicates statistical significance (**$p < 0.001$, ***$p < 0.005$) with respect to control (without inhibitors). **(B)** Activity of HEV protease was studied in the presence of twelve protease inhibitors. lanes 1 undigested ORF1, lane 2 digested ORF1 without any inhibitor. Lanes 3–14 represent ORF1 over digestion (5 h at 37°C) in the presence of 1× concentration of various inhibitors. By this time, active protease without any inhibitor (lane 2) had cleaved the entire pORF1. The most effective inhibition was observed with E-64 and chymostatin (lanes 7 and 8, respectively).

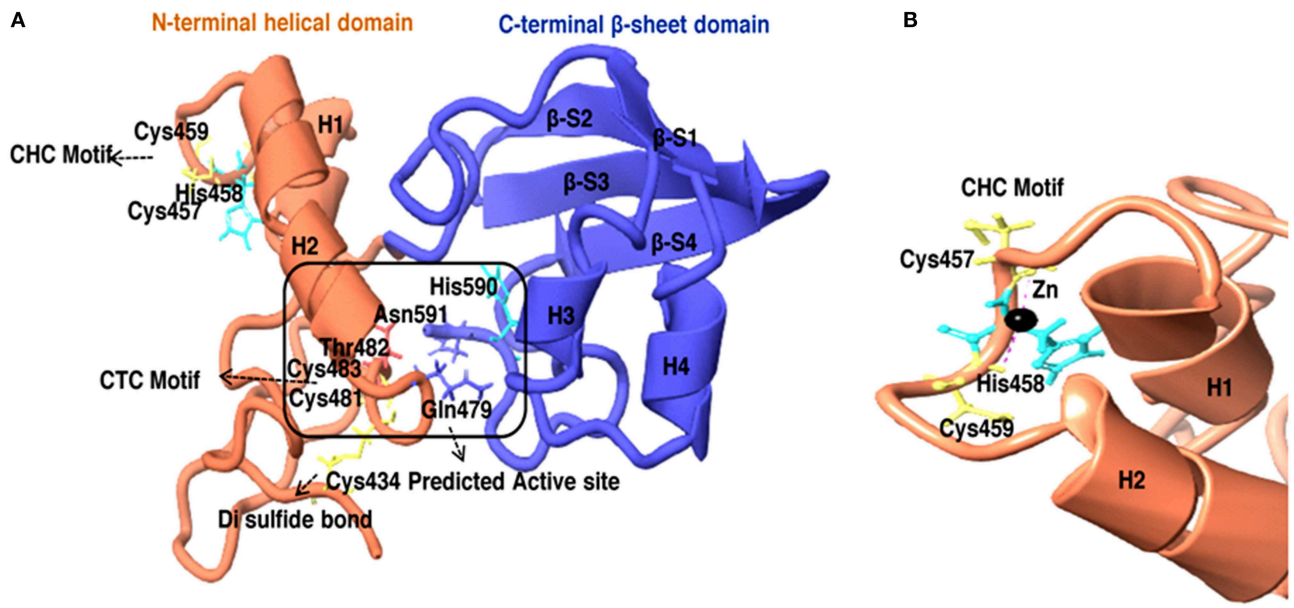

FIGURE 9 | (A) 3D model of HEV-Protease found to be similar with Papain like cysteine protease as to have conserved catalytic triad and "papain-like β-barrel fold." **(B)** Predicted Zinc coordination in the HEV PCP model, the diagrammatic representation of CHC motif and Zn binding site.

interactions with nitrogen atom of Glu479 and oxygen atom of Glu583, respectively. Eight hydrophobic interactions observed with Val507, His590, Leu592, Arg589, Leu581, Asn591 residues. Among the remaining inhibitors, PMSF Phosparamidon and AEBSF which were found to be inactive in the HEV PCP enzyme inhibition assay, ligand–receptor interaction analysis showed that inhibitor PMSF and Phosparamidon did not formed H-bond interactions (**Table 3**). Three inhibitors AEBSF, Bestatin and Pepstatin showed week H-bond and hydrohobic interactions. Interestingly, two inhibitors EDTA and Antipain which were inactive in experimental results remain undocked.

TABLE 1 | Peptide sequence of antibodies generated against epitope of all non-structural proteins of HEV genotype-1.

S.no.	Protein name	Peptide sequence	Location on ORF1
1	Methyl transferase	AGRDVQRWYTAPTRC	111–124
2	HEV-protease	LDPRVLVFDESAPC	444–457
3	Helicase	TADARGLIQSSRAH	1,505–1,518
4	RNA dependent RNA polymerase	PKESLKGFWKKHSG	1,156–1,169

TABLE 2 | Correlation between relative protease activity of recombinant HEV-PCP and Docking score of the inhibitors.

	Relative protease activity	Docking score	Correlation
Without Inhibitor	100	–	0.75
PMSF	100	−2.6	
E-64	4	−6	
Chymostatin	6	−5.1	
Leupeptin	13	−5.8	
ALLN	11	−4.3	
AEBSF	82	−4.8	
Phosparamidon	95	*	
EDTA	77	–	
Antipain	23	–	

Although very good docking score −6.8 was found with Phosparamidon but its binding site was different to others and no H-bond interaction were seen (Table 3**).*

TABLE 3 | Interaction and distance between the inhibitors and key amino acids of HEV-PCP in XP docking complex determined using LIGPLOT program.

Inhibitors	H-bonds (residue (atom number-distance in Å-ligand atom number) ligand)	Other interactions (total hydrophobic interacting residues)
E64	B-Leu477 (O-3.13-N4)L, B-Leu477 (O-2.91-N5)L, S-Glu586 (OE2-2.60-O3)L, B-Lys475 (O-2.95-N5)L.	(11) Gln479, Cys483, Met474, Ala513, Val507, Ile561, His590, Leu592, Arg589, Leu581, Asn591.
Leupeptin	B-Asn591(N-3.22-O4)L	(12) Gln479, Met474, Thr482, Ala513, Val507, Ile517, Ile561, Phe576, His590, Leu592, Arg589, Leu581.
Chymostatin	S-Thr482 (OG1-3.30-N2) L, B-Met474 (O-2.83-N7) L, B-Leu477 (O-2.89-N7) L, B-Asn591 (N-3.33-O6) L, S-Glu479 (OE1-2.95-N2) L.	(8) Val507, His590, Leu592, Phe576, Glu586, Leu581, Glu583, Leu535.
ALLN	S-Glu479 (NE2-3.01-O2)L, S-Glu583 (OE1-2.84-N2)L.	(8) Val507, His590, Leu592, Arg589, Leu581, Asn591.
PMSF	–	(4) Val507, His590, Leu581, Leu592.
AEBSF	B-Met474(O-2.9-N1)L, B-Leu477(O2-2.92-N1)L.	(5) Gln479, Val507, Leu581, Leu592, Thr482.
Phosphoramidon	–	(10) Lys475, Gln479, Leu477, Leu581, Phe576, Ile561, Leu592, Glu583, Glu588, Arg589.
Bestatin	S-His590(ND1-3.05-O1)L.	(5) Gln479, Leu581, Val507, Asp589, Leu592.
Pepstatin	S-Gln479(OE1-3.14-N4)L, S-Gln479(NE2-2.90-O2)L, S-Glu583(OE1-3.01-N2)L.	(8) Val507, His590, Glu588, Leu582, Leu592, Asp536, Leu535, Phe576

S, Side chain; B, Backbone.

DISCUSSION

Viral proteases are good targets for development of antiviral therapeutics due to their crucial role in viral polyprotein processing. Thus, as a pre-requisite for screening of small molecule inhibitors (SMIs) against HEV protease, we expressed and purified a soluble, catalytically active recombinant viral protease with good yield and homogeneity in baculovirus expression system. Further, we developed a robust cell free assay with high sensitivity, selectivity and reproducibility to screen targeted compounds with anti-HEV protease activity. We validate HEV cysteine protease as a papain like protease on the basis of *in silico* 3D modeling and inhibition with specific inhibitors.

Positive-strand RNA viruses are supposed to encode proteases to process their polyproteins usually required for enzymatic activities, interactions with other proteins, subcellular localization, and the viral assembly (Debing et al., 2016). Processing of HEV ORF1 by its protease domain remains controversial due to unavailability of well-characterized native HEV protease. It was hypothesized that a putative region between residues 433 and 592 of HEV-ORF1 encodes protease (Koonin et al., 1992; Parvez and Khan, 2014) but the nature of protease, its biochemical and biophysical characterization need to be understood. In some reports, role of cysteine protease in HEV processing has been identified but possibility of other proteases could not be ruled out (Ropp et al., 2000; Sehgal et al., 2006).

In previous study HEV protease was expressed from different genotype of HEV in *E. coli* (Accession no: FJ457024 region 440-610) containing extra 9 amino acid (SFDASQSTM) at the C-terminal region have 170 amino acids. This refolded protein was also found to be active and classified as chymotrypsin like protease (Paliwal et al., 2014). In the present study a 161 amino acid long protein of Accession no: AF444002_1 region 432-592 of genotype1, similar to the one predicted by putative domain of HEV (Koonin et al., 1992; Parvez, 2013) has been expressed using baculovirus expression system and purified in native condition. These constructs having significant variation, could result in difference as mentioned by Paliwal et al. (2014) and our study. With the present data it cannot be interpreted the nature of protein with dual properties of papain like Cysteine protease or Chymotrypsin like properties. Further studies will be required to validate this fact. In the present study, recombinant HEV protease was expressed using the baculovirus expression system since it is considered to be an efficient insect expression system with the ability to carry post-translational

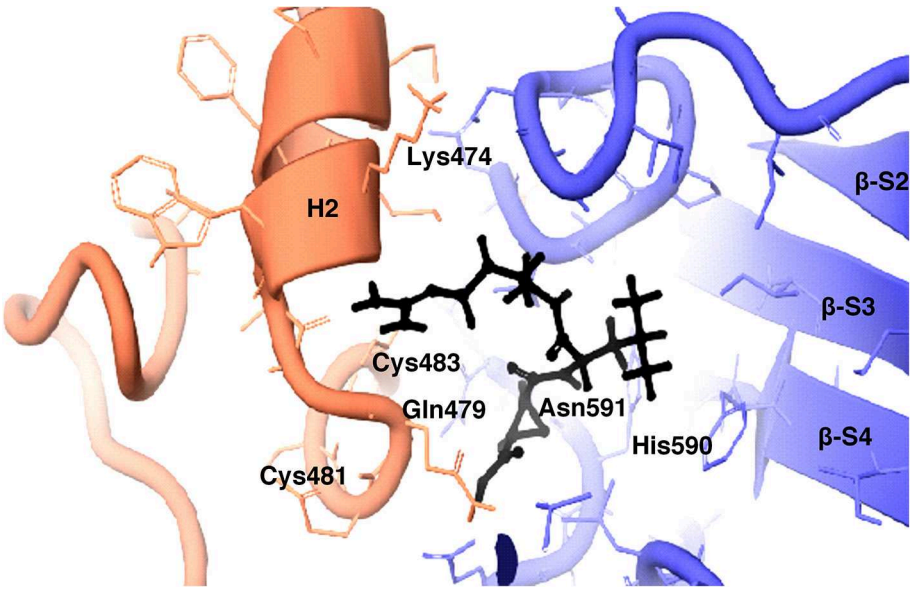

FIGURE 10 | 3D view of cysteine protease inhibitor E64 docked in the binding pocket of the HEV-protease model. Inhibitor E64 is shown as stick with color code pink. The H- bonds are highlighted by dotted yellow lines. Some part of the ribbon has been removed for clarity. Residues present in active site are shown as CPK in Gray color. Only catalytically important residues are marked. These residues are located in the substrate binding cleft.

modifications (Chambers et al., 2018). Previously it has been reported that baculovirus system can express toxic proteins and proteases of different organisms (Keyvani-Amineh et al., 1995; Sali et al., 1998). The cell free assay was developed to quantify the activity of HEV protease since no robust protocols for protease digestion have been described so far. For development of cell free assays, three different approaches have been used to measure protease activity i.e., gelatin zymography, FTC-casein based assay and digestion of full lengthORF1 polyprotein. In pevious report gelatin zymography based assays has been used for hepatitis E viruses (Paliwal et al., 2014), whereby a clearing zone on the slide due to digestion of gelatin was formed. Similar to that, a clear zone was observed on zymogram when the native HEV protease was used. To determine the conditions for the optimal activity of the protease, it has been reported that cysteine protease activates at lower pH (Sundararaj et al., 2012). In our study the protease activity has been shown at lower pH which is typical of a cysteine protease. Digestion of gelatin in zymography gave the first direct evidence of protease activity by the expressed putative protease domain (432–592 aa) of pORF1 leading us to express pORF1 in bacteria to be used as the substrate. The natural activity of HEV-protease could be studied by proteolysis of ORF1 polyprotein which was expressed via *E. coli*. Bl21-DE3 cells. HEV-protease cleaves ORF1 polyprotein in a time dependent manner. After 1 h of incubation, bands of ∼100 and ∼84 kDa were seen, which further cleaved into smaller products with time and after 5 h, multiple band of smaller size were seen due to proteolysis of ORF1. Digestion of ORF1 by cysteine protease resulted in ∼84 kDa RdRp-Hel, and ∼67 kDa Met-PCP fragments which were further processed into ∼55 kDa RdRp, ∼35 kDa Met, and ∼27 kDa Hel fragments with higher incubation time. The above obtained fragments were similar in molecular mass to the ones observed in previous immunoprecipitation studies with replicon transfected HepG2 cells (Panda et al., 2000) and after expression of ORF1 polyprotein in cell free system as well as in mammalian cells (Ropp et al., 2000). In addition, ∼55 kDa intermediately processed form of the RdRp and∼35 kDa Met protein has also been seen in previous study after digestion of 84 kDa RdRp-Hel and 67 kDa Met-PCP fragments by immunoprecipitation (Paliwal et al., 2014). Similar size of products also has been seen in self-digestion of baculovirus derived ORF1 polyprotein (Sehgal et al., 2006). These results suggest role of HEV-protease in ORF1 polyprotein processing and HEV life cycle.

For the first time, enzyme kinetics of native active HEV protease has been determined in this study using FTC-casein substrate based assay to validate enzymatic activity and kinetics of HEV-protease. The values of Km and Vmax were found to be 0.054 mM and 0.77 mM/h, respectively. The optimal temperature for protease activity was found to be 37–48°C which corresponds well to the appropriate environments for HEV growth in the cells (Emerson et al., 2005; Tanaka et al., 2007; Johne et al., 2016). Activity of HEV protease was found to be pH dependent. The protease activity was found to be optimal at low pH of 4 which is the crucial factor to activate Papain like cysteine proteases (Richau et al., 2012; Sundararaj et al., 2012). A number of reports have shown that cysteine proteases can be auto catalytically activated *in vitro* from zymogen to mature enzyme even at reduced pH (Lowther et al., 2009; Sundararaj et al., 2012; Verma et al., 2016) indicating it to be a cysteine protease. In an attempt to validate the nature of the protease we used various inhibitors

to monitor its activity. Twelve inhibitors were used to study the inhibition and it was found that the enzyme was completely resistant to the inhibitors of serine proteases (PMSF, AEBSF, aprotinin), aspartic proteases (pepstatin) and metalloproteases (EDTA) while it was moderately inhibited by cysteine protease inhibitor leupeptin, chymostatin and E-64. HEV protease was strongly inhibited by E-64 (99%) and chymostatin (98%), which had been reported to inhibit papain like cysteine protease (Saha et al., 2018). To confirm these results, modeled HEV protease structure has been docked with above inhibitors which shows that cysteine protease inhibitors E64, Chymostatin, Leupeptin, and ALLN have good docking score and strong binding affinity whereas remaining inhibitors PMSF, Phosparamidon, AEBSF, Bestatin and Pepstatin showed no or weak interactions and EDTA and Antipain remain undocked. Correlation coefficient was found 0.75 which showed good agreement between *in vitro* and *in silico* studies, suggesting strongly that the HEV-protease is a Papain like cysteine protease. Besides, *in silico* modeled structure of HEV-protease was found to be similar with Papain like cysteine proteases as it has structurally similar N-terminal helix domain and C-terminal β-sheet domain and conserved Cys–His–Asn triad at the active site (Koonin et al., 1992; Coulombe et al., 1996). Cys483 and His590 form a catalytic triad with Asn 591 which is present in active site between N-terminal helical domain and a C-terminal β-sheet domain of HEV-protease. A histidine residue, presents in the active site act as proton donor and increase the nucleophilicity of the cysteine residue. Nucleophilic cysteine, act up on the carbon of the reactive peptide bond, release of an amine or amino terminus fragment of the substrate and producing the first tetrahedral thioester intermediate (Coulombe et al., 1996). This intermediate is now stabilized by hydrogen bonding between highly conserved glutamine residue and substrate oxyanion. Subsequently, thioester bond is hydrolyzed and form a carboxylic acid moiety from the remaining substrate fragment (Verma et al., 2016). Earlier, the Papain like proteases are characterized by the presence of two domains, an α- helix and a β-sheet domain forming a deep cleft which contains Cys-His-Asn residues along with Gln acting as a substrate-binding site (Turk et al., 2001). Similar observation has been recorded in our predicted 3D model showing two domain architecture structures where the Cys-His-and Asn triad is formed along with Gln at the active site. Further, according to our findings, the Cys483 and His590 forms a catalytic triad with Asn 591 present in active site between N-terminal helical domain and a C-terminal β-sheet domain of HEV-protease. Further, our findings are also in agreement with previous study where HEV-protease has been categorized as a Papain like cysteine protease (Koonin et al., 1992; Parvez and Khan, 2014). In this study HEV protease was found to have these characteristics and on the basis of structural similarity with papain like protease it has been characterized as papain like cysteine protease. These findings are in the agreement of previous study where HEV-protease has been categorized as a Papain like cysteine protease (Koonin et al., 1992; Parvez and Khan, 2014).

Effect of different divalent cations like Ca^{2+}, Cu^{2+}, Mg^{2+}, Mn^{2+}, Ni^{2+}, Zn^{2+}, Fe^{2+}, and Pb^{2+} were studied on activity of HEV protease. Out of these divalent cations Zn^{2+} remarkably decreased protease activity. Divalent cations like zinc and its conjugates have been identified as protease inhibitors for SARS-CoV proteases (Hsu et al., 2004), also zinc have been found to be essential for Structural stability, folding of NS3 protease of HCV (Urbani et al., 1998) and catalytic activity of Rubella protease (Liu et al., 1998). In another report, Zn has been found to be an essential structural cofactor for human corona virus papain like protease (Herold et al., 1999). Thus, we were interested in testing the influence of metal conjugated compound on HEV protease activity. Further, *in silico* studies have been performed to determine the zinc binding sites present in HEV protease. Two zinc binding sites have been identified, as "Zn^{2+} binding motif" Cys457-His458-Cys459 (CHC) and Cys481-Thr482-Cys483 (CTC) and these findings are in agreement with previous report (Parvez and Khan, 2014) who studied that mutation in Cys 481 and Cys 483 leads to loss of protease activity (Parvez, 2013; Paliwal et al., 2014). These residues present in the zinc binding site may play role in its structural stability and proper folding. It was reported that zinc binding site mediates proteolytic activity of Corona viral papain like protease (Berg and Shi, 1996). These findings support our report where the loss of protease activity has been found in the presence of zinc, which may act as a cofactor and confer the structural stability.

Most of the RNA viral proteases are categorized either as chymotrypsin like or papain-like proteases (Neurath, 1984). Chymotrypsin like proteases have been found to exhibited with three different catalytic triads Ser-His-Asp, Cys-His-Asp, and Cys- His-Glu (Bazan and Fletterick, 1988; Gorbalenya et al., 1989; Matthews et al., 1994), whereas papain like proteases are found to have the conserved Cys-His dyad which are assisted by unique Asn and Asp residues (Gorbalenya et al., 1991). In both the chymotrypsin-like or papain-like proteases, Zn^{2+} is located at the site opposite to the active center (Herold et al., 1999). Therefore, the classification of HEV protease not only depends on the involvement of cysteine and histidine but also on structure and sequence homology. Papain like cysteine proteases are very stable enzymes and often are found in proteolytically harsh environments (Richau et al., 2012). Besides catalytic dyad/triad prediction we find that HEV-protease activity was found to be optimal at low pH of 4 which is the crucial factor to activate cysteine proteases. It is already reported that cysteine protease activates at lower pH (Sundararaj et al., 2012). In our study the protease activity has been shown at lower pH which is typical of a cysteine protease. On the basis of structural homology, active site residue and class specific inhibition we have classified HEV-protease as a "Papain-like cysteine protease."

MATERIALS AND METHODS

Cells and Virus

Spodoptera frugiperda (Sf21) cells (Invitrogen, California, US) were used for generation, propagation and titration of recombinant baculovirus. Sf21 cells were maintained in Sf900III insect cell medium (Gibco, Newyork, US) and supplemented

with 10% fetal bovine serum (Gibco, Newyork, US) at 27°C in refrigerated incubator. HEV cDNA clone pSK-HEV-2 genotype 1 GenBank accession no. AF444002 was used as a reference virus in this study. All the virus experiments were performed in BSL-2 facility in Shiv Nadar University, Dadri, India.

Cloning of HEV Protease Using Bac to Bac Expression System

The HEV protease domain (nts 1319–1801t of HEV; GenBank accession no. AF444002) was PCR-amplified by 5′CTCAGA ATTCATGGCTCAGTGTAGGCGCTG3′ and 5′TCTAGC GGCCGC GAGATTGTGGCGCTC6TGG3′ forward and reverse primer from full length HEV cDNA clone pSK-HEV-2 using Pfu DNA polymerase (NEB, Massachusetts, US). Amplified product was cloned into pFastBac/CT-TOPO vector (Invitrogen, California, US) following manufacture's protocol and transformed into One Shot™ Mach1™ T1R Chemically Competent *E. coli* (Invitrogen, California, US). Positive transformants were screened by PCR and confirmed by DNA sequencing. Further, pFastBac/CT-HEV protease construct was transformed into MAX Efficiency™ DH10Bac™ Competent *E. coli* (Invitrogen, California, US) that contains baculovirus shuttle vector or bacmid. Positive Colonies were confirmed by PCR amplification using pUC/M13 reverse and forward primers. The recombinant bacmid was purified using PureLink HiPure Plasmid Miniprep Kit (Invitrogen, California, US) following manufacture's protocol.

Generation of Recombinant Baculovirus Containing HEV-Protease

Recombinant bacmid containing HEV protease gene was transfected in Sf21 cells using Cellfectin™ II reagent (Invitrogen, California, US). Briefly 8×10^5 Sf21 cells /well were seeded in six well plates. Five-hundred nanogram bacmid DNA was mixed with cellfectinII reagent and transfected into Sf21 cells. After 1 h incubation at 27°C, complete Sf900III medium was added and plate incubated at 27°C for 72 h. Supernatant was collected and titrated using plaque assay. Further, plaques were purified and amplified in Sf21 cells while the recombinant baculovirus was confirmed through PCR of genomic DNA of the infected Sf21 cells.

Demonstration of HEV Protease Expression in Sf21 Cells by Immunofluorescence Assay

In order to demonstrate the expression of HEV-protease in Sf21 cells, 1×10^6 Sf21 cells were seeded in six well plates and infected at 1 MOI (multiplicity of infection) with recombinant baculovirus clone having HEV-protease gene. After 48 h of infection, cells were fixed with chilled methanol for 30 min, followed by permeabilisation with 0.1% Triton X-100 for 15 min. The cells were blocked for 1 h at room temperature with 3% BSA in PBST (PBS with 0.1% Triton X100). Infected Sf21 cells were probed with HEV-protease epitope specific antibodies constructed by Genscript against 444–457 peptide region of HEV-protease (**Table 1**) for 1 h at room temperature. After three washing with PBS, the cells were stained with goat anti-rabbit IgG-Alexa Fluor 488 (Biogenix) for 60 min at room temperature. Subsequently, the cells were washed with PBS and their nuclei were stained with DAPI (4′,6-diamidino-2-phenylindole) (Sigma) for 10 min at room temperature. The cells were washed and fluorescence was visualized using a fluorescence microscope (Olympus IX 71, Germany).

Expression of Recombinant HEV-Protease in Sf21 Insect Cells

Expression of HEV-protease was performed in Sf21 cells as described previously (Sehgal et al., 2006). Briefly 2×10^7 Sf21 cells were seeded in T175 tissue culture flask and incubated at 27°C to attach the cells. Cells were washed with incomplete SF900 III medium and infected with the recombinant baculovirus at MOI of 10. The cells were incubated at 27°C for 90 min followed by addition of 20 ml SF900III medium (Invitrogen, California, US) containing 10% FBS and incubated at 27°C for 48 h. The infected Sf21 cells were daily observed for cytopathic effect (CPE) and harvested after 48 h of infection, when the CPE was ∼95%. The harvested cells were centrifuged at 1,500 × g for 10 min at 4°C, washed using PBS and stored at −80°C until further use.

Solubilization and Purification of Recombinant HEV-Protease

Extraction of HEV-protease from Sf21 cells was performed, as described earlier (Ramya et al., 2011) with some modifications. In order to solubilise the HEV-protease, 2×10^7 infected Sf21cells were resuspended in 1 ml resuspension buffer (50 mM Tris-HCl pH 8.0, 150 mM NaCl, 10% DMSO and 1% CHAPS) and incubated on ice for 30 min. The cells were sonicated for 2 min (2 s on 30 s off) at 20% amplitude on ice and incubated for 4 h at 4°C in end to end rotator. Cell lysate was centrifuged at 21,000 x g for 1 h at 4°C. Solubilized protein was purified through immobilized metal affinity chromatography (IMAC) using Ni–NTA super flow chelating agarose column (Qiagen, Germany). The column was equilibrated with buffer A (50 mM Tris-HCl, 150 mM NaCl, 0.5% CHAPS and 10 mM Imidazole pH 8.0), followed by washing with buffer B (50 mM Tris-HCl, 150 mM NaCl, 0.5% CHAPS and 20 mM Imidazole pH 8.0). The protein fraction was eluted in buffer C (50 mM Tris-HCl, 150 mM NaCl, 0.5% CHAPS and 250 mM Imidazole pH 8.0) and analyzed on 12% SDS-PAGE. Theelutes were pooled and dialyzed against PBS and analyzed by Western blot using HEV-protease epitope specific antibodies (Genscript, US) (**Table 1**).

Determination of Protease Activity by Gelatin Zymography Assay

Activity of purified recombinant HEV-protease was determined by gelatin zymography, as described earlier (Saitoh et al., 2007). Briefly 12% SDS-PAGE having 4 mg/ml gelatin was polymerized in 1 mM thickness plate. Different quantities of recombinant

HEV-protease (1–10 μg), cell lysate of uninfected cells and trypsin were loaded as negative and positive control, respectively. The gel was run at 100 Volt until separation, washed twice for 30 min at 37°C with wash buffer (2.5% Triton X-100, 50 mM Tris-HCl, pH 7.5, 5 mM $CaCl_2$ and 1 μM $ZnCl_2$) to remove SDS. The gel was rinsed twice with distilled water and incubated at 37°C in incubation buffer (1% Triton x 100, 50 mM Tris-HCl, pH 6.8, 5 mM $CaCl_2$ and 1 μM $ZnCl_2$) for 24 h. After incubation, gel was stained by coomassie brilliant blue R (CBBR) (0.5 g in 40% methanol, 10% acetic acid, and 50% distilled water). A clear zone was visualized after destaining with 40% methanol, 10% acetic acid, and 50% distilled water.

ORF1 Polyprotein Digestion Assay

The role of HEV-protease in ORF1 polyprotein processing was determined by digestion assay. Briefly, full length ORF1 polyprotein was expressed in *E. coli*. BL21 cells and purified by Ni-NTA chromatography and characterized by Western blotting using HEV epitope specific antibodies (**Table 1**). The 186 kDa protein was used as a substrate for HEV-protease. To set up digestion assay, 100 ng of ORF1 polyprotein was incubated with 1 ng of HEV-protease in 0.1 M Tris-HCl (pH 7.2) and incubated at 37°C for 1–5 h. Further, to check internal protease activity in full length ORF1, it was incubated without HEV-protease for 24 h. After incubation, protein was fractioned on SDS-PAGE and size of digested products was checked by Western blotting using epitope specific antibodies against all four enzymes present on ORF1 viz. Methyl transferase, Cysteine protease, Helicase and RdRP (**Table 1**).

Fluorescein Thiocarbamoyl-Casein Based Protease Assay

FTC-casein based assay was performed to check the activity of protease as described earlier (Twining, 1984). Fifty micrometer FTC-casein was incubated with 1 μM HEV-protease for 1–12 h at 37°C. Similar reaction was set up with trypsin as a positive control and without any protease. Protease cleaves FTC- casein into smaller, TCA-soluble, FTC-peptides. 0.5% TCA was added to the reaction mixture, to precipitate any remaining undigested FTC-casein. The supernatant was collected following centrifugation at 12,000 g at 4°C and the FTC-peptides were quantified by measuring the absorbance at 492 nm in spectrophotometer. The intensity of color estimated by the assay was found to be proportional to the total protease activity present in the sample.

Biochemical Characterization of HEV-Protease

Biochemical properties of HEV-protease were characterized through kinetic studies under varying reaction conditions like pH (4–12), temperature (4–60°C), salt concentration (0−300 mM NaCl), presence of glycerol (0–50%) and various enzyme and substrate concentration described previously (Ahmed et al., 2011). Finally apparent kinetic parameters (V_{max} and K_m) of the HEV-protease were determined by FTC-casein based protease assay. The initial velocity was measured using varying substrate concentration and the reciprocal of initial velocity and substrate concentration were plotted using Lineweaver-Burk curve to determine Briefly, Different concentration of the substrate (0.001–1.2 mM) was incubated with 1 μM HEV-protease in 4X incubation buffer (200 mM Tris-HCl, pH 7.8, 20 mM $CaCl_2$) at 37°C. To measure enzyme kinetics, absorbance was taken in multiplate reader (Bio-rad) at 492 nm for 1–12 h and initial velocity of each reaction was determined. Finally, the reaction rate was calculated using Michaelis-Menten equation (Michaelis and Menten, 1913)

$$V = Vmax\,[S]/Km + [S]$$

Vmax is the maximum rate of reaction and Km is the substrate concentration at which reaction rate is half of the obtained Vmax.

Further, the effect of various activators or divalent cations on the protease activity was examined by supplementing the reaction with 20 mM of $CuCl_2$, $NiCl_2$, $MgCl_2$, $CaCl_2$, $ZnCl_2$, $MnCl_2$, $FeCl_2$, and $PbCl_2$ as described above. Similar reaction was also performed in the presence of various types of protease inhibitors (Protease inhibitor set; G Biosciences) to determine the nature of protease by inhibition assay, Briefly, 100 μl (1 μM) HEV protease was pre-incubated with 1× protease inhibitors AEBSF, ALLN, antipain dihydro chloride, aprotonin, bestatin, chymostatin, sodium EDTA, E-64, leupeptin, pepstatin, phosphoramidon and PMSF and the inhibition assay was performed using FTC-casein. Inhibition of protease activity was measured as relative absorbance at 492 nm. For relative inhibition activity, same reaction was performed without any inhibitors. In order to validate the inhibition, ORF1 digestion was performed in presence of these inhibitors. A protease-negative control with 100 ng pORF1 was incubated in parallel under the same conditions to monitor pORF1 autolysis. These reactions were incubated for 5 h at 37°C for over-digestion. All the reactions and controls were resolved by 10% SDS-PAGE.

In silico Studies of HEV Protease

The 3D model of HEV PCP (AAL50055.1, region 432–592) was generated using homology modeling, fold recognition and threading techniques (Zhang, 2008; Roy et al., 2010; Yang et al., 2015). Initially I-TASSER was used for modeling of 161 amino acid residues; unfortunately only C-Terminal region could be modeled using 6NU9 as a template and N-Terminal region remain unmodeled. Integrated Protein Structure and Function Prediction Server IntFOLD Version 5.0 (Roche et al., 2011; McGuffin et al., 2015, 2019) was used for modeling of N-Terminal residues 432–513 Amino Acids of ORF1. Finally easy modeler was used for final model generation (Kuntal et al., 2010). The generated model was energy minimized in water using OPLS (optimized potencials for liquid simulations) force field with the convergence threshold of 0.05 by using Macromodel of Maestro (MacroModel, 2017), to remove steric clashes between atoms and to improve overall structural quality of predicted models (Sastry et al., 2013; Protein Preparation Wizard, 2017). 3D model was validated on the basis of stereochemical and geometric consideration and docking studies (Glide, 2017). The top ranked model was further validated

and analyzed based on their Ramachandran plot, Verify 3D and ERRAT analysis (Bowie et al., 1991; Lüthy et al., 1992; Laskowski et al., 1993; Colovos and Yeates, 1993). To identify possible binding sites, site map of maestro was used for binding site prediction (Halgren, 2007, 2009; SiteMap, 2017). Further, Receptor grid generation was done using Glide module. Docking study was done in using Grid based ligand docking with energetic (GLIDE) (Friesner et al., 2004, 2006; Halgren et al., 2004). The 3D model of HEV PCP was docked with inhibitors retrieved from Pubchem search. Eleven known protease inhibitors were docked against HEV-PCP structural model. The different conformations of the compounds were docked flexibly and maximum 1,000 poses per compound were generated (Ligprep, 2017). The analysis of the poses, complexes and the binding affinities between the receptor and ligands was analyzed using Schrodinger's software Glide and correlation coefficient between inhibitory concentration and docking score was calculated using "CORREL" function of MS Excel (Microsoft corp., USA).

Statistical Analysis

For enzyme kinetics, initial velocities were calculated using the linear regression function in the Microsoft Office excel software. Data was analyzed and plotted using Michaelis-Menten equation with Graph Pad Prism to obtain kinetic parameters. All the assays were performed in triplicate and results were graphed, with error bars indicating the SD. Inhibition assay data was analyzed using student's t-test $p < 0.05$ was considered statistically significant. Each experiment was performed thrice in triplicate.

DATA AVAILABILITY STATEMENT

All datasets generated for this study are included in the article/**Supplementary Material**.

AUTHOR CONTRIBUTIONS

DS conceived the study, designed the experiments and prepared the manuscript. SS designed, carried out the experiments performed the data analysis and drafted the manuscript. MC designed, carried out the insilco work and data analysis. All the authors reviewed the manuscript.

FUNDING

This study was funded by Department of Science and Technology, India SERB grant EMR/2015/00107, PI: DS and NPDF-SERB grant PDF/2016/002887, PI: SS.

ACKNOWLEDGMENTS

We thank Dr. S. Emerson for providing pSKHEV2 plasmid. The authors would like to thank Shiv Nadar University for its support and providing infrastructure to carry out this work.

SUPPLEMENTARY MATERIAL

The Supplementary Material for this article can be found online at: https://www.frontiersin.org/articles/10.3389/fcimb.2019.00478/full#supplementary-material

REFERENCES

(2017). *Glide*. New York, NY: Schrödinger, LLC.
(2017). *Ligprep*. New York, NY: Schrödinger, LLC.
(2017). *MacroModel*. New York, NY: Schrödinger, LLC.
(2017). *Maestro*. New York, NY: Schrödinger, LLC.
(2017). *Protein Preparation Wizard*. New York, NY: Schrödinger, LLC.
(2017). *SiteMap*. New York, NY: Schrödinger, LLC.
Aggarwal, R., and Naik, S. (2009). Epidemiology of hepatitis E: current status. *J. Gastroenterol. Hepatol.* 24, 1484–1493. doi: 10.1111/j.1440-1746.2009.05933.x
Agrawal, S., Gupta, D., and Panda, S. K. (2001). The 3′ end of hepatitis E virus (HEV) genome binds specifically to the viral RNA-dependent RNA polymerase (RdRp). *Virology* 282, 87–101. doi: 10.1006/viro.2000.0819
Ahmad, I., Holla, R. P., and Jameel, S. (2011). Molecular virology of hepatitis E virus. *Virus Res.* 161, 47–58. doi: 10.1016/j.virusres.2011.02.011
Ahmed, I., Anjum Zia, M., and Nasir Iqbal, H. M. (2011). Purification and kinetic parameters characterization of an alkaline protease produced from Bacillus subtilisthrough submerged fermentation technique. *World Appl. Sci. J.* 12, 751–775. doi: 10.1016/j.viruses.2011.02.011
Ansari, I. H., Nanda, S. K., Durgapal, H., Agrawal, S., Mohanty, S. K., Gupta, D., et al. (2000). Cloning, sequencing, and expression of the hepatitis E virus (HEV) nonstructural open reading frame 1 (ORF1). *J. Med. Virol.* 60, 275–283. doi: 10.1002/(SICI)1096-9071(200003)60:3<275::AID-JMV5>3.0.CO;2-9
Arasappan, A., Njoroge, F. G., Chan, T. Y., Bennett, F., Bogen, S. L., Chen, K., et al. (2005). Hepatitis C virus NS3-4A serine protease inhibitors: SAR of P'2 moiety with improved potency. *Bioorg. Med. Chem. Lett.* 15, 4180–4184. doi: 10.1016/j.bmcl.2005.06.091
Barbato, G., Cicero, D. O., Nardi, M. C., Steinkühler, C., Cortese, R., De Francesco, R., et al. (1999). The solution structure of the N-terminal proteinase domain of the hepatitis C virus (HCV) NS3 protein provides new insights into its activation and catalytic mechanism. *J. Mol. Biol.* 289, 371–384. doi: 10.1006/jmbi.1999.2745
Bazan, J. F., and Fletterick, R. J. (1988). Viral cysteine proteases are homologous to the trypsin-like family of serine proteases: structural and functional implications. *Proc. Natl. Acad. Sci. U.S.A.* 85, 7872–7876. doi: 10.1073/pnas.85.21.7872
Bendall, R., Ellis, V., Ijaz, S., Thurairajah, P., and Dalton, H. R. (2008). Serological response to hepatitis E virus genotype 3 infection: IgG quantitation, avidity, and IgM response. *J. Med. Virol.* 80, 95–101. doi: 10.1002/jmv.21033
Berg, J. M., and Shi, Y. (1996). The galvanization of biology: a growing appreciation for the roles of zinc. *Science* 271, 1081–1085. doi: 10.1126/science.271.5252.1081
Bowie, J. U., Lüthy, R., and Eisenberg, D. (1991). A method to identify protein sequences that fold into a known three-dimensional structure. *Science* 253, 164–170. doi: 10.1126/science.1853201
Cao, D., and Meng, X. J. (2012). Molecular biology and replication of hepatitis E virus. *Emerg. Microbes Infect.* 1:e17. doi: 10.1038/emi.2012.7
Chambers, A. C., Aksular, M., Graves, L. P., Irons, S. L., Possee, R. D., and King, L. A. (2018). Overview of the baculovirus expression system. *Curr. Protoc. Protein Sci.* 91, 5.4.1–5.4.6. doi: 10.1002/cpps.47
Chandra, V., Kar-Roy, A., Kumari, S., Mayor, S., and Jameel, S. (2008). The hepatitis E virus ORF3 protein modulates epidermal growth factor receptor trafficking, STAT3 translocation, and the acute-phase response. *J. Virol.* 82, 7100–7110. doi: 10.1128/JVI.00403-08
Colovos, C., and Yeates, T. O. (1993). Verification of protein structures: patterns of nonbonded atomic interactions. *Protein Sci.* 2, 1511–1519. doi: 10.1002/pro.5560020916

Coulombe, R., Grochulski, P., Sivaraman, J., Ménard, R., Mort, J. S., and Cygler, M. (1996). Structure of human procathepsin L reveals the molecular basis of inhibition by the prosegment. *EMBO J.* 15, 5492–5503. doi: 10.1002/j.1460-2075.1996.tb00934.x

Debing, Y., Moradpour, D., Neyts, J., and Gouttenoire, J. (2016). Update on hepatitis E virology: Implications for clinical practice. *J. Hepatol.* 65, 200–212. doi: 10.1016/j.jhep.2016.02.045

Emerson, S. U., Arankalle, V. A., and Purcell, R. H. (2005). Thermal stability of hepatitis E virus. *J. Infect. Dis.* 192, 930–933. doi: 10.1086/432488

Friesner, R. A., Banks, J. L., Murphy, R. B., Halgren, T. A., Klicic, J. J., Mainz, D. T., et al. (2004). Glide: a new approach for rapid, accurate docking and scoring. Method *and Assessment of Docking Accuracy. J. Med. Chem.* 7, 1739–1749. doi: 10.1021/jm0306430

Friesner, R. A., Murphy, R. B., Repasky, M. P., Frye, L. L., Greenwood, J. R., Halgren, T. A., et al. (2006). Extra precision glide: docking and scoring incorporating a model of hydrophobic enclosure for protein-ligand complexes. *J. Med. Chem.* 49, 6177–6196. doi: 10.1021/jm051256o

Gorbalenya, A. E., Donchenko, A. P., Blinov, V. M., and Koonin, E. V. (1989). Cysteine proteases of positive strand RNA viruses and chymotrypsin-like serine proteases. A *distinct protein superfamily with a common structural fold. FEBS Lett.* 243, 103–114. doi: 10.1016/0014-5793(89)80109-7

Gorbalenya, A. E., Koonin, E. V., and Lai, M. M. (1991). Putative papain-related thiol proteases of positive-strand RNA viruses. Identification of rubi- and aphthovirus proteases and delineation of a novel conserved domain associated with proteases of rubi-, alpha- and coronaviruses. *FEBS Lett.* 288, 201–205. doi: 10.1016/0014-5793(91)81034-6

Graff, J., Nguyen, H., Yu, C., Elkins, W. R., St. Claire, M., Purcell, R. H., et al. (2005). The open reading frame 3 gene of hepatitis E virus contains a cis-reactive element and encodes a protein required for infection of macaques. *J. Virol.* 79, 6680–6689. doi: 10.1128/JVI.79.11.6680-6689.2005

Guarne, A., Hampoelz, B., Glaser, W., Carpena, X., Tormo, J., Fita, I., et al. (2000). Structural and biochemical features distinguish the foot-and-mouth disease virus leader proteinase from other papain-like enzymes. *J. Mol. Biol.* 302, 1227–1240. doi: 10.1006/jmbi.2000.4115

Gupta, E., and Agarwala, P. (2018). Hepatitis E virus infection: An old virus with a new story! *Ind. J. Med. Microbiol.* 36, 317–323. doi: 10.4103/ijmm.IJMM_18_149

Halgren, T. (2007). New method for fast and accurate binding-site identification and analysis. *Chem. Biol. Drug Des.* 69, 146–148. doi: 10.1111/j.1747-0285.2007.00483.x

Halgren, T. A. (2009). Identifying and characterizing binding sites and assessing druggability. *J. Chem. Inf. Model.* 49, 377–389. doi: 10.1021/ci800324m

Halgren, T. A., Murphy, R. B., Friesner, R. A., Beard, H. S., Frye, L. L., Pollard, W. T., et al. (2004). Glide: a new approach for rapid, accurate docking and scoring. 2. Enrichment factors in database screening. *J. Med. Chem.* 47, 1750–1759. doi: 10.1021/jm030644s

Herold, J., Siddell, S. G., and Gorbalenya, A. E. (1999). A human RNA viral cysteine proteinase that depends upon a unique Zn2+-binding finger connecting the two domains of a papain-like fold. *J. Biol. Chem.* 274, 14918–14925. doi: 10.1074/jbc.274.21.14918

Hsu, J. T., Kuo, C. J., Hsieh, H. P., Wang, Y. C., Huang, K. K., Lin, C. P., et al. (2004). Evaluation of metal-conjugated compounds as inhibitors of 3CL protease of SARS-CoV. *FEBS Lett.* 574, 116–120. doi: 10.1016/j.febslet.2004.08.015

Jameel, S. (1999). Molecular biology and pathogenesis of hepatitis E virus. *Exp. Rev. Mol. Med.* 1999, 1–16. doi: 10.1017/S1462399499001271

Johne, R., Trojnar, E., Filter, M., and Hofmann, J. (2016). Thermal stability of hepatitis e virus as estimated by a cell culture method. *Appl. Environ. Microbiol.* 82, 4225–4231. doi: 10.1128/AEM.00951-16

Kamar, N., Dalton, H. R., Abravanel, F., Izopet, J. (2014). Hepatitis E virus infection. *Clin Microbiol. Rev.* 27, 116–38. doi: 10.1128/CMR.00057-13

Kanade, G. D., Pingale, K. D., and Karpe, Y. A. (2018). Activities of thrombin and factor Xa are essential for replication of hepatitis E virus and are possibly implicated in ORF1 polyprotein processing. *J. Virol.* 92:e01853-17. doi: 10.1128/JVI.01853-17

Karpe, Y. A., and Lole, K. S. (2010a). NTPase and 5′ to 3′ RNA duplex-unwinding activities of the hepatitis E virus helicase domain. *J. Virol.* 84, 3595–3602. doi: 10.1128/JVI.02130-09

Karpe, Y. A., and Lole, K. S. (2010b). RNA 5′-triphosphatase activity of the hepatitis E virus helicase domain. *J. Virol.* 84, 9637–9641. doi: 10.1128/JVI.00492-10

Keyvani-Amineh, H., Labrecque, P., Cai, F., Carstens, E. B., and Weber, J. M. (1995). Adenovirus protease expressed in insect cells cleaves adenovirus proteins, ovalbumin and baculovirus protease in the absence of activating peptide. *Virus Res.* 37, 87–97. doi: 10.1016/0168-1702(95)00018-L

Koonin, E. V., Gorbalenya, A. E., Purdy, M. A., Rozanov, M. N., Reyes, G. R., and Bradley, D. W. (1992). Computer-assisted assignment of functional domains in the nonstructural polyprotein of hepatitis E virus: delineation of an additional group of positive-strand RNA plant and animal viruses. *Proc. Natl. Acad. Sci. U.S.A.* 89, 8259–8263. doi: 10.1073/pnas.89.17.8259

Kuntal, B. K., Aparoy,. P., and Reddanna, P. (2010). EasyModeller: a graphical interface to MODELLER. *BMC Res. Notes* 3:226. doi: 10.1186/1756-0500-3-226

Laskowski, R. A., Macarthur, M. W., Moss, D. S., and Thornton, J. M. (1993). PROCHECK: a program to check the stereochemical quality of protein structures. *J. Appl. Cryst.* 26, 283–291. doi: 10.1107/S0021889892009944

Liu, X., Ropp, S. L., Jackson, R. J., and Frey, T. K. (1998). The rubella virus nonstructural protease requires divalent cations for activity and functions in trans. *J. Virol.* 72, 4463–4466.

Lowther, J., Robinson, M. W., Donnelly, S. M., Xu, W., Stack, C. M., Matthews, J. M., et al. (2009). The importance of pH in regulating the function of the *Fasciola hepatica* cathepsin L1 cysteine protease. *PLoS Negl. Trop. Dis.* 3:e369. doi: 10.1371/journal.pntd.0000369

Lüthy, R., Bowie, J. U., and Eisenberg, D. (1992). Assessment of protein models with three-dimensional profiles. *Nature* 356, 83–85. doi: 10.1038/356083a0

Lv, Z., Chu, Y., and Wang, Y. (2015). HIV protease inhibitors: a review of molecular selectivity and toxicity. *HIV AIDS* 7, 95–104. doi: 10.2147/HIV.S79956

Magden, J., Takeda, N., Li, T., Auvinen, P., Ahola, T., Miyamura, T., et al. (2001). Virus-specific mRNA capping enzyme encoded by hepatitis E virus. *J. Virol.* 75, 6249–6255. doi: 10.1128/JVI.75.14.6249-6255.2001

Matthews, D. A., Smith, W. W., Ferre, R. A., Condon, B., Budahazi, G., Sisson, W., et al. (1994). Structure of human rhinovirus 3C protease reveals a trypsin-like polypeptide fold, RNA-binding site, and means for cleaving precursor polyprotein. *Cell* 77, 761–771. doi: 10.1016/0092-8674(94)90059-0

McGuffin, L. J., Adiyaman, R., Maghrabi AHA, Shuid, A. N., Brackenridge, D. A., Nealon, J. O., et al. (2019). IntFOLD: an integrated web resource for high performance protein structure and function prediction. *Nucleic Acids Res.* 2, 408–413. doi: 10.1093/nar/gkz322

McGuffin, L. J., Atkins, J. D., Salehe, B. R., Shuid, A. N., and Roche, D. B. (2015). IntFOLD: an integrated server for modelling protein structures and functions from amino acid sequences. *Nucleic Acids Res.* 1, 69–73. doi: 10.1093/nar/gkv236

Michaelis, L., and Menten, M. L. (1913). Die Kinetik der Invertinwirkung. *Biochem. Z.* 49, 333–369.

Minuk, G. Y., Sun, A., Sun, D. F., Uhanova, J., Nicolle, L. E., Larke, B., et al. (2007). Serological evidence of hepatitis E virus infection in an indigenous North American population. *Can. J. Gastroenterol.* 21, 439–442. doi: 10.1155/2007/289059

Mushahwar, I. K. (2008). Hepatitis E virus: molecular virology, clinical features, diagnosis, transmission, epidemiology, and prevention. *J. Med. Virol.* 80, 646–658. doi: 10.1002/jmv.21116

Nair, V. P., Anang, S., Subramani, C., Madhvi, A., Bakshi, K., Srivastava, A., et al. (2016). Endoplasmic reticulum stress induced synthesis of a novel viral factor mediates efficient replication of genotype-1 hepatitis E virus. *PLoS Pathog.* 12:e1005521. doi: 10.1371/journal.ppat.1005521

Nan, Y., and Zhang, Y. J. (2016). Molecular biology and infection of hepatitis E virus. *Front. Microbiol.* 7:1419. doi: 10.3389/fmicb.2016.01419

Navaneethan, U., Al Mohajer, M., and Shata, M. T. (2008). Hepatitis E and pregnancy: understanding the pathogenesis. *Liver Int.* 28, 1190–1199. doi: 10.1111/j.1478-3231.2008.01840.x

Neurath, H. (1984). Evolution of proteolytic enzymes. *Science* 224, 350–357. doi: 10.1126/science.6369538

Paliwal, D., Panda, S. K., Kapur, N., Varma, S. P., and Durgapal, H. (2014). Hepatitis E virus (HEV) protease: a chymotrypsin-like enzyme that processes both non-structural (pORF1) and capsid (pORF2) protein. *J. Gen. Virol.* 95(Pt. 8), 1689–1700. doi: 10.1099/vir.0.066142-0

Panda, S. K., Ansari, I. H., Durgapal, H., Agrawal, S., and Jameel, S. (2000). The in vitro-synthesized RNA from a cDNA clone of hepatitis E virus is infectious. *J. Virol.* 74, 2430–2437. doi: 10.1128/JVI.74.5.2430-2437.2000

Parvez, M. K. (2013). Molecular characterization of hepatitis E virus ORF1 gene supports a papain-like cysteine protease (PCP)-domain activity. *Virus Res.* 178, 553–556. doi: 10.1016/j.virusres.2013.07.020

Parvez, M. K. (2017). The hepatitis E virus nonstructural polyprotein. *Future Microbiol.* 12, 915–924. doi: 10.2217/fmb-2017-0016

Parvez, M. K., and Khan, A. A. (2014). Molecular modeling and analysis of hepatitis E virus (HEV) papain-like cysteine protease. *Virus Res.* 179, 220–224. doi: 10.1016/j.virusres.2013.11.016

Ramya, R., Mohana Subramanian, B., Sivakumar, V., Senthilkumar, R. L., Sambasiva Rao, K. R., and Srinivasan, V. A. (2011). Expression and solubilization of insect cell-based rabies virus glycoprotein and assessment of its immunogenicity and protective efficacy in mice. *Clin. Vaccine Immunol.* 18, 1673–1679. doi: 10.1128/CVI.05258-11

Richau, K. H., Kaschani, F., Verdoes, M., Pansuriya, T. C., Niessen, S., Stüber, K., et al. (2012). Subclassification and biochemical analysis of plant papain-like cysteine proteases displays subfamily-specific characteristics. *Plant Physiol.* 158, 1583–1599. doi: 10.1104/pp.112.194001

Roche, D. B., Buenavista, M. T., Tetchner, S. J., and McGuffin, L. J. (2011). The IntFOLD server: an integrated web resource for protein fold recognition, 3D model quality assessment, intrinsic disorder prediction, domain prediction and ligand binding site prediction. *Nucleic Acids Res.* 39, 171–176. doi: 10.1093/nar/gkr184

Ropp, S. L., Tam, A. W., Beames, B., Purdy, M., and Frey, T. K. (2000). Expression of the hepatitis E virus ORF1. *Arch. Virol.* 145, 1321–1337. doi: 10.1007/s007050070093

Roy, A., Kucukural, A., and Zhang, Y. (2010). I-TASSER: a unified platform for automated protein structure and function prediction. *Nat. Protoc.* 5, 725–738. doi: 10.1038/nprot.2010.5

Saha, A., Acharya, B. N., Priya, R., Tripathi, N. K., Shrivastava, A., Rao, M. K., et al. (2018). Development of nsP2 protease based cell free high throughput screening assay for evaluation of inhibitors against emerging Chikungunya virus. *Sci. Rep.* 8:10831. doi: 10.1038/s41598-018-29024-2

Saitoh, E., Yamamoto, S., Okamoto, E., Hayakawa, Y., Hoshino, T., Sato, R., et al. (2007). Identification of cysteine proteases and screening of cysteine protease inhibitors in biological samples by a two-dimensional gel system of zymography and reverse zymography. *Anal. Chem. Insights* 2, 51–59. doi: 10.4137/117739010700200011

Sali, D. L., Ingram, R., Wendel, M., Gupta, D., McNemar, C., Tsarbopoulos, A., et al. (1998). Serine protease of hepatitis C virus expressed in insect cells as the NS3/4A complex. *Biochemistry* 37, 3392–3340. doi: 10.1021/bi972010r

Sastry, G. M., Adzhigirey, M., Day, T., Annabhimoju, R., and Sherman, W. (2013). Protein and ligand preparation: parameters, protocols, and influence on virtual screening enrichments. *J. Comput. Aid Mol. Des.* 27, 221–234. doi: 10.1007/s10822-013-9644-8

Sehgal, D., Thomas, S., Chakraborty, M., and Jameel, S. (2006). Expression and processing of the Hepatitis E virus ORF1 nonstructural polyprotein. *Virol. J.* 3:38. doi: 10.1186/1743-422X-3-38

Stempniak, M., Hostomska, Z., Nodes, B. R., and Hostomsky, Z. (1997). The NS3 proteinase domain of hepatitis C virus is a zinc-containing enzyme. *J. Virol.* 71, 2881–2886.

Sundararaj, S., Singh, D., Saxena, A. K., Vashisht, K., Sijwali, P. S., Dixit, R., et al. (2012). The ionic and hydrophobic interactions are required for the auto activation of cysteine proteases of Plasmodium falciparum. *PLoS ONE* 7:e47227. doi: 10.1371/journal.pone.0047227

Tam, A. W., Smith, M. M., Guerra, M. E., Huang, C. C., Bradley, D. W., Fry, K. E., et al. (1991). Hepatitis E virus (HEV): molecular cloning and sequencing of the full-length viral genome. *Virology* 185, 120–131. doi: 10.1016/0042-6822(91)90760-9

Tanaka, T., Takahashi, M., Kusano, E., and Okamoto, H. (2007). Development and evaluation of an efficient cell-culture system for hepatitis E virus. *J. Gen. Virol.* 88, 903–911. doi: 10.1099/vir.0.82535-0

Tsarev, S. A., Emerson, S. U., Reyes, G. R., Tsareva, T. S., Legters, L. J., Malik, I. A., et al. (1992). Characterization of a prototype strain of hepatitis E virus. *Proc. Natl. Acad. Sci. U.S.A.* 89, 559–563. doi: 10.1073/pnas.89.2.559

Turk, B. E., Huang, L. L., Piro, E. T., and Cantley, L. C. (2001). Determination of protease cleavage site motifs using mixture-based oriented peptide libraries. *Nat. Biotechnol.* 19, 661–667. doi: 10.1038/90273

Twining, S. S. (1984). Fluorescein isothiocyanate-labeled casein assay for proteolytic enzymes. *Anal. Biochem.* 143, 30–34. doi: 10.1016/0003-2697(84)90553-0

Urbani, A., Bazzo, R., Nardi, M. C., Cicero, D. O., De Francesco, R., Steinkühler, C., et al. (1998). The metal binding site of the hepatitis C virus NS3 protease. A spectroscopic investigation. *J. Biol. Chem.* 273, 18760–18769. doi: 10.1074/jbc.273.30.18760

Verma, S., Dixit, R., and Pandey, K. C. (2016). Cysteine proteases: modes of activation and future prospects as pharmacological targets. *Front. Pharmacol.* 7:107. doi: 10.3389/fphar.2016.00107

Yamada, K., Takahashi, M., Hoshino, Y., Takahashi, H., Ichiyama, K., Nagashima, S., et al. (2009). ORF3 protein of hepatitis E virus is essential for virion release from infected cells. *J. Gen. Virol.* 90, 1880–1891. doi: 10.1099/vir.0.010561-0

Yang, J., Yan, R., Roy, A., Xu, D., Poisson, J., and Zhang, Y. (2015). The I-TASSER suite: protein structure and function prediction. *Nat. Methods* 12, 7–8. doi: 10.1038/nmeth.3213

Yu, S. F., and Lloyd, R. E. (1992). Characterization of the roles of conserved cysteine and histidine residues in poliovirus 2A protease. *Virology* 186, 725–735. doi: 10.1016/0042-6822(92)90039-R

Zhang, Y. (2008). I-TASSER server for protein 3D structure prediction. *BMC Bioinformatics* 9:40. doi: 10.1186/1471-2105-9-40

Zhou, Y., Tzeng, W. P., Yang, W., Zhou, Y., Ye, Y., Lee, H. W., et al. (2007). Identification of a Ca2+-binding domain in the rubella virus nonstructural protease. *J. Virol.* 81, 7517–7528. doi: 10.1128/JVI.00605-07

Ziebuhr, J., Schelle, B., Karl, N., Minskaia, E., Bayer, S., Siddell, S. G., et al. (2007). Human coronavirus 229E papain-like proteases have overlapping specificities but distinct functions in viral replication. *J. Virol.* 81, 3922–3932. doi: 10.1128/JVI.02091-06

Conflict of Interest: The authors declare that the research was conducted in the absence of any commercial or financial relationships that could be construed as a potential conflict of interest.

frontiers in Cellular and Infection Microbiology

MINI REVIEW
published: 04 February 2020
doi: 10.3389/fcimb.2020.00032

The Heat Stability of Hepatitis B Virus: A Chronological Review From Human Volunteers and Chimpanzees to Cell Culture Model Systems

Jochen Steinmann[1]*, *Joerg Steinmann*[2,3] *and Eike Steinmann*[4]

[1] Brill + Partner GmbH Institute for Hygiene and Microbiology, Bremen, Germany, [2] Institute of Medical Microbiology, University Hospital of Essen, Essen, Germany, [3] Institute of Clinical Hygiene, Medical Microbiology and Infectiology, General Hospital Nürnberg, Paracelsus Medical University, Nuremberg, Germany, [4] Department for Molecular and Medical Virology, Faculty of Medicine, Ruhr University Bochum, Bochum, Germany

OPEN ACCESS

Edited by:
Milan Surjit,
Translational Health Science and Technology Institute (THSTI), India

Reviewed by:
Vijay Kumar,
Institute of Liver and Biliary Sciences, India
Perumal Vivekanandan,
Indian Institute of Technology Delhi, India
Ravi Jhaveri,
Northwestern University Feinberg School of Medicine, United States

***Correspondence:**
Jochen Steinmann
jochen.steinmann@brillhygiene.com

Specialty section:
This article was submitted to Clinical Microbiology, a section of the journal Frontiers in Cellular and Infection Microbiology

Received: 11 October 2019
Accepted: 17 January 2020
Published: 04 February 2020

Citation:
Steinmann J, Steinmann J and Steinmann E (2020) The Heat Stability of Hepatitis B Virus: A Chronological Review From Human Volunteers and Chimpanzees to Cell Culture Model Systems.
Front. Cell. Infect. Microbiol. 10:32.
doi: 10.3389/fcimb.2020.00032

During the World War II jaundice and hepatitis in the US army were observed after vaccination with the yellow fever vaccine containing human plasma for stabilization. This led to first heat experiments with volunteers without knowledge of the causative agents. Finally, experiments of human serum with volunteers and chimpanzees led to the conclusion that the hepatitis B virus (HBV) which had been identified as the responsible agent of the contamination of the vaccine, could not be inactivated at 98°C after 1 min, whereas 2 min in two chimpanzees were enough. Meanwhile, a cell culture system became available showing that 2 min exposure time is not enough depending on the virus strain used whereas 5 min means complete inactivation of HBV. The great stability of the blood-borne HBV was also of interest in hospital hygiene due to the use of moist heat for disinfection of heat-stable medical devices in washer-disinfectants. The requirements for washer-disinfectors and the parameters describing disinfection with moist heat are defined in the EN ISO 15883. In this standard, the efficacy of this thermal disinfection is described by the A_0 value. For heat-resistant viruses a higher A_0 = 3,000 is often recommended including semi-critical instruments that undergo thermal disinfection and no final sterilization. All experiments including volunteers, chimpanzees and now cell culture were performed with greater A_0 values than 3,000. Therefore, an A_0 value of 3,000 e.g., being reached by 90°C and 5 min in washer-disinfectants, can easily elevated to 6,000 by prolongation of the exposure time to 10 min. In contrast to the different laboratory experiments with high virus titers it should be considered that in practice the necessary cleaning step upfront will help to reduce virus load and then protect the personnel in the medical area.

Keywords: hepatitis B virus, thermostability, inactivation, cell culture, moist heat, A0 value

HBV AND THERMAL DISINFECTION

Despite the availability of vaccination, infections with hepatitis B virus (HBV) are still a severe global health burden, with ~2 billion infected individuals and more than 250 million carriers worldwide. HBV, a small, enveloped, hepatotropic DNA virus is the major cause of chronic liver diseases, the primary causative agent of hepatocellular carcinoma (HCC) and responsible

for 887,000 deaths worldwide annually (WHO, 2017). Chronic hepatitis B (CHB) is still an incurable disease.

HBV is highly contagious circulating in patients' blood with a minimal infectious dose of only 10 genomes (Komiya et al., 2008). Healthcare workers are at constant risk of acquiring HBV infection from occupational exposure. Moreover, nosocomial transmissions of HBV with an increasing number of outbreaks have been reported worldwide over the past few years. Common routes of HBV transmission include the use of multi-dose vials (Fisker et al., 2006; Sauerbrei, 2014), dental or biopsy equipment (Drescher et al., 1994), dialysis unit (Carrilho et al., 2004), contaminated finger-stick devices (Bender et al., 2012; Lanini et al., 2012), acupuncture needles (Walsh et al., 1999), reuse of syringes (Thompson et al., 2009), endoscopes (Santos et al., 2004) and unsafe surgical and injection procedures (Welch et al., 1989; Goldmann, 2002; Buster et al., 2003; Redd et al., 2007). Most of these HBV infections remain clinically asymptomatic and are not immediately recognized by medical personnel.

HBV can survive and remain infectious on environmental surfaces for at least 7 days (Bond et al., 1981). Since moist heat is known to kill microorganisms including viruses, thermal disinfection in the hospital for decontamination of heat-stable reusable medical devices is an essential process in the prevention of nosocomial infections including HBV. After a cleaning step, the thermal disinfection of medical devices is running in automated washer-disinfectors machines.

The requirements for washer-disinfectors and the parameters describing disinfection with moist heat are defined in the European (EN) and International Organization for Standardization (ISO) 15883 (*DIN EN ISO 15883-2:2009-09*)[1]. In this standard, the efficacy of this thermal disinfection is described by the A_0 value. The A_0 value is defined as $\Sigma 10^{(T-80)/z} \times \Delta t$. This value is based on exposure times and temperatures necessary for inactivation of microorganisms with a defined z value. By this, various time-temperature relationships can be compared. A low value of $A_0 = 60$ is regarded as minimum for devices coming into contact with intact skin and pathogens like heat-sensitive viruses, whereas $A_0 = 600$ is necessary for surgical instruments (*DIN EN ISO 15883-2:2009-09*)[1]. For heat-resistant viruses a higher $A_0 = 3{,}000$ is often recommended including semi-critical instruments that undergo thermal disinfection and no final sterilization (Röhm-Rodowald et al., 2013). In the past, the conclusion that a high A_0 value = 3,000 must be chosen if an efficacy against heat-resistant viruses such as HBV is necessary was questioned (Rosenberg, 2003). Furthermore, in the discussion of the necessary A_0 value for heat resistance viruses it also has to be considered that the amount of HBV in the human serum of chronic carriers can be very high and is not part of the A_0 value. Virus titers up to 10^9/mL HBV DNA copies can be found in sera of patients. However, disinfection is always performed after a cleaning step which should reduce the number of microorganisms on the instruments by some orders of magnitude. This reduction has important consequence for the requirements of thermal heating. Moreover, this is a very important step for the protection of processing personnel (Rosenberg, 2003). However, before the concept of the DIN EN ISO 15883 was established the choice of biological indicators was the basis of describing general requirements regarding disinfection with moist heat in washer-disinfectors. The high thermal resistance of HBV as a blood-borne virus was already a key question when the A_0 concept was introduced first.

[1]DIN EN ISO 15883-2:2009-09: Washer-disinfectors - Part 2: Requirements and tests for washer-disinfectors employing thermal disinfection for surgical instruments, anaesthetic equipment, bowls, dishes, receivers, utensils, glassware, etc. DIN 15883-2 (2009).

A HISTORICAL OVERVIEW OF THE THERMOSTABILITY OF HBV

A recent study described the heat stability of HBV resulting from cell culture assays under defined laboratory conditions (König et al., 2019). The reported data on heat-resistant HBV were the first using patient-derived viruses and a HBV cell culture model system in parallel. These results are important for the requirements of thermal disinfection in washer-disinfectors using moist heat. All other data which are already used for recommendations of thermal disinfection in the past were based on experiments with human volunteers and chimpanzees due to the lack of a suitable cell culture system. Therefore, the comprehensive story of heat stability of HBV can be continued and perhaps finished.

Our first knowledge of HBV heat stability started with several experiments with human volunteers after jaundice and hepatitis occurring after yellow fever vaccination in World War II. A vaccine might contain viruses if blood-products like plasma were used for production. Already in 1885, Lürmann described vaccination against smallpox glycerinised with human lymph in a shipyard in Bremen resulting in 191 men becoming jaundiced within 2–8 months (Lürmann, 1885). This was one of the first observations in the nineteenth century without knowledge of the etiologic agent that blood containing products like vaccines were responsible for epidemic transmission of homologous serum hepatitis (**Figure 1**). Another large outbreak was then described by the office of the Surgeon General of the US army in April 1942 (Office of the Surgeon General, 1942). At that time cases of jaundice and hepatitis occurred in US military personnel who received yellow fever vaccine during World War II. The observed symptoms were linked to a specific lot of vaccine named 17D (Oliphant et al., 1943; Neefe et al., 1944a). An experiment with nine volunteers for confirmation and detailed clinical observations followed (Neefe et al., 1944b). Finally, 23,664 cases of hepatitis in Armed Forces personnel were reported in 1944 (Sawyer et al., 1944). In parallel, identical observations after vaccination were made in Brazil (Fox et al., 1942). At that time human immune serum was used to stabilize the vaccine after being heating at 56°C for 30–60 min. Consequently, the use of human serum in vaccine production was stopped. In a review describing mortality and morbidity among military personnel between 1930 and the end of World War II after yellow fever vaccination in total 49,233 cases of jaundice or hepatitis were reported among US troops (Thomas et al., 2013). Consequently, studies with volunteers were initiated to examine

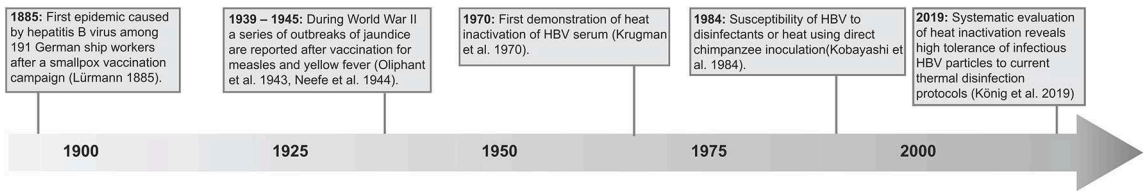

FIGURE 1 | Timeline of landmarks HBV transmission and inactivation studies.

the effect of heat to the unknown agent of homologous serum hepatitis. Sawyer et al. (1944) and MacCallum and Bauer (1944) confirmed that heating at 56°C for 30–60 min was not enough for complete inactivation of the responsible agent. At that time the agent was described as filterable and resistant to heating to 56°C for 30 min (Havens, 1945). In contrast, the virus of the homologous serum hepatitis appeared to be inactivated in a human albumin solution at 60 and 64°C for 10 h (Gellis et al., 1948). Later, this activity by heating against HBV was not confirmed by Shikata et al. showing that heat treatment at 60°C for 10 h provided only a four $\log_{10}$ reduction of virus titer, but no complete inactivation when inoculated in chimpanzees (Shikata et al., 1978). In addition, introducing a shortage of incubation time at 60°C to 4 h samples of plasma containing the agent of homologous serum hepatitis also retained the ability to produce hepatitis in volunteers (Murray and Diefenbach, 1953). Finally, the studies of Krugman et al. at the Willowbrook State School for mentally disabled children in 1970 when describing two types of hepatitis MS-1 and MS-2, HBV serum underwent heat inactivation at 98°C for 1 min after 43 s of heat-up time in a flask over an electric burner (**Figure 1**). After cooling to room temperature in 25 min, serum was inoculated (0.1 mL) to each of 29 volunteers (Krugman et al., 1970). The titer was given as $10^{7.5}$ chimpanzee infective dose $(CID)_{50}$ mL before 1:10 dilution and inoculation of 0.1 mL. Later, the A_0 value for this experiment was calculated to a value of 3,786 (Uetera et al., 2010). The data showed no evidence of infection clinically or in the laboratory tests available in this year. But in 1979, a more sensitive test (radioimmunoassay) revealed three subclinically infected volunteers without liver involvement. At that time the frozen sera were re-examined for HBsAg (Krugman et al., 1979).

In another experiment serum with subtype adr of HBV after 1:1,000 dilutions was treated at 98°C for 2 min after 4 min of heat-up time in a thermostat bath. After cooling in an ice-water bath the sample was inoculated two chimpanzees without any evidence of infection (Kobayashi et al., 1984). The calculated A_0 value for this moist heat treatment of 10^5 CIC_{50}/mL was 7,571 following the calculation of Uetera et al. (2010).

To confirm or disprove the data of Krugman et al. and Kobayashi et al. it was recently shown with a newly developed HBV cell culture system that cell culture-derived virus was still detectable after 2 min incubation at 98°C (**Figure 1**). The tests were run in thin-wall PCR tubes in a thermal cycler with immediate cooling to ice (König et al., 2019). Inactivation profiles of three HBV isolates from patients showed that one isolate was inactivated after 1 min, whereas the isolates from the two other patients could not be inactivated after 2 min exposure time. After treatment at 98°C for 5 min no virus infection was detectable testing all isolates (König et al., 2019).

The difference between the data from human volunteers, chimpanzees, and cell culture might partly be derived from the technical standard used in the laboratories at different times. In 1970, the heating was performed with an electric burner with 43 s of heat-up time and cooling down time within 25 min before inoculation of the volunteers (Krugman et al., 1970). In 1984, the heating was performed in a bath of liquid paraffin after 4 min heat-up time and a rapidly cooling in an ice-water bath before chimpanzees were inoculated (Kobayashi et al., 1984). In the recent study in 2019 with cell culture, thermo heaters were used which allowed a more precise control of all parameters used compared to those in the past (König et al., 2019).

Furthermore, it cannot be excluded, that different virus strains/genotypes influence thermal stability, since the different studies used various virus strains. Krugman et al. used the MS-2 strain, while Kobayashi et al. performed the experiments with the JTB001 strain (subtypes adr) in 1984. In the recent study, the different virus isolates from the patient material were genotype C, whereas the other viruses derived from HepAD38 cells were genotype D.

Besides the technical changes described and the different viruses incorporated, the HBV titers will influence the results in the largest extent. In the voluntary active immunization of volunteers, a 1:10 dilution of an infectivity titer of $10^{7.5}$ was used (Krugman et al., 1970). Both chimpanzees received a 1:1,000 dilutions of a serum with 10^8 units/mL (Kobayashi et al., 1984). In the recently published study of Koenig et al. virus titers ranged from 5.8×10^{10} GEq/mL (genome equivalent) for the cell culture virus to 1.1×10^7 to 5.5×10^9 GEq/mL for patient-derived viruses.

Uetera et al. calculated that the A_0 value was 3,786 when the experiments with the volunteers at the Willowbrook State School were performed (Uetera et al., 2010). Here no complete inactivation was observed after 1 min exposure time. In the chimpanzee infection model with 2 min exposure the A_0 reached 7,571 thus confirming virus inactivation. Concerning the failure in the study at the Willowbrook State School in comparison to the chimpanzee model, it was argued that the serum infectivity titer of the human volunteer study was more than 30 times higher than that used in the animal model (Uetera et al., 2010). In the study

of Koenig et al. an A_0 value resulted of 5,400 without complete abrogation of infectivity within 2 min exposure time using high titers for the cell culture and the patient-derived viruses.

Nowadays, the capacity of washer-disinfectors must be not less than $A_0 = 3{,}000$ and at least $A_0 = 600$ (*DIN EN ISO 15883-2:2009-09*)[1]. In summary, all experiments reviewed here with volunteers, chimpanzees and cell culture models now confirm a necessary A_0 value of >3,000. An A_0 value of 3,000 in washer-disinfectors is often reached by 90°C and 5 min exposure time. After prolongation to 10 min an A_0 value of 6,000 can be reached. Furthermore, the material compatibility must additionally be considered and the important fact that a cleaning step up front is included which also will increase the safety of the staff thus lowering a possible viral contamination with HBV (Röhm-Rodowald et al., 2013).

CONCLUSION

In conclusion, there are data available derived from volunteers and chimpanzees concerning the heat stability of HBV in serum under not ideally defined conditions. A newly developed cell culture system should allow more precise information on this characteristic of an important virus in human medicine. The pronounced heat stability after experiments with volunteers and chimpanzees in the past was even surpassed. Finally, the still ongoing discussion on thermal stability of HBV with consequences for moist heat disinfection can be finished.

AUTHOR CONTRIBUTIONS

ES, JocS, and JoeS drafted the article.

FUNDING

JocS and ES were supported by a grant from the Deutsche Gesellschaft für Krankenhaushygiene e.V. (DGKH).

ACKNOWLEDGMENTS

We thank Dr. Yannick Brüggemann for critically reading the manuscript and Dr. Daniel Todt and Mathias Kunzmann for discussion.

REFERENCES

Bender, T. J., Wise, M. E., Utah, O., Moorman, A. C., Sharapov, U., Drobeniuc, J., et al. (2012). Outbreak of hepatitis B virus infections associated with assisted monitoring of blood glucose in an assisted living facility-Virginia, 2010. *PLoS ONE* 7:e50012. doi: 10.1371/journal.pone.0050012

Bond, W. W., Favero, M. S., Petersen, N. J., Gravelle, C. R., Ebert, J. W., Maynard, J. E., et al. (1981). Survival of hepatitis B virus after drying and storage for one week. *Lancet* 317, 550–551. doi: 10.1016/S0140-6736(81)92877-4

Buster, E. H., van der Eijk, A. A., and Schalm, S. W. (2003). Doctor to patient transmission of hepatitis B virus: implications of HBV DNA levels and potential new solutions. *Antiviral Res.* 60, 79–85. doi: 10.1016/j.antiviral.2003.08.014

Carrilho, F. J., Moraes, C. R., Pinho, J. R., Mello, I. M., Bertolini, D. A., Lemos, M. F., et al. (2004). Hepatitis B virus infection in haemodialysis centres from Santa Catarina State, Southern Brazil. Predictive risk factors for infection and molecular epidemiology. *BMC Public Health* 4:13. doi: 10.1186/1471-2458-4-13

Drescher, J., Wagner, D., Flik, J., Stachan-Kunstyr, R., Verhagen, W., Haverich, A., et al. (1994). Nosocomial hepatitis B virus infections in cardiac transplant recipients transmitted during transvenous endomyocardial biopsy. *J. Hosp. Infect.* 26, 81–92. doi: 10.1016/0195-6701(94)90049-3

Fisker, N., Carlsen, N. L. T., Kolmos, H. J., Tønning-Sørensen, L., Høst, A., and Christensen, P. B. (2006). Identifying a hepatitis B outbreak by molecular surveillance: a case study. *BMJ* 332, 343–345. doi: 10.1136/bmj.332.7537.343

Fox, J. P., Manso, C., Penna, H. A., and Para, M. (1942). Observations on the occurrence of icterus in Brazil following vaccination against yellow fever. *Am. J. Epidemiol.* 36, 68–116. doi: 10.1093/oxfordjournals.aje.a118810

Gellis, S. S., Neefe, J. R., Stokes, J. Jr., Strong, L. E., Janeway, C. A., and Scatchard, G. (1948). Chemical, clinical, and immunological studies on the products of human plasma fractionation. XXXVI. Inactivation of the virus of homologous serum hepatitis in solutions of normal human serum albumin by means of heat. *J. Clin. Invest.* 1948, 239–244. doi: 10.1172/JCI101939

Goldmann, D. A. (2002). Blood-borne pathogens and nosocomial infections. *J. Allergy Clin. Immunol.* 110, S21–S26. doi: 10.1067/mai.2002.125337

Havens, W. P. (1945). Properties of the etiologic agent of infectious hepatitis. *Exp. Biol. Med.* 58, 203–204. doi: 10.3181/00379727-58-14897

Kobayashi, H., Tsuzuki, M., Koshimizu, K., Toyama, H., Yoshihara, N., Shikata, T., et al. (1984). Susceptibility of hepatitis B virus to disinfectants or heat. *J. Clin. Microbiol.* 20, 214–216. doi: 10.1128/JCM.20.2.214-216.1984

Komiya, Y., Katayama, K., Yugi, H., Mizui, M., Matsukura, H., Tomoguri, T., et al. (2008). Minimum infectious dose of hepatitis B virus in chimpanzees and difference in the dynamics of viremia between genotype A and genotype C. *Transfusion* 48, 286–294. doi: 10.1111/j.1537-2995.2007.01522.x

König, A., Than, T. T., Todt, D., Yoon, S. K., Steinmann, J., Steinmann, E., et al. (2019). High tolerance of hepatitis B virus to thermal disinfection. *J. Hepatol.* 71, 1249–1251. doi: 10.1016/j.jhep.2019.08.022

Krugman, S., Giles, J. P., and Hammond, J. (1970). Hepatitis virus: effect of heat on the infectivity and antigenicity of the MS-1 and MS-2 strains. *J. Infect. Dis.* 122, 432–436. doi: 10.1093/infdis/122.5.432

Krugman, S., Overby, L. R., Mushahwar, I. K., Ling, C. M., Frösner, G. G., and Deinhardt, F. (1979). Viral hepatitis, type B. Studies on natural history and prevention re-examined. *N. Engl. J. Med.* 300, 101–106. doi: 10.1056/NEJM197901183000301

Lanini, S., Garbuglia, A. R., Puro, V., Solmone, M., Martini, L., Arcese, W., et al. (2012). Hospital cluster of HBV infection: molecular evidence of patient-to-patient transmission through lancing device. *PLoS ONE* 7:e33122. doi: 10.1371/journal.pone.0033122

Lürmann, A. (1885). Eine Ikterusepidemie. *Berlin. Klin. Wschr.* 12, 20–23.

MacCallum, F. O., and Bauer, D. J. (1944). Homologous serum jaundice transmission experiments with human volunteers. *Lancet* 243, 622–627. doi: 10.1016/S0140-6736(00)74842-2

Murray, R., and Diefenbach, W. C. (1953). Effect of heat on the agent of homologous serum hepatitis. *Proc. Soc. Biol. Med.* 84, 230–231. doi: 10.3181/00379727-84-20599

Neefe, J. R., Miller, T., and Chornock, F. W. (1944a). Homologous serum jaundice. A review of the literature and report of a case. *Am. J. Med. Sci.* 207, 626–638. doi: 10.1097/00000441-194405000-00007

Neefe, J. R., Stokes, J., Reinhold, J. G., and Lukens, F. D. (1944b). Hepatitis due to the injection of homologous blood products in human volunteers. *J. Clin. Invest.* 23, 836–855. doi: 10.1172/JCI101557

Office of the Surgeon General (1942). Circular letter No. 95. Outbreak of jaundice in the army. *JAMA* 120:51.

Oliphant, J. W., Gilliam, A. G., and Larson, C. L. (1943). Jaundice following administration of human serum. *Public Health Reo* 58, 1233–1237. doi: 10.2307/4584567

Redd, J. T., Baumbach, J., Kohn, W., Nainan, O., Khristova, M., and Williams, I. (2007). Patient-to-patient transmission of hepatitis B virus associated with oral surgery. *J. Infect. Dis.* 195, 1311–1314. doi: 10.1086/513435

Röhm-Rodowald, E., Jakimiak, B., Chojecka, A., Wiercinska, O., Ziemba, B., and Kanclerski, K. (2013). Recommendations for thermal disinfection based on the A0 concept according to EN ISO 15883. *Przegl. Epidemiol.* 67, 687–690.

Rosenberg, U. (2003). Thermal disinfection – the A_0 concept and the biological background. *Cent. Serv.*11, 118–120. doi: 10.1054/arth.2003.50108

Santos, N. C., Pinho, J. R. R., Lemos, M. F., Moreira, R. C., Lopes, C. M. C., Sacilotto, M. T. J., et al. (2004). Risk of hepatitis B virus transmission by diagnostic hysteroscopy. *Braz. J. Med. Biol. Res.* 37, 683–689. doi: 10.1590/S0100-879X2004000500009

Sauerbrei, A. (2014). Is hepatitis B-virucidal validation of biocides possible with the use of surrogates? *World J. Gastroenterol.* 20, 436–444. doi: 10.3748/wjg.v20.i2.436

Sawyer, W. A., Meyer, K. F., Eaton, M. D., Bauer, J. H., Putnam, P., and Schwentker, F. F. (1944). Jaundice in army personnel in the western region of the United States and its relation to vaccination against yellow fever: (Part I, II, III and IV). *Am. J. Epidemiol.* 40, 35–107. doi: 10.1093/oxfordjournals.aje.a118977

Shikata, T., Karasawa, T., Abe, K., Takahashi, T., Mayumi, M., and Oda, T. (1978). Incomplete inactivation of hepatitis B virus after heat treatment at 60 C for 10 hours. *J. Infect. Dis.* 138, 242–244. doi: 10.1093/infdis/138.2.242

Thomas, R. E., Lorenzetti, D. L., and Spragins, W. (2013). Mortality and morbidity among military personnel and civilians during the 1930s and World War II from transmission of hepatitis during yellow fever vaccination: systematic review. *Am. J. Public Health* 103, e16–29. doi: 10.2105/AJPH.2012.301158

Thompson, N. D., Perz, J. F., Moorman, A. C., and Holmberg, S. D. (2009). Nonhospital health care-associated hepatitis B and C virus transmission: United States, 1998-2008. *Ann. Intern. Med.* 150, 33–39. doi: 10.7326/0003-4819-150-1-200901060-00007

Uetera, Y., Kawamura, K., Kobayashi, H., Saito, Y., Yasuhara, H., and Saito, R. (2010). Studies on viral disinfection: an evaluation of moist heat disinfection for HBV by using A0 concept defined in ISO 15883-washer-disinfectors. *PDA J. Pharm. Sci. Technol.* 64, 327–336.

Walsh, B., Maguire, H., and Carrington, D. (1999). Outbreak of hepatitis B in an acupuncture clinic. *Commun. Dis. Public Health* 2, 137–140. doi: 10.1111/j.1752-0606.1999.tb01117.x

Welch, J., Webster, M., Tilzey, A. J., Noah, N. D., and Banatvala, J. E. (1989). Hepatitis B infections after gynaecological surgery. *Lancet* 1, 205–207. doi: 10.1016/S0140-6736(89)91213-0

WHO (2017). *Global Hepatitis Report, 2017*. Geneva: World Health Organization.

Conflict of Interest: JocS was employed by Brill + Partner GmbH.

The remaining authors declare that the research was conducted in the absence of any commercial or financial relationships that could be construed as a potential conflict of interest.

frontiers in Cellular and Infection Microbiology

ORIGINAL RESEARCH
published: 27 February 2020
doi: 10.3389/fcimb.2020.00074

E-cadherin Plays a Role in Hepatitis B Virus Entry Through Affecting Glycosylated Sodium-Taurocholate Cotransporting Polypeptide Distribution

Qin Hu[1,2†], Feifei Zhang[1†], Liang Duan[1], Bo Wang[1], Yuanyuan Ye[1], Pu Li[1], Dandan Li[1], Shengjun Yang[1], Lan Zhou[2] and Weixian Chen[1*]*

[1] Department of Laboratory Medicine, The Second Affiliated Hospital of Chongqing Medical University, Chongqing, China, [2] Key Laboratory of Laboratory Medical Diagnostics of Ministry of Education, Chongqing Medical University, Chongqing, China

Hepatitis B virus (HBV) infection is a major cause of chronic liver disease and hepatocellular carcinoma. Current antiviral therapy does not effectively eradicate HBV and further investigations into the mechanisms of viral infection are needed to enable the development of new therapeutic agents. The sodium-taurocholate cotransporting polypeptide (NTCP) has been identified as a functional receptor for HBV entry in liver cells. However, the NTCP receptor is not sufficient for entry and other membrane proteins contribute to modulate HBV entry. This study seeks to understand how the NTCP functions in HBV entry. Herein we show that knockdown of the cell-cell adhesion molecule, E-cadherin significantly reduced infection by HBV particles and entry by HBV pseudoparticles in infected liver cells and cell lines. The glycosylated NTCP localizes to the plasma membrane through interaction with E- cadherin, which increases interaction with the preS1 portion of the Large HBV surface antigen. Our study contributes novel insights that advance knowledge of HBV infection at the level of host cell binding and viral entry.

Keywords: hepatitis B virus (HBV), virus entry, HBV co-receptor, E-cadherin, NTCP

OPEN ACCESS

Edited by:
Cheng Kao,
Indiana University Bloomington, United States

Reviewed by:
Lucie Etienne,
UMR5308 Centre International de Recherche en Infectiologie (CIRI), France
Eric Baranowski,
Institut National de la Recherche Agronomique de Toulouse, France

***Correspondence:**
Lan Zhou
zhoulan@cqmu.edu.cn
Weixian Chen
300801@cqmu.edu.cn

† These authors have contributed equally to this work

Specialty section:
This article was submitted to Virus and Host, a section of the journal Frontiers in Cellular and Infection Microbiology

Received: *15 November 2019*
Accepted: *13 February 2020*
Published: *27 February 2020*

Citation:
Hu Q, Zhang F, Duan L, Wang B, Ye Y, Li P, Li D, Yang S, Zhou L and Chen W (2020) E-cadherin Plays a Role in Hepatitis B Virus Entry Through Affecting Glycosylated Sodium-Taurocholate Cotransporting Polypeptide Distribution. Front. Cell. Infect. Microbiol. 10:74. doi: 10.3389/fcimb.2020.00074

INTRODUCTION

Hepatitis B virus (HBV), a member of the *Hepadnaviridae* family, is a small, enveloped DNA virus (Glebe and Bremer, 2013) that infects human liver parenchymal cells. Although the widespread use of vaccines has greatly reduced the rate of infection, HBV continues to pose a serious threat to global health, affecting more than 350 million individuals worldwide, all of whom are at increased risk of developing liver cirrhosis and hepatocellular carcinoma (HCC) (Trepo et al., 2014). Current therapeutic regimens that employ direct-acting antivirals, with or without ribavirin, have significantly increased the prevalence of escape mutants, caused significant adverse effects while eliciting a low curative rate in HBV patients (Gish et al., 2012).

The lack of effective therapeutic options for HBV is partially due to our incomplete understanding of the HBV life cycle, including the stages during which the virus enters host cells, undergoes DNA replication, and assembles and releases virions from the cells. Productive HBV

infection occurs following viral entry into a host cell, which is initiated through the binding of preS1 the domain of HBV large envelope protein (LHBs) with high affinity HBV receptors on hepatocytes (Le Duff et al., 2009; Glebe and Urban, 2017). The sodium-taurocholate cotransporting polypeptide (NTCP), a bile acid transporter expressed at the basolateral membrane of human hepatocytes, has been identified as a functional receptor for HBV (Yan et al., 2012). Exogenous expression of NTCP in human hepatoma cell lines, such as HepG2 or Huh7, confers susceptibility to HBV infection, and thus, constitute effective cell culture models for examining HBV entry (Yan et al., 2012; Ni et al., 2014). However, the overexpression of NTCP in human or extrahepatic human cell lines, such as HeLa cells, or in mouse hepatocytes, is insufficient for productive HBV infection in these cells, suggesting that additional molecules are also required for efficient HBV infection (Tong and Li, 2014).

The overexpression of the hepatitis B surface antigen binding (SBP) protein in HepG2 cells (HepG2-SBP) induced susceptibility to HBV infection. SBP was shown to interact directly with HBV envelope proteins (Sun et al., 2018). Moreover, heparin sulfate proteoglycans can function to bind HBV and bring the virus to the proximity of the NTCP receptor (Schulze et al., 2007). Verrier et al. (2016) also reported that Glypican 5 attaches to the surface of HBV particles prior to NTCP binding, thereby assisting in host cell entry. These studies indicated that other molecules in addition to NTCP have important roles in efficient and productive HBV infection.

Cadherin adhesion molecules are core components in adherens junctions, located on the basement membrane aspect of polarized epithelial cells. E-cadherin is a calcium-dependent adhesion integrin that is abundant in epithelial tissues and plays an important role in cell-cell adhesion complexes including desmosomes and adherens junctions (Fonseca et al., 2018). E-cadherin play a role in pathogen infection (Bonazzi and Cossart, 2011). Herein, we investigated the role and mechanism for E-cadherin to modulate HBV infection.

MATERIALS AND METHODS

Cell Lines

HepG2-NTCP, HepAD38 (in which HBV replication can be regulated by tetracycline), and Huh-7cells, were provided by Professor Juan Chen of the Chongqing Medical University, Chongqing, China. HepG2-NTCP and HepAD38 cells were maintained in Dulbecco's Modified Eagle Medium (DMEM, Hyclone, Logan, UT, USA) supplemented with 10% fetal bovine serum (FBS, Gibco, Franklin Lakes, NJ, USA) and 400 μg/mL G418. HepG2-NTCP cells were cultured with collagen pretreatment. Huh-7 cells were maintained in DMEM containing 10% FBS. HepaRG cells were purchased from Beijing Beina Science and Technology (Beijing, China) and were cultured in William's E Medium (Sigma-Aldrich, St. Louis, MO, USA) with 10% FBS, 2 mM L-glutamine, 5 μg/mL insulin (Sigma-Aldrich), and 50 μM hydrocortisone hemisuccinate (Sigma-Aldrich). Primary human hepatocytes (PHH) were obtained from ScienCell Research Laboratories (Carlsbad, CA, USA) and were maintained in Hepatocyte Medium (HM, Catalog no. 5210, ScienCell Research Laboratories). All cells were cultured in a humidified incubator at 37°C with 5% CO_2.

Plasmids and Gene Products

The pNL4-3.Luc.R-E- reporter plasmid was obtained through the NIH AIDS Reagent Program. The plasmid of pNL4-3.Luc.R-E- was constructed by rendering this clone Env- and Vpr- with frameshift and inserting the luciferase into the pNL4-3 nef gene, the HIV-1 proviral clone (Connor et al., 1995; He et al., 1995). The pcDNA3.1-E-cadherin plasmid was obtained from Addgene (Cambridge, MA, USA). Partial cDNA for human E-cadherin subcloned into the pcDNA3.1 to generate the pcDNA3.1-Ecad-Δ 35 and then the 425-bp fragment encoding the missing COOH-terminal residues and generated by PCR was sub-cloned into pcDNA3.1-Ecad-Δ 35 to generate full-length pcDNA3.1-E-cadherin plasmid (Gottardi et al., 2001). The pcDNA3.1-HBV1.3 (replication-competent 1.3-fold overlength HBV) and the pcDNA3.1 (vector) plasmids were provided by Professor Juan Chen of Chongqing Medical University (Chongqing, China).To study the effect of E-cadherin on HBV binding to HepG2-NTCP cells, the FITC- and Biotin-labeled preS1 peptides encoding the stable region of preS1 (2-47aa) was synthesized by Zhejiang Baitai Biological Company (Zhejiang, China). The sequence used to produce the FITC- and Biotin-labeled preS1 peptides was: Myr-GTNLSVPNPLGFFPDHQLDPAFGA NSNNPDWDFNPNKDHWEANQVK (Yan et al., 2012). The second amino acid of the preS1 peptides was myristoylated.

Protein Extraction and Western Blotting Analysis

Total protein was extracted from cells using a Protein Extraction Kit (KaiJi, Tianjin, China) according to the manufacturer's instructions. The concentration of protein was quantified via bicinchoninic acid (BCA) protein assay (Beyotime, Shanghai, China) according to the manufacturer's instructions. Equal amounts of total protein from each sample (50 μg) were separated using sodium dodecyl sulfate-polyacrylamide gel electrophoresis (SDS-PAGE) and transferred to a nitrocellulose membrane. The membranes were incubated with rabbit anti-E-cadherin (1:1,000; Cell Signaling Technology, Boston, MA, USA), rabbit anti-HBc (1:1,000; Dako, Glostrup, Denmark), rabbit anti-NTCP (1:1,000; Sigma-Aldrich), rabbit anti-Na^+-K^+-ATPase (1:1,000; Abgent, San Diego, CA, USA), and anti-actin (1:1;000; Boster, Wuhan, China) primary antibodies at 4°C overnight, and subsequently incubated with horseradish peroxidase (HRP)-conjugated secondary antibodies (1:10,000; Boster) at 37°C for 1 h. Blots were developed using an enhanced chemiluminescence reagent (Pierce, Rockford, IL, USA) according to the manufacturer's instructions. The gray value of blots was calculated by the Image Lab.

Preparation of Cell Membrane Fractions

Cell membrane proteins were isolated using Minute™ Plasma Membrane Protein Isolation and Cell Fractionation Kit (ScienCell Research Laboratories) according to the manufacturer's instructions. Protein concentrations in the

extraction samples were quantified using BCA protein assays (Beyotime) according to the manufacturer's instructions.

Immunofluorescence Assay

Coverslips containing cells were washed with phosphate buffered saline (PBS) twice, fixed with 4% paraformaldehyde at 37°C for 10 min, blocked with goat serum at 37°C for 1 h, and incubated with primary antibodies, such as rabbit anti-HBs (1:100; Abcam, Catalog no. ab68520, Cambridge, UK) and rabbit anti-NTCP (1:100; Sigma-Aldrich) at 4°C overnight. The coverslips were then incubated with secondary antibodies (FITC-anti-rabbit IgG, 1:100; Boster) at 37°C for 1 h, and stained with 4′,6-diamidino-2-phenylindole (DAPI) at 37°C for 8 min. Immunofluorescence analysis were performed using a DFC5000 camera (Leica, Wetzlar, Germany) attached to an FV500 Confocal Laser Scanning microscope (Olympus, Tokyo, Japan). The virus infection rate of the cells is the percentage of cells expressing green fluorescence calculated by the ImageJ-win 64.

Analysis of Messenger RNA Expression by Quantitative Real-Time Polymerase Chain Reaction

Total RNA was extracted from cells using TRIzol reagent (Invitrogen, Carlsbad, CA, USA) according to the manufacturer's instructions. Reverse-transcription of total RNA was performed using PrimeScript RT Reagent Kit with gDNA Eraser (Takara Shiga, Japan). Quantitative real-time polymerase chain reaction (qRT-PCR) of the HBV 3.5 kb mRNA was performed using SYBR Green Master Mix (Roche, Basel, Switzerland). The primers for the HBV 3.5 kb were: forward: 5′-GCCTTAGAG TCTCCTGAGCA-3′ and reverse: 5′-GAGGGAGTTCTTCTT CTAGG-3′. The primers for the E-cadherin were: forward: 5′-CCCACCACGTACAAGGGTCAGGT-3′ and reverse: 5′-ACG CTGGGGTATTGGGGGCA-3′. The primers for the NTCP were: forward: 5′-CCACAACGCGTCTGCCCCAT-3′ and reverse: 5′-TGCAGCCCAGCGAGAGCATG-3′.The primers for β-actin were: forward: 5′- TCCCTGGAGAAGAGCTACGA-3′ and reverse: 5′-AGCACTGTGTTGGCGTACAG−3′. The qRT-PCR was run on a Bio-Rad with the following protocol: 2 min at 95°C to pre-denaturation, followed by 40 cycles of denaturation at 95°C for 20 s, annealing at 60°C for 20 s, extension at 72°C for 20 s. All values were normalized to β-actin expression and were calculated using the $2^{\Delta\Delta CT}$ method.

siRNA Transfections

The concentration of siRNAs is 20 pmol/μl. 100 pmol of targeting small interfering or non-targeting siRNAs were transfected into HepG2-NTCP, HepaRG or PHH cell lines planted into 6-well plate using siRNA-mate (Genephama, Shanghai, China) according to the manufacturer's protocol. Further treatments were typically performed 72 h after siRNA transfection began, when gene silencing was determined to reach peak efficiency. The sequence used for siRNA targeting E-cadherin was: 5′-CAGACA AAGACCAGGACUA-3′. The sequence of the siRNA targeting NTCP was: 5′-CAGUUCUCUCUGCCAUCAA-3′. The sequence of the negative control siRNA was: 5′- UUCUCCGAACGUGUC ACGUdTdT-3′.

HBV Particle Production and Infection

HBV particles were enriched from the supernatant of HepAD38 cells using 8% PEG8000 (Sigma-Aldrich) (Ladner et al., 1997). HepG2-NTCP, HepaRG and PHH cells were seeded in 24-well plates and maintained in William's E Medium supplemented with 10% FBS, 2 mM L-glutamine, and 2% DMSO for 1 d at the time of HBV infection. HBV infection was assessed at 2 d by qRT-PCR quantification of HBV 3.5 kb RNA, and at 3 d via western blotting analysis of HBV core protein (1:1,000; Dako), and immunofluorescence assay of HBsAg, using the rabbit anti-HBsAg antibody (1:100; Abcam).

HBV particles from adult chronic HBV patients were obtained and used for infection as previously described (Sun et al., 2018). Briefly, HepG2-NTCP and PHH cells were seeded at a density of 5×10^4 per well into 24-well plates. On the following day, cells were incubated with the HBV-positive serum ($>5 \times 10^7$ copies/mL) diluted in DMEM at a multiplicity of infection (MOI) of 100. Infected cells were maintained in DMEM or HM with 2% FBS. The HBV 3.5 kb RNA, HBc and HBsAg were assessed at 4d post-infection.

Packaging and Infection of HBV Pseudotyped Particles

HBV pseudotyped particles (HBVpps) can infect liver cells but cannot replicate in human hepatocytes. Infection and packaging of HBVpps were achieved as previously described (Meredith et al., 2016). Infectious virus can be produced by co-transfection with HBV membrane protein expression vector. Therefore, HBVpps were produced by co-transfecting pNL4-3.Luc.R-E- and pcDNA3.1-HBV1.3 plasmids into Huh7 cells using Lipofectamine 2000 Transfection Reagent (Invitrogen). The supernatants containing HBVpps were harvested 72 h after transfection and centrifuged at 1,500 × *g* for 15 min to remove debris. The pseudotyped particles were then added to 96-well microplates, which had been seeded with target cells at a density of 5×10^3 on the previous day, at a volume of 100 μL/well. The medium was supplemented with polybrene (Santa Cruz, CA, USA) at a final concentration of 4 μg/mL. Twenty-four hours after infection, 100 μL of fresh medium was changed per well. Luciferase assays were performed after 72 h using a GloMaxTM 96 Microplate Luminometer (Promega, Madison, WI, USA).

Co-immunoprecipitation Assay

Co-immunoprecipitation assay was performed as previously described (Sun et al., 2018). Cells were lysed in immunoprecipitation buffer supplemented with complete protease inhibitor. After lysing with ultrasound, lysates were centrifuged to remove insoluble components. Lysates were then incubated overnight with rabbit anti-E-cadherin (Cell Signaling Technology) or rabbit IgG primary antibodies at 4°C. Protein G beads (Beyotime) were then added to the lysates. The precipitated proteins were measured via western blot analysis as described above.

Pull-Down Assay

Magnetic beads (ThermoFisher Scientific, Waltham, MA, USA) were incubated with biotin-labeled preS1 antibodies at 37°C for 1 h according to the manufacturer's instructions. The beads were washed thrice with TBST, incubated with 500 μL HepG2-NTCP cell lysate at 4°C overnight, and washed a further three times. Thirty microliters of SDS-PAGE reducing sample buffer was then added to each tube and heated at 100°C in a heating block for 5 min. The precipitated proteins were quantified via western blotting analysis.

CCK-8 Cell Proliferation Assay

HepG2-NTCP and HepaRG cells were seeded in 96-well plates (5×10^3 cells in 100 μl per well). At different time points, 10 μl of cell counting kit-8 (CCK-8) solution (Dojindo, Shanghai, China) was added and incubated for 2 h. The value of OD was measured at 450 nm in a microplate reader (ThermoFisher Scientific, Waltham, MA, USA).

Detection of HBsAg Expression With ELISA

HBsAg in culture samples collected from the infected cells at 4 days was detected with ELISA kits (LiZhu, Guangdong, China) according to the manufacturer's instructions. The value of cut off is equal to the negative value plus 0.09. The value of S/CO is the ratio of OD to the value of cut off.

HBV Pre-S1 Binding and Internalization Assay

The experiment was performed as the previous study (Sun et al., 2018). Five microgram of FITC-preS1 was added into the HepG2-NTCP or PHH cells in 96-well plate. The cells were incubated at 4°C for 2 h and then washed with PBS for three times. We determined the binding of pre-S1 by observing cells with linear or dot-like fluorescence on the cell membrane with fluorescence microscope. Besides, incubate it at 37°C for 2 h and then wash it with PBS for three times. We determined the internalization of pre-S1 by observing the green fluorescence inside the cell. We counted the number of cells in white light and then counted the number of cells that express fluorescence in the cell membrane or inside the cell.

Ethics Statement

We collected fresh serum from adult chronic HBV patients. The study was approved by the Ethics Committee of the Second Affiliated Hospital of Chongqing Medical University. This research was conducted according to the relevant guidelines, and all participants gave written informed consent before the experiment.

Statistical Analyses

Statistical Package for the Social Sciences (SPSS) 16.0 was used to perform unpaired Student's *t*-tests. Results with $p < 0.05$ were considered statistically significant. Each experiment was repeated a minimum of three times.

RESULTS

Downregulation of E-cadherin Reduces Infection Efficacy of HBV Particles

HepG2-NTCP cells that stably express a recombinant NTCP receptor, PHH from human donors, and HepaRG cells that differentiated into hepatocytes can be infected by HBV in culture (Schulze et al., 2012; Ren et al., 2018). We used these cells to elucidate the role of E-cadherin in modulating HBV infection. HepG2-NTCP, HepaRG, and PHH cells were transfected with 20 pmol of siRNA-NC, siRNA-E-cadherin, siRNA-NTCP or a combination of siRNA-E-cadherin and siRNA-NTCP before infection with 1×10^3 genome equivalents/cell of HBV produced from HepAD38 cells in 24-well plate. The mRNA level of E-cadherin and NTCP were downregulated about or more than 50% following siRNA treatment in HepG2-NTCP and HepaRG cell lines (**Figures 1A,B**). Transfection with siRNA had no effect on viability in HepG2-NTCP and HepaRG cells (**Figures 1C,D**). Moreover, silencing of E-cadherin and NTCP significantly reduced the level of HBV 3.5 kb mRNA in HepG2-NTCP, HepaRG, and PHH cell lines (**Figure 1E**); while silencing of both E-cadherin and NTCP in HepG2-NTCP and PHH cells served to further reduce the level of HBV 3.5 kb mRNA compared to that observed by either E-cadherin or NTCP separately. Western blot, ELISA and immunofluorescence analysis determined that downregulation of E-cadherin or NTCP independently, or together, reduced the levels of HBV core protein and HBsAg (**Figures 1E–J**). These results suggest that reducing E-cadherin levels reduced productive HBV infection.

Silencing of E-cadherin Inhibits Infection With HBV Particles Isolated From the Serum of an HBV Carrier

To further elucidate the relationship between E-cadherin and HBV infection, HepG2-NTCP and PHH cells were infected with HBV particles obtained from a chronic HBV patient. Infection were detected after 4 days. Silencing of E-cadherin or NTCP alone or at the same time, the levels of HBV 3.5 kb mRNA were downregulated about or more than 50% in HepG2-NTCP and PHH cells (**Figure 2A**). Moreover, silencing of E-cadherin also significantly inhibited the level of HBV core and HBsAg proteins (**Figures 2B–E**). These results demonstrate that reducing E-cadherin inhibited infection by HBV isolated from an HBV patient.

Overexpression of E-cadherin Promotes HBV Particles Infection

The concentration of E-cadherin was lower in HepaRG cells by about 50% compared to HepG2-NTCP cells (**Figures 3A,B**). Therefore, to elucidate the effect of E-cadherin overexpression on HBV infection, HepaRG cells were transfected with either pcDNA3.1-E-cadherin (E-cadherin) or pcDNA3.1 (vector). After transfected with pcDNA3.1-E-cadherin, the level of E-cadherin was upregulated double (**Figures 3C,D**). At 3 days post-transfection, HepaRG cells were infected with enriched HBV particles. E-cadherin overexpression increased the level

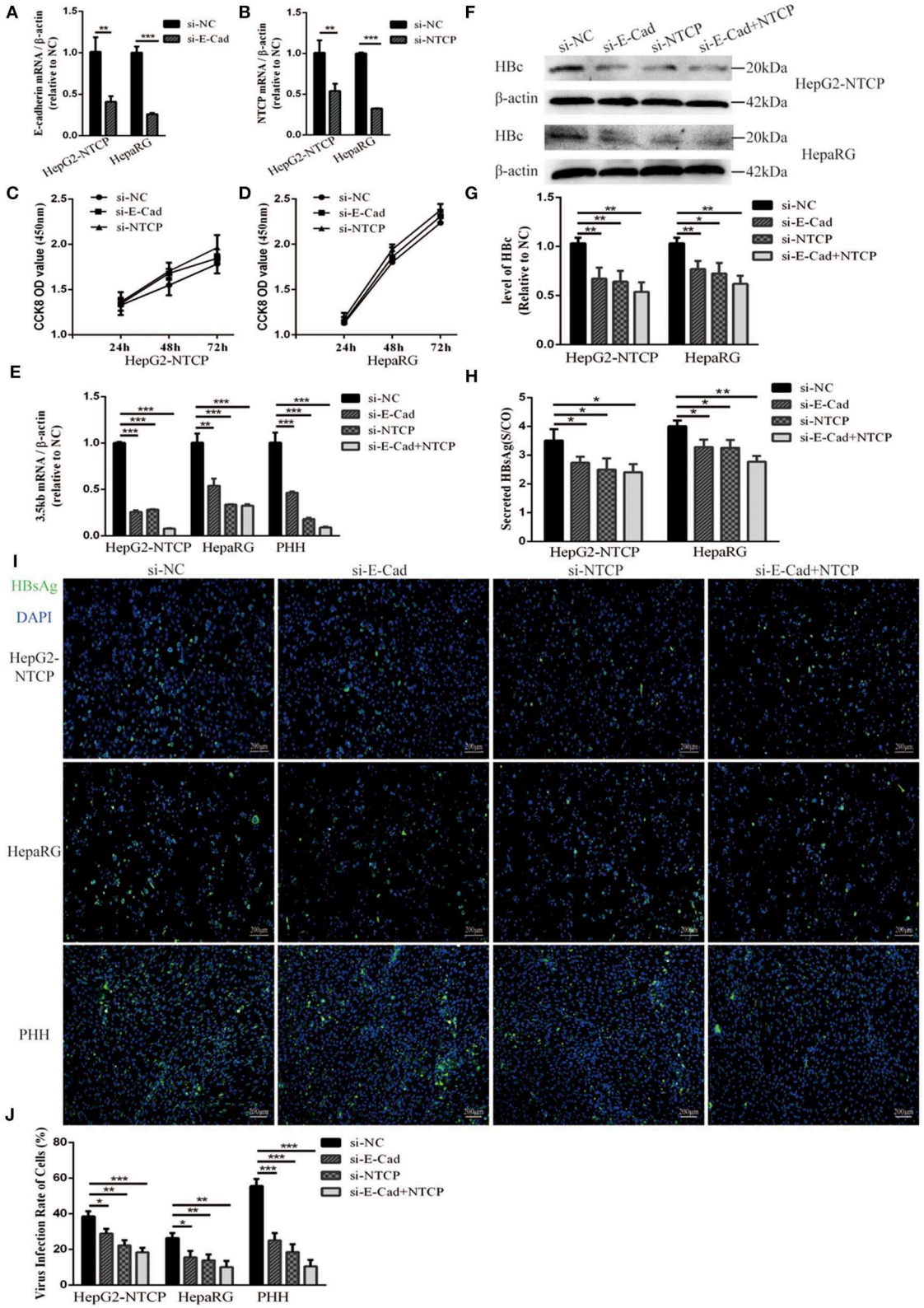

FIGURE 1 | Downregulation of E-cadherin reduces infection efficacy of HBV particles enriched from supernatants of HepAD38 cells. **(A)** E-cadherin expression was silenced in HepG2-NTCP and HepaRG cells by siRNAs. **(B)** NTCP expression was silenced in HepG2-NTCP and HepaRG cells by siRNAs. Silencing efficacy was

(Continued)

FIGURE 1 | assessed for E-cadherin and NTCP by qRT-PCR 2 days post-transfection. The value of si-NC group was normalized to 1. **(C,D)** CCK8 assay showed proliferation of HepG2-NTCP and HepaRG cells transfected with si-NC, si-E-cadherin, and si-NTCP. There was no significant difference between the groups. **(E)** Total RNA was extracted 2 days post-infection and HBV infection was assessed by qRT-PCR quantification of HBV 3.5 kb mRNA normalized to β-actin mRNA. The value of si-NC group was also normalized to 1. **(F)** Total protein was extracted 3 days post-infection and expression of HBV core (HBc) was assessed by western blot analysis in HepG2-NTCP and HepaRG cells. **(G)** The densitometric ratios were normalized to the β-actin and then compared to the controls. **(H)** HBsAg in culture collected from the infected cells at 4 days was detected with ELISA kits in HepG2-NTCP and HepaRG cells. The value of S/CO is the ratio of OD to the value of cut off. **(I)** HBsAg expression was assessed by immunofluorescence 3 days post-infection in HepG2-NTCP, HepaRG and PHH cells treated with si-NC, si-E-cadherin, si-NTCP or si-E-cadherin and si-NTCP together. **(J)** The virus infection rate of the cells is the percentage of cells expressing green fluorescence calculated by the ImageJ-win 64. Representative data is shown from triplicate experiments. $^{*}p < 0.05$, $^{**}p < 0.01$, $^{***}p < 0.001$; error bars: standard deviation (SD).

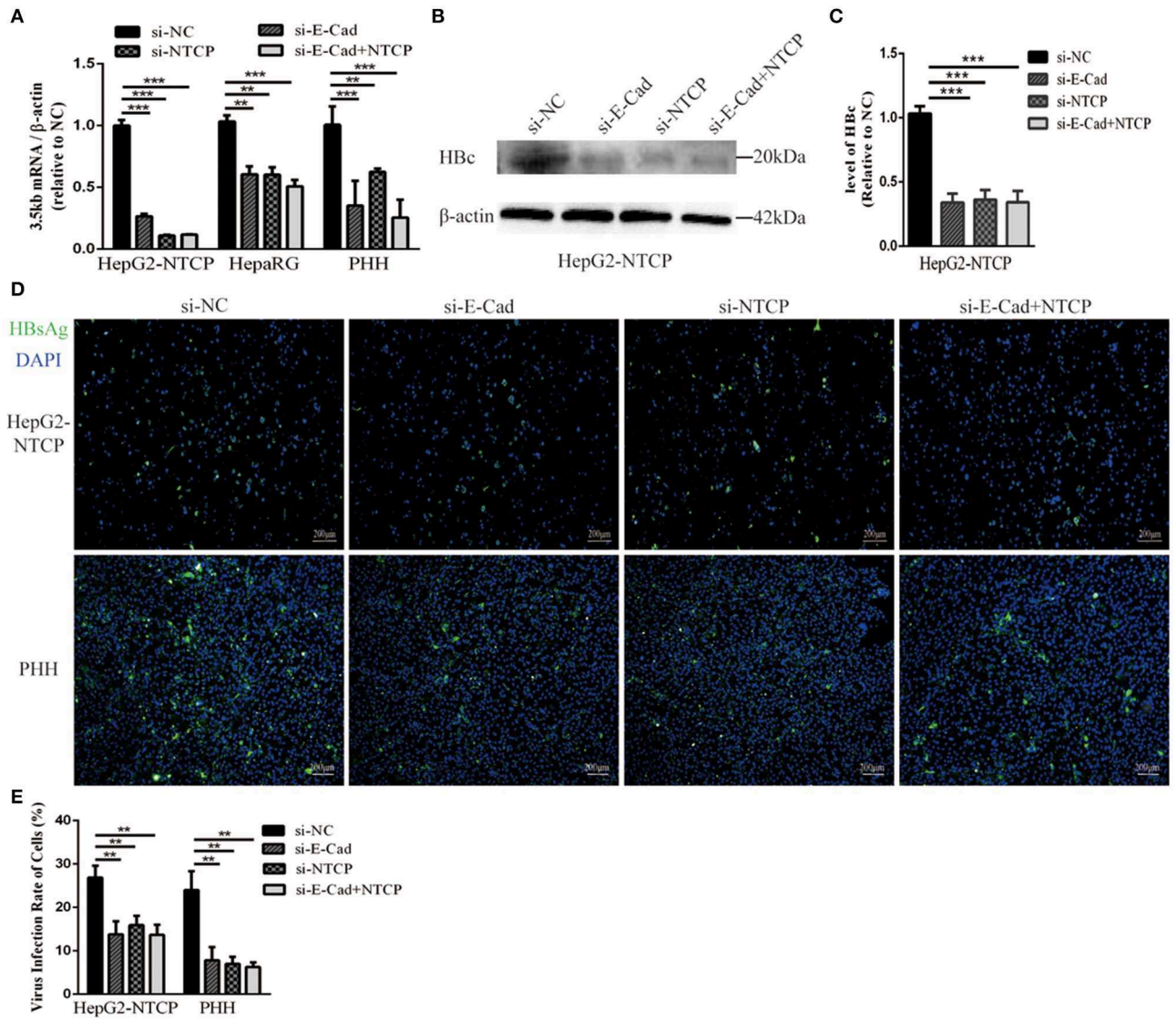

FIGURE 2 | Downregulation of E-cadherin inhibits infection of HBV particles from the serum of an HBV carrier. HepG2-NTCP, HepaRG and PHH cells were incubated with the HBV-positive serum diluted in DMEM at an MOI of 100 after 3 days post-transfection with si-NC, si-E-cadherin, si-NTCP, or si-E-cadherin and si-NTCP together. **(A)** Total RNA was extracted 4 days post-infection and HBV infection was assessed via qRT-PCR quantification of HBV 3.5 kb mRNA normalized to β-actin mRNA. The value of si-NC group was also normalized to 1. **(B)** Total protein was extracted 4 days post-infection and HBV core (HBc) expression was assessed by western blot analysis in HepG2-NTCP cells. **(C)** The densitometric ratios were normalized to the β-actin and then compared to the controls. **(D)** HBsAg expression was assessed by immunofluorescence 4 days post-infection in Hep2-NTCP and PHH cells. **(E)** The virus infection rate of the cells is the percentage of cells expressing green fluorescence calculated by the ImageJ-win 64. Representative data is shown from triplicate experiments. $^{**}p < 0.01$; $^{***}p < 0.001$; error bars: standard deviation (SD).

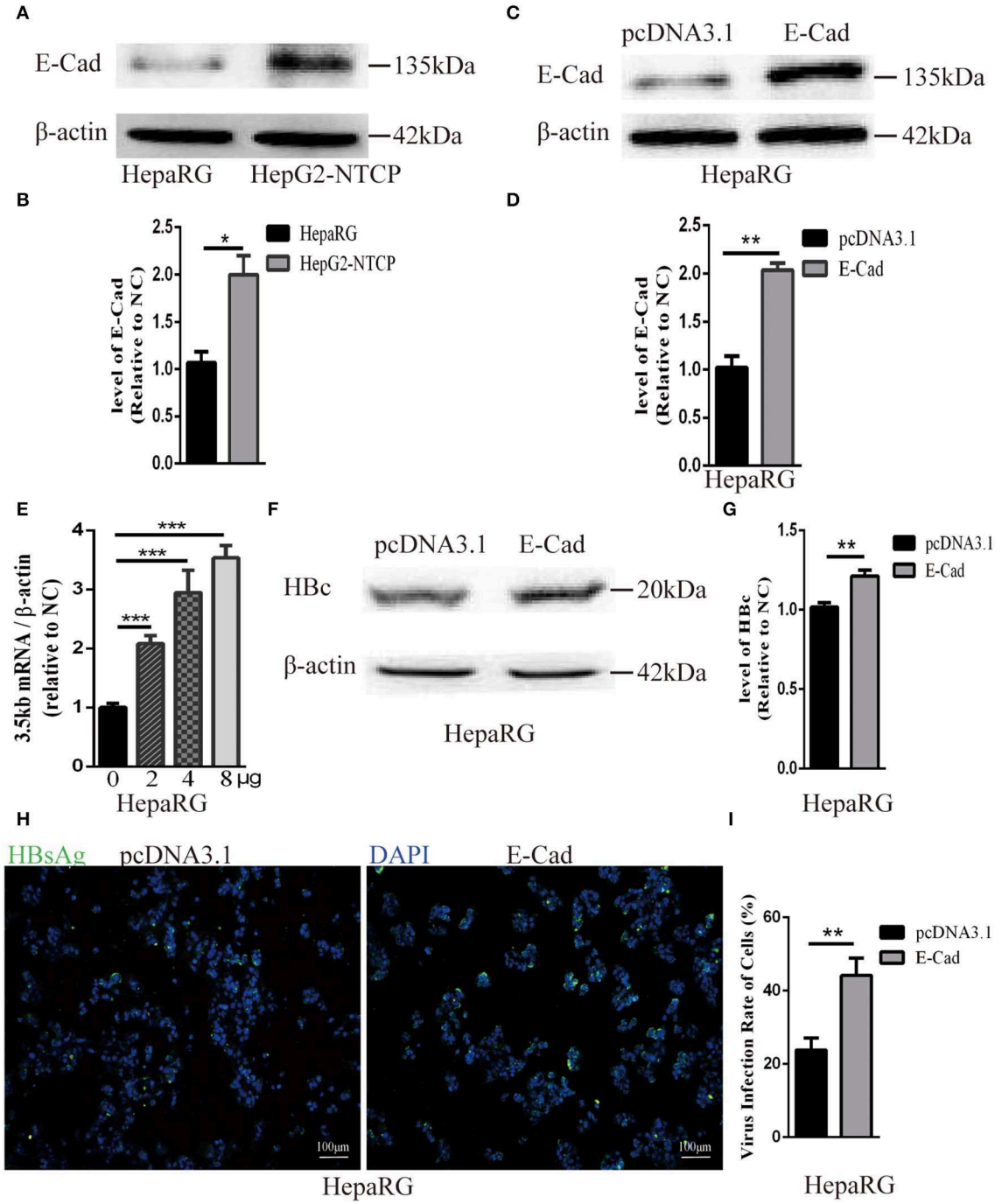

FIGURE 3 | Overexpression of E-cadherin promotes HBV particles infection in HepaRG cells. **(A)** E-cadherin expression was assessed via western blot analysis in HepaRG and HepG2-NTCP cells. **(B)** The densitometric ratios were normalized to the β-actin and then compared to the controls. **(C)** Four microgram of pcDNA3.1-E-cadherin was transfected into HepaRG cells planted in 6-well plate. E-cadherin expression was assessed via western blot analysis 3 days post-transfection. **(D)** The densitometric ratios were normalized to the β-actin and then compared to the controls. **(E)** 0, 2, 4, and 8μg of pcDNA3.1-E-cadherin was transfected into HepaRG cells planted in 6-well plate. Then the cells were planted into 24-well plate at 2 days after transfection and then infected with HBV virus. Total RNA was extracted 2 days post-infection and the amount of HBV was assessed via qRT-PCR quantification of HBV 3.5 kb mRNA normalized to β-actin mRNA. **(F–I)** Four microgram of pcDNA3.1-E-cadherin was transfected into HepaRG cells planted in 6-well plate. Then the cells were planted into 24-well plate at 2 days after transfection and then infected with HBV virus. **(F)** Total protein was extracted 3 days post-infection and HBV core (HBc) expression was assessed by western blot analysis in HepaRG cells. **(G)** The densitometric ratios were normalized to the β-actin and then compared to the controls. **(H)** HBsAg expression was assessed by immunofluorescence 3 days post-infection in HepaRG cells. **(I)** The virus infection rate of the cells is the percentage of cells expressing green fluorescence calculated by the ImageJ-win 64. Representative data is shown from triplicate experiments. E-Cad, E-cadherin. $^{*}p < 0.05$; $^{**}p < 0.01$; $^{***}p < 0.001$; error bars: standard deviation (SD).

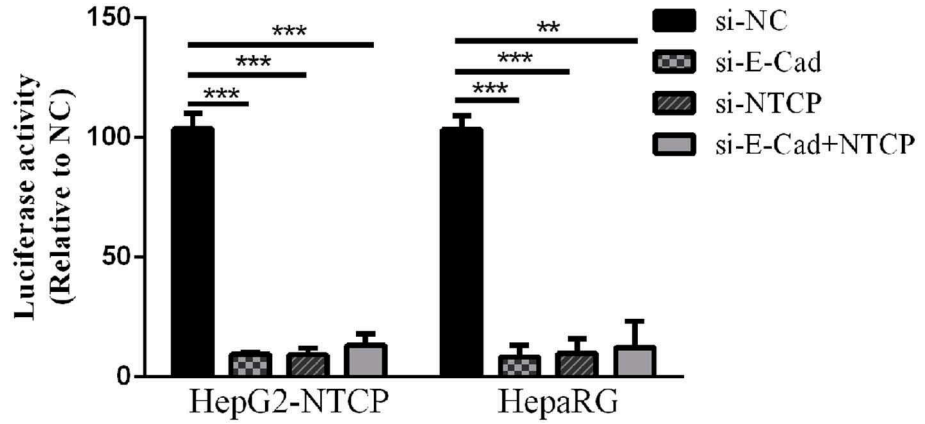

FIGURE 4 | Downregulation of E-cadherin inhibits entry of HBV pseudoparticles. HepG2-NTCP and HepaRG cells were infected with luciferase-encoding pseudotyped virus particles bearing HBV large envelope glycoprotein LHBs 3 days post-transfection with siRNA. Luciferase assays were performed 72 h after infection. The value of si-NC group was normalized to 100 and the values of other groups were compared to the controls. Representative data is shown from triplicate experiments. $^{**}p < 0.01$; $^{***}p < 0.001$; error bars: standard deviation (SD).

of HBV 3.5 kb mRNA and in a concentration-dependent manner (**Figure 3E**). Furthermore, expression of recombinant E-cadherin enhanced the level of HBV core and HBsAg proteins (**Figures 3F–I**). These results suggest that E-cadherin contributed to HBV infection.

E-cadherin Specifically Modulates HBV pseudoparticle Entry

Lentivirus-based pseudoparticles had been used to study the entry pathways of a range of viruses, including human immunodeficiency virus (HIV) and hepatitis C virus (Moller-Tank and Maury, 2015). To further clarify the steps of the HBV life cycle impacted by E-cadherin expression, HBV pseudotyped virus (HBVpps) was conducted. HBVpps could only infect cells, but could not replicate within cells. Therefore, the amount of virus entering into the cell could be detected by measuring the luciferase activity. Silencing of E-cadherin or NTCP individually or together by siRNAs served to significantly inhibit HBVpps entry into HepG2-NTCP and HepaRG cells (**Figure 4**), suggesting that E-cadherin impacts HBV binding/entry.

Silencing of E-cadherin Inhibits HBV Pre-S1 Binding and Internalization to HepG2-NTCP and PHH Cells

We next sought to determine the mechanism employed by E-cadherin to enhance HBV binding. We, therefore, quantified the binding of HBV pre-S1 (Myr-2-47aa) via immunofluorescence assays in HepG2-NTCP and PHH cells after 120 min incubation at 4°C, which is the conditions in which viral binding most readily occurs, or at 37°C, when uptake of pre-S1 occurs. Results revealed that when E-cadherin or NTCP were silenced separately or at the same time, significant inhibition of preS1 binding and uptake were observed in HepG2-NTCP and PHH cells (**Figure 5**). These results suggest that E-cadherin modulates HBV entry by affecting preS1 binding and internalization by host cells.

E-cadherin Regulates NTCP Cell Surface Distribution

To further explore the mechanism by which E-cadherin mediates HBV particle entry, we examined whether it influenced the total NTCP concentration. The densitometric ratios of every bands were normalized to the β-actin and then compared to the controls. Results show that silencing of E-cadherin did not affect the level of NTCP in HepG2-NTCP and HepaRG cells (**Figures 6A–D**), which suggests that E-cadherin does not modulate HBV entry by directly affecting the expression and stability of NTCP. We, therefore, speculated that E-cadherin might influence the membrane distribution of NTCP. Our results showed that silencing E-cadherin in HepG2-NTCP cells significantly impacted the subcellular distribution of NTCP. Specifically, NTCP which primarily localizes to the cell surface was instead gathered in the cytoplasm (**Figure 6E**). We next separated membrane proteins to confirm the observed changes in NTCP cell surface distribution. Na^+-K^+-ATPase mainly distributed in the cell membrane was used as an internal reference. As shown in **Figures 6F,G**, knockdown of E-cadherin resulted in reduced levels of NTCP at the cell membrane in HepG2-NTCP cells. Besides, the data also indicated that overexpression of E-cadherin increased the levels of NTCP at the cell membrane in HepaRG cells (**Figures 6H,I**).

To elucidate the mechanism employed by E-cadherin to impact the cellular distribution of NTCP, we further examined the interactions between E-cadherin and NTCP via co-immunoprecipitation (co-IP). Surprisingly, when an E-cadherin antibody was used to precipitate the cellular lysate of HepG2-NTCP cells, an ∼50 kDa protein band was detected in the precipitates with the NTCP antibody. To confirm whether the

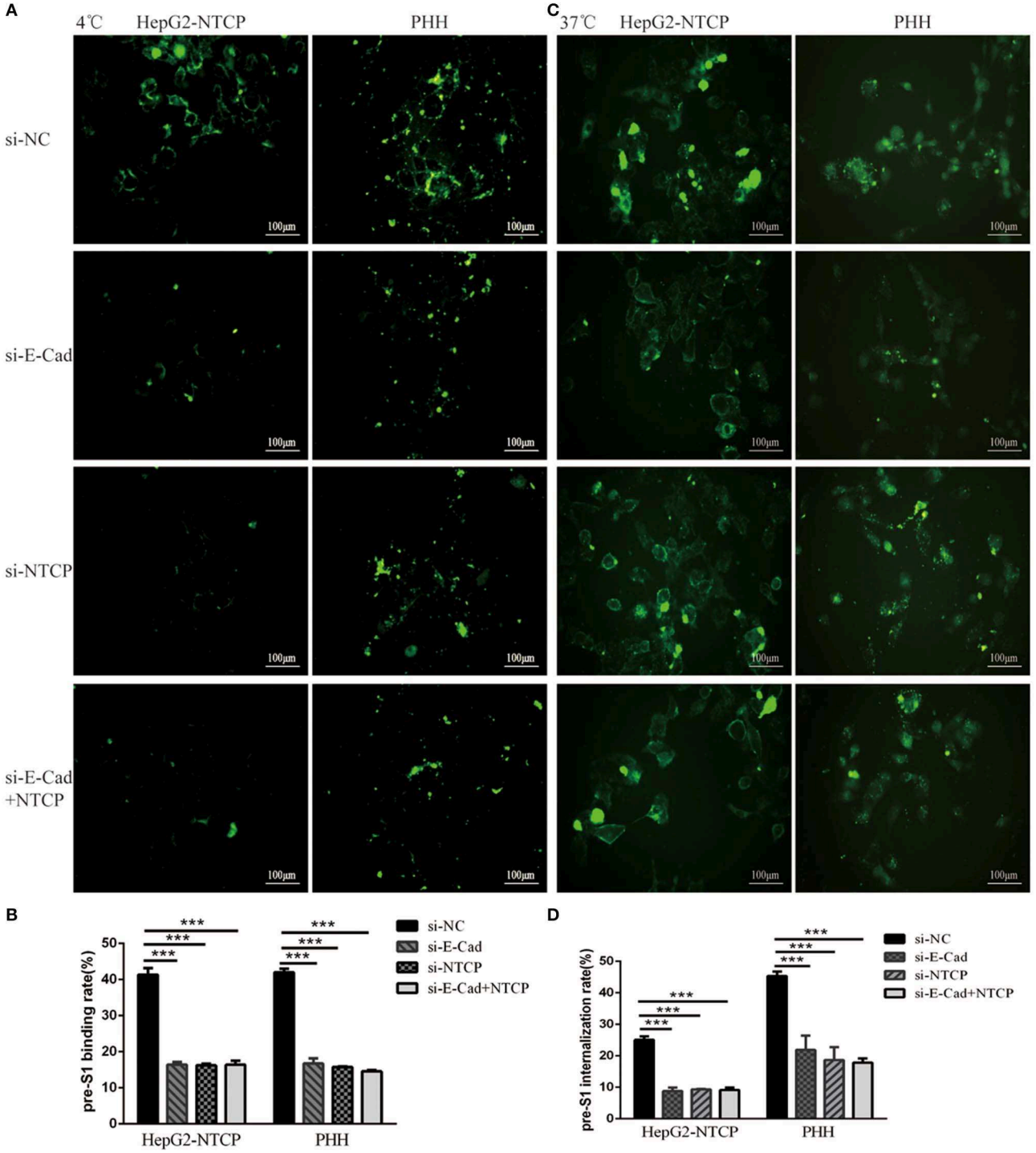

FIGURE 5 | Silencing E-cadherin inhibits HBV preS1 binding and internalization by HepG2-NTCP and PHH cells. HepG2-NTCP and PHH cells were cultured with HBV preS1 for 2 h at **(A)** 4°C or **(C)** 37°C 3 days after transfection with si-NC, si-E-cadherin, si-NTCP or si-E-cadherin, and si-NTCP together. The binding or internalization rate was quantified by counting the total number of cells in the white light and the number of cells expressing fluorescence in the cell membrane or inside the cell. ***$p < 0.001$; error bars: standard deviation (SD) **(B,D)**. Representative data is shown from triplicate experiments.

50 kDa protein was glycosylated NTCP, the precipitate was treated by PNGase F and further probed with NTCP antibodies. Results demonstrated that PNGase F treatment caused the 50 kDa protein to change into a 39 kDa variant; suggesting the 50 kDa protein was a glycosylated form of NTCP (**Figure 6J**). Furthermore, after treating cell membrane proteins with PNGase

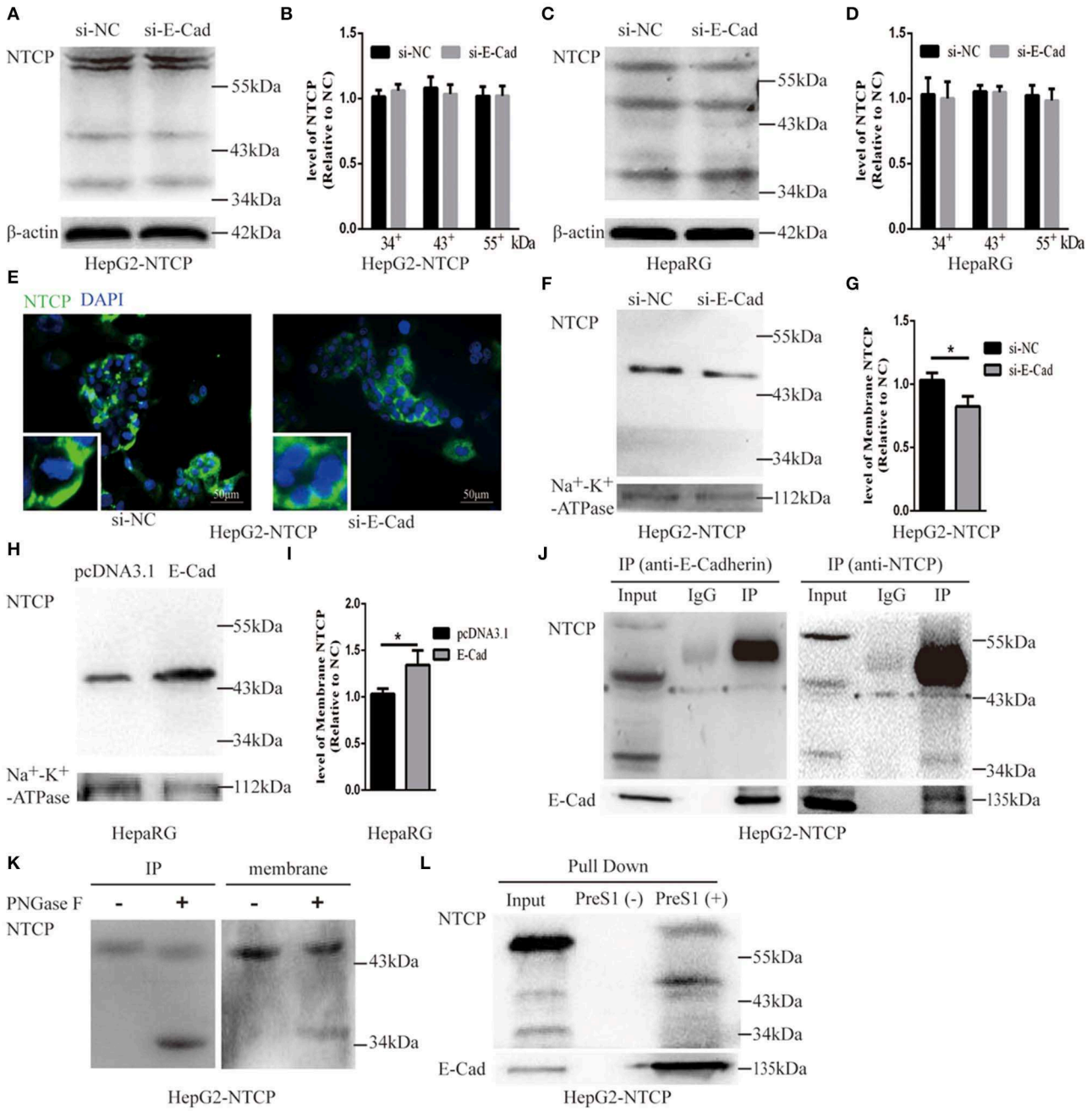

FIGURE 6 | E-cadherin facilitates NTCP localization to the cell surface through interacting with glycosylated NTCP. Total protein was extracted 3 days post-transfection with siRNA-NC or siRNA-E-cadherin. NTCP expression was assessed by western blot analysis in **(A)** HepG2-NTCP and **(C)** HepaRG cells. The samples were derived from the same experiment and gels were processed in parallel. **(B,D)** The densitometric ratios of every band were normalized to the β-actin and then compared to the controls. There was no significant difference between the groups. **(E)** NTCP expression was assessed by immunofluorescence 3 days post-transfection with E-cadherin siRNA in HepG2-NTCP cells. **(F)** Membrane protein was extracted 3 days post-transfection with siRNA-NC (left panel) or siRNA-E-cadherin (right panel) and NTCP expression was assessed by western blot analysis in HepG2-NTCP cells. **(G)** The densitometric ratios were normalized to the Na^+-K^+-ATPase and then compared to the controls. **(H)** Membrane protein was extracted 4 days post-transfection with pcDNA3.1 plasmid or pcDNA3.1-E-cadherin and NTCP expression was assessed by western blot analysis in HepaRG cells. **(I)** The densitometric ratios were normalized to the Na^+-K^+-ATPase and then compared to the controls. **(J)** Co-immunoprecipitation was performed to confirm the interaction between E-cadherin and NTCP. Input: Total protein from cell extract. IgG of rabbit was used as the control group. IP: Total protein from Hep2-NTCP cells was incubated with anti-E-cadherin, or anti-NTCP at 4°C overnight. **(K)** The precipitate of IP and membrane protein were treated by PNGase F at 37°C for 1 h and detected by western blot. **(L)** The HepG2-NTCP cell lysates were incubated with pre-S1 to confirm that preS1 was bound to glycosylated NTCP. Representative data is shown from triplicate experiments. *$p < 0.05$; error bars: standard deviation (SD).

F, we also observed a shift in electrophoresis size from 50 to 39 kDa, indicating that a large fraction of the NTCP localized at the cell membrane was glycosylated (**Figure 6K**). Lastly, after incubating preS1 with HepG2-NTCP cell lysates, we observed the formation of preS1, glycosylated NTCP and E-cadherin complexes (**Figure 6L**). Taken together these results suggest that E-cadherin binds to glycosylated NTCP, allowing for efficient localization to the cell surface.

DISCUSSION

HBV entry into the host cell is the critical step in their life cycle. This process includes particle delivery and capture, complex internalization, and membrane fusion (Hayes et al., 2016). HBV entry requires a tightly coordinated group of specific viral proteins and multiple host receptors (Miao et al., 2017). In the current study, we report that E-cadherin acts as a novel host factor that facilitates HBV entry. The functional role of E-cadherin as a host entry factor was confirmed by numerous studies. Specifically we showed that silencing of E-cadherin acted to inhibit HBV particle entry into HepG2-NTCP, HepaRG and PHH cells (**Figures 1**, **2**); overexpression of E-cadherin contributed to HBV particle entry in HepaRG cells (**Figure 3**) and silencing of E-cadherin inhibited HBVpps entry in HepG2-NTCP and HepaRG cells (**Figure 4**). Moreover, E-cadherin silencing caused a significant decrease in the binding and internalization of the HBV pre-S1 peptide by HepG2-NTCP and PHH cells (**Figure 5**). Mechanistic studies suggested that E-cadherin regulates the cell-surface distribution of NTCP (**Figure 6**). This study represents an important step forward in understanding the molecular mechanisms and cellular regulatory events involved in HBV entry.

Although Li J. et al. (2016) reported that HepG2-NTCP cells exhibited poor susceptibility to HBV particles derived from patient serum, our study demonstrated the opposite effect with HepG2-NTCP cells being efficiently infected with HBV particles from serum of chronic HBV patients. These results were confirmed by quantifying specific markers of HBV infection (HBV 3.5 kb RNA, HBc and HBsAg) to confirm infection of HepG2-NTCP cells (**Figure 2**). Similarly, Yan et al. (2012) successfully infected HepG2-NTCP cells with an HBV genotype B virus from the plasma of a carrier with HBV. An additional study also reported successful infection of HepG2-NTCP cells with an HBV genotype D virus isolated from serum to determine the effect of glypican-5 (GPC5) expression on HBV entry (Verrier et al., 2016).

E-cadherin is a type I classical cadherin and a calcium-dependent adhesion glycoprotein expressed in the epithelium (Harris and Tepass, 2010). E-cadherin has been described as a critical component in the regulation of pathways highly associated with cancer development, including cellular proliferation, apoptosis, invasiveness, metabolism, and metastasis, through mediating multiple cellular signaling pathways (Yulis et al., 2018). Many additional studies have focused on the effect that E-cadherin has on pathogenic infections caused by bacteria and viruses (Bonazzi and Cossart, 2011). *Listeria monocytogenes* is a foodborne pathogen that crosses the intestinal barrier upon binding between its surface protein InlA and the host receptor E-cadherin occurs (Nikitas et al., 2011). *Candida albicans* produces two types of invasins, namely, Als1 and Als3, in combination with E-cadherin or N-cadherin, which together facilitate the internalization of bacteria (Phan et al., 2007). Moreover, E-cadherin associates directly with nectin-1 which is critical for HSV-1 infection (Drees et al., 2005). Connolly et al. (2005) also reported that E-cadherin overexpression may strengthen intercellular junctions and shorten the distance between infected and uninfected cells, thereby increasing the regional concentration of nectin-1 to facilitate efficient viral spread. E-cadherin was also found to play a critical role in HCV entry through regulating membrane distribution of the HCV receptors, claudin-1 (CLDN1) and occludin (OCLN) (Li Q. et al., 2016). These studies provide evidence that E-cadherin acts directly as a receptor while also modulating the expression and activity of other receptors to mediate pathogenic infections.

Herein we show that E-cadherin plays a critical role in HBV entry by influencing the distribution of NTCP, the functional receptor of HBV. NTCP, a 349 residue glycoprotein, becomes glycosylated at N5 and N11 in the endoplasmic reticulum and Golgi apparatus before being trafficked to the cell surface, resulting in a band that spans from 39 to 56 kDa (Appelman et al., 2017). Surprisingly, we found that E-cadherin interacts with the glycosylated form of NTCP (**Figure 6E**). Therefore, when E-cadherin is distributed on the cell membrane, the glycated NTCP bound to E-cadherin could also be localized to the cell membrane. A previous study indicated that glycosylation is essential for NTCP to act as a receptor for HBV since the non-glycosylated form of NTCP is rapidly internalized and degraded (Appelman et al., 2017). Yan et al. (2012) also found that Myr-preS1 cross-links with glycosylated NTCP. However, another study claimed that both the glycosylated and non-glycosylated forms of NTCP effectively mediate HBV infection, since differentiated HepaRG cells only express non-glycosylated NTCP (Lee et al., 2018). In our study, both glycosylated and non-glycosylated NTCP were detected in differentiated HepaRG and HepG2-NTCP cells, however, only glycosylated NTCP were detected in membrane proteins. Moreover, Myr-2-47aa was found to bind to the glycosylated form (**Figure 6G**). Our results showed that E-cadherin was associated with glycosylated NTCP (**Figure 6E**), and, thus, we propose that E-cadherin exerts a regulatory role on the cellular entry of HBV through interacting with glycosylated NTCP and facilitating its membrane localization in hepatocytes. Moreover, NTCP is a hepatic Na^+ bile acid symporter and is responsible for cotransportation of sodium and bile acids across cellular membranes to maintain the enterohepatic circulation of bile acids (Stieger, 2011). Whether E-cadherin could affect the physiological roles of NTCP such as transportation of sodium and bile acids need to be further studied.

Furthermore, E-cadherin is the primary component of adherens junctions at the basolateral surfaces of polarized epithelial cells and function to establish cellular polarity

(Shneider et al., 1997). Cell polarization, defined as the asymmetric distribution of components and functions in a cell, is not only required for proper cellular functioning but has also been defined as being associated with pathogenic infection (Ruch and Engel, 2017). The archetypal polarized animal cell is the epithelial cell, however, hepatocytes are also highly polarized. Pathogens such as *Helicobacter pylori* (Tammer et al., 2007), *Salmonella typhimurium* (Liao et al., 2008), *Shigella dysenteriae* (Beau et al., 2007), and Rotavirus (Guglielmi et al., 2007), either interfere with the establishment of cellular polarization, or adapt to use polarized molecules as their functional receptors, thereby facilitating self-infection of host cells. Furthermore, Schulze et al. (2012) reported that hepatocyte polarization is essential for HBV entry. So, E-cadherin may affect HBV entry through affecting hepatocyte polarization and this need to be studied in the future.

In summary, E-cadherin improved the rate of HBV entry through binding to glycosylated NTCP thereby, impacting the membrane distribution of NTCP. This study provides novel insights that advance the current understanding of the HBV life cycle as well as inform the development of pharmaceutical interventions targeting E-cadherin as a means to prevent HBV infection.

DATA AVAILABILITY STATEMENT

All datasets generated for this study are included in the article/supplementary material.

ETHICS STATEMENT

The studies involving human participants were reviewed and approved by Ethics Committee of the Second Affiliated Hospital of Chongqing Medical University. The patients/participants provided their written informed consent to participate in this study.

AUTHOR'S NOTE

The following reagent was obtained through the NIH AIDS Reagent Program, Division of AIDS, NIAID, NIH: pNL4-3.Luc.R–.E– from Dr. Nathaniel Landau. This manuscript has been released as a Pre-Print at https://www.biorxiv.org/content/10.1101/729822v1 (Hu et al., 2019).

AUTHOR CONTRIBUTIONS

WC designed the study. QH, FZ, LD, and BW conduct the experiments. QH, FZ, PL, YY, DL, and SY conducted analyses. QH wrote the manuscript. WC and LZ edited the manuscript.

FUNDING

This study was supported by researches grant from National Natural Science Foundation of China (81873971, 81672080).

REFERENCES

Appelman, M. D., Chakraborty, A., Protzer, U., McKeating, J. A., and van de Graaf, S. F. (2017). N-glycosylation of the Na^+-taurocholate cotransporting polypeptide (NTCP) determines its trafficking and stability and is required for Hepatitis B virus infection. *PLoS ONE* 12:e0170419. doi: 10.1371/journal.pone.0170419

Beau, I., Cotte-Laffitte, J., Amsellem, R., and Servin, A. L. (2007). A protein kinase A-dependent mechanism by which rotavirus affects the distribution and mRNA level of the functional tight junction-associated protein, occludin, in human differentiated intestinal Caco-2 cells. *J. Virol.* 81, 8579–8586. doi: 10.1128/JVI.00263-07

Bonazzi, M., and Cossart, P. (2011). Impenetrable barriers or entry portals? the role of cellcell adhesion during infection. *J. Cell Biol.* 195, 349–358. doi: 10.1083/jcb.201106011

Connolly, S. A., Landsburg, D. J., Carfi, A., Whitbeck, J. C., Zuo, Y., Wiley, D. C., et al. (2005). Potential nectin-1 binding site on herpes simplex virus glycoprotein d. *J. Virol.* 79, 1282–1295. doi: 10.1128/JVI.79.2.1282-1295.2005

Connor, R. I., Chen, B. K., Choe, S., and Landau, N. R. (1995). Vpr is required for efficient replication of human immunodeficiency virus type-1 in mononuclear phagocytes. *Virology* 206, 935–944. doi: 10.1006/viro.1995.1016

Drees, F., Pokutta, S., Yamada, S., Nelson, W. J., and Weis, W. I. (2005). Alpha-catenin is a molecular switch that binds E-cadherin-beta-catenin and regulates actin-filament assembly. *Cell* 123, 903–915. doi: 10.1016/j.cell.2005.09.021

Fonseca, I. C. C. F. E., da Luz, F. A. C., Uehara, I. A., and Silva, M. J. B. (2018). Cell-adhesion molecules and their soluble forms: Promising predictors of "tumor progression" and relapse in leukemia. *Tumour Biol.* 40:1010428318811525. doi: 10.1177/1010428318811525

Gish, R., Jia, J. D., Locarnini, S., and Zoulim, F. (2012). Selection of chronic hepatitis B therapy with high barrier to resistance. *Lancet Infect. Dis.* 12, 341–353. doi: 10.1016/S1473-3099(11)70314-0

Glebe, D., and Bremer, C. M. (2013). The molecular virology of hepatitis B virus. *Semin. Liver Dis.* 33, 103–112. doi: 10.1055/s-0033-1345717

Glebe, D., and Urban, S. (2017). Viral and cellular determinants involved in hepadnaviral entry. *World J. Gastroenterol.* 13, 22–38. doi: 10.3748/wjg.v13.i1.22

Gottardi, C. J., Wong, E., and Gumbiner, B. M. (2001). E-cadherin suppresses cellular transformation by inhibiting beta-catenin signaling in an adhesion-independent manner. *J Cell Biol.* 153, 1049–1060. doi: 10.1083/jcb.153.5.1049

Guglielmi, K. M., Kirchner, E., Holm, G. H., Stehle, T., and Dermody, T. S. (2007). Reovirus binding determinants in junctional adhesion molecule-A. *J. Biol. Chem.* 282, 17930–17940. doi: 10.1074/jbc.M702180200

Harris, T. J., and Tepass, U. (2010). Adherens junctions: from molecules to morphogenesis. *Nat. Rev. Mol. Cell Biol.* 11, 502–514. doi: 10.1038/nrm2927

Hayes, C. N., Zhang, Y., Makokha, G. N., Hasan, M. Z., Omokoko, M. D., and Chayama, K. (2016). Early events in hepatitis B virus infection: from the cell surface to the nucleus. *J. Gastroenterol. Hepatol.* 31, 302–309. doi: 10.1111/jgh.13175

He, J., Choe, S., Walker, R., Di Marzio, P., Morgan, D. O., and Landau, N. R. (1995). Human immunodeficiency virus type 1 viral protein R (Vpr) arrests cells in the G2 phase of the cell cycle by inhibiting p34cdc2 activity. *J. Virol.* 69, 6705–6711. doi: 10.1128/JVI.69.11.6705-6711.1995

Hu, Q., Zhang, F. F., Duan, L., Wang, B., Li, P., Li, D. D., et al. (2019). E-cadherin binds glycosylated sodium-taurocholate cotransporting polypeptide to facilitate hepatitis B virus entry. *bioRxiv [Preprint]*. doi: 10.1101/729822

Ladner, S. K., Otto, M. J., Barker, C. S., Zaifert, K., Wang, G. H., Guo, J. T., et al. (1997). Inducible expression of human hepatitis B virus (HBV) in stably transfected hepatoblastoma cells: a novel system for screening potential inhibitors of HBV replication. *Antimicrob. Agents Chemother.* 41, 1715–1720. doi: 10.1128/AAC.41.8.1715

Le Duff, Y., Blanchet, M., and Sureau, C. (2009). The pre-S1 and antigenic loop infectivity determinants of the hepatitis B virus envelope proteins are functionally independent. *J. Virol.* 83, 12443–12451. doi: 10.1128/JVI.01594-09

Lee, J., Zong, L., Krotow, A., Qin, Y., Jia, L., Zhang, J., et al. (2018). N-linked glycosylation is not essential for sodium taurocholate cotransporting polypeptide to mediate Hepatitis B Virus infection *in vitro*. *J. Virol*. 92:e00732-18. doi: 10.1128/JVI.00732-18

Li, J., Zong, L., Sureau, C., Barker, L., Wands, J. R., and Tong, S. (2016). Unusual features of sodium taurocholate cotransporting polypeptide as a hepatitis B Virus receptor. *J. Virol*. 90, 8302–8313. doi: 10.1128/JVI.01153-16

Li, Q., Sodroski, C., Lowey, B., Schweitzer, C. J., Cha, H., Zhang, F., et al. (2016). Hepatitis C virus depends on E-cadherin as an entry factor and regulates its expressio on in pithelial-to-mesenchymal transition. *Proc. Natl. Acad. Sci. U.S.A*. 113, 7620–5. doi: 10.1073/pnas.1602701113

Liao, A. P., Petrof, E. O., Kuppireddi, S., Zhao, Y., Xia, Y., Claud, E. C., et al. (2008). Salmonella type III effector AvrA stabilizes cell tight junctions to inhibit inflammation in intestinal epithelial cells. *PLoS ONE* 3:e2369. doi: 10.1371/journal.pone.0002369

Meredith, L. W., Hu, K., Cheng, X., Howard, C. R., Baumert, T. F., Balfe, P., et al. (2016). Lentiviral hepatitis B pseudotype entry requires sodium taurocholate co-transporting polypeptide and additional hepatocyte-specific factors. *J. Gen. Virol*. 97, 121–127. doi: 10.1099/jgv.0.000317

Miao, Z., Xie, Z., Miao, J., Ran, J., Feng, Y., and Xia, X. (2017). Regulated entry of Hepatitis C virus into hepatocytes. *Viruses* 9:100. doi: 10.3390/v9050100

Moller-Tank, S., and Maury, W. (2015). Ebola virus entry: a curious and complex series of events. *PLoS Pathog*. 11:e1004731. doi: 10.1371/journal.ppat.1004731

Ni, Y., Lempp, F. A., Mehrle, S., Nkongolo, S., Kaufman, C., Falth, M., et al. (2014). Hepatitis B and D viruses exploit sodium taurocholate co-transporting polypeptide for species-specific entry into hepatocytes. *Gastroenterology* 146, 1070–1083. doi: 10.1053/j.gastro.2013.12.024

Nikitas, G., Deschamps, C., Disson, O., Niault, T., Cossart, P., and Lecuit, M. (2011). Transcytosis of Listeria monocytogenes across the intestinal barrier upon specific targeting of goblet cell accessible E-cadherin. *J. Exp. Med*. 208, 2263–2277. doi: 10.1084/jem.20110560

Phan, Q. T., Myers, C. L., Fu, Y., Sheppard, D. C., Yeaman, M. R., Welch, W. H., et al. (2007). Als3 is a Candida albicans invasin that binds to cadherins and induces endocytosis by host cells. *PLoS Biol*. 5:e64. doi: 10.1371/journal.pbio.0050064

Ren, J. H., Hu, J. L., Cheng, S. T., Yu, H. B., Wong, V. K. W., Law, B. Y. K., et al. (2018). SIRT3 restricts hepatitis B virus transcription and replication through epigenetic regulation of covalently closed circular DNA involving suppressor of variegation 3-9 homolog 1 and SET domain containing 1A histone methyltransferases. *Hepatology* 68, 1260–1276. doi: 10.1002/hep.29912

Ruch, T. R., and Engel, J. N. (2017). Targeting the mucosal barrier: how pathogens modulate the cellular polarity network. *Cold Spring Harb Perspect Biol*. 9:a027953. doi: 10.1101/cshperspect.a027953

Schulze, A., Gripon, P., and Urban, S. (2007). Hepatitis B virus infection initiates with a large surface protein-dependent binding to heparan sulfate proteoglycans. *Hepatology* 46, 1759–1768. doi: 10.1002/hep.21896

Schulze, A., Mills, K., Weiss, T. S., and Urban, S. (2012). Hepatocyte polarization is essential for the productive entry of the hepatitis B virus. *Hepatology* 55, 373–383. doi: 10.1002/hep.24707

Shneider, B. L., Fox, V. L., Schwarz, K. B., Watson, C. L., Ananthanarayanan, M., Thevananther, S., et al. (1997). Hepatic basolateral sodium-dependent-bile acid transporter expression in two unusual cases of hypercholanemia and in extrahepatic biliary atresia. *Hepatology* 25, 1176–1183. doi: 10.1002/hep.510250521

Stieger, B. (2011). The role of the sodium-taurocholate cotransporting polypeptide (NTCP) and of the bile salt export pump (BSEP) in physiology and pathophysiology of bile formation. *Handb. Exp. Pharmacol*. 205–59. doi: 10.1007/978-3-642-14541-4_5

Sun, Y., Wang, S., Yi, Y., Zhang, J., Duan, Z., Yuan, K., et al. (2018). The hepatitis B surface antigen binding protein: an immunoglobulin G constant region-like protein that interacts with HBV envelop proteins and mediates HBV entry. *Front. Cell Infect. Microbiol*. 8:338. doi: 10.3389/fcimb.2018.00338

Tammer, I., Brandt, S., Hartig, R., Konig, W., and Backert, S. (2007). Activation of Abl by Helicobacter pylori: a novel kinasefor CagA and crucial mediator of host cell scattering. *Gastroenterology* 132, 1309–1319. doi: 10.1053/j.gastro.2007.01.050

Tong, S., and Li, J. (2014). Identification of NTCP as an HBV receptor: the beginning of the end or the end of the beginning? *Gastroenterology* 146, 902–905. doi: 10.1053/j.gastro.2014.02.024

Trepo, C., Chan, H. L., and Lok, A. (2014). Hepatitis B virus infection. *Lancet* 384, 2053–2063. doi: 10.1016/S0140-6736(14)60220-8

Verrier, E. R., Colpitts, C. C., Bach, C., Heydmann, L., Weiss, A., and Renaud, M. (2016). A targeted functional RNA interference screen uncovers glypican 5 as an entry factor for hepatitis B and D viruses. *Hepatology* 63, 35–48. doi: 10.1002/hep.28013

Yan, H., Zhong, G., Xu, G., He, W., Jing, Z., Gao, Z., et al. (2012). Sodium taurocholate cotransporting polypeptide is functional receptor for human hepatitis B and D virus. *Elife* 1:e00049. doi: 10.7554/eLife.00049

Yulis, M., Kusters, D. H. M., and Nusrat, A. (2018). Cadherins: cellular adhesive molecules serving as signalling mediators. *J. Physiol*. 596, 3883–3898. doi: 10.1113/JP275328

Conflict of Interest: The authors declare that the research was conducted in the absence of any commercial or financial relationships that could be construed as a potential conflict of interest.

frontiers in Cellular and Infection Microbiology

ORIGINAL RESEARCH
published: 16 April 2020
doi: 10.3389/fcimb.2020.00158

Difluoromethylornithine, a Decarboxylase 1 Inhibitor, Suppresses Hepatitis B Virus Replication by Reducing HBc Protein Levels

*Binli Mao†, Zhuo Wang†, Sidie Pi, Quanxin Long, Ke Chen, Jing Cui, Ailong Huang and Yuan Hu**

Key Laboratory of Molecular Biology on Infectious Diseases, Ministry of Education, Institute for Viral Hepatitis, Department of Infectious Diseases, Second Affiliated Hospital, Chongqing Medical University, Chongqing, China

OPEN ACCESS

Edited by:
C. T. Ranjith-Kumar, Guru Gobind Singh Indraprastha University, India

Reviewed by:
Song Yang, Capital Medical University, China
Raphael Gaudin, UMR9004 Institut de Recherche en Infectiologie de Montpellier (IRIM), France

***Correspondence:**
Yuan Hu
biotottyhy@hotmail.com

†*These authors have contributed equally to this work*

Specialty section:
This article was submitted to Virus and Host, a section of the journal Frontiers in Cellular and Infection Microbiology

Received: *21 December 2019*
Accepted: *24 March 2020*
Published: *16 April 2020*

Citation:
Mao B, Wang Z, Pi S, Long Q, Chen K, Cui J, Huang A and Hu Y (2020) Difluoromethylornithine, a Decarboxylase 1 Inhibitor, Suppresses Hepatitis B Virus Replication by Reducing HBc Protein Levels. Front. Cell. Infect. Microbiol. 10:158. doi: 10.3389/fcimb.2020.00158

Current treatments of hepatitis B virus (HBV) are limited to Interferon-alpha or the nucleos(t)ide analogs antiviral therapies, and it is crucial to develop and define new antiviral drugs to cure HBV. In this study, we explored the anti-HBV effect of difluoromethylornithine (DFMO), an irreversibly inhibitor of decarboxylase 1(ODC1) on HBV replication. Firstly, we found that polyamines contributed to HBV DNA replication via increasing levels of the HBV core protein (HBc) and capsids. In contrast, depletion of polyamines either by silencing the expression of ODC1 or DFMO treatment, resulted in decreasing viral DNA replication and levels of HBc protein and capsids. Furthermore, we found that DFMO decreased the stability of the HBc protein without affecting mRNA transcription and protein translation. Taken together, our findings demonstrate that DFMO inhibits HBV replication by reducing HBc stability and this may provide a new approach for HBV therapeutics.

Keywords: hepatitis B virus, DFMO, ODC1, polyamines, HBc

INTRODUCTION

Despite employing an effective vaccine against Hepatitis B virus (HBV) infection, HBV remains a major serious health problem worldwide (Lampertico et al., 2017). There are about 257 million people chronically infected worldwide and over 887,000 death every year according to a WHO report (Revill et al., 2019). Chronic hepatitis B infection (CHB) often causes cirrhosis and liver cancer (Schweitzer et al., 2015). Currently, there are two approved antiviral treatments for CHB, including interferon-alpha and nucleotide analogs (NAs) (Block et al., 2015). However, due to the side effects of interferon-alpha or drug resistance for NAs (Zoulim and Locarnini, 2009), the current therapeutic efficacy is limited. Therefore, developing new drugs that directly target either virus or host factors for an efficient CHB treatment is viral and urgent (Mitra et al., 2018).

HBV is a small enveloped virus that encodes four overlapping open-reading frames (ORFs) including the HBV polymerase, the HBV core protein (HBc), envelope proteins, and the HBV X protein (HBx) (Seeger and Mason, 2015). Increasing evidence has indicated that HBc displays multiple complex functions during HBV replication (Diab et al., 2018), including capsid formation (Zlotnick et al., 2015) and epigenetic regulation of the cccDNA minichromosomal (Pollicino et al., 2006).

Thus, HBc has been considered to be an attractive and promising target for anti-HBV therapy (Block et al., 2015; Durantel and Zoulim, 2016), and drugs targeting HBc are currently under development (Stray and Zlotnick, 2006; Yang et al., 2016; Ko et al., 2019).

Polyamines (including putrescine, spermidine and spermine) are small and positively charged molecules, which are involved in several cellular processes in mammalian cells, such as gene transcription, mRNA translation, cell growth and apoptosis (Igarashi and Kashiwagi, 2015; Miller-Fleming et al., 2015). Polyamines are implicated in more aspects of the replication cycle of several viruses, such as the herpes simplex viruses (HSV), where polyamines facilitate viral DNA packaging (Gibson and Roizman, 1971) or chikungunya virus (CHIKV) and Zika virus (ZIKV), where polyamines are necessary for translation of the viral mRNAs (Mounce et al., 2016b). In addition, Ornithine decarboxylase (ODC1), spermidine synthase (SRM) and spermine synthase (SMS) are rate-limiting enzymes in intracellular polyamine biosynthetic pathway (Raul, 2007; **Figure 1A**). As an irreversibly inhibitor of ODC1, difluoromethylornithine (DFMO) has been recently demonstrated to inhibit replication of diverse viruses such as Human Cytomegalovirus (HCMV) (Gibson et al., 1984) by reducing the levels of polyamines. DFMO can also inhibit replication of several RNA virus, such as the Dengue virus (DENV), the ZIKV, the CHIKV (Mounce et al., 2016a). These findings have strengthened the importance of the polyamines toward viral replication and highlighted the potential function of DFMO as a promising broad-spectrum antiviral drug. However, whether polyamines are involved in HBV life cycle or DFMO can inhibit HBV replication are remain unclear. In this study, we revealed that polyamines were required for HBV replication, and DFMO could restrict the viral DNA replication via reducing the HBc protein levels. These results highlight the potential role of DFMO as a promising therapeutic target for anti-HBV treatment.

MATERIALS AND METHODS

Cell Culture and Transfection

HepAD38, HepG2, HepG2-NTCP and HepG2.2.15 cells were cultured in the Dulbecco's modified Eagle's medium (DMEM) supplemented with 10% fetal bovine serum (Biological Industries, Israel),100 U/mL penicillin (Gibco, Life Technologies, Carlsbad, CA, USA) and 100 g/mL streptomycin (Gibco, Life Technologies, Carlsbad, CA,USA). To maintain the stably transfected HBV genome, HepG2.2.15 cells were grown with 200 ug/mL G418. As for the HepAD38 cells, 1 μg/mL tetracycline was added to suppress HBV transcription.

The expression vector for 3xFlag-HBc was cloned with a N-terminal 3xFlag-tag in pEZ-M12 vector by Genecopoeia Company. The expression vectors for 3xFlag-HBx and 3xFlag-HBs are plasmids expressing the HBx and HBV surface antigen (HBs), respectively. Small interfering RNAs (siRNAs) were purchased from Shanghai Jima Company and the siRNA sequences targeting human ODC1, SRM, elF5A1 and elF5A2 have been showed in **Supplement Table 1**. Lipofectamine 3000 (Invitrogen, Carlsbad, CA, USA) was used for the transfection of plasmids or siRNAs according to the manufacturer's instructions.

Chemical Reagents

DFMO was purchased from selleckchem company. Exogenous polyamines, spermidine and spermine were purchased from Sigma company. Cycloheximide (CHX) and carbobenzoxy-Leu-Leu-leucinal (MG132) were purchased from AbMole. All drugs were stored at −20°C until further use.

RNA Purification and Real-Time RT-PCR

For RNA purification, cells were washed with PBS and total RNA was extracted by TriZol (Life Technologies, Carlsbad, CA, USA) according to the manufacturer's instructions. Purified RNA was transcribed into cDNA with Primescript RT reagent Kit with gDNA Eraser (Takara,Tokyo, Japan). Real-time RT-PCR was performed to determine the levels of target gene. Expression levels of GAPDH mRNA were used as an internal control, and the $2^{-\Delta\Delta Ct}$ method was used for the final evaluation. Primers have been shown in **Supplement Table 1**.

Western Blotting

The methods for protein measurement in cell lysates and Western blotting were performed as described previously (Chen et al., 2018). The antibodies for immunoblots used in this study are follows: anti-HBc (B0586, Dako, Denmark), anti-flag (MA-1-91878, Thermo, USA), anti-ODC1(sc-398116, Santa Cruz, USA), anti-SRM (bs-17653R, Bioss, China), anti-elF5A (ET1610-49, Hangzhou Hua An Biotechnology, China), anti-HBs (NB100-62652, Novus, USA), anti-GAPDH (100242-MM05, Sino Biological, China). Quantifications of the immunoblot band intensities were analyzed by the Image J software.

Enzyme-Linked Immunosorbent Assay (ELISA)

Hepatitis B surface antigen (HBsAg) in cell supernatant was detected using an ELISA assay kit (KHB, Shang Hai, China) according to the manufacturer's protocol.

Virus Production and HBV Infection

For production of the HBV virions, supernatants of HepAD38 cells were filtered, precipitated with 10% PEG8000, and centrifuged as described previously (Chen et al., 2018). For HBV infection, the HepG2-NTCP cells were infected with HBV viral particles at 1,000 genome equivalents (GE) per cell in the presence of PEG8000. After removing virus from the infected cells, they were maintained in the Williams' E media before harvest.

Extraction and Quantitative Analysis of HBV DNA by Southern Blotting and Real-Time PCR

The method for the extraction and detection of intracellular HBV core-associated DNA was conducted as described previously (Chen et al., 2018). Briefly, the intracellular HBV core-associated DNA was extracted through a sucrose density gradient and purified by phenol/chloroform, then the extracted viral DNA was

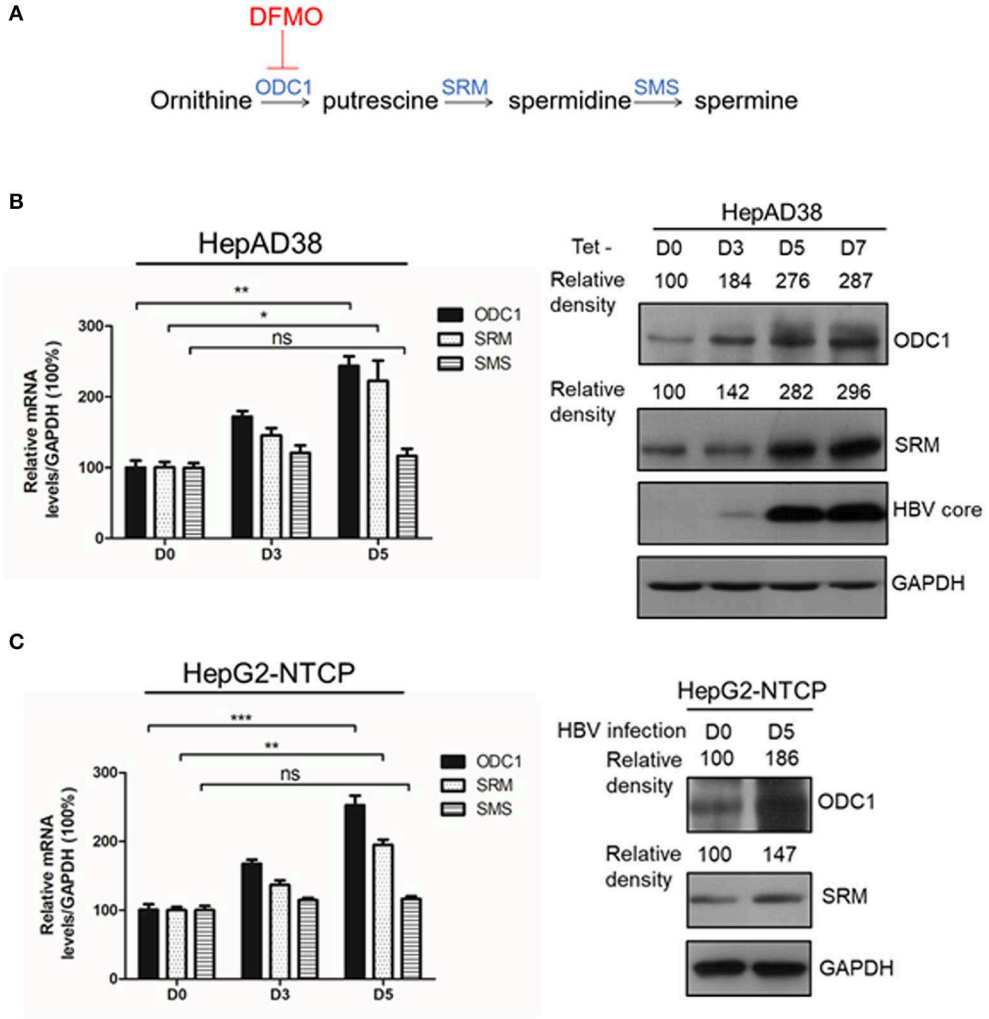

FIGURE 1 | ODC1 and SRM in polyamine metabolism pathway are upregulated in HBV replicating hepatoma cells. **(A)** Schematic representation of polyamine metabolic pathway including enzymes and inhibitors. As shown in the image, DFMO could block ODC1 activity, which converts ornithine into the putrescine. Putrescine is converted into spermidine via spermidine synthase (SRM), the spermidine is then converted into spermine via spermine synthase (SMS). **(B)** Real-time RT-PCR (left panel) and Western blotting (right panel) analysis of ODC1, SRM and SMS expression levels in the HepAD38 cells after removing tetracycline for different time points. **(C)** Real-time RT-PCR (left panel) and Western blotting (right panel) analysis of ODC1, SRM and SMS expression levels in the HepG2-NTCP infected with HBV particles with different time points. The levels of ODC1 and SRM proteins were normalized to the levels of GAPDH and analyzed by the Image J software. Statistical significance was determined by one-way ANOVA with the Tukey *post-hoc* test (*$p < 0.05$, **$p < 0.01$, ***$p < 0.001$; ns, not significant). Data have been represented as the mean ± SD of three independent experiments.

electrophoresed on 1.0% agarose gels and transferred into nylon membranes (Roche, Basel, Switzerland). After immobilization on the membranes, the viral DNA was detected by using the DIG high prime DNA labeling and detection starter kit (Roche Diagnostics). For the assessment of the HBV core-associated DNA levels by real-time PCR was conducted as previously described (Hu et al., 2018).

Native Gel Analysis of HBV Capsids

The method for the detection HBV core particles was conducted as described previously (Hu et al., 2018). Briefly, cell lysates were loaded on native 1% agarose gels, and the viral particles transferred onto a nitrocellulose (NC) membrane were probed with an anti-HBV core antibody (B0586, Dako, Denmark).

Drug Viability Assay

The cytotoxic effects of drugs employed in this research on human hepatoma cells were detected by using the Celltiter 96 aqueous non-radioactive cell proliferation assay (Promega, Madison, WI, USA). For that, cells were seeded into 96-well plates and maintained with drugs for 3 days, followed by measuring the absorbance at 490 nm according to the manufacturer's instruction.

Statistical Analysis

Statistics evaluations were performed using the GraphPad Prism8.0 (GraphPad Software, San Diego, CA, USA). Unpaired *t*-test or ANOVA by one way with Tukey *post-hoc* test was used to determine significant differences. Differences were considered as statistically significant as $p < 0.05$.

RESULTS

ODC1 and SRM in Polyamine Metabolism Pathway Are Up-Regulated in HBV Replicating Hepatoma Cells

ODC1, SRM and SMS are rate-limiting enzymes involved in intracellular polyamine biosynthetic pathway (**Figure 1A**), therefore, we initially investigated the expression of these three enzymes in the presence of HBV. In HBV-stable expressing cells HepAD38, the HBV replication was inducted by removing the tetracycline. The expression of ODC1 and SRM, but not for SMS, was gradually increased both at mRNA and the protein levels with HBc expression (**Figure 1B**). Furthermore, we examined the expression of ODC1, SRM and SMS in HepG2-NTCP cells that support HBV infection. We also found that the expression of ODC1 and SRM increased both at mRNA and the protein levels by an HBV infection (**Figure 1C**). These results suggested that ODC1 and SRM that regulate the levels of cellular polyamines were upregulated in HBV replication and infection cell models.

Silencing the Expression of ODC1 and SRM Decrease Levels of the HBV Core-Associated DNA and the HBc Protein

Next, we continued to test the potential function of ODC1 or SRM in regulating HBV replication. For that, the expression of ODC1 or SRM were knockdown by using specific siRNAs in HepAD38 (**Figure 2A**) and HBV markers, including HBsAg in the supernatant, the core-associated DNA levels or the HBc expression levels were then measured by ELISA, real-time PCR or Western blotting, respectively. As shown in **Figures 2B–D**, silencing of ODC1 or SRM in HepAD38 cells resulted in decreased viral DNA levels, as well as in the levels of the HBc protein and capsids, while it had no noticeable effect on the HBsAg levels in the supernatant. These findings suggest that ODC1 or SRM that regulating polyamine levels may be involved in HBV replication.

DFMO Inhibits HBV Core-Associated DNA Replication by Reducing HBc Protein Levels

To confirm the critical role of ODC1 in regulating HBV replication in hepatoma cells, we used DFMO, a specific inhibitor against ODC1. DFMO treatment had no impact on HBV-stably expressing cells HepAD38 or HepG2.2.15 cell viability even at high concentration of 200 μM (**Figure 3A**). The HepAD38 cells were firstly treated with DFMO under subtoxic concentration, and the HBV markers were then measured. As shown in **Figure 3B**, DFMO treatment reduced 34% of the viral DNA levels and 84% of the HBc protein levels at concentration of 100 μM. Similarly, the levels of viral capsids were also reduced significantly by DFMO treatment (**Figure 3B**). However, DFMO treatment had no effect on the levels of HBsAg in the supernatant or the HBV 3.5kb RNA levels (**Figures 3C,D**). Similar results were observed in HepG2.2.15 cells (**Figures 3E,F**). These results indicate that DFMO inhibits HBV core-associated DNA synthesis mostly by reducing HBc protein levels.

Next, to determine whether the decrease of HBc and HBV DNA levels had a potential impact on the infectiveness of this virus, HepAD38 cells were treated with DFMO for 3 days, followed by a collection of the HBV particles in the supernatants for an HepG2-NTCP cells infection. The cytoplasmic viral DNA was extracted and investigated by real-time PCR analysis. As shown in **Figure 3G**, the levels of viral DNA were decreased by 31% in the DFMO treatment group, suggesting that DFMO treatment reduced the infection capacity of viral particles. As DFMO target HBc, and nucleotide analogs such as LAM, and target HBV polymerase, we tested whether DFMO in combination with LAM led to the increased inhibition of the HBV DNA replication. Both LAM and DFMO reduced the HBV DNA levels. However, no significant combinatorial effect was observed (**Supplement Figure 1**).

Polyamines Facilitate Viral Replication and HBc Protein Levels

Considering that silencing of ODC1 or inhibition of polyamine biosynthesis by DFMO can deplete preexisting polyamines pools in cells (Gupta et al., 2016; Mounce et al., 2016b), we tested whether adding the exogenous polyamines could also affect HBV replication. First, HepAD38 cells were directly treated with polyamines for 3 days, and the intracellular viral DNA was extracted and measured by real-time PCR. As shown in **Figures 4A–C**, polyamines, without the DFMO pretreatment, had a minor effect of stimulating the viral DNA replication and the HBc protein levels, as well as moderate capsids levels, while no noticeable effect on HBsAg levels in the supernatant was observed. However, the addition of exogenous polyamines to the DFMO-pretreated HepAD38 cells significantly rescued the HBc protein and capsids levels (**Figure 4D**), suggesting HBV replication may requires threshold levels of polyamines.

Since spermine and spermidine are essential polyamines in mammals (Yuan et al., 2001; Moinard et al., 2005), then we investigated the potential function of spermine or spermidine toward an HBV replication. As expected, replenishment of spermidine or spermine at a subtoxic concentration to DFMO-pretreated HepAD38 cells rescued the HBc protein and capsids levels (**Figures 4D,E**), suggesting that polyamines stimulate viral replication by increasing HBc protein levels. Based on the data presented in **Figures 2**, **3**, we conclude that polyamines were involved in HBV replication.

DFMO Reduces of HBc Protein Levels Independent of Transcription and Translation Regulation

As DFMO reduced, and polyamines increased the HBc protein levels **Figures 3**, **4**, we investigated the underline mechanism of

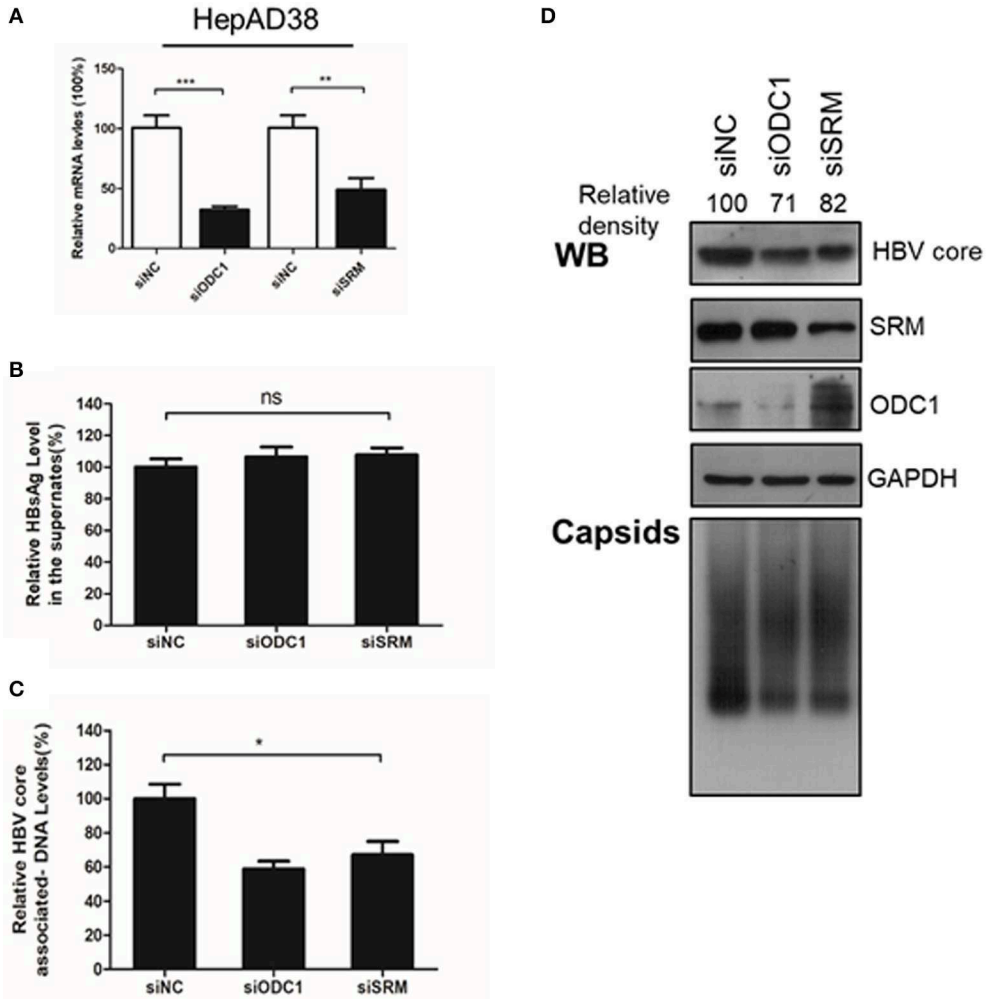

FIGURE 2 | Silencing the expression of ODC1 and SRM restricted the HBV replication and reduced the HBc protein levels. **(A)** HepAD38 cells were transfected siRNA targeting ODC1 or SRM, and the knockdown efficiency was confirmed by using real-time RT-PCR. **(B)** The HBsAg levels in the supernatants were determined by ELISA methods. **(C)** The intracellular HBV DNA was extracted and measured by real-time PCR. **(D)** The protein levels of HBc, SRM and ODC1 were measured by Western blotting using relevant antibodies, as described in **Figure 1**. For viral capsid measurement, HBV particles were analyzed using a Native gel assay. Statistical significance was determined by one-way ANOVA with Tukey *post-hoc* test (*$p < 0.05$, **$p < 0.01$, ***$p < 0.001$; ns, not significant). Data have been represented as the mean ± SD of three independent experiments.

DFMO-mediated inhibition of the HBc protein levels. HepG2 cells were transfected with Flag-tagged HBc, HBx and HBs expression plasmids, and the cells were treated with 50 μM DFMO for 3 days. We observed that only HBc, but not for HBx or HBs protein levels were significantly reduced by DFMO treatment (**Figure 5A**), supporting our suggestion that DFMO inhibits viral replication mainly by targeting the HBc protein. In addition, DFMO treatment led to decreased protein levels of HBc without affecting its mRNA levels in HepG2 cells (**Figure 5B**), suggesting that DFMO inhibits HBc expression at the post-transcriptional level. Similar results were observed by replenishment spermidine or spermine to DFMO-pretreated HepG2 cells (**Figure 5C**).

It had been reported that spermidine is necessary for the hypusination of the eukaryotic initiation factor 5A(eIF5A) (Jao and Chen, 2006; Park, 2006). Hypusinated eIF5A is a translation factor that is currently regarded to be important for peptide chain elongation and broadly participates in the replication of multiple viruses, such as HIV, EBOV and HSV-1 (Malim et al., 1990; Olsen et al., 2016; Mounce et al., 2017). In mammalian cells, there are two isoforms of eIF5A, eIF5A1 and eIF5A2, which share 84% homology and both harbor the hypusine modification (Caraglia et al., 2013). We examined whether eIF5A was necessary for the HBc protein translation. However, silencing the expression of eIF5A1 or eIF5A2 had no noticeable effect on HBc protein levels or viral DNA replication (**Figure 5D**), which indicated that DFMO inhibited HBc protein levels independent of hypusination modification of eIF5A by spermidine.

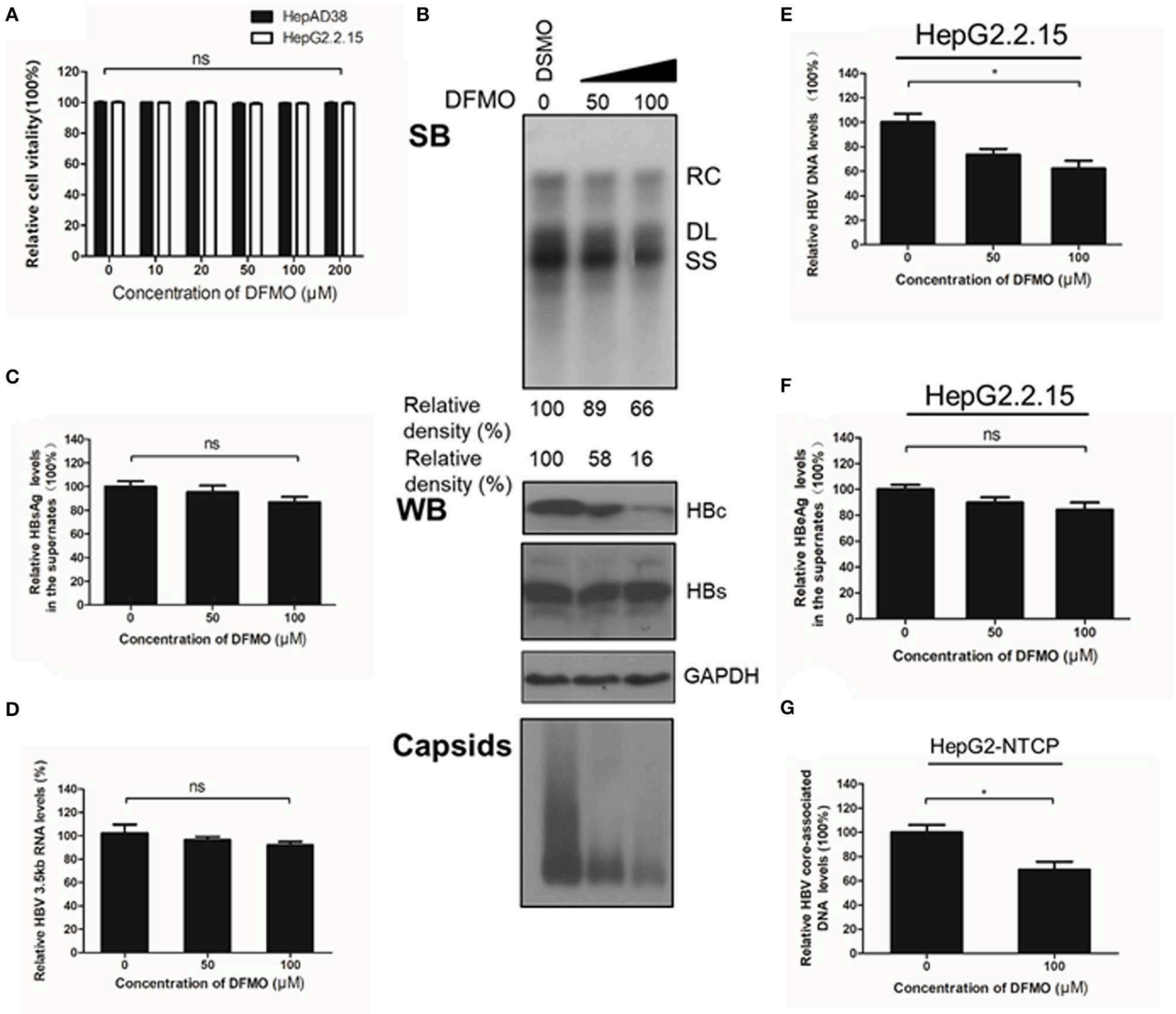

FIGURE 3 | DFMO decreases the HBV core-associated DNA and the HBc protein levels. **(A)** Determination of cytotoxicity of HepAD38 and HepG2.2.15 cells treated DFMO measured by the MTS assay. **(B)** HepAD38 cells were treated with DFMO (50 μM, 100 μM), and the HBV core-associated DNA was extracted 3 days later and measured by Southern blot (upper panel). The levels of HBc and HBs were measured by Western blotting, and capsids levels were determined using a Native gel assay (lower panel) as described above. **(C)** The levels of HBsAg in supernatant were measured by ELISA assay as described above. **(D)** HBV 3.5kb RNA levels were measured by real-time RT-PCR. **(E)** and **(F)** HepG2.2.15 cells treated with DFMO (50, 100 μM) for 3 days, then the levels of intracellular HBV DNA or HBsAg levels in the supernatant were detected by real-time PCR **(E)** or ELISA assay **(F)**. **(G)** DFMO decreased the infection capacity of the HBV particles. HepAD38 cells in the absence of tetracycline were treated with DSMO or DFMO with indicated concentration for 3 days, and the HBV viral particles were then collected and added to the HepG2-NTCP cells. Five days later, the cytoplasmic viral DNA were extracted and measured by real-time PCR. RC, relaxed circular; DL, double stranded linear; SS, single stranded. Experiments were performed in triplicate, and data are represented as means ± SD. Statistical significance was determined by one-way ANOVA with the Tukey *post-hoc* test (*$p < 0.05$; ns, not significant).

DFMO Treatment Decreases the HBc Protein Stability

Finally, we investigated whether DFMO treatment affected the HBc protein stability. HepAD38 cells were pretreated with DFMO for 3 days, and after the removal of tetracycline from the medium to initiate HBV replication, cycloheximide (CHX) was added to the cells in order to block protein synthesis. As shown in **Figure 6A**, DFMO treatment significantly reduced the half-life of HBc protein in HepAD38 cells. Similar results were obtained in the HepG2 cells transfected with Flag-tagged HBc expression plasmid (**Figure 6B**). These findings suggested that DFMO inhibited the HBc protein levels by reducing its stability.

Next, we used a proteasome inhibitor MG132 to determine whether DFMO-mediated HBc degradation was

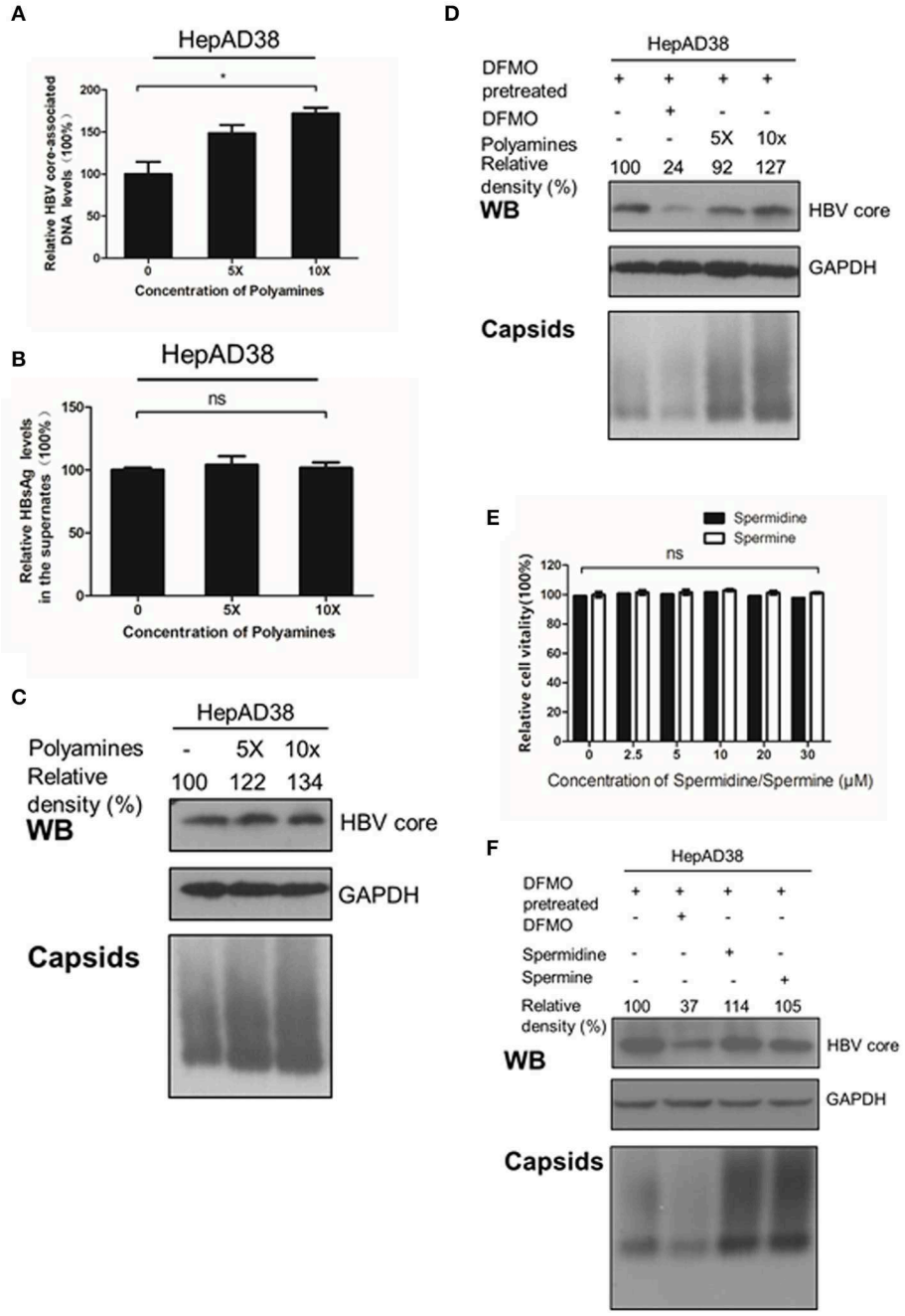

FIGURE 4 | Polyamines enhances the HBc protein levels. **(A–C)** HepAD38 cells were treated with polyamines mixture for 3 days, then the levels of intracellular HBV DNA, HBsAg in supernatant, HBc or capsids were measured using real-time PCR **(A),(B)** ELISA assay or **(C)** Western blotting. **(D)** HepAD38 cells were pretreated with DFMO (100 μM) for 3 days, then divide in four groups: the control (lane 1), DFMO-treated group (lane 2), group replenished with a polyamine mixture (lane 3 and 4) for another 3 days, followed with Western blotting or Native gels to measure the levels of HBc or viral capsids as described above. **(E)** Determination of cytotoxicity of HepAD38 treated spermidine or spermine measured by using the MTS assay. **(F)** HepAD38 cells were pretreated for 3 days with DFMO (100 μM) to deplete the levels of polyamines, followed by an addition of DFMO (100 μM), exogenous spermidine (10 μM) or spermine (10 μM) for another 3 days, then the levels of HBc protein or capsids were determined as described above. Statistical significance was determined by one-way ANOVA with the Tukey *post-hoc* test (*$p < 0.05$, ns, not significant). Mean ± SD values from three independent experiments have been shown.

dependent on the proteasome pathway. Indeed, the effects of DFMO treatment on downregulating the levels of HBc protein were abolished by MG132 treatment both in the HepAD38 and HepG2 cells (**Figures 6C,D**), indicating that DFMO inhibited the HBc protein levels via promoting its ubiquitination.

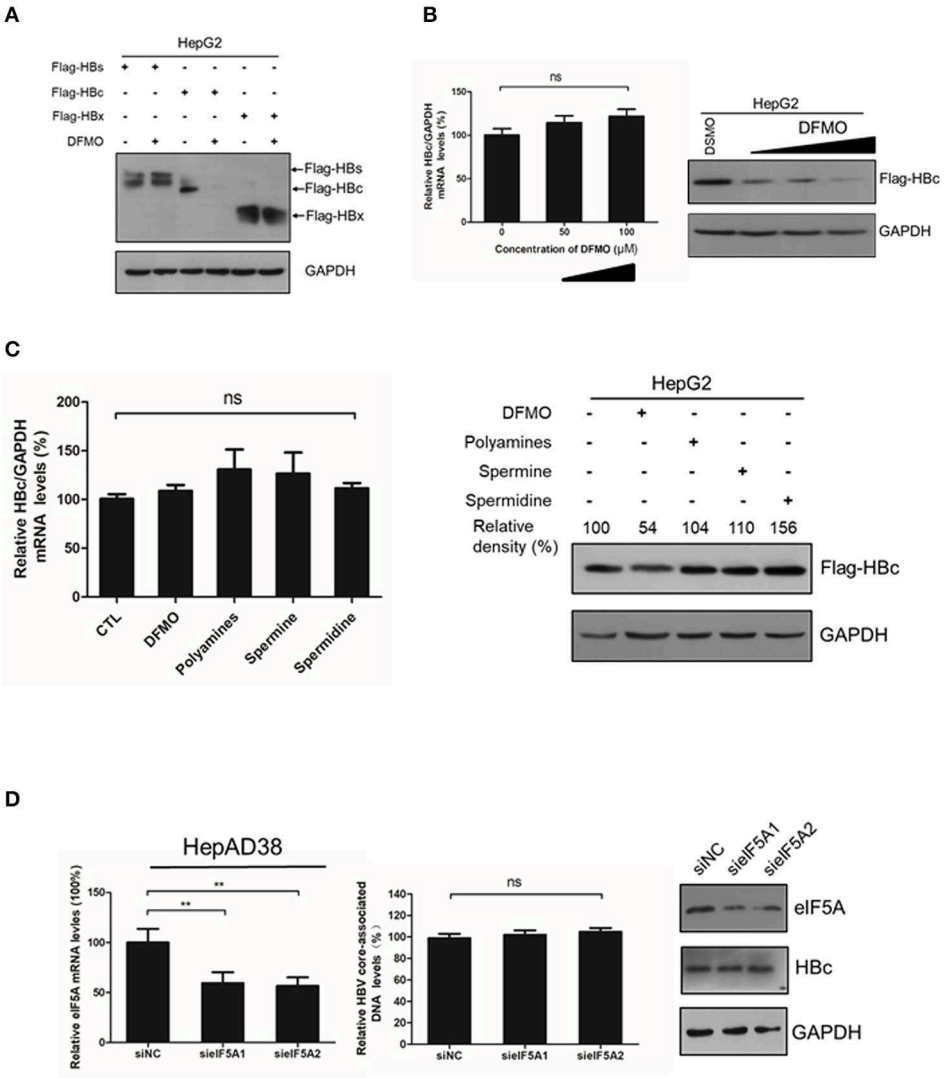

FIGURE 5 | DFMO-mediated reduction of the HBc protein levels was independent of the transcription and translation pattern. **(A)** HepG2 cells were transfected with Flag-tagged HBs, Flag-tagged HBc, and Flag-tagged HBx plasmids, and treated with 50 μM DFMO for 3 days. Total proteins were extracted and subjected to Western Blotting. **(B)** HepG2 cells were transfected with Flag-tagged HBc plasmid, followed by DFMO treatment of different concentration for 3 days. The levels of HBc mRNA and protein were detected by using real-time RT-PCR (left panel) and Western blotting (right panel), respectively. **(C)** HepG2 cells were pretreated with 50 μM DFMO, then transfected with Flag-tagged HBc plasmid, followed by a replenishment using a polyamines mixture (5x), spermidine (10 μM) or spermine (10 μM) for another 3 days as described in **Figure 4**. The levels of HBc mRNA or proteins were determined by using real-time RT-PCR (left panel) or Western blotting (right panel). **(D)** HepAD38 cells were transfected siRNA targeting eIF5A1 or eIF5A2 and the levels of intracellular HBV DNA or HBc protein were determined by real-time PCR or Western blotting. Statistical significance was determined by using one-way ANOVA with the Tukey *post-hoc* test (*$p < 0.05$, ns, not significant). Mean ± SD values from three independent experiments have been shown.

DISCUSSION

It is known that viruses can utilize host cell resources for their own replication. Understanding this process in more detail can provide strategies for the development of antiviral treatment. Polyamines play various roles within the mammalian cells, including gene transcription and mRNA translation (Childs et al., 2003; Pegg, 2009; Igarashi and Kashiwagi, 2015; Kashiwagi et al., 2018). The intracellular levels of polyamines are regulated by several rate-limiting enzymes such as ODC1, SRM and SMS. Recent reports have indicated that viral infection can affect polyamine synthesis, for instance via influencing the expression of the enzymes involved in regulation of the polyamine biosynthetic pathway and polyamine levels, and, as a consequence, contribute to their own replication during viral life cycle (Mounce et al., 2017). For example, the levels of ODC1 have been reported to increase in adenovirus-infected cells (Liu et al., 1985). Similarly, HCMV infection also stimulates the activity of ODC1 (Isom, 1979) and an increment of the spermine and spermidine levels (Clarke and Tyms, 1991). In

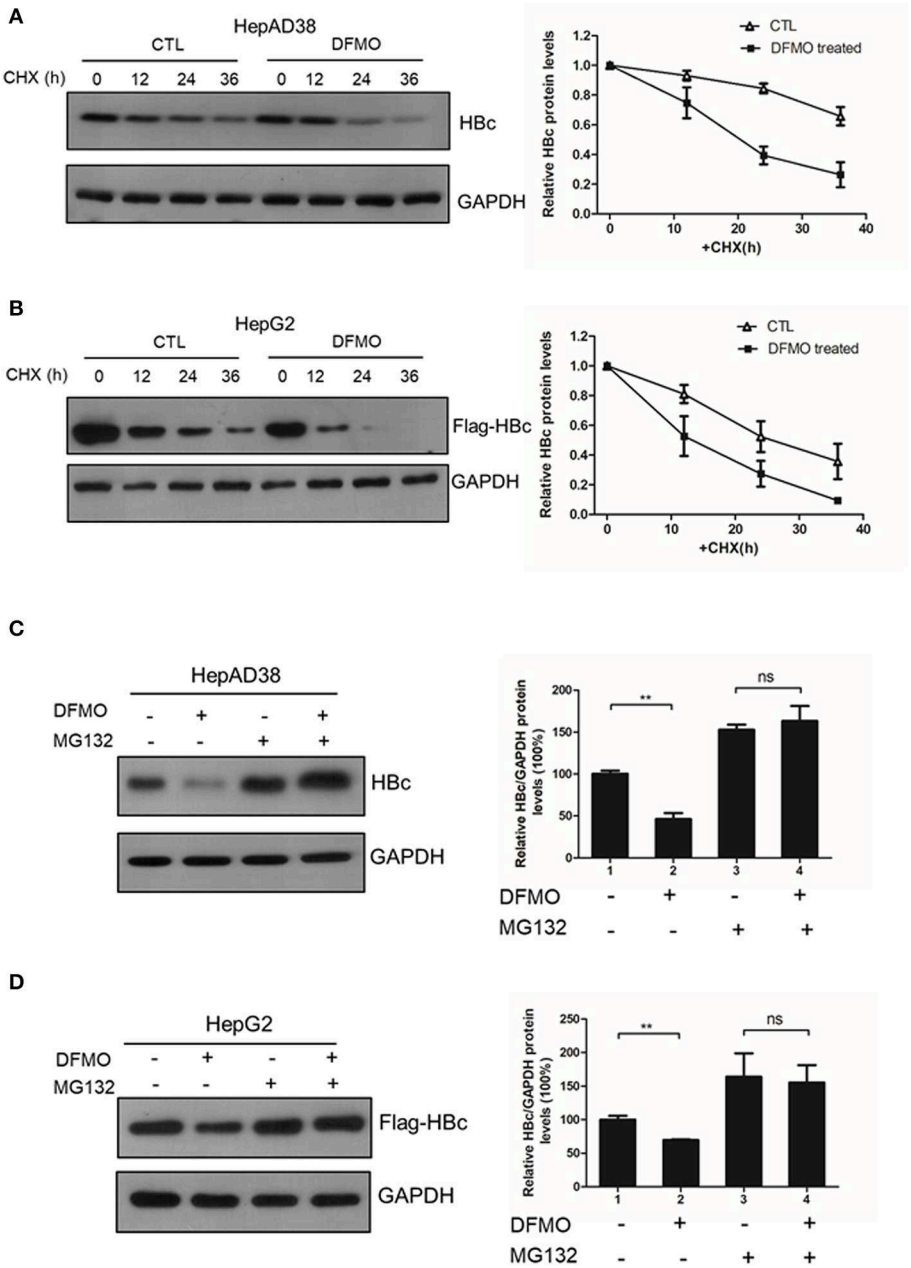

FIGURE 6 | DFMO decreased the HBc protein stability. **(A)** HepAD38 cells were treated with 100 μM DFMO in the absence of tetracycline for 3 days, and cultured then with 100 μg/mL CHX for indicated time periods. The steady-state levels of HBc were determined by Western blotting (left panel). Quantification of the HBc protein by ImageJ has been shown in the right panel. **(B)** HepG2 cells were treated with 50 μM DFMO for 3 days, then transfected with Flag-tagged HBc, followed with 100 μg/mL CHX treatment as described in A. **(C)** HepAD38 cells were treated with 100 μM DFMO for 3 days in the absence of tetracycline for 3 days, followed by a treatment with 10 μM MG132. The levels of HBc were measured by Western blotting analysis. **(D)** HepG2 cells treated with 50 μM DFMO, transfected with Flag-tagged HBc, cultured with MG132 as described in **(C)**. The levels of HBc were measured by Western blotting analysis. Statistical significance was determined by one-way ANOVA with the Tukey *post-hoc* test (*$p < 0.05$, ns, not significant). Mean ± SD values from three independent experiments have been shown.

contrast, the expression of ODC1, as well as the levels of spermine and spermidine have been reported to be reduced in cells harboring a full-length HCV replicon (Smirnova et al., 2017). In our study, we found that the expression of ODC1 and SRM were both upregulated in the HBV replication cells and cell models of infection (**Figure 1**). Furthermore, silencing the expression of ODC1 or SRM (**Figure 2**), as well as inhibition of polyamine biosynthesis with DFMO treatment (**Figure 3**), affected the replication of the viral intracellular DNA, the levels of the HBc protein and capsids, suggesting that HBV infection could utilize polyamine synthesis to regulate its replication. For the further mechanistic clarification of the polyamine metabolism,

the cells pretreated with DFMO were replenished with exogenous polyamines, including the spermine or spermidine, which significantly rescued the HBc protein and capsids levels (**Figure 4**). This observation strengthens the important role of polyamines in promoting HBV replication during the HBV life cycle. However, supplementing cells directly with polyamines had slight effect on the replication of the viral DNA and the HBc protein levels and moderate influence on the capsids levels (**Figure 4**), suggesting that HBV replication required a threshold levels of polyamines. Similar results were observed for polyamines in CHIKV replication (Mounce et al., 2016b).

As a new emerging anti-viral drugs, DFMO inhibits replication of several viruses via complex pathways: for DNA virus, such as HCMV, DFMO represses the production of viruses by interfering with the viral assembly (Tyms and Williamson, 1982; Gibson et al., 1984); while for RNA viruses, such as CHIKV and ZIKV, DFMO exhibits broad spectrum of antiviral functions by depleting the polyamines pools (Mounce et al., 2016a). In addition, hypusination of eIF5A, a unique posttranslational modification of an aminobutyl moiety from the spermidine at the Lys50 site via deoxyhypusine synthase (DHPS), is necessary for viral protein translation (Olsen and Connor, 2017). As a result, reducing the levels of spermidine by DFMO treatment can also inhibits the expression of EBOV minigenome (Olsen et al., 2016, 2018). In our research, we revealed that DFMO reduces the HBc protein levels by promoting its ubiquitination (**Figure 6**), as a consequence, inhibiting HBV capsids levels and DNA replication (**Figure 3**). This finding provides a new insight into DFMO function against viral replication. It has been reported that HBc protein can be modified by ubiquitination, and lysine K7 and K96 were potential target sites for ubiquitination (Rost et al., 2006; Lubyova et al., 2017). In addition, Np95/ICBP90-like RING finger protein (NIRF), a novel E3 ubiquitin ligase, which could promote HBc protein degradation via binding to HBc (Qian et al., 2012). In our study, we found DFMO inhibited the HBc protein levels via promoting its ubiquitination. As DFMO is an inhibitor of ODC1, which would affect the cellular polyamines levels, it is possible that ODC1/polyamines may regulating the ubiquitination of HBc by affect the expression of E3 ubiquitin ligase such as NIRF. Further work for identification of DFMO role in the ubiquitination of HBc protein will help to clarify this mechanism. Of note, the concentration of DFMO for inhibition of HBV replication applied in our study was relatively high (100 μM), meanwhile, the concentration of 500 μM was used in other studies for testing a DFMO-mediated viral RNA replication (Mounce et al., 2016a). As the human ODC1 has a rapid turnover (t1/2 <1 h) (Heby et al., 2003), it is necessary to apply high doses of the treatment in these studies.

In summary, our findings demonstrate that DFMO restricts the HBV replication via targeting the HBc stability, which highlights the importance of DFMO and reveal a new mechanism against viral replication. Given that DFMO is the Food and Drug Administration (FDA)-approved drug used to treat female facial hirsutism (Wolf et al., 2007), human African trypanosomiasis (Pepin et al., 1987), and some cancers (Casero and Woster, 2009). More importantly, DFMO is safe to use and is well tolerated in humans (Creaven et al., 1993), which highlights the its potential values as an anti-HBV therapy.

DATA AVAILABILITY STATEMENT

All datasets generated for this study are included in the article/**Supplementary Material**.

AUTHOR CONTRIBUTIONS

BM and YH conceived the project. BM, ZW and YH designed the study and analyzed the data. BM, ZW, SP, QL and KC performed the study. JC, AH and YH provided the funds. BM prepared the draft manuscript. YH edited and revised the manuscript.

FUNDING

This work was supported by the National Key Research and Development Project of China (2018YFE0107500), a National Science Foundation of China award (NSFC 81101310) and Natural Science Foundation Project of CQ CSTC (cstc2018jcyjAX0166) to YH, an National Sciences Foundation of China award (81661148057) and National Science and Technology Major Project Science & Technology Commission of China (2017ZX10202203) to AH, and by innovative talents promotion plan of Chongqing Municipal Education Commission (CY190405) to JC.

ACKNOWLEDGMENTS

We gratefully thank Professor Ni Tang of Chongqing Medical University for providing plasmids 3xFlag-HBx, Professor Ying Zhu of Wuhan University for providing plasmid Flag-HBs.

SUPPLEMENTARY MATERIAL

The Supplementary Material for this article can be found online at: https://www.frontiersin.org/articles/10.3389/fcimb.2020.00158/full#supplementary-material

Figure S1 | DFMO does not show combinational effect of inhibiting HBV DNA replication with LAM. HepAD38 cells were treated with DFMO (100 μM) or/and LAM (0.5 μM) for 3 days, and HBV core-associated DNA was extracted and measured by real-time PCR.

REFERENCES

Block, T. M., Rawat, S., and Brosgart, C. L. (2015). Chronic hepatitis B: a wave of new therapies on the horizon. *Antiviral Res.* 121, 69–81. doi: 10.1016/j.antiviral.2015.06.014

Caraglia, M., Park, M. H., Wolff, E. C., Marra, M., and Abbruzzese, A. (2013). eIF5A isoforms and cancer: two brothers for two functions? *Amino Acids* 44, 103–109. doi: 10.1007/s00726-011-1182-x

Casero, R. A. Jr., and Woster, P. M. (2009). Recent advances in the development of polyamine analogues as antitumor agents. *J. Med. Chem.* 52, 4551–4573. doi: 10.1021/jm900187v

Chen, Y., Hu, J., Cai, X., Huang, Y., Zhou, X., Tu, Z., et al. (2018). APOBEC3B edits HBV DNA and inhibits HBV replication during reverse transcription. *Antiviral Res.* 149, 16–25. doi: 10.1016/j.antiviral.2017.11.006

Childs, A. C., Mehta, D. J., and Gerner, E. W. (2003). Polyamine-dependent gene expression. *Cell Mol. Life Sci.* 60, 1394–1406. doi: 10.1007/s00018-003-2332-4

Clarke, J. R., and Tyms, A. S. (1991). Polyamine biosynthesis in cells infected with different clinical isolates of human cytomegalovirus. *J. Med. Virol.* 34, 212–216. doi: 10.1002/jmv.1890340403

Creaven, P. J., Pendyala, L., and Petrelli, N. J. (1993). Evaluation of alpha-difluoromethylornithine as a potential chemopreventive agent: tolerance to daily oral administration in humans. *Cancer Epidemiol. Biomarkers Prev.* 2, 243–247.

Diab, A., Foca, A., Zoulim, F., Durantel, D., and Andrisani, O. (2018). The diverse functions of the hepatitis B core/capsid protein (HBc) in the viral life cycle: implications for the development of HBc-targeting antivirals. *Antiviral Res.* 149, 211–220. doi: 10.1016/j.antiviral.2017.11.015

Durantel, D., and Zoulim, F. (2016). New antiviral targets for innovative treatment concepts for hepatitis B virus and hepatitis delta virus. *J. Hepatol.* 64, S117–S131. doi: 10.1016/j.jhep.2016.02.016

Gibson, W., and Roizman, B. (1971). Compartmentalization of spermine and spermidine in the herpes simplex virion. *Proc. Natl. Acad. Sci. U.S.A.* 68, 2818–2821. doi: 10.1073/pnas.68.11.2818

Gibson, W., Van Breemen, R., Fields, A., Lafemina, R., and Irmiere, A. (1984). D,L-alpha-difluoromethylornithine inhibits human cytomegalovirus replication. *J. Virol.* 50, 145–154.

Gupta, E. D., Pachauri, M., Ghosh, P. C., and Rajam, M. V. (2016). Targeting polyamine biosynthetic pathway through RNAi causes the abrogation of MCF 7 breast cancer cell line. *Tumour Biol.* 37, 1159–1171. doi: 10.1007/s13277-015-3912-2

Heby, O., Roberts, S. C., and Ullman, B. (2003). Polyamine biosynthetic enzymes as drug targets in parasitic protozoa. *Biochem. Soc. Trans.* 31, 415–419. doi: 10.1042/bst0310415

Hu, J., Qiao, M., Chen, Y., Tang, H., Zhang, W., Tang, D., et al. (2018). Cyclin E2-CDK2 mediates SAMHD1 phosphorylation to abrogate its restriction of HBV replication in hepatoma cells. *FEBS Lett.* 592, 1893–1904. doi: 10.1002/1873-3468.13105

Igarashi, K., and Kashiwagi, K. (2015). Modulation of protein synthesis by polyamines. *IUBMB Life* 67, 160–169. doi: 10.1002/iub.1363

Isom, H. C. (1979). Stimulation of ornithine decarboxylase by human cytomegalovirus. *J. Gen. Virol.* 42, 265–278. doi: 10.1099/0022-1317-42-2-265

Jao, D. L., and Chen, K. Y. (2006). Tandem affinity purification revealed the hypusine-dependent binding of eukaryotic initiation factor 5A to the translating 80S ribosomal complex. *J. Cell Biochem.* 97, 583–598. doi: 10.1002/jcb.20658

Kashiwagi, K., Terui, Y., and Igarashi, K. (2018). Modulation of protein synthesis by polyamines in mammalian cells. *Methods Mol. Biol.* 1694, 325–336. doi: 10.1007/978-1-4939-7398-9_27

Ko, C., Bester, R., Zhou, X., Xu, Z., Blossey, C., Sacherl, J., et al. (2019). A new role for capsid assembly modulators to target mature hepatitis B virus capsids and prevent virus infection. *Antimicrob. Agents Chemother.* 64:aac.01440-19. doi: 10.1128/aac.01440-19

Lampertico, P., Agarwal, K., Berg, T., Buti, M., Janssen, H., Papatheodoridis, G., et al. (2017). EASL 2017 clinical practice guidelines on the management of hepatitis B virus infection. *J. Hepatol.* 67, 370–398. doi: 10.1016/j.jhep.2017.03.021

Liu, H. T., Baserga, R., and Mercer, W. E. (1985). Adenovirus type 2 activates cell cycle-dependent genes that are a subset of those activated by serum. *Mol. Cell Biol.* 5, 2936–2942. doi: 10.1128/mcb.5.11.2936

Lubyova, B., Hodek, J., Zabransky, A., Prouzova, H., Hubalek, M., Hirsch, I., et al. (2017). PRMT5: a novel regulator of hepatitis B virus replication and an arginine methylase of HBV *core*. *PLoS ONE* 12:e0186982. doi: 10.1371/journal.pone.0186982

Malim, M. H., Tiley, L. S., Mccarn, D. F., Rusche, J. R., Hauber, J., and Cullen, B. R. (1990). HIV-1 structural gene expression requires binding of the rev trans-activator to its RNA target sequence. *Cell* 60, 675–683. doi: 10.1016/0092-8674(90)90670-a

Miller-Fleming, L., Olin-Sandoval, V., Campbell, K., and Ralser, M. (2015). Remaining mysteries of molecular biology: the role of polyamines in the cell. *J. Mol. Biol.* 427, 3389–3406. doi: 10.1016/j.jmb.2015.06.020

Mitra, B., Thapa, R. J., Guo, H., and Block, T. M. (2018). Host functions used by hepatitis B virus to complete its life cycle: implications for developing host-targeting agents to treat chronic hepatitis B. *Antiviral. Res.* 158, 185–198. doi: 10.1016/j.antiviral.2018.08.014

Moinard, C., Cynober, L., and de Bandt, J. P. (2005). Polyamines: metabolism and implications in human diseases. *Clin. Nutr.* 24, 184–197. doi: 10.1016/j.clnu.2004.11.001

Mounce, B. C., Cesaro, T., Moratorio, G., Hooikaas, P. J., Yakovleva, A., Werneke, S. W., et al. (2016a). Inhibition of polyamine biosynthesis is a broad-spectrum strategy against RNA viruses. *J. Virol.* 90, 9683–9692. doi: 10.1128/jvi.01347-16

Mounce, B. C., Olsen, M. E., and Vignuzzi, M. (2017). Polyamines and their role in virus infection. *Microbiol. Mol. Biol. Rev.* 81:00029-17. doi: 10.1128/mmbr.00029-17

Mounce, B. C., Poirier, E. Z., Passoni, G., Simon-Loriere, E., Cesaro, T., Prot, M., et al. (2016b). Interferon-induced spermidine-spermine acetyltransferase and polyamine depletion restrict zika and chikungunya viruses. *Cell Host Microbe.* 20, 167–177. doi: 10.1016/j.chom.2016.06.011

Olsen, M. E., and Connor, J. H. (2017). Hypusination of eIF5A as a target for antiviral therapy. *DNA Cell Biol.* 36, 198–201. doi: 10.1089/dna.2016.3611

Olsen, M. E., Cressey, T. N., Muhlberger, E., and Connor, J. H. (2018). Differential Mechanisms for the involvement of polyamines and hypusinated eIF5A in ebola virus gene expression. *J. Virol.* 92:01260-18. doi: 10.1128/jvi.01260-18

Olsen, M. E., Filone, C. M., Rozelle, D., Mire, C. E., Agans, K. N., Hensley, L., et al. (2016). Polyamines and hypusination are required for ebolavirus gene expression and replication. *mBio* 7:00882-16. doi: 10.1128/mBio.00882-16

Park, M. H. (2006). The post-translational synthesis of a polyamine-derived amino acid, hypusine, in the eukaryotic translation initiation factor 5A (eIF5A). *J. Biochem.* 139, 161–169. doi: 10.1093/jb/mvj034

Pegg, A. E. (2009). Mammalian polyamine metabolism and function. *IUBMB Life* 61, 880–894. doi: 10.1002/iub.230

Pepin, J., Milord, F., Guern, C., and Schechter, P. J. (1987). Difluoromethylornithine for arseno-resistant Trypanosoma brucei gambiense sleeping sickness. *Lancet* 2, 1431–1433. doi: 10.1016/s0140-6736(87)91131-7

Pollicino, T., Belloni, L., Raffa, G., Pediconi, N., Squadrito, G., Raimondo, G., et al. (2006). Hepatitis B virus replication is regulated by the acetylation status of hepatitis B virus cccDNA-bound H3 and H4 histones. *Gastroenterology* 130, 823–837. doi: 10.1053/j.gastro.2006.01.001

Qian, G., Jin, F., Chang, L., Yang, Y., Peng, H., and Duan, C. (2012). NIRF, a novel ubiquitin ligase, interacts with hepatitis B virus core protein and promotes its degradation. *Biotechnol. Lett.* 34, 29–36. doi: 10.1007/s10529-011-0751-0

Raul, F. (2007). Revival of 2-(difluoromethyl)ornithine (DFMO), an inhibitor of polyamine biosynthesis, as a cancer chemopreventive agent. *Biochem. Soc. Trans.* 35, 353–355. doi: 10.1042/bst0350353

Revill, P. A., Chisari, F. V., Block, J. M., Dandri, M., Gehring, A. J., Guo, H., et al. (2019). A global scientific strategy to cure hepatitis B. *Lancet Gastroenterol. Hepatol.* 4, 545–558. doi: 10.1016/s2468-1253(19)30119-0

Rost, M., Mann, S., Lambert, C., Doring, T., Thome, N., and Prange, R. (2006). Gamma-adaptin, a novel ubiquitin-interacting adaptor, and Nedd4 ubiquitin ligase control hepatitis B virus maturation. *J. Biol. Chem.* 281, 29297–29308. doi: 10.1074/jbc.M603517200

Schweitzer, A., Horn, J., Mikolajczyk, R. T., Krause, G., and Ott, J. J. (2015). Estimations of worldwide prevalence of chronic hepatitis B virus infection: a systematic review of data published between 1965 and 2013. *Lancet* 386, 1546–1555. doi: 10.1016/s0140-6736(15)61412-x

Seeger, C., and Mason, W. S. (2015). Molecular biology of hepatitis B virus infection. *Virology* 479-480, 672–686. doi: 10.1016/j.virol.2015.02.031

Smirnova, O. A., Keinanen, T. A., Ivanova, O. N., Hyvonen, M. T., Khomutov, A. R., Kochetkov, S. N., et al. (2017). Hepatitis C virus alters metabolism of biogenic polyamines by affecting expression of key enzymes of their metabolism. *Biochem. Biophys. Res. Commun.* 483, 904–909. doi: 10.1016/j.bbrc.2017.01.032

Stray, S. J., and Zlotnick, A. (2006). BAY 41-4109 has multiple effects on Hepatitis B virus capsid assembly. *J. Mol. Recognit.* 19, 542–548. doi: 10.1002/jmr.801

Tyms, A. S., and Williamson, J. D. (1982). Inhibitors of polyamine biosynthesis block human cytomegalovirus replication. *Nature* 297, 690–691. doi: 10.1038/297690a0

Wolf, J. E. Jr., Shander, D., Huber, F., Jackson, J., Lin, C. S., Mathes, B. M., et al. (2007). Randomized, double-blind clinical evaluation of the efficacy and safety of topical eflornithine HCl 13.9% cream in the treatment of women with facial hair. *Int. J. Dermatol.* 46, 94–98. doi: 10.1111/j.1365-4632.2006.03079.x

Yang, L., Wang, Y. J., Chen, H. J., Shi, L. P., Tong, X. K., Zhang, Y. M., et al. (2016). Effect of a hepatitis B virus inhibitor, NZ-4, on capsid formation. *Antiviral Res.* 125, 25–33. doi: 10.1016/j.antiviral.2015.11.004

Yuan, Q., Ray, R. M., Viar, M. J., and Johnson, L. R. (2001). Polyamine regulation of ornithine decarboxylase and its antizyme in intestinal epithelial cells. *Am. J. Physiol. Gastrointest. Liver Physiol.* 280, G130–G138. doi: 10.1152/ajpgi.2001.280.1.G130

Zlotnick, A., Venkatakrishnan, B., Tan, Z., Lewellyn, E., Turner, W., and Francis, S. (2015). Core protein: a pleiotropic keystone in the HBV lifecycle. *Antiviral. Res.* 121, 82–93. doi: 10.1016/j.antiviral.2015.06.020

Zoulim, F., and Locarnini, S. (2009). Hepatitis B virus resistance to nucleos(t)ide analogues. *Gastroenterology* 137, 1593–1608. doi: 10.1053/j.gastro.2009.08.063

Conflict of Interest: The authors declare that the research was conducted in the absence of any commercial or financial relationships that could be construed as a potential conflict of interest.

frontiers in Cellular and Infection Microbiology

ORIGINAL RESEARCH
published: 21 April 2020
doi: 10.3389/fcimb.2020.00135

Marmoset Viral Hepatic Inflammation Induced by Hepatitis C Virus Core Protein via IL-32

Bochao Liu[1], Xiaorui Ma[1], Qi Wang[1], Shengxue Luo[1], Ling Zhang[1], Wenjing Wang[1], Yongshui Fu[2], Jean-Pierre Allain[3], Chengyao Li[1] and Tingting Li[1]**

[1] Department of Transfusion Medicine, School of Laboratory Medicine and Biotechnology, Southern Medical University, Guangzhou, China, [2] Guangzhou Blood Center, Guangzhou, China, [3] Emeritus Professor of Transfusion Medicine, University of Cambridge, Cambridge, United Kingdom

Common marmosets infected with GB virus-B (GBV-B) chimeras containing hepatitis C virus (HCV) core and envelope proteins (CE1E2p7) developed more severe hepatitis than those infected with HCV envelope proteins (E1E2p7), suggesting that HCV core protein might be involved in the pathogenesis of viral hepatitis. The potential role of HCV core in hepatic inflammation was investigated. Six individual cDNA libraries of liver tissues from HCV CE1E2p7 or E1E2p7 chimera-infected marmosets (three animals per group) were constructed and sequenced. By differential expression gene analysis, 30 of 632 mRNA transcripts were correlated with the immune system process, which might be associated with hepatitis. A protein–protein interaction network was constituted by STRING database based on these 30 differentially expressed genes (DEGs), showing that IL-32 might play a central regulatory role in HCV core-related hepatitis. To investigate the effect of HCV core protein on IL-32 production, HCV core expressing and mock constructs were transfected into Huh7 cells. IL-32 mRNA and secretion protein were detected at significantly higher levels in cells expressing HCV core protein than in those without HCV core expression ($P < 0.01$ and $P < 0.001$, respectively). By KEGG enrichment analysis and using the specific signaling pathway inhibitor LY294002 for inhibition of PI3K, IL-32 expression was significantly reduced ($P < 0.001$). In conclusion, HCV core protein induces an increase of IL-32 expression via the PI3K pathway in hepatic cells, which played a major role in development of HCV-related severe hepatitis.

Keywords: HCV core protein, viral hepatic inflammation, IL-32, PI3K pathway, common marmosets

OPEN ACCESS

Edited by:
C. T. Ranjith-Kumar, Guru Gobind Singh Indraprastha University, India

Reviewed by:
Alec Jay Hirsch, Oregon Health and Science University, United States
Arup Banerjee, Translational Health Science and Technology Institute (THSTI), India

****Correspondence:***
Chengyao Li
chengyaoli@hotmail.com
Tingting Li
apple-ting-007@163.com

Specialty section:
This article was submitted to Virus and Host, a section of the journal Frontiers in Cellular and Infection Microbiology

Received: *27 November 2019*
Accepted: *13 March 2020*
Published: *21 April 2020*

Citation:
Liu B, Ma X, Wang Q, Luo S, Zhang L, Wang W, Fu Y, Allain J-P, Li C and Li T (2020) Marmoset Viral Hepatic Inflammation Induced by Hepatitis C Virus Core Protein via IL-32. Front. Cell. Infect. Microbiol. 10:135. doi: 10.3389/fcimb.2020.00135

INTRODUCTION

Hepatitis C virus (HCV), a serious infectious disease that is transmitted through blood, is one of the most common viral causes of liver disease, affecting more than 170 million people worldwide. Chronic HCV infection causes chronic viral hepatitis C and liver dysfunction, which relates to the progression of cirrhosis and human hepatocellular carcinoma (HCC) (Choo et al., 1991). HCV is a single-stranded RNA flavivirus and has a 9.6-kilobase genome (kb) that encodes 10 proteins: structural core and envelope E1, E2, and p7, non-structural NS2, NS3, NS4A, NS4B, NS5A, and NS5B, respectively. Some of these proteins could interact with host cellular factors and promote tumor growth *in vivo* and *in vitro* (Ray et al., 1996; Gale et al., 1999; Park et al., 2000; Lerat et al., 2002). Previous studies found that core, NS3, NS5A, and NS5B could affect cell proliferation

(Machida et al., 2001; Massague, 2004; Hara et al., 2006) or enhance oncogenic transformation (Banerjee et al., 2010).

HCV core protein is involved in the regulation of liver cell proliferation and cell transformation. It is thought that HCV is an important factor leading to HCC, although the molecular mechanisms determining such functions of virus remained unclear. HCV core protein may interact with transcription factors of p53, p21, NF-kB, and 14-3-3 protein, which are known to be involved in the development of HCC (Banerjee et al., 2010). HCV core protein could inhibit apoptosis, which is mediated by TNF-α (Ray et al., 1998; Marusawa et al., 1999) and interacted with TNF receptor 1 and lymphotoxin-β receptor that is involved in apoptotic signaling (Marusawa et al., 1999). HCV core protein expression reportedly affected the cell cycle of hepatocytes (HepG2) by increasing the levels of cell-cycle-dependent kinase inhibitor (CdkI) p21 (Nguyen et al., 2003). Common marmosets (*Callithrix jacchus*) are a kind of New World small primates and can be infected by GB virus B (GBV-B), a flavivirus closer to HCV (Bukh et al., 1999). Marmosets infected with GBV-B exhibited typical viral hepatitis similar to hepatitis C patients (Lanford et al., 2003; Jacob et al., 2004) and could be used as a surrogate animal model for HCV infection (Bright et al., 2004). In order to explore the core protein function, the marmosets infected with chimeric viruses of HCV structural core and envelope protein (CE1E2p7) or envelope protein (E1E2p7) sequences integrated within GBV-B genome were comparatively analyzed in combination with previous infected animals (Li et al., 2014).

De novo transcriptome sequencing has been used widely for studying specific gene expression patterns in different tissues or at different developmental stages, prediction of new transcripts (Denoeud et al., 2008), identification of alternative splicing (Lin et al., 2016), detection of single-nucleotide polymorphisms (SNPs) (Trick et al., 2009), and discovery of insertions/deletions in transcripts (Trapnell et al., 2010). In this study, cDNA libraries of liver tissue samples from two groups of marmosets infected with HCV-CE1E2p7/GBV-B or HCV-E1E2p7/GBV-B chimeras were sequenced. The IL-32 expression induced by HCV core protein was identified, which was demonstrated to play a critical role in occurrence of hepatic inflammation during HCV infection.

MATERIALS AND METHODS

Ethics Statement

The use of common marmoset experimentation was approved by the Southern Medical University (SMU) Animal Care and Use Committee (permit numbers: SYXK[Yue]2010-0056). All animal care and procedures (NFYYLASOP-037) were in accordance with national and institutional policies for animal health and well-being. All efforts were made to minimize suffering of animals.

Animal Liver Tissue Samples

Six common marmosets (*C. jacchus*) were obtained from Tianjin Medical University and individually fed in Laboratory Animal Research Center of Nanfang Hospital, Guangzhou, China. Liver tissue samples were collected specifically for this study from the animals infected with HCV/GBV-B chimeras in our previous study (Li et al., 2014).

Histopathological Examination

Small sections of liver tissue from left, right, and caudate lobes of each animal liver were examined with hematoxylin and eosin (H&E) staining as described previously (Li et al., 2014). The necrosis and inflammation were graded on a 0–18 scale according to the modified HAI system (Knodell et al., 1981).

CDNA Libraries and Sequencing

Total RNA was isolated from liver tissue samples using TRIzol reagents according to the manufacturer's introduction (Invitrogen, Carlsbad, USA). Hepatic mRNAs were isolated from the extracted total RNA by Oligo (dT) after treatment with DNase I and then reversely transcribed to cDNAs. The purified cDNA fragments were connected with adapters and the suitable fragments were amplified by PCR. The quality control (QC) was implemented in cDNA library establishment by using Agilent 2100 Bioanalyzer and ABI StepOnePlus Real-Time PCR System. The cDNA libraries were sequenced by using Illumina HiSeq4000.

Sequence Data Processing and Analysis

In order to get clean sequencing data, the raw sequence reads were filtered for the low-quality sequences by eliminating the adaptors or a large amount of unknown sequencing reads. After mapping clean reads to reference genome, novel transcript prediction, SNP and INDEL detection, and differentially splicing gene (DSG) detection were performed. When obtaining novel transcripts, the coding sequences were compared with references to obtain a complete reference, and then gene expression analysis against this reference was performed. Differentially expressed genes (DEGs) were detected, in which possible function and pathway were analyzed by the Gene Ontology (GO) annotation system and the KEGG database, respectively. GO terms or pathways with a corrected $P \leq 0.05$ were considered significantly enriched for DEGs. GO annotation results were analyzed by the Web Gene Ontology Annotation Plot (WEGO) software.

Cells and Plasmids

Huh7 (human hepatocellular cell line) cells were cultured at 37°C in a 5% CO_2 incubator in Dulbecco's modified Eagle medium (DMEM) supplemented with 10% FBS, 100 g/ml streptomycin, and 100 g/ml penicillin. The HCV or GBV-B core-expressing plasmid pcDNA3.1 constructs were generated by inserting either the full-length HCV core (genotype 1b) or the GBV-B core sequence as described previously (Li et al., 2014). T-vector containing the same sequence of HCV core or GBV-B core was used as non-expressing construct.

Cell Transfection and Inhibition

A density of 4×10^5 Huh7 cells in 2 ml of complete RPMI 1640 medium without antibiotics were plated in a 6-well plate for 24 h incubation. For transfection, 10 μl of Lipofectamine 2000 (Invitrogen) was diluted in 250 μl of FBS and antibiotic-free

Opti-MEM (Invitrogen) and incubated for 5 min. Meanwhile, 2-μg DNA constructs (pcDNA3.1-HCV or -GBV-B core, T-vector-HCV or -GBV-B core) were diluted in 250 μl of Opti-MEM and incubated for 5 min. Then, the mixture of Lipofectamine and construct solutions and 1.5 ml of Opti-MEM were added onto the cells and incubated for 6 h. The medium was replaced with 10% FBS RPMI 1640 and incubated for 24–72 h for detection. Inhibition of signaling pathway in transfected Huh7 cells was conducted by incubation with the specific inhibitors (LY294002, SB203580, and SH-4-54) at different concentrations (5, 10, and 20 μM), respectively.

Verification by Quantitative Real-Time RT-PCR

Total RNA of liver tissue samples or Huh7 cells were extracted using TRIzol method (Invitrogen) and reverse-transcripted using Reverse Transcription System according to the manufacturer's instructions (Roche, Basel, Switzerland). RT-PCR reactions were performed with SYBR Master Mix following the manufacturer's protocol (Roche, Basel, Switzerland). Amplification reactions were started for 2 min at 95°C, and then performed for 40 cycles at 95°C for 15 s, 55°C for 30 s, and 72°C for 30 s. All quantifications were carried out in triplicate and glyceraldehyde-3-phosphatedehydrogenase (GAPDH) was taken as internal control. Results were presented as mean value ± standard deviation (SD). IL-32-specific primers included a forward primer, 5′-CGACTTCAGAGAGTGCATGTT-3′, and a reverse primer, 5′-TGTTGCCTCTGAGTCGTAATTC-3′. The primers for the other analyzed proteins (IL-6, TNFa, IL18, IL8, IL1b, and GAPDH) were cited appropriately (Fujii et al., 2013; Jagessar et al., 2013). The fold change (FC) for the level of mRNA was calculated by the following equations: $\Delta CT = \Delta CT(\text{target}) - \Delta CT(\text{GAPDH})$; $\Delta\Delta CT = \Delta CT(\text{infected}) - \Delta CT(\text{control})$; mRNA fold change $= 2^{-\Delta\Delta CT}$.

Immunohistochemistry

Immunohistochemical staining (IHC) was performed as previously described (Li et al., 2014). Briefly, after dewaxing and dehydration, the tissue slides were incubated with anti-IL-32 antibody (BioLegend, San Diego, CA). Then, the HRP-conjugated secondary antibody (PV-6002 Two-step IHC Detection Reagent, ZSGB company, Beijing, China) was added to the tissue sections and incubated for 30 min. Slides were developed with DAB and counterstained with hematoxylin, and then dehydrating in ethanol and xylene. The scoring was evaluated according to the intensity of staining and the frequency of stained cells (Koo et al., 2009).

Enzyme Immunoassay (EIA)

The amount of IL-32 in culture supernatants was measured by a kit with Human IL-32 DuoSet ELISA (R&D Systems, Minneapolis, MN, USA).

Immunofluorescence Staining (IFS)

Huh7 cells were seeded onto 24-well plates and transfected with pcDNA3.1-HCV core, pcDNA3.1-GBV-B core, or mock plasmid by Lipofectamine 2000 (Invitrogen, Guangzhou, China). The monoclonal antibody (mAb) to HCV core (C1F5 clone) or GBV-B core (1E5 clone) was used as primary antibody provided in the laboratory (Li et al., 2014), whereas Alexa Fluor 594 (red) goat anti-mouse IgG (Invitrogen) was used as secondary antibody for detection of the core protein in transfected cells. Diamidinophenylindoldiacetate (DAPI) was added to stain cell nuclei.

Western Blot

Cells were lysed with RIPA buffer containing protease inhibitors at 24–72 h after transfection or treatment, and total protein lysate of each group was separated by 12% SDS-PAGE, and then transferred to a PVDF membrane (Millipore). The membranes were saturated with blocking solution (containing 1% BSA) for 2 h at room temperature and then incubated with specific primary antibody overnight at 4°C. After washing with PBST, the membranes were incubated with HRP-conjugated secondary antibody for 1 h at room temperature. Immunostaining was detected using an ECL substrate and GAPDH served as the internal reference.

Statistical Analysis

All experiments were performed at least three times independently. The data were analyzed using the statistical package SPSS v. 16.0. The results were presented as the mean ± SD. Difference between groups were analyzed by using Student's *t*-test, and $P < 0.05$ was considered statistically significant.

RESULTS

Difference of Necroinflammatory Grade in Histopathological Changes of Liver Tissues Between Marmosets Infected by HCV Chimeras With or Without HCV Core Protein

Among HCV/GBV-B chimera-infected marmoset models, we observed that the necroinflammatory grades of pathological changes in liver tissues from HCV-CE1E2p7/GBV-B chimera-infected marmosets (M3, M6, and M15) were obviously severe than those from marmosets (M1, M10, and M18) infected by HCV-E1E2p7/GBV-B chimera without HCV core protein. To further confirm this phenomenon, the liver tissue sections from left, right, and caudate lobes of each animal liver were examined for histopathological changes (**Figure 1A**). The HAI scores were evaluated for significant difference between two chimeric virus-infected marmosets with HCV core or without HCV core protein (mean of HAI score: 3.89 vs. 1.56; **Table 1** and **Figure 1B**, $P < 0.001$). The viral loads in the liver tissues at the time points used for cDNA library construction and sequencing are shown in **Figure 1C**. The data suggested that HCV core might play a role in leading to severely hepatic inflammation of HCV chimera-infected marmosets.

De novo Assembly of Illumina Sequencing Reads and Annotation of DEGs

To reveal the difference of genomic transcripts in liver tissues between HCV chimera-infected marmosets with or without HCV core protein, six cDNA libraries of individual liver tissues

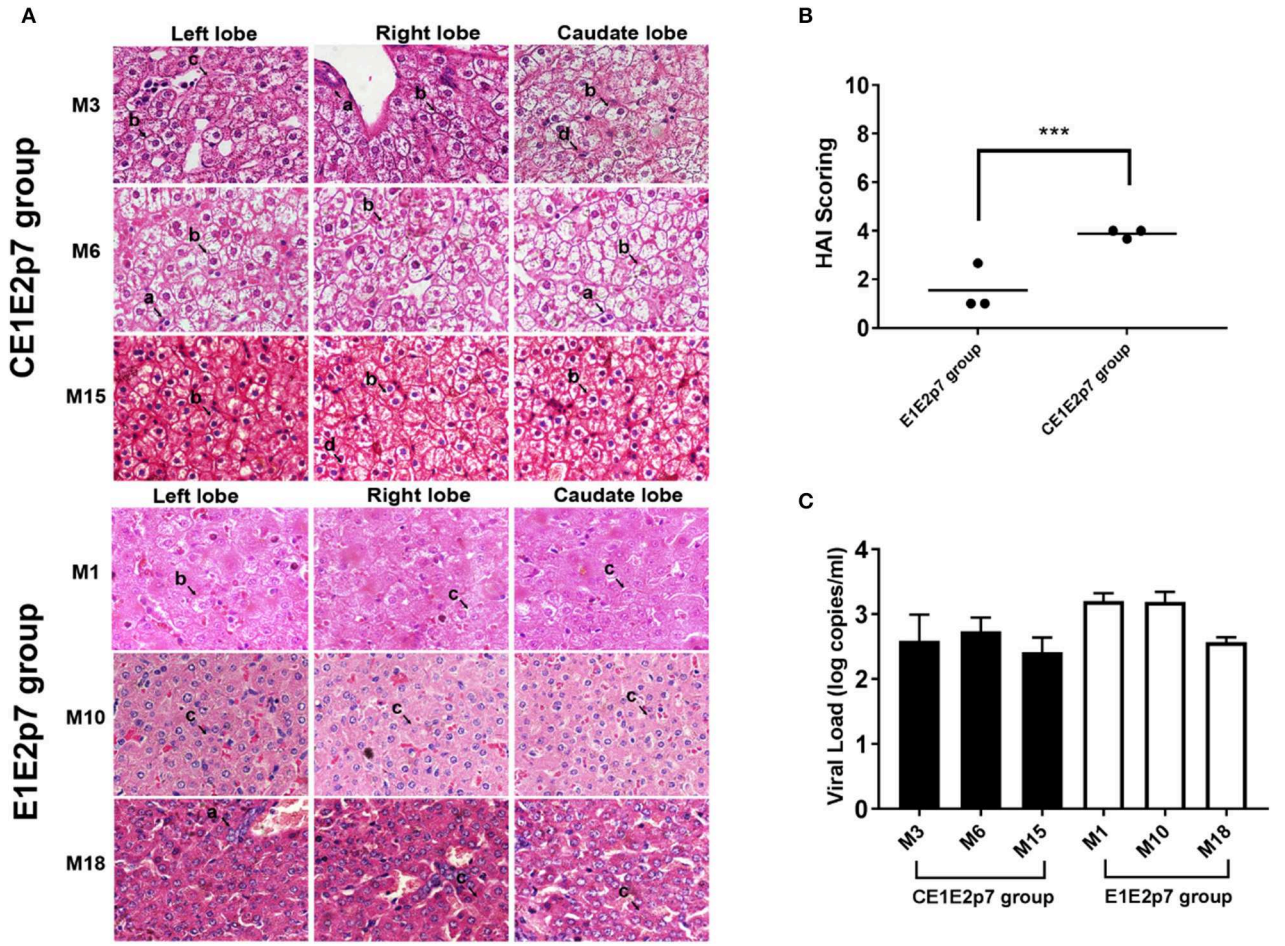

FIGURE 1 | Difference of necroinflammatory grade in histopathological changes of liver tissues between marmosets infected by HCV chimeras with or without HCV core protein. **(A)** H&E staining was conducted on the liver tissues collected by left, right, and caudate lobes of each liver from marmosets. The original magnification was × 800. (a) Lymphocytic infiltrates, (b) ballooning degeneration (edema), (c) ground glass liver cells, and (d) eosinophilic cells. **(B)** Necroinflammatory grades in histopathological changes of liver tissues were scored by the modified HAI system, in which inflammation grades were on a scale of 0 to 18. $^{***}P < 0.001$. **(C)** The viral loads in the liver tissues infected with HCV-CE1E2p7/GBV-B or HCV-E1E2p7/GBV-B for the time points used for cDNA library construction and sequencing.

from two groups of HCV-CE1E2p7 or -E1E2p7 chimera-infected marmosets were constructed and sequenced in a single run. After mapping the sequence reads against reference genomes and the reconstructed transcripts, 26,758 novel transcripts were obtained, in which 17,413 were previously unknown. Splicing events for known genes generated 1,113 novel coding transcripts with unknown features, and the remaining 8,232 were long non-coding RNAs.

A transcript-level expression analysis was conducted to detect the differentially expressed mRNAs between two groups of HCV chimera-infected liver tissues using ballgown R package. Taking $P < 0.05$ and fold change (FC) > 1.5 as cutoff, 235 mRNAs were found to be down-regulated, while 397 mRNAs were up-regulated in the group infected by CE1E2p7 chimera with HCV core protein (**Figure 2A**). The MA plot (**Figure 2B**) and the volcano plot (**Figure 2C**) showed the distribution and significance of the differentially expressed genes (DEGs).

Using DEGs, we performed GO classification and functional enrichment. Among 632 DEGs, 30 genes were correlated with immune system process, which played an important role in hepatitis and contained in biological process (**Figure 2D**). By comprehensive analysis of data obtained from these 30 DEGs, a protein–protein interaction network was constituted by STRING database (**Figure 2E**), which indicated that IL-32 played a core regulatory role in the immune system. To validate the RNA-seq results, the relative fold changes of IL-32 and the five DEGs including IL-6, TNF-α, IL-18, IL-8, and IL-1β that correlated with IL-32 in this network in liver tissue samples from HCV CE1E2p7 or E1E2p7 chimera-infected marmosets were measured by RT-qPCR (**Figure 2F**). The Pearson correlation of fold changes in gene expression between RT-qPCR and RNA-seq analysis was significant (**Figure 2G**), which suggested that RT-qPCR results were consistent with RNA-seq results. Immunohistochemical staining results showed that the relative mean density of

TABLE 1 | Histopathological observations.

Virus	Marmoset	Time point (week)	Necroinflammatory grade*			
			Left lobe	Right lobe	Caudate lobe	Mean value
CE1E2p7	M3	26	3	4	4	3.67
	M6	20	4	4	4	4
	M15	44	4	4	4	4
E1E2p7	M1	37	4	2	2	2.67
	M10	29	1	1	1	1
	M18	17	1	1	1	1

**The histological status was determined by the modified HAI system (Kondell score), which grades necrosis and inflammation on a scale of 0–18 (periportal inflammation and necrosis, 0–10; lobular inflammation and necrosis, 0–4; portal inflammation, 0–4).*

hepatic IL-32 staining in liver tissues from HCV-CE1E2p7/GBV-B chimera-infected marmosets was significantly increased compared with that of animals infected with HCV-E1E2p7/GBV-B chimera (mean of IHC scores: 8.63 vs. 3.23; **Figures 3A,B**, $P < 0.01$). The levels of IL-32 expression (IHC scoring) in liver tissues were positively correlated with the HAI scores of histopathological changes in liver tissues from six marmosets (**Figure 3C**, $P = 0.001$, $R^2 = 0.9462$), but not correlated with viral loads.

As shown in **Figures 3D,E**, level of hepatic or serum IL-32 from HCV-CE1E2p7/GBV-B chimera-infected marmosets was significantly higher than that from HCV-E1E2p7/GBV-B chimera-infected animals ($P < 0.05$).

HCV Core Protein Induces IL-32 Production in Huh7 Cells

To investigate the effect of HCV core protein on IL-32 expression, pcDNA3.1-HCV core, pcDNA3.1-GBV-B core, and mock construct DNAs were transfected into Huh7 cells. Forty-eight hours later, the production of HCV core or GBV-B core protein was confirmed in the expressing vector-transfected cells but not in mock plasmid-transfected cells by immunofluorescence staining (**Figure 4A**) and Western blot (**Figures 4B,C**), suggesting that HCV core or GBV-B core protein was present in the cells, respectively. Meanwhile, IL-32 mRNA from transfected cells was measured by RT-qPCR (**Figure 5A**), showing that IL-32 mRNA level increased significantly in the cells transfected with HCV core expressing construct. It was five times higher than that in the cells transfected with GBV-B core expressing construct ($P < 0.01$).

To confirm the effect of HCV core protein on IL-32 expression, culture supernatants from transfected cells were tested for secreted IL-32 protein by ELISA. As shown in **Figure 5B**, IL-32 protein concentration was twofold higher in the supernatant of pcDNA3.1-HCV core construct-transfected cells than that in pcDNA3.1-GBV-B core-transfected cells ($P < 0.001$). The results suggested

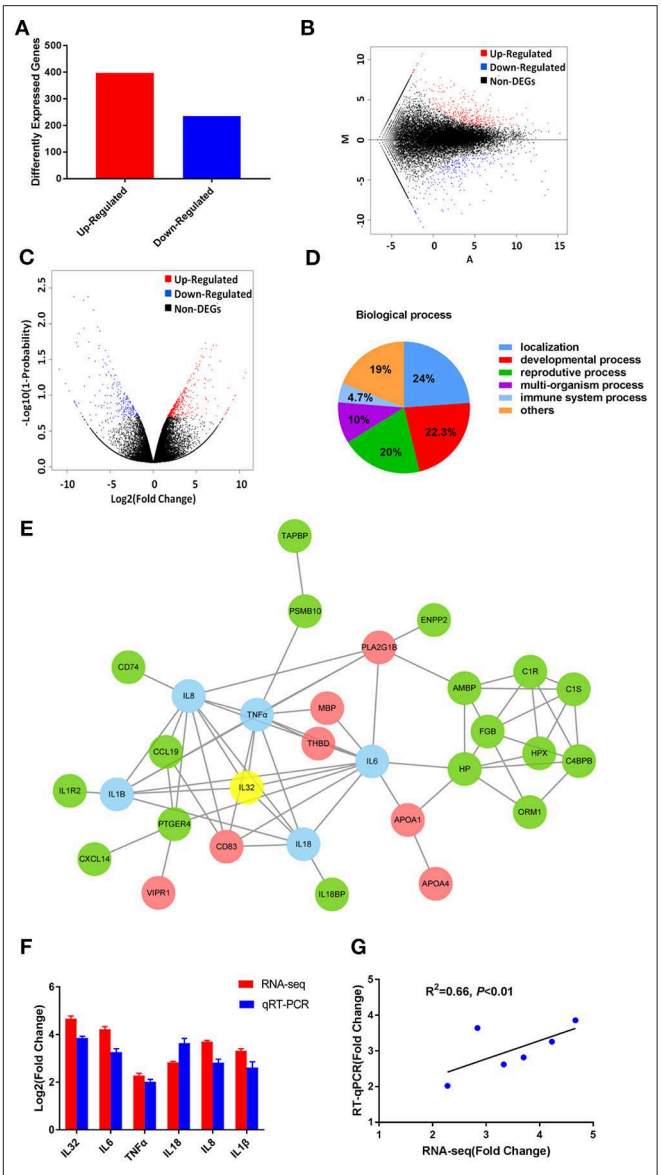

FIGURE 2 | The RNA-seq results revealed the critical role of HCV core in the development of severe hepatic inflammation in HCV/GBV-B chimera-infected marmosets. **(A)** Among 632 DEGs, 235 genes were found to be down-regulated, while 397 genes were up-regulated in the group infected by CE1E2p7 chimera with HCV core protein. The MA plot **(B)** and the volcano plot **(C)** showed the distribution and significance of the differentially expressed genes (DEGs). **(D)** Among 632 DEGs, 30 genes were correlated with immune system process, which were contained in the biological process when performing GO classification and functional enrichment. **(E)** IL-32 played a core regulatory role in protein–protein interaction network constituted by the 30 DEGs involved in immune system process. The interaction network map was constructed by STRING database. Green indicated up-regulation, red indicated down-regulation, and blue indicated the DEGs correlated with IL-32, which was marked in yellow. The data were obtained from the transcriptome sequencing results. **(F)** The relative fold changes of IL-32 mRNA and the DEGs correlated with IL-32 in samples of marmoset's liver tissues were quantified by RT-qPCR and RNA-seq. Total RNA of liver tissue samples were extracted and reversely transcripted. All quantitative measurements were carried out in triplicate and normalized to GAPDH control in every reaction. Results were expressed as mean value ± standard deviation (SD) from three independent experiments. **(G)** Pearson correlation of fold changes (FC) in gene expression between RT-qPCR results and RNA-seq results ($P < 0.01$).

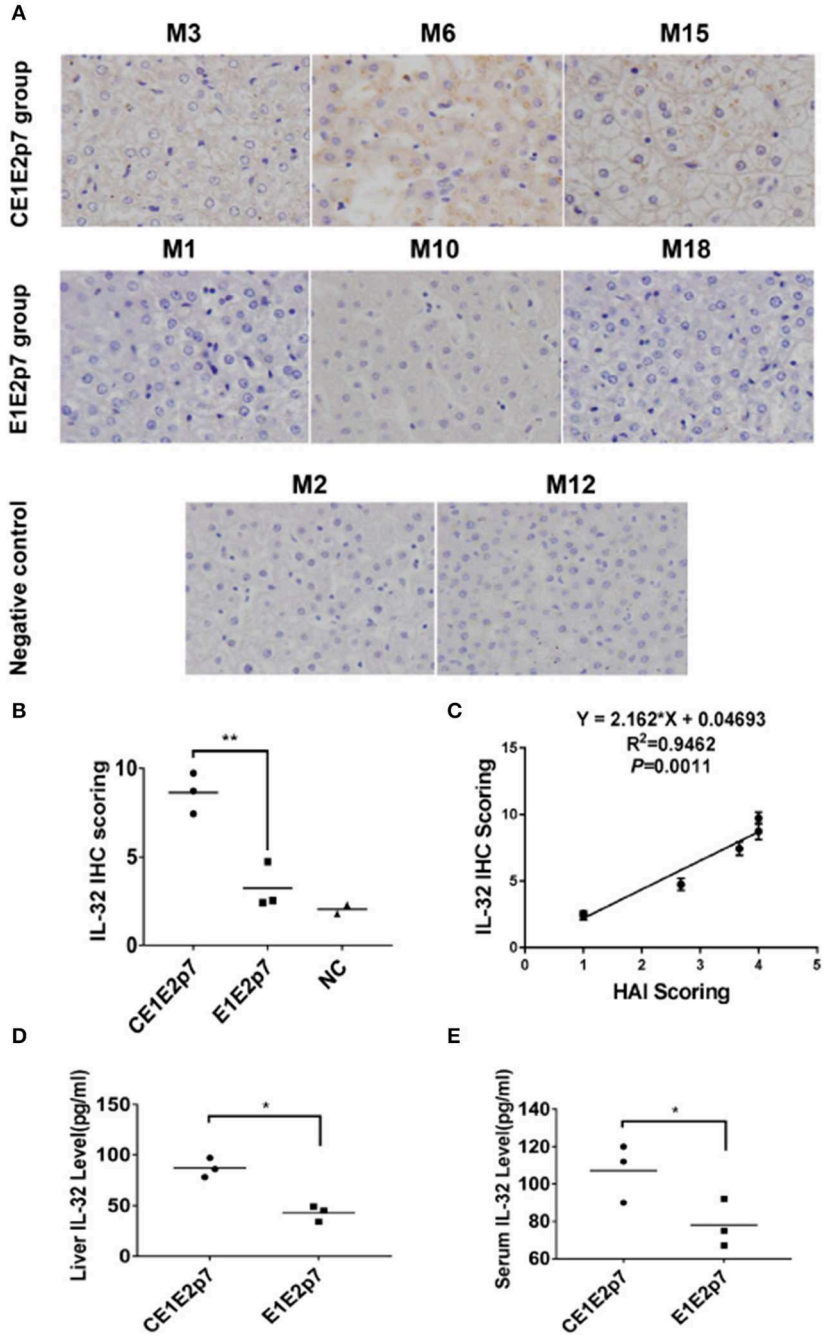

FIGURE 3 | IL-32 protein was detected in liver tissues or sera from HCV chimera-infected marmosets. **(A)** Immunohistochemical staining of IL-32 protein in liver tissues from marmosets M3, M6, and M15 infected with HCV-CE1E2p7 chimera, or M1, M10, and M18 infected with HCV-E1E2p7 chimera. The original magnification was × 200. **(B)** The IHC score was assessed according to the intensity of staining (no staining, 0; weak staining, 1; moderate staining, 2; strong staining, 3) and the extent of stained cells (0%, 0; 1 to 10%, 1; 11 to 50%, 2; 51 to 80%, 3; 81 to 100%, 4). The final score was determined by multiplying the intensity scores by the extent of positivity scores of stained cells. The difference between HCV CE1E2p7 and E1E2p7 chimera-infected marmosets was significant ($P < 0.01$). **(C)** Level of IL-32 expression in liver tissues from six marmosets is correlated with necroinflammatory grades (HAI scores) in histopathological changes of liver tissues scored by the modified HAI. **(D)** Liver IL-32 protein or **(E)** serum IL-32 protein from six marmosets (the last week before sacrifice) was tested by ELISA. The difference between the two groups was significant ($P < 0.05$). Data were presented as mean value ± SD from three separate experiments. *$P < 0.05$, **$P < 0.01$.

that the presence of HCV core protein could significantly increase IL-32 secretion in the supernatant of transfected Huh7 cells.

To eliminate the possibility that HCV core DNA might induce IL-32 expression, T-vector-HCV core, T-vector-GBV-B core, and empty-pcDNA3.1 or empty-T-vector mock plasmids

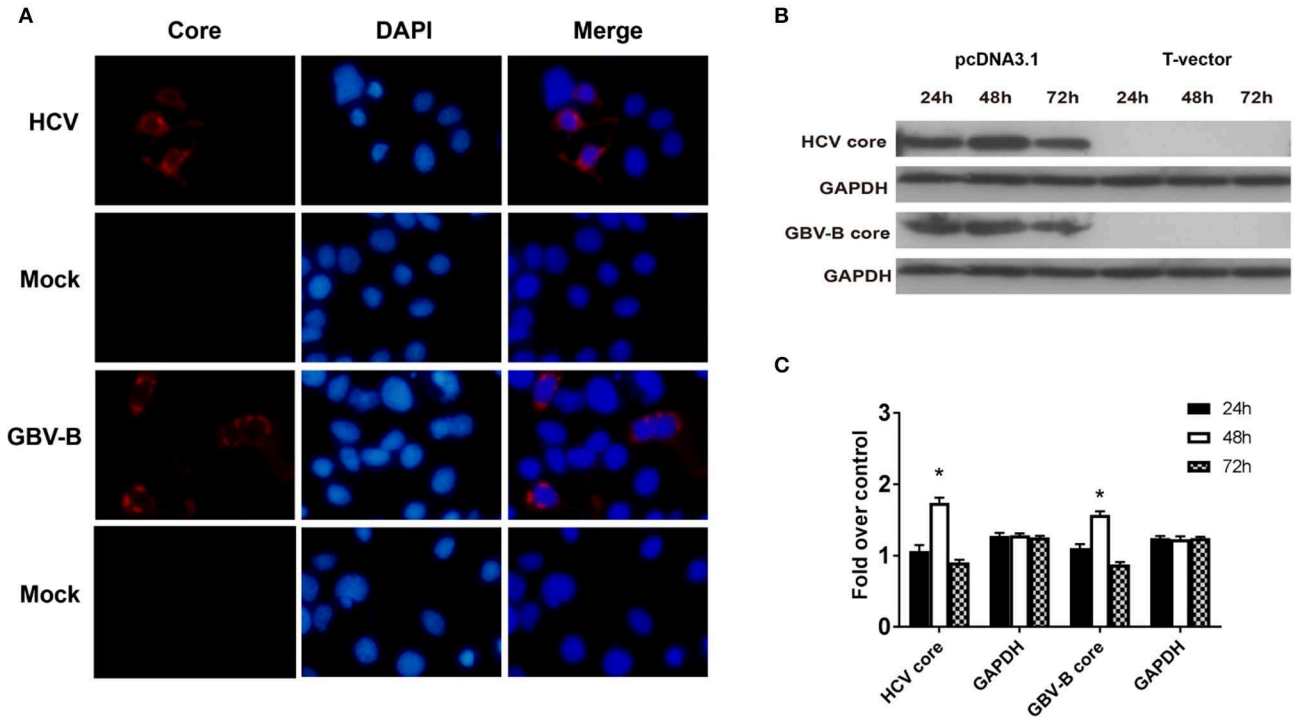

FIGURE 4 | The expression of HCV core or GBV-B core protein was confirmed in the expressing vector transfected Huh7 cells. **(A)** Immunofluorescence staining for HCV or GBV-B core protein in transfected Huh7 cells. Huh7 cells were seeded onto 24-well plates and transfected with 1 μg of pcDNA3.1-HCV core or pcDNA3.1-GBV-B core or mock plasmid, respectively. After 48 h, the cells were stained with mAb to HCV core or GBV-B core. Cell nuclei were stained in blue with DAPI. Original magnification was ×200. **(B,C)** Western blot analysis for HCV core and GBV-B core proteins in transfected Huh7 cells at the time point of 24, 48, and 72 h. *$P < 0.05$ vs. the 24-h group. All experiments were repeated three times.

were transfected into Huh7 cells. Forty-eight hours later, IL-32 at mRNA and supernatant protein levels from transfected Huh7 cells were measured by RT-qPCR and ELISA, respectively. The results showed no difference among T-vectorial HCV core DNA, GBV-B core DNA, and empty-vector controls (**Figures 5A,B**), suggesting that only HCV core protein could induce IL-32 expression in these cells.

HCV Core-Induced IL-32 Expression via the PI3K/AKT Pathway

Since little was known about the regulation of IL-32 production, we further examined which signaling pathway was involved in production of IL-32 stimulated by HCV core protein in Huh7 cells. Here, 562 out of 632 DEGs were categorized to 268 KEGG pathways. To identify the most impacted pathways, a KEGG enrichment analysis was performed for HCV-CE1E2p7/GBV-B chimera-infected marmosets, which contained 92 pathways of $P < 0.05$. Among these pathways, PI3K/AKT, JAK/STAT, and MAPK were previously described relative to IL-32 (Nishida et al., 2008; Ko et al., 2011; Moschen et al., 2011).

To identify which pathway was involved in HCV core protein for inducing IL-32 production, the specific signaling pathway inhibitors of LY294002 (PI3K inhibitor), SB203580 (MAPK inhibitor), and SH-4-54 (STAT inhibitor) were utilized in pcDNA3.1-HCV core construct-transfected Huh7 cells. Levels of IL-32 mRNA transcripts and proteins were quantified by RT-qPCR and ELISA, respectively (**Figures 5C,D**). Approximately 60–80% reduction of IL-32 mRNA level in transfected cells was observed by PI3K and MAPK inhibitors ($P < 0.001$; **Figure 5C**), while a 46% reduction of IL-32 protein secretion in the supernatant of transfected cells was solely found by PI3K inhibitor ($P < 0.001$; **Figure 5D**). Furthermore, the levels of PI3K, pAKT, AKT, and IL-32 expression were quantified by Western blot (**Figure 5E**). When compared with the control group, HCV core protein increased the expression levels of PI3K, pAKT, and IL-32 in Huh7 cells. In contrast, when compared with the HCV core expression group, the inhibitor LY294002 (with concentrations of 5, 10, and 20 μM) inhibited the expression of PI3K, pAKT, and IL-32 in Huh7 cells in a dose-dependent fashion (**Figure 5F**). These results suggested that HCV core protein may induce IL-32 production via the PI3K/AKT pathway. Further, to identify the regulatory role of IL-32 associating with inflammatory cytokines, levels of mRNA transcripts for IL-6, IL-1β, TNFα, IL-18, and IL-8 were detected from Huh7 cells in 48 h incubated with the supernatants from pcDNA3.1-HCV core-transfected Huh7 cells only (**Figure 5G**a), supernatants from transfected Huh7 cells treated with 20 μM LY294002 (**Figure 5G**b), and anti-IL-32 antibody neutralized supernatants from transfected Huh7 cells

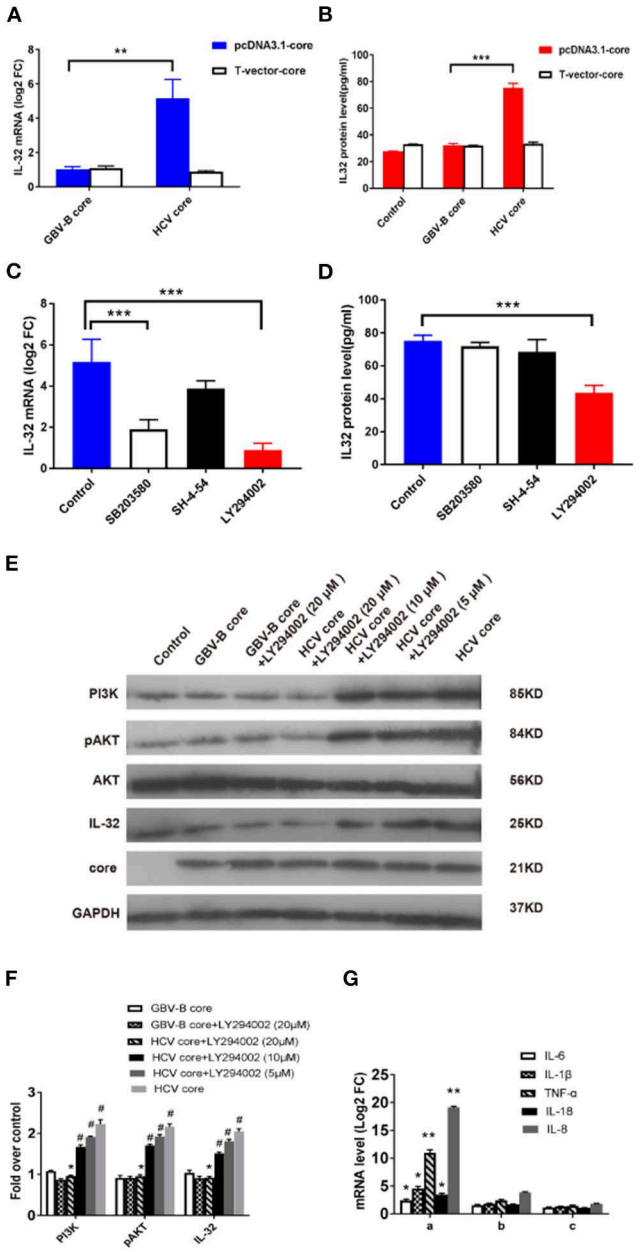

FIGURE 5 | HCV core-induced IL-32 expression via the PI3K/AKT pathway. **(A)** The level of IL-32 mRNA (relative fold change, FC) in samples of Huh7 cells transfected for 48 h with pcDNA3.1-HCV core, pcDNA3.1-GBV-B core, or mock plasmid was quantified by RT-qPCR. **(B)** The level of IL-32 protein in culture supernatants of Huh7 cells in 48 h after transfecting with pcDNA3.1-HCV core, pcDNA3.1-GBV-B core, or mock plasmid was quantified by ELISA. **(C–E)** Inhibition of HCV core induced IL-32 expression in Huh7 cells by specific signaling pathway inhibitors. Huh7 cells were treated with the specific signaling pathway inhibitors of LY294002 (PI3K inhibitor), SB203580 (MAPK inhibitor), and SH-4-54 (STAT inhibitor), respectively, by following transfection with pcDNA3.1-HCV core construct DNA. After 48 h, **(C)** levels of IL-32 mRNA transcripts and **(D)** secretion protein were quantified by RT-qPCR and ELISA. Huh7 cells transfected with pcDNA3.1-HCV core but without inhibitor were used as negative control (NC). A reduction of IL-32 mRNA or protein in transfected cells was compared between inhibitor and control. **(E,F)** The levels of downstream molecules including PI3K, AKT, pAKT, *(Continued)*

FIGURE 5 | and IL-32 were detected by Western blot for analyzing PI3K pathway. Huh7 cells transfected with mock plasmids were used as control. PI3K and IL-32 were normalized against GAPDH, and pAKT were normalized against GAPDH as well as total AKT. #$P < 0.05$ vs. control; *$P < 0.05$ vs. HCV core group; **$P < 0.01$; ***$P < 0.001$. **(G)** The level of inflammatory cytokine mRNAs from Huh7 cells in 48 h incubated with the (a) supernatants from pcDNA3.1-HCV core-transfected Huh7 cells; (b) supernatants from pcDNA3.1-HCV core-transfected Huh7 cells treated with 20 μM LY294002; (c) anti-IL-32 antibody neutralized supernatants from pcDNA3.1-HCV core-transfected Huh7 cells. The levels of inflammatory cytokine mRNAs from Huh7 cells in 48 h incubated with supernatants from mock plasmid-transfected Huh7 cells were set as controls. *$P < 0.05$ vs. control; **$P < 0.01$ vs. control. Data were presented as mean value ± SD from three separate experiments, in which each measurement was carried out in triplicate.

(**Figure 5G**c), respectively. Compared with the controls from mock plasmid-transfected Huh7 cells, these five inflammatory cytokine mRNAs were significantly elevated, especially 10.96-fold for TNFα and 19.13-fold for IL-8 (**Figure 5G**a). After treating with LY294002 or anti-IL32 antibody, these mRNA levels decreased significantly (**Figure 5G**b,c). These results suggested that IL-32 might act as a central role in the hepatic inflammation regulatory network.

DISCUSSION

Chronic HCV infection is a risk factor for development of hepatic steatosis, cirrhosis, and HCC (Raimondi et al., 2009). However, the exact molecular pathogenesis of chronic HCV infection-mediated hepatitis is not entirely explored. A study suggested that expression of the core protein increased cell proliferation, DNA synthesis, apoptosis, cell cycle progression, cell transformation, steatosis, and HCC in transgenic mice (Moriya et al., 1998). Looking back at our previously reported study (Li et al., 2014), we observed that the marmosets infected with HCV core protein-containing viral chimera experienced more severe hepatic inflammation than animals infected with viral chimera that did not express HCV core protein. These data suggested that HCV core might lead to hepatic inflammation. Despite the availability of complete genome sequence from marmosets (Worley et al., 2014), no data covers the transcriptome of liver tissue for marmosets. Based on the mRNA transcripts of liver tissues from HCV chimera-infected marmosets in the present study, we found that the presence of HCV core protein was positively correlated with the severe viral hepatitis in marmosets (**Figure 3C**), which might be a stage toward progression to HCC as demonstrated previously in mice for HCV core protein inducing HCC (Moriya et al., 1998).

In this study, the complexity of liver transcriptome of marmosets was analyzed by high-throughput RNA sequencing. We found 632 genes with expression patterns differentiating between two groups of marmosets infected with HCV CE1E2p7 chimera and E1E2p7 chimera, respectively. Among those mRNA transcripts, IL-32 was considered the most important factor leading to hepatitis in infected marmosets. IL-32 is a cytokine produced by T-cells, natural killer (NK) cells,

monocyte/macrophage, and epithelial cells, that includes six isoforms of IL-32α, β, γ, δ, ε, and ζ. IL-32α is the most abundant isoform (Ko et al., 2011). IL-32 could activate the NF-kB and p38-MAPK pathways to induce proinflammatory cytokines (IL-1β, IL-6, and TNFα) and chemokines (IL-8 and MIP-2) by stimulating monocytes and macrophages (Yousif et al., 2013). A previous study indicated that the levels of IL-32 mRNA were significantly correlated with hepatic inflammation and that HCV infection of Huh 7.5 cells increases IL-32 expression (Moschen et al., 2011). However, this study indicated that HCV infection induced IL-32 transcription in Huh7.5 cells without clarifying whether the IL-32 expression was induced by HCV core protein. Further, to confirm IL-32 relating to the hepatic inflammation regulatory network, five inflammatory cytokine mRNAs (IL-6, IL-1β, TNFα, IL-18, and IL-8) were measured from Huh7 cells incubated with or without the functional IL-32 (**Figure 5G**). The data supported the idea that IL-32 promoted the production of inflammatory cytokines. To test the hypothesis that HCV core protein induced IL-32 expression, pcDNA3.1-HCV core or -GBV-B core expressing constructs, pT-Vector-HCV core or -GBV-B core non-expressing constructs, and empty-vector controls were transfected into Huh7 cells. We first found that HCV core protein expression induced an increase of IL-32 mRNA transcripts and secretion proteins in transfected cells. Since IL-32 exerts pro-inflammatory effects in various cell types including epithelial, endothelial, and mononuclear cells (Kim et al., 2005; Nold-Petry et al., 2009), our results might explain the important role of HCV core protein in developing viral hepatitis.

As described previously, the PI3K/AKT pathway regulates IL-32α production in human alveolar epithelial cells (Ko et al., 2011) and also mediates IL-32α induction in human pancreatic periacinar myofibroblasts (Nishida et al., 2008). MAPK signaling pathway is also related to MyD88-dependent IL-32α production in IL-1β-stimulated human alveolar epithelial cells (Moschen et al., 2011). TNFα alone or in combination with IFNα could induce IL-32 production in Huh7.5 cells as well as in Hep3B cells. The IL-32 induction was completely abrogated by inhibition of NF-kB signaling (by BAY11-7082) but not JAK/STAT signaling (by Jak Inhibitor I). In contrast to hepatocytes, IL32 induction was dependent on both NF-kB and JAK/STAT signaling pathways in $CD14^{+}$ monocytes (Moschen et al., 2011). Since the NF-kB pathway was not found in the 92 pathways obtained from DEG sequencing results ($P < 0.05$), we focused on PI3K/AKT, JAK/STAT, and MAPK as the potential targets for the pathways involved in IL-32 induction stimulated by HCV core protein. To explore the critical role of those signaling pathways, specific signaling pathway inhibitors of PI3K (LY294002), MAPK (SB203580), or STAT inhibitor (SH-4-54) were added to HCV core expressing construct-transfected Huh7 cells. A reduction of IL-32 mRNA level in transfected cells was obtained by PI3K and MAPK inhibitors, while only a reduction of secretion IL-32 protein was identified in the supernatant of transfected cells by PI3K inhibitor. This suggested that HCV core protein-induced IL-32 production was mainly through the PI3K pathway. Western blot results show that (**Figures 5E,F**) HCV core protein increased the expression of PI3K, pAKT, and IL-32 in Huh7 cells. In contrast, LY294002 inhibited the expressions of PI3K, pAKT, and IL-32 in Huh7 cells. Thus, the changes in the expression levels of IL-32 in HCV core construct-transfected Huh7 cells were regulated by the PI3K/AKT signaling pathway.

The secretion of IL-32α could be stimulated by IL-1β in A549 cells, regulated by the PI3K/AKT signaling pathway, and suppressed by inhibitors of SFKs, PKCδ, or p38 (Ko et al., 2011). IL-32 could also be constitutively produced in Huh7.5 cells stimulated by IL-1β and TNFα (Moschen et al., 2011), and it also could be induced in monocyte by HCV (Pang et al., 2016). IL-1β acts an important role in various cellular responses such as inflammation (Charles, 1997). The binding of IL-1β to type I IL-1 receptors (IL-1RI) could trigger recruitment of the adapter protein MyD88, which could affect PI3K/AKT signaling pathway by regulating PKCδ and PI3K (Braddock and Quinn, 2004). HCV could activate production of IL-1β through the NLRP3 inflammasome pathway (Ramos et al., 2012), which could show response in both acute and chronic inflammation (Allen et al., 2009). The exact mechanism by which HCV core protein stimulates IL-32 expression and secretion through the PI3K/AKT pathway may be dependent on inflammatory cytokines like IL-1β or TNFα. As the relationship between HCV core and IL-1β (or TNFα) was not explored in this study, we focused on how HCV core protein affected PI3K/AKT signaling pathway, and we would examine that if IL-1β or TNFα was involved in this progression in the future.

In summary, an increase of IL-32 production was induced by HCV core protein via the PI3K/AKT pathway, which might explain the association with a high grade of hepatic inflammation in HCV-infected individuals. Clearance of HCV core protein or modulation of IL-32 activity might be an option to reduce inflammation in patients with chronic hepatitis C.

DATA AVAILABILITY STATEMENT

All data associated with this study are available in the main text or the Supplementary Materials, and HCV/GBV-B chimeras or constructs are available in the Department of Transfusion Medicine, Southern Medical University, Guangzhou, China.

ETHICS STATEMENT

The animal study was reviewed and approved by Southern Medical University (SMU) Animal Care and Use Committee (permit numbers: SYXK(Yue)2010-0056).

AUTHOR CONTRIBUTIONS

CL and TL designed research. BL, XM, QW, SL, LZ, WW, and TL performed research. CL, BL, TL, and YF analyzed data. BL, TL, CL, and J-PA wrote the paper.

FUNDING

This work was supported by grants from the National Natural Science Foundation of China (Nos. 31770185 and 31500134),

the National Key Research and Development Program (No. 2017YFD0500300), the Guangdong Province Universities and Colleges Pearl River Scholar Funded Scheme (2017), and the Guangzhou major project of industry–university–research cooperation and collaborative innovation (Nos. 201508020061 and 201704020083). The funders have no role in study design, data collection and analysis, decision to publish, or preparation of the manuscript.

REFERENCES

Allen, I. C., Scull, M. A., Moore, C. B., Holl, E. K., McElvania-Tekippe, E., Taxman, D. J., et al. (2009). The NLRP3 inflammasome mediates *in vivo* innate immunity to influenza A virus through recognition of viral RNA. *Immunity* 30, 556–565. doi: 10.1016/j.immuni.2009.02.005

Banerjee, A., Ray, R. B., and Ray, R. (2010). Oncogenic potential of hepatitis C virus proteins. *Viruses* 2, 2108–2133. doi: 10.3390/v2092108

Braddock, M., and Quinn, A. (2004). Targeting IL-1 in inflammatory disease: new opportunities for therapeutic intervention. *Nat. Rev. Drug Discov.* 3, 330–339. doi: 10.1038/nrd1342

Bright, H., Carroll, A. R., Watts, P. A., and Fenton, R. J. (2004). Development of a GB virus B marmoset model and its validation with a novel series of Hepatitis C virus NS3 protease inhibitors. *J. Virol.* 78, 2062–2071. doi: 10.1128/JVI.78.4.2062-2071.2004

Bukh, J., Apgar, C. L., and Yanagi, M. (1999). Toward a surrogate model for hepatitis C virus: an infectious molecular clone of the GB virus-B hepatitis agent. *Virology* 262, 470–478. doi: 10.1006/viro.1999.9941

Charles, A. (1997). Interleukin-1. *Cytokine Growth Factor Rev.* 8, 253–265. doi: 10.1016/S1359-6101(97)00023-3

Choo, Q. L., Richman, K. H., Han, J. H., Berger, K., Lee, C., Dong, C., et al. (1991). Genetic organization and diversity of the hepatitis C virus. *Proc. Natl. Acad. Sci. U. S. A.* 88, 2451–2455. doi: 10.1073/pnas.88.6.2451

Denoeud, F., Aury, J. M., Da Silva, C., Noel, B., Rogier, O., Delledonne, M., et al. (2008). Annotating genomes with massive-scale RNA sequencing. *Genome Biol.* 9:175. doi: 10.1186/gb-2008-9-12-r175

Fujii, Y., Kitaura, K., Matsutani, T., Shirai, K., Suzuki, S., Takasaki, T., et al. (2013). Immune-related gene expression profile in laboratory common marmosets assessed by an accurate quantitative real-time PCR using selected reference genes. *PLoS ONE* 8:e56296. doi: 10.1371/journal.pone.0056296

Gale, M. Jr, Kwieciszewski, B., Dossett, M., Nakao, H., and Katze, M. G. (1999). Antiapoptotic and oncogenic potentials of hepatitis C virus are linked to interferon resistance by viral repression of the PKR protein kinase. *J. Virol.* 73, 6506–6516. doi: 10.1128/JVI.73.8.6506-6516.1999

Hara, Y., Hino, K., Okuda, M., Furutani, T., Hidaka, I., Yamaguchi, Y., et al. (2006). Hepatitis C virus core protein inhibits deoxycholic acid-mediated apoptosis despite generating mitochondrial reactive oxygen species. *J. Gastroenterol.* 41, 257–268. doi: 10.1007/s00535-005-1738-1

Jacob, J. R., Lin, K. C., Tennant, B. C., and Mansfield, K. G. (2004). GB virus B infection of the common marmoset (*Callithrix jacchus*) and associated liver pathology. *J. Gen. Virol.* 85, 2525–2533. doi: 10.1099/vir.0.80036-0

Jagessar, S. A., Vierboom, M., Blezer, E. L., Bauer, J., Hart, B. A., and Kap, Y. S. (2013). Overview of models, methods,and reagents developed for translationalautoimmunity research in the common marmoset (*Callithrix jacchus*). *Exp. Anim.* 62, 159–171. doi: 10.1538/expanim.62.159

Kim, S. H., Han, S. Y., Azam, T., Yoon, D. Y., and Dinarello, C. A. (2005). Interleukin-32: a cytokine and inducer of TNFalpha. *Immunity* 22, 131–142. doi: 10.1016/S1074-7613(04)00380-2

Knodell, R. G., Ishak, K. G., Black, W. C., Chen, T. S., Craig, R., Kaplowitz, N., et al. (1981). Formulation and application of a numerical scoring system for assessing histological activity in asymptomatic chronic astive hepatitis. *Hepatology* 1, 431–435. doi: 10.1002/hep.1840010511

Ko, N. Y., Mun, S. H., Lee, S. H., Kim, J. W., Kim, D. K., Kim, H. S., et al. (2011). Interleukin-32α production is regulated by MyD88-dependent and independent pathways in IL-1β-stimulated human alveolar epithelial cells. *Immunobiology* 216, 32–40. doi: 10.1016/j.imbio.2010.03.007

Koo, C. L., Kok, L. F., Lee, M. Y., Wu, T. S., Cheng, Y. W., Hsu, J. D., et al. (2009). Scoring mechanisms of p16INK4a immunohistochemistry based on either independent nucleic stain or mixed cytoplasmic with nucleic expression can significantly signal to distinguish between endocervical and endometrial adenocarcinomas in a tissue microarray study. *J. Transl. Med.* 7:25. doi: 10.1186/1479-5876-7-25

Lanford, R. E., Chavez, D., Notvall, L., and Brasky, K. M. (2003). Comparison of tamarins and marmosets as hosts for GBV-B infections and the effect of immunosuppression on duration of viremia. *Virology* 311, 72–80. doi: 10.1016/S0042-6822(03)00193-4

Lerat, H., Honda, M., Beard, M. R., Loesch, K., Sun, J., Yang, Y., et al. (2002). Steatosis and liver cancer in transgenic mice expressing the structural and nonstructural proteins of hepatitis C virus. *Gastroenterology* 122, 352–365. doi: 10.1053/gast.2002.31001

Li, T., Zhu, S., Shuai, L., Xu, Y., Yin, S., Bian, Y., et al. (2014). Infection of common marmosets with hepatitis C virus/GB virus-B chimeras. *Hepatology* 59, 789–802. doi: 10.1002/hep.26750

Lin, L., Park, J. W., Ramachandran, S., Zhang, Y., Tseng, Y. T., Shen, S., et al. (2016). Transcriptome sequencing reveals aberrant alternative splicing in Huntington's disease. *Hum. Mol. Genet.* 25, 3454–3466. doi: 10.1093/hmg/ddw187

Machida, K., Tsukiyama-Kohara, K., Seike, E., Ton,é S., Shibasaki, F., Shimizu, M., et al. (2001). Inhibition of cytochrome c release in Fas-mediated signaling pathway in transgenic mice induced to express hepatitis C viral proteins. *J. Biol. Chem.* 276, 12140–12146. doi: 10.1074/jbc.M010137200

Marusawa, H., Hijikata, M., Chiba, T., and Shimotohno, K., (1999). Hepatitis C virus core protein inhibits Fas- and tumor necrosis factor alpha-mediated apoptosis via NF-kappaB activation. *J. Virol.* 73, 4713–4720. doi: 10.1128/JVI.73.6.4713-4720.1999

Massague, J. (2004). G1 cell-cycle control and cancer. *Nature* 432, 298–306. doi: 10.1038/nature03094

Moriya, K., Fujie, H., Shintani, Y., Yotsuyanagi, H., Tsutsumi, T., Ishibashi, K., et al. (1998). The core protein of hepatitis C virus induces hepatocellularcarcinoma in transgenic mice. *Nat. Med.* 4, 1065–1067. doi: 10.1038/2053

Moschen, A. R., Fritz, T., Clouston, A. D., Rebhan, I., Bauhofer, O., Barrie, H. D., et al. (2011). Interleukin-32: a new proinflammatory cytokine involved in hepatitis C virus-related liver inflammation and fibrosis. *Hepatology* 53, 1819–1829. doi: 10.1002/hep.24285

Nguyen, H., Mudryj, M., Guadalupe, M., and Dandekar, S. (2003). Hepatitis C virus core protein expression leads to biphasic regulation of the p21 cdk inhibitor and modulation of hepatocyte cell cycle. *Virology* 312, 245–253. doi: 10.1016/S0042-6822(03)00209-5

Nishida, A., Andoh, A., Shioya, M., Kim-Mitsuyama, S., Takayanagi, A., and Fujiyama, Y. (2008). Phosphatidylinositol 3-kinase/Akt signaling mediates interleukin-32alpha induction in human pancreatic periacinarmyofibroblasts. *Am. J. Physiol. Gastrointest. Liver Physiol.* 294, 831–838. doi: 10.1152/ajpgi.00535.2007

Nold-Petry, C. A., Nold, M. F., Zepp, J. A., Kim, S. H., Voelkel, N. F., and Dinarello, C. A. (2009). IL-32-dependent effects of IL-1beta on endothelial cell functions. *Proc. Natl. Acad. Sci. U. S. A.* 106, 3883–3888. doi: 10.1073/pnas.0813334106

Pang, X., Song, H., Zhang, Q., Tu, Z., and Niu, J. (2016). Hepatitis C virus regulates the production of monoytic myeloid-derived suppressor cells from peripheral blood mononuclecar cells through PI3K pathway and autocrine signaling. *Clin. Immunol.* 64, 57–64. doi: 10.1016/j.clim.2016.01.014

Park, J. S., Yang, J. M., and Min, M. K. (2000). Hepatitis C virus nonstructural protein NS4B transforms NIH3T3 cells in cooperation with the Ha-ras oncogene. *Biochem. Biophys. Res. Commun.* 267, 581–587. doi: 10.1006/bbrc.1999.1999

Raimondi, S., Bruno, S., Mondelli, M. U., and Maisonneuve, P. (2009). Hepatitis C virus genotype 1b as a risk factor for hepatocellular carcinomadevelopment: a meta-analysis. *J. Hepatol.* 50, 1142–1154. doi: 10.1016/j.jhep.2009.01.019

Ramos, H. J., Lanteri, M. C., Blahnik, G., Negash, A., Suthar, M. S., Brassil, M. M., et al. (2012). IL-1β signaling promotes CNS-intrinsic immune control of West Nile virus infection. *PLoS Pathog.* 8:e1003039. doi: 10.1371/journal.ppat.1003039

Ray, R. B., Lagging, L. M., Meyer, K., and Ray, R. (1996). Hepatitis C virus core protein cooperates ras and transforms primary rat embryo fibroblasts to tumorigenic phenotype. *J. Virol.* 70, 4438–4443. doi: 10.1128/JVI.70.7.4438-4443.1996

Ray, R. B., Meyer, K., Steele, R., Shrivastava, A., Aggarwal, B. B., and Ray, R., (1998). Inhibition of tumor necrosis factor (TNF-alpha)-mediated apoptosis by hepatitis C virus core protein. *J. Biol. Chem.* 273, 2256–2259. doi: 10.1074/jbc.273.4.2256

Trapnell, C., Williams, B. A., Pertea, G., Mortazavi, A., Kwan, G., Baren, M. J., et al. (2010). Transcript assembly and quantification by RNA-Seq reveals unannotated transcripts and isoform switching during cell differentiation. *Nat. Biotechnol.* 28, 511–515. doi: 10.1038/nbt.1621

Trick, M., Long, Y., Meng, J., and Bancrof, I. (2009). Single nucleotide polymorphism (SNP) discovery in the polyploid *Brassica napus* using Solexa transcriptome sequencing. *Plant. Biotechnol. J.* 7, 334–346. doi: 10.1111/j.1467-7652.2008.00396.x

Worley, K. C., Warren, W. C., Rogers, J., Locke, D., Muzny, D. M., and Mardis, E. R. (2014). The common marmoset genome provides insight into primate biology and evolution. *Nat. Genet.* 46, 850–857. doi: 10.1038/ng.3042

Yousif, N. G., Al-Amran, F. G., Hadi, N., Lee, J., and Adrienne, J. (2013). Expression of IL-32 modulates NF-κB and p38 MAP kinase pathways in human esophageal cancer. *Cytokine* 61, 223–227. doi: 10.1016/j.cyto.2012.09.022

Conflict of Interest: The authors declare that the research was conducted in the absence of any commercial or financial relationships that could be construed as a potential conflict of interest.

frontiers in Cellular and Infection Microbiology

REVIEW
published: 30 June 2020
doi: 10.3389/fcimb.2020.00325

HCV Replicon Systems: Workhorses of Drug Discovery and Resistance

*Shaheen Khan†, Shalini Soni† and Naga Suresh Veerapu**

Virology Section, Department of Life Sciences, Shiv Nadar University, Gautam Buddha Nagar, India

The development of direct-acting antivirals (DAAs) has revolutionized the state-of-the art treatment of HCV infections, with sustained virologic response rates above 90%. However, viral variants harboring substitutions referred to as resistance-associated substitutions (RASs) may be present in baseline levels and confer resistance to DAAs, thereby posing a major challenge for HCV treatment. HCV replicons have been the primary tools for discovering and evaluating the inhibitory activity of DAAs against viral replication. Interest in replicon systems has further grown as they have become indispensable for discovering genotype-specific and cross-genotype RASs. Here, we review functional replicon systems for HCV, how these replicon systems have contributed to the development of DAAs, and the characteristics and distribution of RASs for DAAs.

Keywords: hepatitis C virus, replicon, direct-acting antiviral, resistance-associated substitution, drug discovery, drug resistance, genotype

OPEN ACCESS

Edited by:
Milan Surjit,
Translational Health Science and Technology Institute (THSTI), India

Reviewed by:
Volker Lohmann,
Heidelberg University Hospital, Germany
Song Yang,
Capital Medical University, China

****Correspondence:***
Naga Suresh Veerapu
nagasuresh.veerapu@snu.edu.in

†These authors have contributed equally to this work

Specialty section:
This article was submitted to Virus and Host, a section of the journal Frontiers in Cellular and Infection Microbiology

Received: *12 March 2020*
Accepted: *28 May 2020*
Published: *30 June 2020*

Citation:
Khan S, Soni S and Veerapu NS (2020) HCV Replicon Systems: Workhorses of Drug Discovery and Resistance. Front. Cell. Infect. Microbiol. 10:325. doi: 10.3389/fcimb.2020.00325

INTRODUCTION

The molecular cloning of hepatitis C virus (HCV) in 1989 led to advances in fundamental research to fully decipher the virus life cycle and develop treatments for its eradication (Hoofnagle et al., 1986; Choo et al., 1989; Scheel and Rice, 2013; Alazard-Dany et al., 2019). HCV is a member of the *Flaviviridae* family that also includes the causative viruses of West Nile, Dengue, Yellow fever, and Zika diseases. Following acute HCV infection, 70% of individuals develop chronic hepatitis C. The Word Health Organization (WHO) estimates that ∼71 million people have chronic hepatitis C globally (World Health Organization, 2017). Chronic hepatitis C can lead to cirrhosis and hepatocellular carcinoma (HCC), followed by death in about 5% of individuals (Stanaway et al., 2016). Currently available HCV treatments have successful elimination rates above 95% (Holmes et al., 2019). Successful treatment is confirmed by the absence of HCV RNA via polymerase chain reaction (PCR) assays, with an assessment at 12 weeks after the end of treatment, thereby indicating sustained virologic responses (SVR). There are currently no prophylactic or therapeutic vaccines against hepatitis C (Roingeard and Beaumont, 2020).

Improvement in the treatment and SVR against HCV was facilitated by the discovery of pangenotypic direct-acting antivirals (DAAs), with replicon systems playing significant direct roles. HCV replicons are subgenomic RNA molecules that are capable of autonomously replicating in hepatoma cells. The replicons are primary composed of NS3-to-NS5B sequences that encode enzymes essential for viral replication (Lohmann et al., 1999; Bartenschlager, 2002, 2006; Lohmann, 2009). The underlying mechanism relies on DAAs targeting

viral enzymes that are not expressed by hepatoma cell genomes, and they should also be effective in treating HCV-infected patients, in addition to likely inducing minimal side effects. However, the high genetic variation of HCV poses a major challenge for developing pangenotypic DAAs. The high viral diversity is partly due to high error rates from HCV replication (Ogata et al., 1991; Neumann, 1998; Geller et al., 2016). Resistance to DAAs arises from mutations in NS3-to-NS5B sequences that encode viral enzyme targets of DAAs. Consequently, selection and persistent replication of variants harboring amino acid substitutions that confer resistance to DAAs are major causes for reduced treatment efficacy (Wyles and Luetkemeyer, 2017). Hence, preclinical assessments of drug resistance profiles have gained important roles in the development of DAAs. Further, replicon systems have been used to study treatment-related resistance associated substitutions (RASs) that confer resistance to DAAs across genotypes (GTs) and subtypes (Ng et al., 2017a; Han et al., 2019) .

VIROLOGY

HCV is an enveloped virus comprising an ∼9.6-Kbp-long single-strand RNA genome with positive polarity. The genome constitutes a 5' non-translated region (NTR), and a single large open reading frame, followed by a 3' NTR. An internal ribosomal entry site (IRES) present at the 5' NTR translates the ORF to a large polyprotein of about 3,000 amino acids length that is then processed by viral and cellular proteases into three structural and seven non-structural proteins (**Figure 1**) (Moradpour et al., 2007; Alazard-Dany et al., 2019). The structural protein core forms the virus capsid. E1 and E2 are envelope transmembrane glycoproteins that aid in receptor-mediated endocytosis for viral entry (Bartosch et al., 2003). The P7 protein forms an ion channel in the endoplasmic reticulum (ER) and plays a role in viral infection. Nonstructural proteins, NS2, NS3, NS4A, NS4B, NS5A, and NS5B, act together to form replication complexes on membranous webs derived from the ER (Romero-Brey et al., 2012). NS2 is a cysteine protease that autocatalyzes the polyprotein precursor cleavage between NS2 and NS3 (Grakoui et al., 1993). NS3 also exhibits cysteine and serine protease activities that cleave NS4A-NS5B at junction regions to release individual protein components and also act as a viral helicase, while NS4A is a co-factor of NS3 (Tomei et al., 1993; Lin et al., 1994). NS4B is an integral membrane protein that aids in the formation of the viral replication complex (Egger et al., 2002). NS5A is a membrane phosphoprotein that permits viral binding and assembly of the replication complex (Tanji et al., 1995). NS5B (an RNA-dependent RNA polymerase) directs transcription of the (+) strand for production of the (-) strand that becomes the template for the new (+) strand genomes (Behrens et al., 1996; Lohmann et al., 1997). Given their essential role, the non-structural proteins of replication complex are the targets of DAAs, which can disrupt specific steps in the replication, have now become the core of the HCV treatment strategies (Lontok et al., 2015).

HCV GENETIC HETEROGENEITY AND THE EMERGENCE OF DAA RESISTANCE

Sequencing and phylogenetic analyses of HCV isolates from different geographic regions have revealed that HCV can be classified into eight genotypes (GTs 1–8) and 86 subtypes that differ at the nucleotide (nt) level by 30 and 15%, respectively (Hedskog et al., 2019). The appearance of HCV in at least eight GTs has important implications for HCV treatment, as differences exist in achieved SVR rates against different GTs using various regimens (Mangia and Mottola, 2012). Further, the two inherent replication features of HCV can contribute to suboptimal responses to DAAs at the patient level, including their: (a) high error rate during replication and (b) high virion turnover. Due to the lack of NS5B exonuclease activity, HCV replicates with an error rate of 10^{-3} to 10^{-5} mutations per nt per round of replication and reproduce with an estimated 10^{10}-10^{12} virion turnover per day in an infected individual (Ogata et al., 1991; Neumann, 1998; Geller et al., 2016). The resultant large reservoir of genetic variants circulating at a given time in an infected patient is classically referred to as a "quasispecies" (Perales et al., 2015). The majority of variants are unable to replicate due to deleterious or lethal effects of the new mutations or are otherwise cleared by the host immune system. However, some variants with beneficial mutations are continuously selected upon due to evolutionary advantages or better adaptation to adverse conditions, such as the presence of a DAA (Agarwal et al., 2018; Singh et al., 2020). Consequently, natural variants with various levels of susceptibility to DAAs may exist within patients and can be selected after DAA exposure (Ahmed and Felmlee, 2015). The selection of variants may then confer resistance to DAAs and treatment failure.

Following the discovery of HCV, numerous attempts have been made to recapitulate viral life cycles using *in vitro* cell culture systems. The first significant development was the establishment of a "subgenomic replicon" system wherein replicon cell lines were isolated that persistently harbored autonomously replicating HCV non-structural genes at appreciable levels (Lohmann et al., 1999). These replicons generally lack the viral structural genes involved in capsid formation and are hence subgenomic. The subsequent isolation of more efficient replicons paved the way for understanding HCV replication, the molecular interplay between viruses and cells, and the identification and development of inhibitors that are effective against HCV replication. The second significant breakthrough was the establishment of the infectious "HCV cell culture" system (HCVcc) based on the JFH-1 wild type isolate (GT2a) that exhibits all stages of the virus life cycle (Kato et al., 2001; Wakita et al., 2005). Further advances using JFH-1 HCVcc were made by generating a highly infectious GT2a J6/JFH1 chimera (Lindenbach and Rice, 2005). The repository of infectious HCVcc systems was expanded to include GT1a (Yi et al., 2006), GT1b (Pietschmann et al., 2009), GT2b (Ramirez et al., 2014) GT3a (Saeed et al., 2013), and 6a (Pham et al., 2018). HCVcc systems of intergenotypic are also developed (reviewed in Ramirez and Bukh, 2018). Indeed, infectious HCVcc systems have paved the way for a deeper understanding of HCV biology,

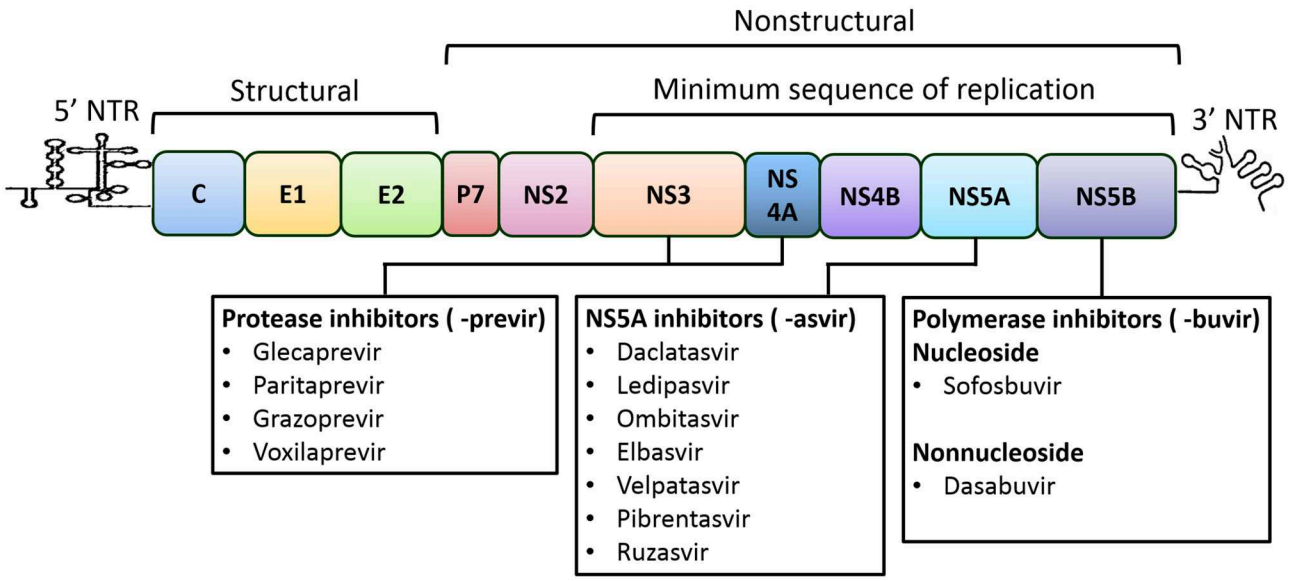

FIGURE 1 | HCV genome organization and direct-acting antivirals for the treatment of HCV Infection. The HCV genome is consisted of single open reading frame (ORF) that is flanked by 5' and 3' non-translated regions (NTRs). The IRES present at the 5' NTR mediates the translation of the ORF leading to the formation of a polyprotein, which is further processed into three structural (core, E1 and E2) and seven nonstructural proteins (P7, NS2, NS3, NS4A, NS4B, NS5A, and NS5B). The NS3-to-NS5B coding region is the minimal sequence required for RNA replication (Lohmann et al., 1999). Recommended direct-acting antivirals are listed below and include the NS3/4A (or protease; names end in -previr) inhibitors, the NS5A inhibitors (names end in -asvir), and the NS5B (or polymerase) inhibitors of nucleoside and non-nucleoside (names end in -buvir).

including the identification of DAA-resistant variants in the context of infectious viral life cycles (Ramirez et al., 2016; Serre et al., 2016; Jensen et al., 2019).

Although infectious HCVcc systems allow the more complete study of complete viral replication cycles and understanding of genotype-specific pathogenesis, HCV replicon technology continues to be critical due to its ease of use in the discovery of candidate DAAs, and also in the identification and evaluation of RASs to improve the effectiveness of HCV treatments. Here, we provide a summary of different aspects of the HCV replicon systems and our current knowledge of RASs associated with resistance to DAAs.

REPLICON SYSTEMS

Structure and Development of the Classical Bicistronic Replicon

Lohmann et al. successful proof-of-principle demonstration that the minimal HCV replication and translation machinery require the NTRs and the NS3-to-NS5B coding sequences forms the basis for HCV replicon technology (Lohmann et al., 1999; Bartenschlager, 2002). Functional replicons have been established for different GTs and several subtypes have now become indispensable tools for preclinical DAA discovery (Fourati and Pawlotsky, 2015). Consensus 1 (Con1), the first HCV replicon that was generated from the consensus GT1b isolate sequence consists of two gene clusters, each with an independent cistron: (i) the HCV 5' NTR and the first 16 codons of the core gene fused in-frame with the selectable neomycin phosphotransferase gene (*neo*), and (ii) the IRES of the encephalomyocarditis virus (EMCV) that directs the translation of fused HCV NS3-to-NS5B coding sequence, and the HCV 3' NTR (**Figure 2A**). A replicon cloned downstream of the T7 promoter in a plasmid serves as template to generate bicistronic transcripts. Huh7 cells that are then transfected with the bicistronic transcripts are propagated for several cell division cycles in the presence of the aminoglycoside antibiotic G418. The *neo* gene that confers resistance to the cytotoxic drug G418 then enabled the selection of "stable replicon cells" that support the autonomous replication of Con1 transcripts, thereby constituting a stable HCV replicon assay. The Con1 replicon carrying the NS5B GND amino acid motif (GND in place of GDD results in loss of NS5B polymerase activity) has been used as a negative control for viral replication. Efficiency of colony formation could then be quantified as the number of selected colonies per microgram of transfected RNA. Northern blot analysis of total RNA isolated from stable Con1 replicon cells that were treated with actinomycin D (an inhibitor of DNA-directed, but not RNA-directed RNA synthesis) could then detect HCV (+)- and (−)-strand RNA (Lohmann et al., 1999; Blight et al., 2000).

The G418-resistant Con1 replicon cells that were generated persistently carried replicating HCV RNAs, albeit with low colony formation efficiency and viral RNA levels that reflected adaptive constraints in the Huh7 cell environment. Sequencing of the viral RNAs from isolated replicon cell clones then revealed key mutations localized to different non-structural genes. Inclusion of these mutations conferred the original Con1 replicon with increased colony formation efficiency,

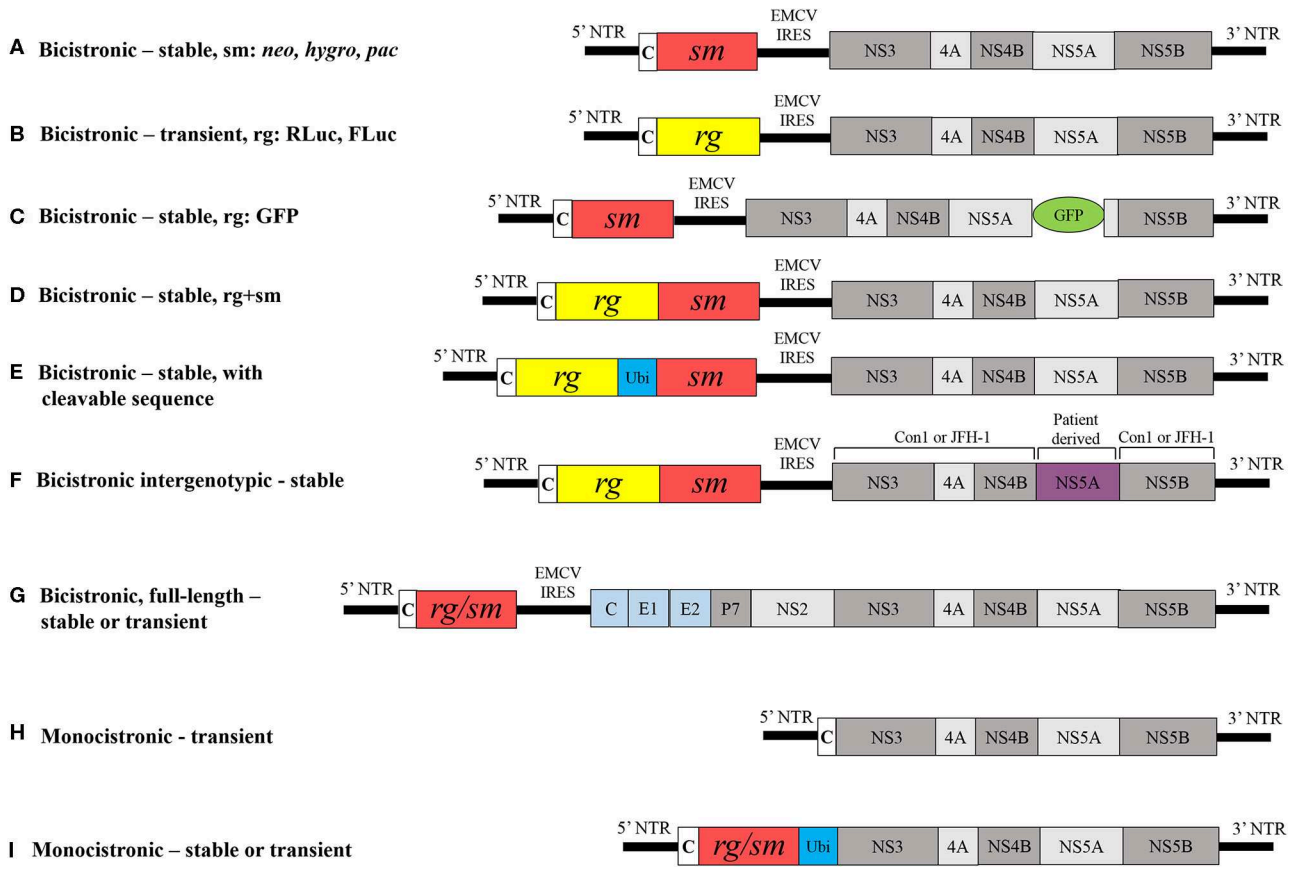

FIGURE 2 | Schematic comparison of different HCV replicons. **(A)** Classical bicistronic subgenomic replicon comprised 5' NTR, first 16 codons of core, *neo* gene, a selectable marker followed by EMCV IRES, HCV NS3-to-NS5B coding region and HCV 3' NTR; Other selectable markers less widely used are *hygro* and *pac*. Modified bicistronic replicons may carry either: **(B)** a *Renilla* luciferase (RLuc) or firefly luciferase (FLuc) (reporter gene) instead of a selectable marker, **(C)** a GFP at certain positions within NS5A, **(D)** a reporter gene that is fused with a selectable marker, **(E)** ubiquitin, a host cell cleavable sequence fused in-frame between a reporter and selectable marker, **(F)** a non-structural sequence derived from patient in Con1 or JFH-1 replicons genetic background or **(G)** an entire HCV ORF, core-to-NS5B and 3' NTR. Monocistronic replicons are composed of **(H)** HCV 5' NTR and first 12 codons of core followed by NS3-to-NS5B coding sequences and 3' NTR and **(I)** ubiquitin in-frame with either a reporter gene or selection marker. NTR, non-translated region; Ubi, ubiquitin, rg, reporter gene; sm, selection marker; neo, gene encoding neomycin phosphotransferase; hygro, hygromycin phosphotransferase; PAC, puromycin N-acetyltransferase; c, core; EMCV IRES, internal ribosomal entry site from encephalomyocarditis virus; GDD, amino acid motif in the catalytic site of RNA polymerse; GFP, green fluorescent protein. Viral and non-viral coding sequences are marked by rectangles; non-coding regions are indicated by horizontal lines.

and this phenomenon subsequently was termed 'adaptive mutation.' Specifically, Con1-based replicons carrying two adaptive mutations located at NS3 E176G and T254I, and one at NS5A S225P (Krieger et al., 2001) or NS4B K129T (Lohmann et al., 2003) conferred synergistically enhanced RNA replication. In addition, Blight et al. (2000) identified S232I as a key adaptive mutation localized in NS5A that appears to correspond to highly efficient replication. However, the GT1b HCV-N replicon was observed to replicate efficiently in Huh7 cells, even in the absence of adaptive mutations (Ikeda et al., 2002). Moreover, two independent studies observed that NS3 P470L and NS5A S232I mutations synergistically enhance H77-based replication of the GT1a replicon (Grobler et al., 2003; Yi and Lemon, 2004). In particular, the NS5A S232I mutation played a key role in expanding the repertoire of efficient non-GT1 replicon systems (Saeed et al., 2012; Peng et al., 2013; Wose Kinge et al., 2014; Yu et al., 2014). Recently, it is shown that Sec14L2 expressing Huh7.5 cells supported replication of natural HCV isolates in cell culture (Saeed et al., 2015). The exact mechanism underlying how adaptive mutations confer enhanced replication of HCV RNAs is not completely understood. A recent study showed that S232I reduces the hyperphosphorylation of NS5A and disrupts the NS5A interaction with human vesicle associated proteins, thereby negatively regulating viral replication and contributing to the adaptive phenotype (Evans et al., 2004). Another recent study has shown that adaptive mutations could prevent a cellular lipid kinase, phosphatidylinositol 4-kinase IIIα (PI4KA) activation, which create a permissive membrane microenvironment in hepatoma cells. Further, inhibition of PI4KA activity was found to promote replication of unadapted viral isolates (Harak et al., 2017). Since the first report, HCV replicons have been further modified to be more suitable for studying viral RNA replication

and to promote drug discovery. A few of the various HCV replicon derivatives are described in further detail below.

Other Bicistronic Replicons and Modifications

The molecular structure of the classical replicon was used to establish the GT1b (Ikeda et al., 2002) GT2a (Kato et al., 2003), GT3a (Saeed et al., 2012), GT4 (Saeed et al., 2012; Peng et al., 2013), GT5a (Wose Kinge et al., 2014) and GT6a (Yu et al., 2014; Camus et al., 2018) replicon systems. In all of these systems, *neo* was used to select stable cell lines. Another selection marker that was less frequently used was puromycin N-acetyltransferase (Liang et al., 2005) and hygromycin phosphotransferase (Sir et al., 2012) (**Figure 2A**). Generating G418-resistant stable cell lines is time consuming, taking up to 3–4 weeks, and is dependent on the replication capacity of the replicon. To produce a rapid and direct means of analyzing transient replication capacity, *neo* was replaced by firefly luciferase (FLuc) or *Renilla* luciferase (Rluc) reporter genes in the replicon, thereby eliminating the need for selection and allowing analysis of replicon RNA replication over 72 h of post-transfection via a transient HCV replicon assay (**Figure 2B**) (Krieger et al., 2001; Lohmann et al., 2001; Camus et al., 2018). Other reporter gene alternatives include β-lactamase or green fluorescent protein (GFP) (Murray et al., 2003). The Con1 replicon carrying an in-frame insertion of GFP at certain positions within the NS5A gene permits the direct visualization of active replication complexes in real time (**Figure 2C**) (Moradpour et al., 2004). However, the insertion of GFP reduces the replication capacity of replicons by about 100-fold relative to the parental replicon without GFP (Appel et al., 2005). The most widely used replicons comprising fused RLuc and *neo* genes allows the simultaneous selection of hepatoma cells while luciferase activity provides direct evaluation of RNA replication levels (**Figure 2D**) (Krieger et al., 2001; Peng et al., 2013; Yu et al., 2014; Camus et al., 2018). A bicistronic replicon has ubiquitin (host cleavable sequence) in-frame between reporter and selection marker helps in assessing inhibitory activity of antivirals (**Figure 2E**) (Vrolijk et al., 2003). Further, the replacement of nonstructural genes in replication-competent GT1b (Con1) and GT2a (JFH-1) replicons by corresponding non-structural genes of patient isolates from different GTs and subtypes resulted in the production of intergenotypic chimeras that have helped substantiate the identification of pangenotypic DAAs and resistance (**Figure 2F**) (Herlihy et al., 2008; Sheaffer et al., 2011; Liu et al., 2015; Ng et al., 2017b; Han et al., 2019). The molecular structures of bicistronic replicons shown in **Figure 2D** have been used as the basis to generate the intergenotypic replicons.

Full-Length Bicistronic Replicons

Full-length bicistronic or genomic HCV replicons encode the entire HCV open reading frame core–NS5B and were generated for GT1b and GT1a that carried adaptive mutations (**Figure 2G**) (Pietschmann et al., 2002; Blight et al., 2003). The presence of *neo* also facilitated the selection of stable cell lines that support full-length RNA replication. However, the replication efficiency of full-length replicons was about 5-fold less than for subgenomic counterparts carrying the same adaptive mutations, and no evidence for infectious progeny release from hepatoma cells was observed. However, selectable JFH-1 full-length replicons are capable of producing infectious progeny (Date et al., 2007).

Monocistronic Subgenomic Replicons

Monocistronic replicons lack EMCV IRES and consist of only HCV 5′ NTR that direct the translation of downstream viral coding sequences. Therefore, they closely resemble the structure of viral genomes (**Figure 2H**). Monocistronic replicons comprise the 5' NTR and first 12 codons of core sequence followed by the in-frame NS2-to-NS5B sequences. In this model, the cellular signaling peptidase mediates the cleavage between the capsid and NS2 (Blight et al., 2000). In other monocistronic replicons, the 5′ NTR translates the reporter gene that is in-frame with ubiquitin and the NS3-to-NS5B coding region, followed by the 3′ NTR (**Figure 2I**) (Reiss et al., 2013). (Frese, 2002) generated a monocistronic replicon containing the selection marker hygromycin phosphotransferase. In this case, cleavage between ubiquitin and NS3 is mediated by a cellular ubiquitin carboxyl-terminal hydrolase (**Figure 2I**). Monocistronic replicon replication can then be assessed by detection of viral proteins using non-structural protein-specific antibodies and viral mRNA with quantitative real-time RT-PCR.

Replicon Systems in the Era of DAAs

The treatment strategies for HCV infections have radically changed in the last two decades, and particularly in the last 10 years (Cuypers et al., 2016). A better understanding of the molecular structure and function of hepatitis C proteins has especially allowed the design of antivirals that directly target non-structural proteins, including NS3/4A, NS5A, or NS5B, that facilitate RNA replication (Bartenschlager et al., 2013; Scheel and Rice, 2013). The NS3/4A inhibitor ciluprevir (BILN-2061) was the first developed DAA using the GT1a (Con1) replicon system and was tested in hepatitis C patients to demonstrate the proof-of-principle (Lamarre et al., 2003). However, ciluprevir was less effective against GT2 and GT3, emphasizing the dire need to develop efficient non-GT1 replicon systems. The non-GT1 replicon systems that have been developed have proven highly useful for testing the pangenoypic HCV replication inhibition activity by DAAs. Hence, HCV replicon systems have become indispensable in the preclinical research and development of effective DAAs, owing to advantages that include: (i) stable replicon cells easily integrate into high-throughput screening assays; (ii) it is reliable to assess and compare levels of HCV replicon replication; (iii) they are efficient for determining preclinical cytotoxicity; (iv) they are robust for determining pangenotypic antiviral activity and have a high genetic barrier to resistance; and (v) replicon systems yield no infectious progeny, thereby minimizing the risk of exposure unlike infectious HCVcc systems.

A candidate DAA would have desirable preclinical attributes that support its clinical development for HCV treatment. Since the identification of the first NS3/4A inhibitor, HCV replicon systems have been widely used to identify safe and effective pangenotypic antivirals. Among many effective, not limited

to, the most effective DAAs that are recommended for HCV treatment include, NS3/4A protease inhibitors (PIs, names end in -previr): glecaprevir (ABT-493) (Ng et al., 2014), grazoprevir (MK-5172) (Summa et al., 2012), paritaprevir (ABT-450) (Pilot-Matias et al., 2015), and voxilaprevir (GS-9857) (Taylor et al., 2019); NS5A inhibitors (names end in -asvir): daclatasvir (BMS-790052) (Gao et al., 2010), ledipasvir (GS-9451) (Yang et al., 2014), elbasvir (MK-8742) (Coburn et al., 2013), velpatasvir (GS-5816) (Cheng et al., 2013), ombitasvir (ABT-267) (DeGoey et al., 2014), pibrentasvir (ABT-530) (Ng et al., 2014) and ruzasvir (MK-8408) (Tong et al., 2017); inhibitors of NS5B nucleoside polymerase (NPIs, names end in -buvir): sofosbuvir (GS-7977) and non-nucleoside (NNPIs): dasabuvir (?ABT-333) (Maring et al., 2009) (**Figure 1**). These DAAs exhibited subnanomolar 50% effective concentrations (EC_{50}s) toward replicons expressing a wide range of HCV GTs with minimal cytotoxicity. Despite the limited inventory of druggable viral enzymes and corresponding low molecular weight DAAs exhibiting high efficacy, current DAA-based treatments have been highly effective for HCV elimination. However, the emergence of HCV resistance to DAAs in small patient populations (< 5%) poses challenges to eradication (Popping et al., 2018). The crystal structures of NS3/4A, NS5A and NS5B are helping to solve the mechanisms of action of various DAAs and the molecular basis for DAA resistance (reviewed in Bartenschlager et al., 2013; Götte and Feld, 2016).

HCV treatment has dramatically improved since 2014 coinciding with the pegIFN and RBV-free co-administration of two or three pangenotypic DAAs that shorten treatment durations and lead to SVR rates above 95% in patients with chronic hepatitis C (EASL, 2018). It is worth to note that all currently recommended DAA regimen consists an NS5A inhibitor. The mode of action of DAAs at molecular level is not yet understood. HCV variants may harbor RASs that are associated with reduced susceptibility given the high mutation rate of HCV, and these may exist naturally and can be selected in patients due to the application of some DAAs. The biological and clinical implications of variant selection that are resistant to DAA and cause treatment failure are well-known (Lontok et al., 2015). Thus, insight into the nature of RASs and their mode of action is important to understand viral resistance to DAAs and to promote the eradication of HCV (Lontok et al., 2015; Cuypers et al., 2016; Wyles and Luetkemeyer, 2017). RASs are reported as "single letter amino acid code-number-single letter amino acid code." For example, the NS5A-specific RAS Y93H manifest as the typically expected amino acid at position 93 of the NS5A protein in the predominant circulating virus has tyrosine (Y) and in some patients, viral variants may harbor the amino acid histidine (H) at position 93 of the NS5A protein. Sequencing technologies can be used to detect drug-specific RASs circulating in patients (Li and Chung, 2019). RASs present in at least 15% of all drug-target encoding viral sequences circulating in patients reduces the SVR for the patient (Pawlotsky, 2016). The number and type of RAS(s) required for a variant to remain fit in the presence of a DAA are referred to as the genetic barrier to resistance, which also differ according to DAA and class (Götte, 2012). A single RAS at a key position in the target protein can confer a low genetic barrier to resistance, while a high genetic barrier to resistance requires at least three RASs (McCown et al., 2008; Pawlotsky, 2011). The emergence of DAA resistance depends on the fitness of RASs and whether they exist at baseline in patients prior to treatment. The fitness of RASs determines the speed of resistant variant selection in the presence of DAAs (Feld, 2017). The individual NS5A-RASs M28T, Q30E/H/R, L31M/V, and Y93H/N are commonly found at baseline in 10–15% of GT1 treatment-naïve patients. These high fitness RASs to NS5A-inhibitors (e.g., daclatasvir, ledipasvir, and ombitasvir) confer a low barrier to resistance, and can emerge early and persist in patients following administration of NS5A-based treatments (Krishnan et al., 2015b; Zeuzem et al., 2017; Dietz et al., 2018; Fourati et al., 2018). The majority of these RAS are also selected in replicon cells and confer resistance to recently recommended pangenotypic NS5A-inhibitors (Cheng et al., 2013; Liu et al., 2015; Ng et al., 2017a; Asante-Appiah et al., 2018). In contrast, the NS5B RAS S282T exhibited reduced fitness and does not appear to emerge in patients following administration of sofosbuvir (NPI) (Lam et al., 2012; Wyles et al., 2017). Consequently, a typical goal of DAA-based combination regimens is to increase the genetic barrier such that resistant variants do not arise so readily (Chacko and Gaglio, 2015).

Considering that any RASs that may confer resistance to a candidate DAA are not known or that they will likely rise, the replicon systems remain innovative, for instance, in the treatment of stable replicon cells with increasing doses of a DAA that may facilitate emergence of RASs (Bartenschlager, 2006). Another instance where replicon systems have proven useful is when new RASs might be selected for in patients following administration of a DAA. These new RASs could be introduced into the replicon by site-directed mutagenesis and are then challenged by DAAs at increasing doses based on EC_{50} or EC_{90} values for replication inhibition compared to the wild-type counterpart, which is commonly expressed as fold resistance (**Figure 3**). These two examples provide opportunities to examine the development of DAA resistance using replicon systems. Moreover, it is reasonable to assume that RASs conferring resistance to DAAs *in vitro* have clinical significance.

REPLICONS OF GENOTYPES 1–6 AND RESISTANCE-ASSOCIATED SUBSTITUTIONS

Genotype 1

HCV GT1 is the most globally widespread group and represents 46% of all infections. Subtype 1b is more prevalent than 1a, at 68 vs. 31%, respectively (Messina et al., 2015). Boceprevir and telaprevir (PIs) were the two first DAAs recommended for use in combination with pegIFN and RBV in patients infected with GT1 HCV in 2011. Although both PIs increased the SVR rate by about 30% in treatment-na?ve and -experienced patients compared to standard pegIFN and RBV, their low genetic barrier to resistance and highly adverse effects in GT1 patients (Pearlman, 2012; Wendt and Bourlière, 2013) led to the development of more effective PIs with higher genetic barriers to resistance. The pegIFN- and RBV-free DAA combination regimens targeting viral enzymes were developed in 2014 and have improved the SVR rate to above 90%, along with shorter

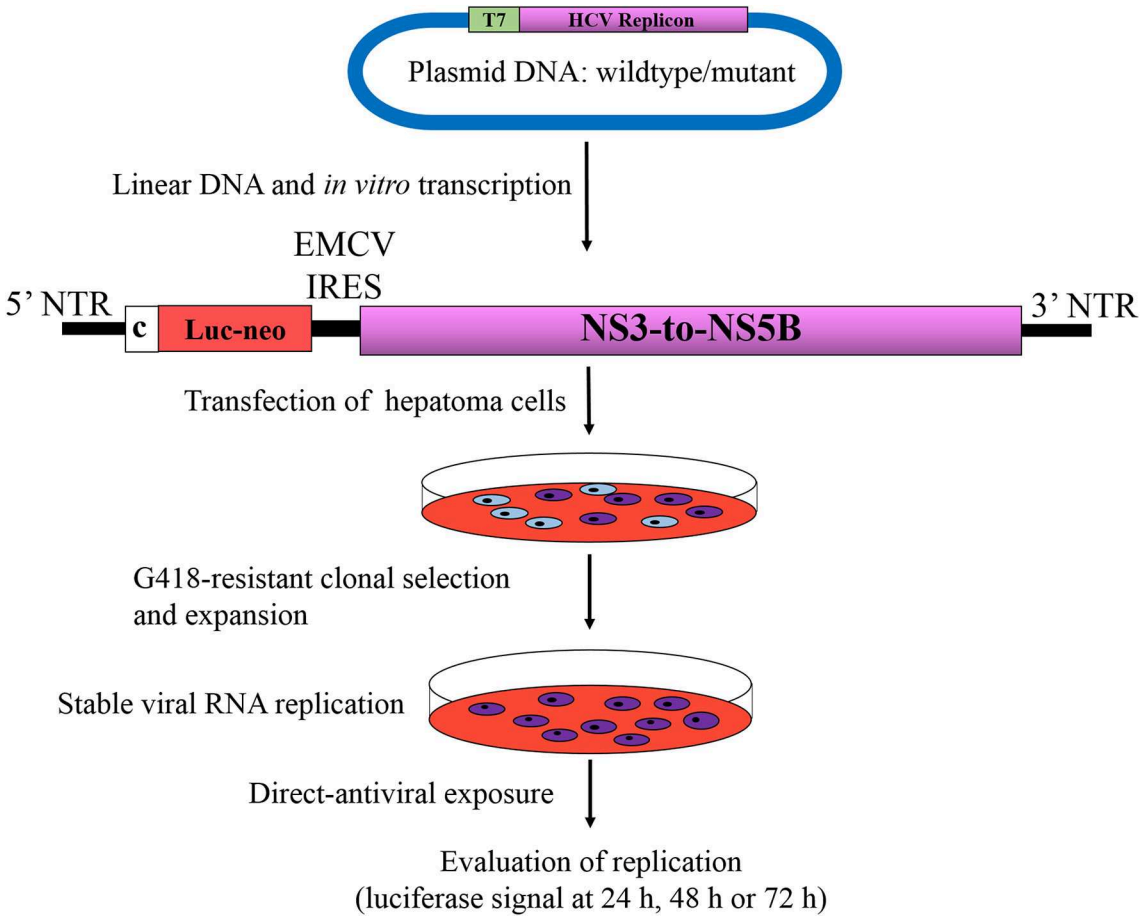

FIGURE 3 | Phenotypic assay of HCV resistance to antivirals. Bicistronic replicons described in **Figure 2D** are the most widely used systems for determination of phenotypic direct-acting antiviral resistance. Replicon RNAs from wild type or mutant are synthesized by *in vitro* transcription of linearized plasmids harboring HCV replicon, which are then transfected into hepatoma cells, subsequently subjected to G418 selection pressure for 3–4 weeks. Cells harboring active replicon RNAs become resistance to G418 due to expression of *neo* gene, whereas untransfected cells or cells that do not support RNA replication will be eliminated during the process. After the establishment of stable cell line supporting HCV autonomous replication, cells are subjected to increasing antiviral concentrations based on of EC_{50} or EC_{90} values. The level of susceptibility is evaluated by measuring the luciferase activity at 24, 48, and 72 h after treatment, in comparison to its wild type counterpart, which is commonly expressed as fold resistance. Luc-Neo, fused luciferase and *neo* gene encoding neomycin phosphotransferase; c, core; EMCV IRES, internal ribosomal entry site from encephalomyocarditis virus. Viral and non-viral coding sequences are marked by rectangles; non-coding regions are indicated by horizontal lines.

treatment durations of about 8 or 12 weeks and minimal adverse effects (Afdhal et al., 2014; Kowdley et al., 2014). The currently recommended four highly effective DAA combination regimes, elbasvir/grazoprevir, glecaprevir/pibrentasvir, ledipasvir/sofosbuvir, or sofosbuvir/velpatasvir, exhibit SVR rates of 98%−100% (Afdhal et al., 2014; Kowdley et al., 2014; Feld et al., 2015; Forns et al., 2015). The amino acid substitutions V36M, T54S, Q80K/H/R, R155K/M, A156T/V, and D168E/V/Y/H/T confer resistance to different PIs in GT1 HCV patients. In addition, the NS5A-associated substitutions M28T/V, L28M/I, Q30H/R, L31M, and Y93H are the most prevalent in GT1 isolates (Zeuzem et al., 2017).

GT1a (H77) and GT1b (Con1) replicons, or their backbones in chimeric form, are extensively used to identify pangenotypic HCV inhibitors. Replicons harboring single NS3 RASs at positions 36, 43, 54, 80, 155, 156, or 168 or in combinations comprising two or three of the mutations have been tested for resistance to PIs. Both replicons with NS3 D168A/E/V conferred significant resistance to paritaprevir and grazoprevir, while A156T/V conferred resistance to glecaprevir. The replicon with NS3 R155K lost susceptibility to paritaprevir, but maintained susceptibility to glecaprevir and grazoprevir (Ng et al., 2017b). The RASs R155W, A156T, and D168K/L/R conferred 20- to 100-fold resistance, whereas A156/L/V exhibited >100-fold resistance to voxilaprevir (Han et al., 2019). The NS5A amino acid substitutions M28T/V and Q30D/E/H/R/K in the GT1a replicon yielded moderate to high resistance to ruzasvir, daclatasvir, ledipasvir, ombitasvir, elbasvir, and pibrentasvir, while L31M/V to GT1b, whereas Y93H/N/C in both the GT1 replicons conferred negligible to significantly high resistance (Krishnan et al., 2015a;

TABLE 1 | Amino acid substitutions that confer resistance to NS3/4A, NS5A and NS5B inhibitors from HCV genotypes 1–6.

Replicon genotype	Amino acid and position	Amino acid substitution(s) (> 2-fold resistance)	Direct-acting antiviral
NS3/4A			
1a	V36	A	GRA/PTV/VOX/GLE/GZR
		C/G	PTV
		L	VOX/GZR
		M	GLE/PTV/GZR/VOX
		L	PTV/GZR
	F43	S	VOX
		A	GZR
	T55	I	VOX
		H	PTV/GZR
	Y56	K	GZR/PTV/VOX
	Q80	L	PTV
		R	GZR/GLE/PTV
		G	GZR/PTV
		K	PTV
	R155	I	PTV
		K	GRA/PTV/VOX/GLE/GZR
		M	PTV
		Q	GRA/PTV/VOX/GLE/GZR
		S/W	PTV
		T	GZR/PTV
		V	GZR
	R156	T	PTV
		S	GRA/PTV/VOX/GLE/GZR
		G	VOX
	A156	T	GLE
		L	VOX
	D168	C	GZR/PTV
		E	GLE/GZR/PTV
		G/T	GZR
		H	GZR/ PTV
		K	GZR/VOX
		L/R	VOX
		N	GZR/PTV
		V	GLE/GZR/PTV
		Y	GZR/PTV
		T	VOX
	I170	V	VOX
		A	GRA/PTV/VOX/GLE/GZR
1b	V36	C/G/K	PTV
		M/G	PTV/GZR
		S	GZR
		R	GZR/GLE/VOX
	Q80	K	PTV
	R155	K	GRA/PTV/VOX/GLE/GZR
		G	GZR/PTV/GLE
	A156	S/A	GZR/PTV
		T	GZR/PTV/GLE/VOX
		V	GZR/GLE/VOX
	D168	E/H/K/T/V/Y	GZR/PTV
		G/N	GZR
		Q	GRA
2	R123	V	GRA/PTV
	I132	A	GZR
	R155	K	GRA/PTV/VOX/GLE/GZR
		T	GZR/PTV
		G	GZR/PTV/GLE
		W	PTV/VOX
	A156	S	GZR/PTV
		V	GZR/GLE/VOX
		T	GLE/VOX
		A/E/G/H/N/V	GZR/PTV
	D168	V	GRA
	I170	F	GRA/PTV
	L175	R	VOX
3	K26	R/K	VOX
	Q41	A	VOX
	T54	R	VOX/GLE
	Q80	K	VOX
		A/C/F/T/Y	VOX
	S122	K	GRA/PTV/VOX/GLE/GZR
	R155	G	GZR/PTV/GLE
	A156	S	GZR/PTV/GLE
		T	GLE
	S166	A	GZR/PTV
	D168	V	PTV
		R	GRA/PTV
	Q168	R/H/I	VOX
		R	VOX/GLE
		L	GLE
	V170	T	GRA/ PTV
	I170	H/R	VOX
4	Q41	S	VOX
	T54	A/N/S/V	VOX
	T122	K	GRA/PTV/VOX/GLE/GZR
	R155	C	VOX/GLE/PTV/GZR
		G	GZR/PTV/GLE
	A156	S	GZR/PTV
		L/T/V	VOX/GLE
		S	VOX
	A166	E/K	VOX
	D168	V	VOX/GLE/PTV/GZR
		H	GLE/PTV/GZR
		I/L	VOX
	V170	V	GRA

(Continued)

TABLE 1 | Continued

Replicon genotype	Amino acid and position	Amino acid substitution(s) (> 2-fold resistance)	Direct-acting antiviral
5	E30	A/G/V	VOX
	T122	K	GRA/PTV/VOX/GLE/GZR
	R155	G	GZR/PTV/GLE
	A156	S	GZR/PTV
		S	VOX
	A166	A	GZR/PTV/VOX
	D168	E/H/V	GZR/PTV/VOX/GLE
		N	GZR/PTV
		K/R/Y	VOX
		V	VOX
		E	GLE
	I170	A	GRA/PTV/VOX/GLE/GZR
6	V36	K/R	VOX
	Q41	C	GRA/PTV
	F43	A	VOX
	V55	H	VOX
	Y56	K/Q/R	VOX
	L80	A/D/G/N/T	VOX
	S122	K	GRA/PTV/VOX/GLE/GZR
	R155	T	PTV
		G	GZR/PTV/GLE
	A156	S/I	GZR/PTV
	V158	A	GZR/PTV/VOX
	D168	E/V	GZR/PTV/VOX
		A/H	GLE/GZR/PTV
		G/N	GZR/PTV
		Y/V	VOX/GLE
NS5A			
1a	K24	G	LDV
		N	LDV
		R	LDV
	M28	A	DCV/LDV/ELB/OMV
		G	DCV/LDV
		T	DCV/LDV/OMV/PBT/ OMV/VEL/ELB
		V	OMV
	Q30	D	ELB
		E	DCV/LDV/OMV/PBT/ OMV/VEL/ELB
		G	LDV/ELB
		H	DCV/LDV/OMV/PBT/ OMV/VEL/ELB
		K	LDV/VEL
		L	LDV/VEL
		R	DCV/LDV/OMV/PBT/ OMV/VEL/ELB
		T	LDV
	L31	F	DCV/LDV/OMV/ELB
		I	LDV/VEL
		M	DCV/LDV/ELB/VEL
		V	DCV/LDV/OMV/PBT/ OMV/VEL/ELB
	P32	L	DCV/LDV/VEL
		S	DCV/LDV/VEL
	S38	F	LDV
	H58	D	DCV/LDV/OMV/PBT/ OMV/VEL/ELB
	A92	T	LDV
	Y93	C	DCV/LDV/OMV/PBT/ OMV/VEL/ELB
		F	LDV/VEL
		H	DCV/LDV/OMV/PBT/ OMV/VEL/ELB
		N	DCV/LDV/OMV/PBT/ OMV/VEL/ELB
		R	DCV/VEL
		S	LDV/VEL/OMV
		W	VEL
1b	L28	M	ELB
		T	DCV/OMV
		I	OMV
	R30	H	DCV
	L31	F	DCV/LDV/OMV/ELB
		M	DCVLDV/OMV/VEL
		V	DCV/LDV/OMV/PBT/ OMV/VEL/ELB
	P32	L	DCV/LDV/VEL
		S	DCV/LDV/VEL
	P58	D	LDV
		S	DCV
	A92	K	LDV
	Y93	H	DCV/LDV/OMV/PBT/ OMV/VEL/ELB
		N	DCV/LDV/OMV/PBT /OMV/VEL/ELB
		C	VEL/DCV
		S	VEL
2	F28	S	DCV/OMV
	L28	F	OMV
	L31	M	DCV/LDV/VEL
		V	DCV/LDV/OMV/PBT/ OMV/VEL/ELB
	C92	R	DCV
	Y93	H	DCV/LDV/OMV/PBT/ OMV/VEL/ELB
3	M28	T	DCV/LDV/OMV/PBT/ OMV/VEL/ELB
	A30	K	DCV/ELB/VEL
		T	DCV
	L31	F	DCV/LDV/ OMV/ELB

(Continued)

TABLE 1 | Continued

Replicon genotype	Amino acid and position	Amino acid substitution(s) (> 2-fold resistance)	Direct-acting antiviral
		M	DCV/LDV/OMV/VEL
		V	DCV/LDV/OMV/PBT/OMV/VEL/ELB
	S62	L	DCV
	Y93	H	DCV/LDV/OMV/PBT/OMV/VEL/ELB
4	L28	V	OMV
	L30	H	DCV
		R	VEL
		F	ELB
		S	VEL
	Y93	C	VEL
		H	DCV/LDV/OMV/PBT/OMV/VEL/ELB
		N	DCV/LDV/OMV/PBT/OMV/VEL/ELB
		R	DCV/VEL
5	L28	I	OMV
	L31	F	DCV/LDV/OMV
		V	DCV/LDV/OMV/PBT/OMV/VEL/ELB
6	L31	M	DCV/LDV/ELB/VEL
		V	DCV/LDV/OMV/PBT/OMV/VEL/ELB
	P32	L	DCV/LDV/V EL
		S	DCV/LDV/VEL
	T58	A	DCV/OMV
		N	DCV/OMV
		S	DCV/OMV
NS5B			
1a	S282	T	SOF
	C316	H	DSV
		Y	DSV
		N	SOF
		F	SOF
	L320	F	SOF
	A395	G	DSV
	M414	T	DSV
	N444	K	DSV
	E446	K	DSV
		Q	DSV
	Y448	C	DSV
		H	DSV
	A553	T	DSV
	S556	G	DSV
		N	DSV
	D559	G	DSV
	Y561	H	DSV
	S565	F	DSV
1b	S282	T	SOF
	C316	H	DSV
		Y	DSV
		N	DSV
	L320	F	SOF
	S368	T	DSV
	N411	S	DSV
	M414	T	DSV
	Y448	C	DSV
		H	DSV
	P495	A	DSV
	A553	V	DSV
	G554	S	DSV
	S556	G	DSV
	D559	G	DSV
2	S282	T	SOF
	M289	L	SOF
3	S282	T	SOF

GZR, grazoprevir; PTV, paritaprevir; GLE, glecaprevir; VOX, voxilaprevir; DCV, daclatasvir; EBR, elbasvir; LDV, ledipasvir; PBT, pibrentasvir; OMV, ombitasvir; DSV, dasabuvir; SOF, sofosbuvir.

Liu et al., 2015; Asante-Appiah et al., 2018). HCV GT1 replicons carrying amino acid substitutions that confer > 2-fold resistance to various DAAs are listed in the **Table 1**.

Genotype 2

HCV GT2 infections comprised 8% of the patients with chronic hepatitis C virus in Europe (Mangia and Mottola, 2012). Treatment of HCV GT2 infections have historically resulted in higher SVRs than with HCV GT1 infections, even with lower doses of RBV and a shorter duration of therapy. SVR rates of 99% have been observed for HCV GT2 with sofosbuvir/velpatasvir or glecaprevir/pibrentasvir treatment in patients that previously failed therapy with pegIFN and RBV or a combined sofosbuvir and RBV treatment (Feld et al., 2015; Forns et al., 2017).

The efficient replication by the JFH-1 replicon makes it among the most extensively used replicon systems for identifying pangenotypic HCV inhibitors. The JFH-1 replicon carrying NS5A-F28S confers resistance to declatasvir, lidipasvir, and velpatasvir while L31V confers resistance to ombitasvir and Y93H to ruzasvir (Asante-Appiah et al., 2018). Several NS3 RASs confer significant resistance, including R155W to voxilaprevir and A156T/V to volxilaprevir and glecaprevir (Ng et al., 2017b; Han et al., 2019). The S282T mutation in the NS5B polymerase region is the only mutation that is associated with resistance to sofosbuvir and was identified in a 2b-infected patient that failed therapy during a clinical trial (Hedskog et al., 2015). HCV GT2 replicons harboring amino acid substitutions that confer > 2-fold resistance to various DAAs are listed in the **Table 1**.

Genotype 3

The GT3 genotype accounts for 20–30% of all of the HCV infections globally and is the second most prevalent reported genotype in several East Asian and some European countries (Gower et al., 2014; Messina et al., 2015). Patients with GT3 infections have relatively faster rates of fibrosis progression in addition to higher incidence of steatosis and HCC when compared with individuals infected with other HCV GTs (Chan et al., 2017). Dual DAA regimens including sofosbuvir/velpatasvir and glecaprevir/pibrentasvir show effective SVR rates ranging from 94 to 100% and have thus become mainstays for treatment-naïve patients (Jacobson et al., 2017; Kwo et al., 2017; Zeuzem et al., 2018). The most commonly observed baseline NS5A RASs that confer high levels of resistance in GT3 infected patients are Y93H, A30K, and L31I/F (Lawitz et al., 2016; Wyles and Luetkemeyer, 2017). The RAS A30K is found in 87% of GT3b infected patients at baseline, while paired RAS A30K + L31M in 100% of patients infected with GT3b and GT3g (Bagaglio et al., 2019; Smith et al., 2019).

The GT3 bicistronic subgenomic replicon was constructed from the consensus sequence of the isolate S310 (SGR-S310) that yielded G418-resistant colonies. The inclusion of NS3 T235I, NS5A-T210A, and NS5B-R465K increased the replication potential of the parental replicon, rendering the replicon amenable for screening and evaluation of DAAs (Saeed et al., 2013). An intergenotypic GT3 replicon cloned in the Con1 genetic background that carried the RAS NS5A-Y93H mutation conferring resistance to different NS5A inhibitors, including daclatasvir, ombitasvir, and elbasvir, also conferred significant loss in susceptibility to the recently discovered pibrentasvir and ruzasvir (Ng et al., 2017a; Asante-Appiah et al., 2018). In addition, a stably replicating GT3a replicon (PR87A7) harboring NS3-168Q, which is a highly conserved amino acid among GT3a isolates, was found to impart resistance to several anti-NS3 DAAs (Guo et al., 2019). Recently, it is reported that RAS NS5b-A150V was shown associated with a reduced response to treatment with sofosbuvir and RBV, with or without pegIFN. Inclusion of A150V in NS5B of GT3a (S52) subgenomic replicon conferred resistance against sofosbuvir (Saeed et al., 2012; Wing et al., 2019). HCV GT3 replicons harboring amino acid substitutions that confer > 2-fold resistance to various DAAs are listed in the **Table 1**.

Genotype 4

GT4 is responsible for more than 80% of all of the HCV infections in Africa and the Middle East, and GT4 infections account for nearly 20% of global infections (Nguyen and Keeffe, 2005; Kamal, 2011). Approved dual DAA regimens for GT4 treatment include glecaprevir/pibrentasvir, sofosbuvir/velpatasvir, elbasvir/grazoprevir, and ledipasvir/sofosbuvir (Curry et al., 2015; Feld et al., 2015). The recommended triple regimens comprise ombitasvir-paritaprevir-ritonavir and sofosbuvir-velpatasvir-voxilaprevir (Bourlière et al., 2017). Current HCV GT4 treatments exhibit SVR rates above 95% (Feld et al., 2015; Bourlière et al., 2017).

The GT4a replicon ED43 was constructed from the cDNA consensus sequence to facilitate the development of antivirals with pangenotypic activity (Gottwein et al., 2010). Although the wild-type bicistronic replicon (fused RLuc-Neo) failed to replicate, stable cell lines were established by the inclusion of the adaptive mutations NS5A Q34R and NS3 T343R in addition to NS5A-S232I, which was previously shown to enhance GT1b (Con1) replication (Peng et al., 2013). Incorporation of the mutation R465G (NS5B), which was also identified in Con1, combined with NS5A S232I yielded few G418 resistant colonies (Saeed et al., 2012). In the ED43 genetic background (carries adaptive mutations NS3 G162R) inclusion of the NS5A RASs L28V or L30H do not confer significant resistance against pibrentasvir, nor do Y93H or L30H against ruzasvir (Ng et al., 2017a; Asante-Appiah et al., 2018). However, incorporation of NS3-R156T/V and D168H/V in the stable chimeric GT4a replicon in a Con1 genetic background conferred resistance to glecaprevir, while NS5A L28V conferred resistance to ombitasvir (Krishnan et al., 2015a; Ng et al., 2017b). HCV GT4 replicons harboring amino acid substitutions that confer > 2-fold resistance to various DAAs are listed in the **Table 1**.

Genotypes 5 and 6

Chronic hepatitis C due to GT5 or GT6 infections has low global prevalence. However, GT5 is widespread in Southern Africa, wherein up to 40% of individuals with chronic HCV have GT5 infections (Al Naamani et al., 2013). In contrast, GT6 is mainly concentrated in Southeast Asia, including in China, Vietnam, Thailand, and Myanmar, with a prevalence of ∼30–40% (Luo et al., 2019). Due to limited numbers of patients with reported GT5 and GT6 infections, data for treatment efficacy are limited to small cohorts. FDA-recommended treatments for patients infected with HCV GT5 and GT6 include sofosbuvir combined with an NS5A inhibitor like velpatasvir or ledipasvir. Such treatments have achieved 95–100% SVR rates among treatment-naive patients with or without cirrhosis (Feld et al., 2015; Jacobson et al., 2017; Nguyen et al., 2019).

GT5a strain SA13 was isolated from the plasma of a chimpanzee infected with a South African patient sample (Bukh et al., 2010) and was used to develop an efficient GT5a replicon and intergenotypic replicons. Inclusion of the NS5A S232G adaptive mutation in the SA13 background has facilitated the generation of a stable replicon, but E176K, E196C, D405N/Y, and E533K have not (Camus et al., 2018). A replicon consisting of the NS5A coding sequence in the GT2a (JFH-1) background was recently synthesized to evaluate the antiviral activity of ruzasvir, which is a pangenotype NS5A inhibitor (Asante-Appiah et al., 2018). The RASs L18F, L31F, and L31S have frequently emerged as resistance-conferring mutations to ruzasvir (Asante-Appiah et al., 2018). Inclusion of the adaptive mutation NS5A S232I that was originally found in the GT1b Con1 replicon within the GT5a replicon [SA1/SG-neo(I)] moderately increases replicon replication compared to its wild-type counterpart. However, inclusion of NS3 E176K and K379S adaptive mutations in addition to the NS5A S393P mutation further enhanced replicon replication and facilitated screening of antivirals (Wose Kinge et al., 2014).

Gilead Sciences has generated GT6a subgenomic replicons containing the NS5A S232I adaptive mutation. Further, additional adaptive mutations including the NS3 mutations

E30V and K272R and the NS4A mutation K34R enhances GT6a replicon replication. Inclusion of these new adaptive mutations allowed the establishment of an efficient replicon that was engineered with RLuc-Neo fusion to achieve reproducible quantification of HCV replication (Yu et al., 2014). Further, inclusion of the adaptive mutations NS3 K272R plus NS5A P237L enhanced the replication capacity of a GT6a replicon (GS16a-1) (Camus et al., 2018). In addition, a chimeric replicon consisting of the complete NS5A sequence GT6 in the GT2a (JFH-1) background was generated to evaluate the antiviral activity of ruzasvir (Asante-Appiah et al., 2018). The GT5a and GT6a replicons harboring the NS3 amino acid substitutions D168H/G/V and D168E/V/Y were associated with reduced susceptibility to glecaprevir and voxilaprevir, respectively (Ng et al., 2017b; Han et al., 2019). The RAS NS3-D168E was found in 48.6% of GT5 natural HCV sequences and 2.7% of those of GT6 (Patiño-Galindo et al., 2016). HCV GT5 and GT6 replicons carrying amino acid substitutions that confer > 2-fold resistance to various DAAs are listed in the **Table 1**.

CONCLUSION

After the molecular cloning of HCV genome, establishing functional Con1 replicon constitutes one of the most significant steps in fundamental research on this pathogen of public health concern. Further improvements are accomplished by the advent of HCV replicons for most of the genotypes. HCV replicon systems are already proving valuable research tools for the discovery of effective pangenotypic DAAs, and to evaluate RAS(s) identified in both preclinical and clinical studies. It is not much of an exaggeration to say that HCV replicon systems have been and will continue to be the primary workhorses of the DAA discovery process and may provide a foundation for the elimination of HCV.

AUTHOR CONTRIBUTIONS

SK, SS, and NV contributed to the manuscript writing and final approval. All authors contributed to the article and approved the submitted version.

FUNDING

The preparation of this review and research in authors' laboratory was supported by research grant BT/PR10906/MED/29/860/2014 to NV from the Department of Biotechnology, Ministry of Science and Technology, Government of India. SK and SS were supported by a graduate scholarship from Shiv Nadar University.

REFERENCES

Afdhal, N., Zeuzem, S., Kwo, P., Chojkier, M., Gitlin, N., Puoti, M., et al. (2014). Ledipasvir and sofosbuvir for untreated HCV genotype 1 infection. *N. Engl. J. Med*. 370, 1889–1898. doi: 10.1056/NEJMoa1402454

Agarwal, S., Baccam, P., Aggarwal, R., and Veerapu, N. S. (2018). Novel synthesis and phenotypic analysis of mutant clouds for hepatitis E virus genotype 1. *J. Virol*. 92:e01932–01917. doi: 10.1128/JVI.01932-17

Ahmed, A., and Felmlee, D. J. (2015). Mechanisms of hepatitis C viral resistance to direct acting antivirals. *Viruses* 7, 6716–6729. doi: 10.3390/v7122968

Al Naamani, K., Al Sinani, S., and Deschênes, M. (2013). Epidemiology and treatment of hepatitis C genotypes 5 and 6. *Can. J. Gastroenterol*. 27, e8–e12. doi: 10.1155/2013/624986

Alazard-Dany, N., Denolly, S., Boson, B., and Cosset, F.-L. (2019). Overview of HCV life cycle with a special focus on current and possible future antiviral targets. *Viruses* 11:30. doi: 10.3390/v11010030

Appel, N., Pietschmann, T., and Bartenschlager, R. (2005). Mutational analysis of hepatitis C virus nonstructural protein 5A: potential role of differential phosphorylation in RNA replication and identification of a genetically flexible domain. *J. Virol*. 79, 3187–3194. doi: 10.1128/JVI.79.5.3187-3194.2005

Asante-Appiah, E., Liu, R., Curry, S., McMonagle, P., Agrawal, S., Carr, D., et al. (2018). *In vitro* antiviral profile of ruzasvir, a potent and pangenotype inhibitor of hepatitis C virus NS5a. *Antimicrob. Agents Chemother*. 62, 1–13. doi: 10.1128/AAC.01280-18

Bagaglio, S., Messina, E., Hasson, H., Galli, A., Uberti-Foppa, C., and Morsica, G. (2019). Geographic distribution of HCV-GT3 subtypes and naturally occurring resistance associated substitutions. *Viruses* 11:148. doi: 10.3390/v11020148

Bartenschlager, R. (2002). Hepatitis C virus replicons: potential role for drug development. *Nat. Rev. Drug Discov*. 1, 911–916. doi: 10.1038/nrd942

Bartenschlager, R. (2006). Hepatitis C virus molecular clones: from cDNA to infectious virus particles in cell culture. *Curr. Opin. Microbiol*. 9, 416–422. doi: 10.1016/j.mib.2006.06.012

Bartenschlager, R., Lohmann, V., and Penin, F. (2013). The molecular and structural basis of advanced antiviral therapy for hepatitis C virus infection. *Nat. Rev. Microbiol*. 11, 482–496. doi: 10.1038/nrmicro3046

Bartosch, B., Dubuisson, J., and Cosset, F. L. (2003). Infectious hepatitis C virus pseudo-particles containing functional E1-E2 envelope protein complexes. *J. Exp. Med*. 197, 633–642. doi: 10.1084/jem.20021756

Behrens, S. E., Tomei, L., and De Francesco, R. (1996). Identification and properties of the RNA-dependent RNA polymerase of hepatitis C virus. *EMBO J*. 15, 12–22. doi: 10.1002/j.1460-2075.1996.tb00329.x

Blight, K. J., Kolykhalov, A. A., and Rice, C. M. (2000). Efficient initiation of HCV RNA replication in cell culture. *Science* 290, 1972–1974. doi: 10.1126/science.290.5498.1972

Blight, K. J., McKeating, J. A., Marcotrigiano, J., and Rice, C. M. (2003). Efficient replication of hepatitis C virus genotype 1a RNAs in cell culture. *J. Virol*. 77, 3181–3190. doi: 10.1128/jvi.77.5.3181-3190.2003

Bourlière, M., Gordon, S. C., Flamm, S. L., Cooper, C. L., Ramji, A., Tong, M., et al. (2017). Sofosbuvir, velpatasvir, and voxilaprevir for previously treated HCV infection. *N. Engl. J. Med*. 376, 2134–2146. doi: 10.1056/NEJMoa1613512

Bukh, J., Meuleman, P., Tellier, R., Engle, R. E., Feinstone, S. M., Eder, G., et al. (2010). Challenge pools of hepatitis C virus genotypes 1–6 prototype strains: Replication fitness and pathogenicity in chimpanzees and human liver–chimeric mouse models. *J. Infect. Dis*. 201, 1381–1389. doi: 10.1086/651579

Camus, G., Xu, S., Han, B., Lu, J., Dvory-Sobol, H., Yu, M., et al. (2018). Establishment of robust HCV genotype 4d, 5a, and 6a replicon systems. *Virology* 514, 134–141. doi: 10.1016/j.virol.2017.11.003

Chacko, K. R., and Gaglio, P. J. (2015). Meet the classes of directly acting antiviral agents. *Clin. Liver Dis*. 19, 605–617. doi: 10.1016/j.cld.2015.06.002

Chan, A., Patel, K., and Naggie, S. (2017). Genotype 3 Infection: The last stand of hepatitis C Virus. *Drugs* 77, 131–144. doi: 10.1007/s40265-016-0685-x

Cheng, G., Yu, M., Peng, B., Lee, Y.-J., Trejo-Martin, A., Gong, R., et al. (2013). 1191 GS-5816, A second generation HCV NS5A inhibitor with potent antiviral activity, broad genotypic coverage and a high resistance barrier. *J. Hepatol*. 58, S484–S485. doi: 10.1016/S0168-8278(13)61192-7

Choo, Q., Kuo, G., Weiner, A., Overby, L., Bradley, D., and Houghton, M. (1989). Isolation of a cDNA clone derived from a blood-borne non-A, non-B viral hepatitis genome. *Science* 244, 359–362. doi: 10.1126/science.2523562

Coburn, C. A., Meinke, P. T., Chang, W., Fandozzi, C. M., Graham, D. J., Hu, B., et al. (2013). Discovery of MK-8742: an HCV NS5A inhibitor with broad genotype activity. *ChemMedChem* 8, 1930–1940. doi: 10.1002/cmdc.201300343

Curry, M. P., O'Leary, J. G., Bzowej, N., Muir, A. J., Korenblat, K. M., Fenkel, J. M., et al. (2015). Sofosbuvir and velpatasvir for HCV in patients with decompensated cirrhosis. *N. Engl. J. Med.* 373, 2618–2628. doi: 10.1056/NEJMoa1512614

Cuypers, L., Ceccherini-Silberstein, F., Van Laethem, K., Li, G., Vandamme, A.-M., and Rockstroh, J. K. (2016). Impact of HCV genotype on treatment regimens and drug resistance: a snapshot in time. *Rev. Med. Virol.* 26, 408–434. doi: 10.1002/rmv.1895

Date, T., Miyamoto, M., Kato, T., Morikawa, K., Murayama, A., Akazawa, D., et al. (2007). An infectious and selectable full-length replicon system with hepatitis C virus JFH-1 strain. *Hepatol. Res.* 37, 433–443. doi: 10.1111/j.1872-034X.2007.00056.x

DeGoey, D. A., Randolph, J. T., Liu, D., Pratt, J., Hutchins, C., Donner, P., et al. (2014). Discovery of ABT-267, a pan-genotypic inhibitor of HCV NS5A. *J. Med. Chem.* 57, 2047–2057. doi: 10.1021/jm401398x

Dietz, J., Susser, S., Vermehren, J., Peiffer, K.-H., Grammatikos, G., Berger, A., et al. (2018). Patterns of resistance-associated substitutions in patients with chronic HCV infection following treatment with direct-acting antivirals. *Gastroenterology* 154, 976–988.e4. doi: 10.1053/j.gastro.2017.11.007

Egger, D., Wolk, B., Gosert, R., Bianchi, L., Blum, H. E., Moradpour, D., et al. (2002). Expression of hepatitis C virus proteins induces distinct membrane alterations including a candidate viral replication complex. *J. Virol.* 76, 5974–5984. doi: 10.1128/JVI.76.12.5974-5984.2002

Evans, M. J., Rice, C. M., and Goff, S. P. (2004). Phosphorylation of hepatitis C virus nonstructural protein 5A modulates its protein interactions and viral RNA replication. *Proc. Natl. Acad. Sci U.S.A.* 101, 13038–13043. doi: 10.1073/pnas.0405152101

Feld, J. J. (2017). Resistance testing: Interpretation and incorporation into HCV treatment algorithms. *Clin. Liver Dis.* 9, 115–120. doi: 10.1002/cld.631

Feld, J. J., Jacobson, I. M., Hézode, C., Asselah, T., Ruane, P. J., Gruener, N., et al. (2015). Sofosbuvir and velpatasvir for HCV Genotype 1, 2, 4, 5, and 6 Infection. *N. Engl. J. Med.* 373, 2599–2607. doi: 10.1056/NEJMoa1512610

Forns, X., Gordon, S. C., Zuckerman, E., Lawitz, E., Calleja, J. L., Hofer, H., et al. (2015). Grazoprevir and elbasvir plus ribavirin for chronic HCV genotype-1 infection after failure of combination therapy containing a direct-acting antiviral agent. *J. Hepatol.* 63, 564–572. doi: 10.1016/j.jhep.2015.04.009

Forns, X., Lee, S. S., Valdes, J., Lens, S., Ghalib, R., Aguilar, H., et al. (2017). Glecaprevir plus pibrentasvir for chronic hepatitis C virus genotype 1, 2, 4, 5, or 6 infection in adults with compensated cirrhosis (EXPEDITION-1): a single-arm, open-label, multicentre phase 3 trial. *Lancet Infect. Dis.* 17, 1062–1068. doi: 10.1016/S1473-3099(17)30496-6

Fourati, S., Feld, J. J., Chevaliez, S., and Luhmann, N. (2018). Approaches for simplified HCV diagnostic algorithms. *J. Int. AIDS Soc.* 21:e25058. doi: 10.1002/jia2.25058

Fourati, S., and Pawlotsky, J.-M. (2015). Virologic tools for HCV drug resistance testing. *Viruses* 7, 6346–6359. doi: 10.3390/v7122941

Frese, M. (2002). Interferon-γ inhibits replication of subgenomic and genomic hepatitis C virus RNAs. *Hepatology* 35, 694–703. doi: 10.1053/jhep.2002.31770

Gao, M., Nettles, R. E., Belema, M., Snyder, L. B., Nguyen, V. N., Fridell, R. A., et al. (2010). Chemical genetics strategy identifies an HCV NS5A inhibitor with a potent clinical effect. *Nature* 465, 96–100. doi: 10.1038/nature08960

Geller, R., Estada, Ú., Peris, J. B., Andreu, I., Bou, J.-V., Garijo, R., et al. (2016). Highly heterogeneous mutation rates in the hepatitis C virus genome. *Nat. Microbiol.* 1:16045. doi: 10.1038/nmicrobiol.2016.45

Götte, M. (2012). The distinct contributions of fitness and genetic barrier to the development of antiviral drug resistance. *Curr. Opin. Virol.* 2, 644–650. doi: 10.1016/j.coviro.2012.08.004

Götte, M., and Feld, J. J. (2016). Direct-acting antiviral agents for hepatitis C: structural and mechanistic insights. *Nat. Rev. Gastroenterol. Hepatol.* 13:338–351. doi: 10.1038/nrgastro.2016.60

Gottwein, J. M., Scheel, T. K. H., Callendret, B., Li, Y. P., Eccleston, H. B., Engle, R. E., et al. (2010). Novel infectious cDNA clones of hepatitis C virus genotype 3a (Strain S52) and 4a (Strain ED43): genetic analyses and *in vivo* pathogenesis studies. *J. Virol.* 84, 5277–5293. doi: 10.1128/JVI.02667-09

Gower, E., Estes, C., Blach, S., Razavi-Shearer, K., and Razavi, H. (2014). Global epidemiology and genotype distribution of the hepatitis C virus infection. *J. Hepatol.* 61, S45–S57. doi: 10.1016/j.jhep.2014.07.027

Grakoui, A., McCourt, D. W., Wychowski, C., Feinstone, S. M., and Rice, C. M. (1993). A second hepatitis C virus-encoded proteinase. *Proc. Natl. Acad. Sci U.S.A.* 90, 10583–10587. doi: 10.1073/pnas.90.22.10583

Grobler, J. A., Markel, E. J., Fay, J. F., Graham, D. J., Simcoe, A. L., Ludmerer, S. W., et al. (2003). Identification of a key determinant of hepatitis C virus cell culture adaptation in domain II of NS3 helicase. *J. Biol. Chem.* 278, 16741–16746. doi: 10.1074/jbc.M212602200

Guo, M., Lu, J., Gan, T., Xiang, X., Xu, Y., Xie, Q., et al. (2019). Construction and characterization of genotype-3 hepatitis C virus replicon revealed critical genotype-3-specific polymorphism for drug resistance and viral fitness. *Antiviral. Res.* 171:104612. doi: 10.1016/j.antiviral.2019.104612

Han, B., Martin, R., Xu, S., Parvangada, A., Svarovskaia, E. S., Mo, H., et al. (2019). Sofosbuvir susceptibility of genotype 1 to 6 HCV from DAA-naïve subjects. *Antiviral Res.* 170:104574. doi: 10.1016/j.antiviral.2019.104574

Harak, C., Meyrath, M., Romero-Brey, I., Shenck, C., Gondeau, C., Schult, P., et al. (2017). Tuning a cellular lipid kinase activity adapts hepatitis C virus to replication in cell culture. *Nat. Microbiol.* 2:16247. doi: 10.1038/nmicrobiol.2016.247

Hedskog, C., Dvory-Sobol, H., Gontcharova, V., Martin, R., Ouyang, W., Han, B., et al. (2015). Evolution of the HCV viral population from a patient with S282T detected at relapse after sofosbuvir monotherapy. *J. Viral Hepat.* 22, 871–881. doi: 10.1111/jvh.12405

Hedskog, C., Parhy, B., Chang, S., Zeuzem, S., Moreno, C., Shafran, S. D., et al. (2019). Identification of 19 Novel hepatitis C virus subtypes—further expanding HCV classification. *Open Forum Infect. Dis.* 6:ofz076. doi: 10.1093/ofid/ofz076

Herlihy, K. J., Graham, J. P., Kumpf, R., Patick, A. K., Duggal, R., and Shi, S. T. (2008). Development of intergenotypic chimeric replicons to determine the broad-spectrum antiviral activities of hepatitis C virus polymerase inhibitors. *Antimicrob. Agents Chemother.* 52, 3523–3531. doi: 10.1128/AAC.00533-08

Holmes, J. A., Rutledge, S. M., and Chung, R. T. (2019). Direct-acting antiviral treatment for hepatitis C. *Lancet* 393, 1392–1394. doi: 10.1016/S0140-6736(18)32326-2

Hoofnagle, J. H., Mullen, K. D., Jones, D. B., Rustgi, V., Di Bisceglie, A., Peters, M., et al. (1986). Treatment of chronic non-A, non-B hepatitis with recombinant human alpha interferon. *N. Engl. J. Med.* 315, 1575–1578. doi: 10.1056/NEJM198612183152503

Ikeda, M., Yi, M., Li, K., and Lemon, S. M. (2002). Selectable subgenomic and genome-length dicistronic RNAs derived from an infectious molecular clone of the HCV-N strain of hepatitis C virus replicate efficiently in cultured Huh7 cells. *J. Virol.* 76, 2997–3006. doi: 10.1128/JVI.76.6.2997-3006.2002

Jacobson, I. M., Lawitz, E., Gane, E. J., Willems, B. E., Ruane, P. J., Nahass, R. G., et al. (2017). Efficacy of 8 weeks of sofosbuvir, velpatasvir, and voxilaprevir in patients with chronic HCV infection: 2 phase 3 randomized trials. *Gastroenterology* 153, 113–122. doi: 10.1053/j.gastro.2017.03.047

Jensen, S. B., Fahnøe, U., Pham, L. V., Serre, S. B. N., Tang, Q., Ghanem, L., et al. (2019). Evolutionary pathways to persistence of highly fit and resistant hepatitis C virus protease inhibitor escape variants. *Hepatology* 70, 771–787. doi: 10.1002/hep.30647

Kamal, S. M. (2011). Hepatitis C virus genotype 4 therapy: progress and challenges. *Liver Int.* 31, 45–52. doi: 10.1111/j.1478-3231.2010.02385.x

Kato, T., Date, T., Miyamoto, M., Furusaka, A., Tokushige, K., Mizokami, M., et al. (2003). Efficient replication of the genotype 2a hepatitis C virus subgenomic replicon. *Gastroenterology* 125, 1808–1817. doi: 10.1053/j.gastro.2003.09.023

Kato, T., Furusaka, A., Miyamoto, M., Date, T., Yasui, K., Hiramoto, J., et al. (2001). Sequence analysis of hepatitis C virus isolated from a fulminant hepatitis patient. *J. Med. Virol.* 64, 334–339. doi: 10.1002/jmv.1055

Kowdley, K. V., Gordon, S. C., Reddy, K. R., Rossaro, L., Bernstein, D. E., Lawitz, E., et al. (2014). Ledipasvir and sofosbuvir for 8 or 12 weeks for chronic HCV without cirrhosis. *N. Engl. J. Med.* 370, 1879–1888. doi: 10.1056/NEJMoa1402355

Krieger, N., Lohmann, V., and Bartenschlager, R. (2001). Enhancement of hepatitis C virus RNA replication by cell culture-adaptive mutations. *J. Virol.* 75, 4614–4624. doi: 10.1128/jvi.75.10.4614-4624.2001

Krishnan, P., Beyer, J., Mistry, N., Koev, G., Reisch, T., DeGoey, D., et al. (2015a). *In vitro* and *in vivo* antiviral activity and resistance profile of ombitasvir, an inhibitor of hepatitis C virus NS5A. *Antimicrob. Agents Chemother.* 59, 979–987. doi: 10.1128/AAC.04226-14

Krishnan, P., Tripathi, R., Schnell, G., Reisch, T., Beyer, J., Irvin, M., et al. (2015b). Resistance analysis of baseline and treatment-emergent variants in hepatitis C virus genotype 1 in the AVIATOR study with paritaprevir-ritonavir, ombitasvir, and dasabuvir. *Antimicrob. Agents Chemother.* 59, 5445–5454. doi: 10.1128/AAC.00998-15

Kwo, P. Y., Poordad, F., Asatryan, A., Wang, S., Wyles, D. L., Hassanein, T., et al. (2017). Glecaprevir and pibrentasvir yield high response rates in patients with HCV genotype 1–6 without cirrhosis. *J. Hepatol.* 67, 263–271. doi: 10.1016/j.jhep.2017.03.039

Lam, A. M., Espiritu, C., Bansal, S., MicolochickSteuer, H. M., Niu, C., Zennou, V., et al. (2012). Genotype and subtype profiling of PSI-7977 as a nucleotide inhibitor of hepatitis C virus. *Antimicrob. Agents Chemother.* 56, 3359–3368. doi: 10.1128/AAC.00054-12

Lamarre, D., Anderson, P. C., Bailey, M., Beaulieu, P., Bolger, G., Bonneau, P., et al. (2003). An NS3 protease inhibitor with antiviral effects in humans infected with hepatitis C virus. *Nature* 426, 186–189. doi: 10.1038/nature02099

Lawitz, E. J., Dvory-Sobol, H., Doehle, B. P., Worth, A. S., McNally, J., Brainard, D. M., et al. (2016). Clinical resistance to velpatasvir (GS-5816), a novel pan-genotypic inhibitor of the hepatitis C virus NS5A protein. *Antimicrob. Agents Chemother.* 60, 5368–5378. doi: 10.1128/AAC.00763-16

Li, D. K., and Chung, R. T. (2019). Overview of direct-acting antiviral drugs and drug resistance of hepatitis C virus. *Methods Mol. Biol.* 1911, 3–32. doi: 10.1007/978-1-4939-8976-8_1

Liang, C., Rieder, E., Hahm, B., Key Jang, S., Paul, A., and Wimmer, E. (2005). Replication of a novel subgenomic HCV genotype 1a replicon expressing a puromycin resistance gene in Huh-7 cells. *Virology* 333, 41–53. doi: 10.1016/j.virol.2004.12.031

Lin, C., Prágai, B. M., Grakoui, A., Xu, J., and Rice, C. M. (1994). Hepatitis C virus NS3 serine proteinase: trans-cleavage requirements and processing kinetics. *J. Virol.* 68, 8147–8157. doi: 10.1128/JVI.68.12.8147-8157.1994

Lindenbach, B. D., and Rice, C. M. (2005). Unravelling hepatitis C virus replication from genome to function. *Nature* 436, 933–938. doi: 10.1038/nature04077

Liu, R., Curry, S., McMonagle, P., Yeh, W. W., Ludmerer, S. W., Jumes, P. A., et al. (2015). Susceptibilities of genotype 1a, 1b, and 3 hepatitis C virus variants to the NS5A inhibitor elbasvir. *Antimicrob. Agents Chemother.* 59, 6922–6929. doi: 10.1128/AAC.01390-15

Lohmann, V. (2009). "HCV Replicons: Overview and basic protocols," in *Methods in Molecular Biology*, ed H. Tang (Totowa, NJ: Humana Press), 145–163. =

Lohmann, V., Hoffmann, S., Herian, U., Penin, F., and Bartenschlager, R. (2003). Viral and cellular determinants of hepatitis C virus RNA replication in cell culture. *J. Virol.* 77, 3007–3019. doi: 10.1128/JVI.77.5.3007-3019.2003

Lohmann, V., Kdrner, F., Koch, O. J., Herian, U., Theilmann, L., and Bartenschlager, R. (1999). Replication of subgenomic hepatitis C virus RNAs in a hepatoma cell line. *Science* 285, 110–113. doi: 10.1126/science.285.5424.110

Lohmann, V., Korner, F., Dobierzewska, A., and Bartenschlager, R. (2001). Mutations in hepatitis C virus RNAs conferring cell culture adaptation. *J. Virol.* 75, 1437–1449. doi: 10.1128/JVI.75.3.1437-1449.2001

Lohmann, V., Körner, F., Herian, U., and Bartenschlager, R. (1997). Biochemical properties of hepatitis C virus NS5B RNA-dependent RNA polymerase and identification of amino acid sequence motifs essential for enzymatic activity. *J. Virol.* 71, 8416–8428. doi: 10.1128/JVI.71.11.8416-8428.1997

Lontok, E., Harrington, P., Howe, A., Kieffer, T., Lennerstrand, J., Lenz, O., et al. (2015). Hepatitis C virus drug resistance-associated substitutions: state of the art summary. *Hepatology* 62, 1623–1632. doi: 10.1002/hep.27934

Luo, A., Xu, P., Wang, J., Li, Z., Wang, S., Jiang, X., et al. (2019). Efficacy and safety of direct-acting antiviral therapy for chronic hepatitis C genotype 6. *Medicine.* 98:e15626. doi: 10.1097/MD.0000000000015626

Mangia, A., and Mottola, L. (2012). What's new in HCV genotype 2 treatment? *Liver Int.* 32, 135–140. doi: 10.1111/j.1478-3231.2011.02710.x

Maring, C., Wagner, R., Hutchinson, D., Flentge, C., Kati, W., Koev, G., et al. (2009). 955 Preclinical potency, pharmacokinetic and ADME characterization of ABT-333, a novel non-nucleoside HCV polymerase inhibitor. *J. Hepatol.* 50:S347. doi: 10.1016/S0168-8278(09)60957-0

McCown, M. F., Rajyaguru, S., Le Pogam, S., Ali, S., Jiang, W.-R., Kang, H., et al. (2008). The hepatitis C virus replicon presents a higher barrier to resistance to nucleoside analogs than to nonnucleoside polymerase or protease inhibitors. *Antimicrob. Agents Chemother.* 52, 1604–1612. doi: 10.1128/AAC.01317-07

Messina, J. P., Humphreys, I., Flaxman, A., Brown, A., Cooke, G. S., Pybus, O. G., et al. (2015). Global distribution and prevalence of hepatitis C virus genotypes. *Hepatology* 61, 77–87. doi: 10.1002/hep.27259

Moradpour, D., Evans, M. J., Gosert, R., Yuan, Z., Blum, H. E., Goff, S. P., et al. (2004). Insertion of green fluorescent protein into nonstructural protein 5A allows direct visualization of functional hepatitis C virus replication complexes. *J. Virol.* 78, 7400–7409. doi: 10.1128/JVI.78.14.7400-7409.2004

Moradpour, D., Penin, F., and Rice, C. M. (2007). Replication of hepatitis C virus. *Nat. Rev. Microbiol.* 5, 453–463. doi: 10.1038/nrmicro1645

Murray, E. M., Grobler, J. A., Markel, E. J., Pagnoni, M. F., Paonessa, G., Simon, A. J., et al. (2003). Persistent replication of hepatitis C virus replicons expressing the β-Lactamase reporter in subpopulations of highly permissive Huh7 Cells. *J. Virol.* 77, 2928–2935. doi: 10.1128/JVI.77.5.2928-2935.2003

Neumann, A. U. (1998). Hepatitis C viral dynamics *in vivo* and the antiviral efficacy of interferon- therapy. *Science* 282, 103–107. doi: 10.1126/science.282.5386.103

Ng, T., Pilot-Matias, T., Liangjun, L., Reisch, T., Dekhtyar, T., Krishnan, P., et al. (2014). "A next generation HCV DAA combination: potent, pangenotypic inhibitors ABT-493 and ABT-530 with high barriers to resistance. [abstract]," in *65th Annual Meeting of the American Association for the Study of Liver Diseases 2014.* (Boston, MA: AbbVie Inc), 7–11.

Ng, T. I., Krishnan, P., Pilot-Matias, T., Kati, W., Schnell, G., Beyer, J., et al. (2017a). *In Vitro* antiviral activity and resistance profile of the next-generation hepatitis C virus NS5A inhibitor pibrentasvir. *Antimicrob. Agents Chemother.* 61, 1–14. doi: 10.1128/AAC.02558-16

Ng, T. I., Tripathi, R., Reisch, T., Lu, L., Middleton, T., Hopkins, T. A., et al. (2017b). *In vitro* antiviral activity and resistance profile of the next-generation hepatitis C Virus NS3/4A protease inhibitor glecaprevir. *Antimicrob. Agents Chemother.* 62, 1–16. doi: 10.1128/AAC.01620-17

Nguyen, E., Trinh, S., Trinh, H., Nguyen, H., Nguyen, K., Do, A., et al. (2019). Sustained virologic response rates in patients with chronic hepatitis C genotype 6 treated with ledipasvir+sofosbuvir or sofosbuvir+velpatasvir. *Aliment. Pharmacol. Ther.* 49, 99–106. doi: 10.1111/apt.15043

Nguyen, M. H., and Keeffe, E. B. (2005). Prevalence and treatment of hepatitis C virus genotypes 4, 5, and 6. *Clin. Gastroenterol. Hepatol.* 3(Suppl. 2), 97–101. doi: 10.1016/S1542-3565(05)00711-1

Ogata, N., Alter, H. J., Miller, R. H., and Purcell, R. H. (1991). Nucleotide sequence and mutation rate of the H strain of hepatitis C virus. *Proc. Natl. Acad. Sci. U.S.A.* 88, 3392–3396. doi: 10.1073/pnas.88.8.3392

Patiño-Galindo, J. Á., Salvatierra, K., González-Candelas, F., and López-Labrador, F. X. (2016). Comprehensive screening for naturally occurring hepatitis C virus resistance to direct-acting antivirals in the NS3, NS5A, and NS5B genes in worldwide isolates of viral genotypes 1 to 6. *Antimicrob. Agents Chemother.* 60, 2402–2416. doi: 10.1128/AAC.02776-15

Pawlotsky, J.-M. (2011). Treatment failure and resistance with direct-acting antiviral drugs against hepatitis C virus. *Hepatology* 53, 1742–1751. doi: 10.1002/hep.24262

Pawlotsky, J.-M. (2016). Hepatitis C virus resistance to direct-acting antiviral drugs in interferon-free regimens. *Gastroenterology* 151, 70–86. doi: 10.1053/j.gastro.2016.04.003

Pearlman, B. L. (2012). Protease inhibitors for the treatment of chronic hepatitis C genotype-1 infection: the new standard of care. *Lancet Infect. Dis.* 12, 717–728. doi: 10.1016/S1473-3099(12)70060-9

Peng, B., Yu, M., Xu, S., Lee, Y., Tian, Y., Yang, H., et al. (2013). Development of robust hepatitis C virus genotype 4 subgenomic replicons. *Gastroenterology* 144, 59–61.e6. doi: 10.1053/j.gastro.2012.09.033

Perales, C., Quer, J., Gregori, J., Esteban, J., and Domingo, E. (2015). Resistance of hepatitis C virus to inhibitors: complexity and clinical implications. *Viruses* 7, 5746–5766. doi: 10.3390/v7112902

Pham, L. V., Ramirez, S., Gottwein, J. M., Fahnøe, U., Li, Y.-P., Pedersen, J., et al. (2018). HCV genotype 6a escape from and resistance to velpatasvir, pibrentasvir, and sofosbuvir in robust infectious cell culture models. *Gastroenterology* 154, 2194–2208.e12. doi: 10.1053/j.gastro.2018.02.017

Pietschmann, T., Lohmann, V., Kaul, A., Krieger, N., Rinck, G., Rutter, G., et al. (2002). Persistent and transient replication of full-length hepatitis C virus genomes in cell culture. *J. Virol.* 76, 4008–4021. doi: 10.1128/JVI.76.8.4008-4021.2002

Pietschmann, T., Zayas, M., Meuleman, P., Long, G., Appel, N., Koutsoudakis, G., et al. (2009). Production of infectious genotype 1b virus particles in cell culture and impairment by replication enhancing mutations. *PLoS Pathog.* 5:e1000475. doi: 10.1371/journal.ppat.1000475

Pilot-Matias, T., Tripathi, R., Cohen, D., Gaultier, I., Dekhtyar, T., Lu, L., et al. (2015). *In vitro* and in vivo antiviral activity and resistance profile of the hepatitis C virus NS3/4A protease inhibitor ABT-450. *Antimicrob. Agents Chemother.* 59, 988–997. doi: 10.1128/AAC.04227-14

Popping, S., El-Sayed, M., Feld, J., Hatzakis, A., Hellard, M., Lesi, O., et al. (2018). Report from the international viral hepatitis elimination meeting (IVHEM), 17-18 November 2017, Amsterdam, the Netherlands: gaps and challenges in the WHO 2030 hepatitis C elimination framework. *J. Virus Erad.* 4, 193–195.

Ramirez, S., and Bukh, J. (2018). Current status and future development of infectious cell-culture models for the major genotypes of hepatitis C virus: essential tools in testing of antivirals and emerging vaccine strategies. *Antiviral Res.* 158, 264–287. doi: 10.1016/j.antiviral.2018.07.014

Ramirez, S., Li, Y.-P., Jensen, S. B., Pedersen, J., Gottwein, J. M., and Bukh, J. (2014). Highly efficient infectious cell culture of three hepatitis C virus genotype 2b strains and sensitivity to lead protease, nonstructural protein 5A, and polymerase inhibitors. *Hepatology* 59, 395–407. doi: 10.1002/hep.26660

Ramirez, S., Mikkelsen, L. S., Gottwein, J. M., and Bukh, J. (2016). Robust HCV genotype 3a infectious cell culture system permits identification of escape variants with resistance to sofosbuvir. *Gastroenterology* 151, 973–985.e2. doi: 10.1053/j.gastro.2016.07.013

Reiss, S., Harak, C., Romero-Brey, I., Radujkovic, D., Klein, R., Ruggieri, A., et al. (2013). The lipid kinase phosphatidylinositol-4 kinase iii alpha regulates the phosphorylation status of hepatitis C virus NS5A. *PLoS Pathog.* 9:e1003359. doi: 10.1371/journal.ppat.1003359

Roingeard, P., and Beaumont, E. (2020). Hepatitis C vaccine: 10 good reasons for continuing. *Hepatology* 71, 1845–1850. doi: 10.1002/hep.31182

Romero-Brey, I., Merz, A., Chiramel, A., Lee, J.-Y., Chlanda, P., Haselman, U., et al. (2012). Three-dimensional architecture and biogenesis of membrane structures associated with hepatitis C virus replication. *PLoS Pathog.* 8:e1003056. doi: 10.1371/journal.ppat.1003056

Saeed, M., Andreo, U., Chung, H.-Y., Espiritu, C., Branch, A. D., Silva, J. M., et al. (2015). SEC14L2 enables pan-genotype HCV replication in cell culture. *Nature* 524, 471–475. doi: 10.1038/nature14899

Saeed, M., Gondeau, C., Hmwe, S., Yokokawa, H., Date, T., Suzuki, T., et al. (2013). Replication of hepatitis C virus genotype 3a in cultured cells. *Gastroenterology* 144, 56–58.e7. doi: 10.1053/j.gastro.2012.09.017

Saeed, M., Scheel, T. K. H., Gottwein, J. M., Marukian, S., Dustin, L. B., Bukh, J., et al. (2012). Efficient replication of genotype 3a and 4a hepatitis C virus replicons in human hepatoma cells. *Antimicrob. Agents Chemother.* 56, 5365–5373. doi: 10.1128/AAC.01256-12

Scheel, T. K. H., and Rice, C. M. (2013). Understanding the hepatitis C virus life cycle paves the way for highly effective therapies. *Nat. Med.* 19, 837–849. doi: 10.1038/nm.3248

Serre, S. B. N., Jensen, S. B., Ghanem, L., Humes, D. G., Ramirez, S., Li, Y.-P., et al. (2016). Hepatitis C virus genotype 1 to 6 protease inhibitor escape variants: *In vitro* selection, fitness, and resistance patterns in the context of the infectious viral life cycle. *Antimicrob. Agents Chemother.* 60, 3563–3578. doi: 10.1128/AAC.02929-15

Sheaffer, A. K., Lee, M. S., Hernandez, D., Chaniewski, S., Yu, F., Falk, P., et al. (2011). Development of a chimeric replicon system for phenotypic analysis of NS3 protease sequences from HCV clinical isolates. *Antivir. Ther.* 16, 705–718. doi: 10.3851/IMP1825

Singh, D., Soni, S., Khan, S., Sarangi, A. N., Yennamalli, R. M., Aggarwal, R., et al. (2020). Genome-wide mutagenesis of hepatitis C virus reveals ability of genome to overcome detrimental mutations. *J. Virol.* 94, 1–21. doi: 10.1128/JVI.01327-19

Sir, D., Kuo, C., Tian, Y., Liu, H. M., Huang, E. J., Jung, J. U., et al. (2012). Replication of hepatitis C virus RNA on autophagosomal membranes. *J. Biol. Chem.* 287, 18036–18043. doi: 10.1074/jbc.M111.320085

Smith, D., Magri, A., Bonsall, D., Ip, C. L. C., Trebes, A., Brown, A., et al. (2019). Resistance analysis of genotype 3 hepatitis C virus indicates subtypes inherently resistant to nonstructural protein 5A inhibitors. *Hepatology* 69, 1861–1872. doi: 10.1002/hep.29837

Stanaway, J. D., Flaxman, A. D., Naghavi, M., Fitzmaurice, C., Vos, T., Abubakar, I., et al. (2016). The global burden of viral hepatitis from 1990 to 2013: findings from the global burden of disease study. *Lancet* 388, 1081–1088. doi: 10.1016/S0140-6736(16)30579-7

Summa, V., Ludmerer, S. W., McCauley, J. A., Fandozzi, C., Burlein, C., Claudio, G., et al. (2012). MK-5172, a selective inhibitor of hepatitis C virus NS3/4A protease with broad activity across genotypes and resistant variants. *Antimicrob. Agents Chemother.* 56, 4161–4167. doi: 10.1128/AAC.00324-12

Tanji, Y., Kaneko, T., Satoh, S., and Shimotohno, K. (1995). Phosphorylation of hepatitis C virus-encoded nonstructural protein NS5A. *J. Virol.* 69, 3980–3986. doi: 10.1128/jvi.69.7.3980-3986.1995

Taylor, J. G., Zipfel, S., Ramey, K., Vivian, R., Schrier, A., Karki, K. K., et al. (2019). Discovery of the pan-genotypic hepatitis C virus NS3/4A protease inhibitor voxilaprevir (GS-9857): a component of Vosevi®. *Bioorg. Med. Chem. Lett.* 29, 2428–2436. doi: 10.1016/j.bmcl.2019.03.037

Tomei, L., Failla, C., Santolini, E., De Francesco, R., and La Monica, N. (1993). NS3 is a serine protease required for processing of hepatitis C virus polyprotein. *J. Virol.* 67, 4017–4026. doi: 10.1128/JVI.67.7.4017-4026.1993

Tong, L., Yu, W., Chen, L., Selyutin, O., Dwyer, M. P., Nair, A. G., et al. (2017). Discovery of ruzasvir (MK-8408): A potent, pan-genotype HCV NS5A inhibitor with optimized activity against common resistance-associated polymorphisms. *J. Med. Chem.* 60, 290–306. doi: 10.1021/acs.jmedchem.6b01310

Vrolijk, J. M., Kaul, A., Hansen, B. E., Lohmann, V., Haagmans, B. L., Schalm, S. W., et al. (2003). A replicon-based bioassay for the measurement of interferons in patients with chronic hepatitis C. *J. Virol. Methods* 110, 201–209. doi: 10.1016/S0166-0934(03)00134-4

Wakita, T., Pietschmann, T., Kato, T., Date, T., Miyamoto, M., Zhao, Z., et al. (2005). Production of infectious hepatitis C virus in tissue culture from a cloned viral genome. *Nat. Med.* 11, 791–796. doi: 10.1038/nm1268

Wendt, A., and Bourlière, M. (2013). An update on the treatment of genotype-1 chronic hepatitis C infection: lessons from recent clinical trials. *Ther. Adv. Infect. Dis.* 1, 191–208. doi: 10.1177/2049936113502647

Wing, P. A. C., Jones, M., Cheung, M., DaSilva, S., Bamford, C., Jason Lee, W.-Y., et al. (2019). Amino acid substitutions in genotype 3a hepatitis c virus polymerase protein affect responses to sofosbuvir. *Gastroenterology* 157, 692–704.e9. doi: 10.1053/j.gastro.2019.05.007

World Health Organization (2017). *Global Hepatitis Report 2017*. Geneva: World Health Organization.

Wose Kinge, C. N., Espiritu, C., Prabdial-Sing, N., Sithebe, N. P., Saeed, M., and Rice, C. M. (2014). Hepatitis C Virus Genotype 5a subgenomic replicons for evaluation of direct-acting antiviral agents. *Antimicrob. Agents Chemother.* 58, 5386–5394. doi: 10.1128/AAC.03534-14

Wyles, D., Dvory-Sobol, H., Svarovskaia, E. S., Doehle, B. P., Martin, R., Afdhal, N. H., et al. (2017). Post-treatment resistance analysis of hepatitis C virus from phase II and III clinical trials of ledipasvir/sofosbuvir. *J. Hepatol.* 66, 703–710. doi: 10.1016/j.jhep.2016.11.022

Wyles, D. L., and Luetkemeyer, A. F. (2017). Understanding hepatitis C virus drug resistance: clinical implications for current and future regimens. *Top. Antivir. Med.* 25, 103–109.

Yang, H., Robinson, M., Corsa, A. C., Peng, B., Cheng, G., Tian, Y., et al. (2014). Preclinical characterization of the novel hepatitis C virus NS3 protease inhibitor GS-9451. *Antimicrob. Agents Chemother.* 58, 647–653. doi: 10.1128/AAC.00487-13

Yi, M., and Lemon, S. M. (2004). Adaptive mutations producing efficient replication of genotype 1a hepatitis C virus RNA in normal huh7 cells. *J. Virol.* 78, 7904–7915. doi: 10.1128/JVI.78.15.7904-7915.2004

Yi, M., Villanueva, R. A., Thomas, D. L., Wakita, T., and Lemon, S. M. (2006). Production of infectious genotype 1a hepatitis C virus (Hutchinson strain) in cultured human hepatoma cells. *Proc. Natl. Acad. Sci. U.S.A.* 103, 2310–2315. doi: 10.1073/pnas.0510727103

Yu, M., Peng, B., Chan, K., Gong, R., Yang, H., Delaney, W., et al. (2014). Robust and persistent replication of the genotype 6a hepatitis C virus replicon in cell culture. *Antimicrob. Agents Chemother.* 58, 2638–2646. doi: 10.1128/AAC.01780-13

Zeuzem, S., Foster, G. R., Wang, S., Asatryan, A., Gane, E., Feld, J. J., et al. (2018). Glecaprevir–pibrentasvir for 8 or 12 weeks in HCV genotype 1 or 3 infection. *N. Engl. J. Med*. 378, 354–369. doi: 10.1056/NEJMoa1702417

Zeuzem, S., Mizokami, M., Pianko, S., Mangia, A., Han, K. H., Martin, R., et al. (2017). NS5A resistance-associated substitutions in patients with genotype 1 hepatitis C virus: prevalence and effect on treatment outcome. *J. Hepatol*. 66, 910–918. doi: 10.1016/j.jhep.2017.01.007

Conflict of Interest: The authors declare that the research was conducted in the absence of any commercial or financial relationships that could be construed as a potential conflict of interest.

frontiers in Cellular and Infection Microbiology

REVIEW
published: 11 August 2020
doi: 10.3389/fcimb.2020.00341

Role of Microbiota in Pathogenesis and Management of Viral Hepatitis

*Rashi Sehgal, Onkar Bedi and Nirupma Trehanpati**

Department of Molecular and Cellular Medicine, Institute of Liver and Biliary Sciences, New Delhi, India

Hepatitis is a condition that can be self-limiting or can progress to fibrosis (scarring), cirrhosis, or liver cancer. These days, gut microbiota becomes an important part of our immune system, which is important for disease progression or recovery. Translocation of gut microbial and metabolic products causes intestinal inflammation by modulating immune cells leading to impairment of the primary barrier. But there are limited studies discussing pathogenesis and management of hepatitis with gut microbiota. In this review, we have discussed the role of gut microbiota in pathogenesis and management of various hepatitis, especially hepatitis B and C. We have discussed the role of bacterial products, LPS-TLR4 pathway, and unmethylated CpG DNA, which ultimately affects downstream NF-kB signaling in hepatitis. Finally, we have discussed the role of fecal microbiota transplantation in the management of hepatitis.

Keywords: hepatitis, fecal microbiota transplantation, gut microbiota, lipopolysaccharides (LPS), probiotic, bacteria

OPEN ACCESS

Edited by:
Milan Surjit,
Translational Health Science and Technology Institute (THSTI), India

Reviewed by:
Jawed Iqbal,
Jamia Millia Islamia, India
Binod Kumar,
Loyola University Chicago, United States

****Correspondence:***
Nirupma Trehanpati
trehanpati@gmail.com

Specialty section:
This article was submitted to Virus and Host, a section of the journal Frontiers in Cellular and Infection Microbiology

Received: *12 March 2020*
Accepted: *04 June 2020*
Published: *11 August 2020*

Citation:
Sehgal R, Bedi O and Trehanpati N (2020) Role of Microbiota in Pathogenesis and Management of Viral Hepatitis. Front. Cell. Infect. Microbiol. 10:341. doi: 10.3389/fcimb.2020.00341

INTRODUCTION

Hepatitis is generally known as an inflammation of the liver that can be caused by hepatic and non-hepatic viruses, can be caused by alcohol, can be drug induced, and can be caused by autoimmunity. Gut microbiota composition is known to be associated with disease pathogenesis. However, dynamic alteration of the gut microbiota in disease pathogenesis is not well-understood.

Microbiota involves communities of commensal, symbiotic, as well as pathogenic microorganisms found in organisms, i.e., plants and animals. Microbiota of a healthy individual shows more of commensalism or symbiosis without causing any disease. These microbes mainly colonize humans during birth or shortly thereafter and remain throughout the course of life. These can be found in many areas like skin, respiratory tract, urinary tract, and digestive tract, while brain, lungs, and the circulatory system are free of microbes. Approximately 10^{14} microbes are present in a healthy individual gut (Minemura and Shimizu, 2015). Therefore, gut microbiota has an important role to modulate the immune system in disease progression or recovery.

Translocation of microbes or their metabolic products cause intestinal inflammation leading to impairment of the primary barrier (Hill et al., 2010). There is limited available information regarding the role of gut microbiota in hepatitis, which makes it important to majorly focus on clinical data of gut microbiota linked with hepatitis B and C virus.

GUT MICROBIOTA

Gut or gastrointestinal tract starts from the mouth and ends at the back passage (anus). Gut helps in the digestion of food by absorbing energy and nutrients. Majority of gut microbiota (80 to 85%) contains good bacteria, and only 15 to 20% are harmful bacteria in different parts of the intestine

(Bajaj et al., 2014). In mouth and upper respiratory tract, normal flora is more of **the** commensal bacteria like *Streptococcus*, *Moraxella*, *Neisseria*, and *Haemophilus*. Very few species of bacteria are present in the stomach and small intestine, while the large intestine and colon contain dense population of microbes, i.e., up to 10^{12} cells/g. Along with bacteria, many other microorganisms like fungi, protists, archaea, and viruses also symbiotically harbor in the gut.

There are four dominant phyla of bacteria present in the gut, and they are *Firmicutes*, Bacteroidetes, *Actinobacteria*, and Proteobacteria (Khanna and Tosh, 2014). Most important genera in which bacteria belong are *Bacteroides, Clostridium, Faecalibacterium, Eubacterium, Ruminococcus*, *Peptococcus*, *Peptostreptococcus*, and *Bifidobacterium* (Fernández et al., 2018). Some of the fungal species that also coexist in the gut are *Candida*, *Saccharomyces*, *Aspergillus*, *Penicillium*, *Rhodotorula*, *Trametes*, *Pleospora*, *Sclerotinia*, *Bullera*, and *Galactomyces*, among others (Raimondi et al., 2019).

Functions of Gut Microbiota

Gut microbiota plays an important but diverse role such as barrier effect, vitamin synthesis, and fermentation. Resident bacteria of the gut acts as a barrier and protect the intestinal mucosa from invasion of the other potential pathogens (Hooper et al., 1999). Many factors including diet, age, medication, illness, stress, and lifestyle influence the gut microbiota, which have a great impact on disease pathogenesis. In fact, many bacteria, i.e., *Bacteroides*, *Eubacterium*, *Propionibacterium*, and *Fusobacterium*, are instrumental in the synthesis of vitamins K and B (i.e., folate, B12, and biotin) (Canny and McCormick, 2008). They are also involved in the fermentation of non-digestible carbohydrates for the production of short-chain fatty acids (SCFAs), which are helpful in maintaining metabolic homeostasis. In addition to the production of SCFA, glycolysis and pentose phosphate pathway also produce butyrate, which promotes the growth of *Lactobacilli* and *Bifidobacteria* bacteria in the colon (Venegas et al., 2019). Various studies supported the fact that nutrients derived from microbiota play a pivotal role in the normal functioning of the hepatic system (Li et al., 2012; Zheng et al., 2013; Moratalla et al., 2014; Jiminez et al., 2016; Cremer et al., 2017; Wang et al., 2017a).

Gut Microbiota in Liver Diseases

Commensal bacteria play a decisive role in maintaining immune homeostasis (**Figure 1**) and also guard immune reactions at mucosal surfaces (Ichinohe et al., 2011). Intestinal microflora is a dynamic and complex ecosystem, which helps in proliferation, growth, and differentiation of epithelial cells to fight infections and improve immunity. Despite its crucial role in the synthesis of vitamin K, folate, SCFA, and peroxides, gut microbiota acts as a chief environmental as well as etiological factor for the progression of many liver diseases (O'Hara and Shanahan, 2007). Particularly, gut microbiota has a larger influence on alcoholic liver disease, non-alcoholic fatty liver disease, viral hepatitis (hepatitis B and C), autoimmune hepatitis (AIH), primary sclerosing cholangitis (PSC), and primary biliary cholangitis (PBC) (Mohamadkhani, 2018). *Lactobacillus, Bifidobacterium, Saccharomyces boulardii,* and *Lactobacillus plantarum* play a bigger role in the management of various metabolic disorders and hepatitis (Mohamadkhani, 2018).

Several pathogens, including viruses and intestinal microorganisms, use mucous membranes as a doorway (Karst, 2016). Hepatic viruses breach the intestinal permeability leading to gut dysbiosis and release pro-inflammatory cytokines instrumental in developing liver cirrhosis and HCC. It is also observed that the use of probiotics reduces the tolerogenic response and enhances the mucosal defense against viral pathogens (Rigo-Adrover M del et al., 2018). *Lactobacillus* alone can influence the production of interferon by modulating the antiviral effects of vitamin A (Lee and Ko, 2016). The mixture of various probiotics and *Bifidobacterium* with galacto-oligosaccharides and fructo-oligosaccharides has a defensive effect against *Rotavirus* infection by aggregating the production of TNF-α, IL-4, IFN-γ, and TLR2 expression (Rigo-Adrover M del et al., 2018). In most of the liver disease, especially cirrhosis, dysbiosis of the gut increases Proteobacteria, *Enterobacteriaceae*, and *Veillonellaceae*, while it decreases Bacteroidetes and *Lachnospiraceae* (Sanduzzi Zamparelli et al., 2017). Recently, the cirrhosis dysbiosis ratio (CDR) is coined for defining the changes in gut microbiome in cirrhosis patients with beneficial *Lachnospiraceae* and *Ruminococcaceae* and harmful *Enterobacteriaceae* bacteria (Bajaj et al., 2014). Other groups have also associated patients with severe cirrhosis and hepatic encephalopathy with overgrowth of *Enterobacteriaceae* bacteria (Chen et al., 2011).

ROLE OF GUT MICROBIOTA IN HEPATIC VIRAL INFECTIONS

Acute viral hepatitis due to hepatitis A and E viral infections is a major community health problem especially in developing countries. Hepatitis A and E cause acute infection which could be short-lived and self-clearing unless the subjects are immunocompromised or in transplant settings. Acute hepatitis E infection also becomes detrimental and life-threatening during pregnancy, affecting both the mother and the child.

Both hepatitis A and E are RNA viruses that transmit through oral fecal routes (Lemon et al., 2018) and may have devastating effects on intestinal microflora. It was observed that administration of the healthy probiotic bacterium like *Enterococcus faecium* NCIMB 10415 affects the reduction as well as the removal of enteric HEV viruses in pigs (Kreuzer et al., 2012). However, there is lack of relevant data in humans.

As per the World Health Organization (WHO), hepatitis B virus (HBV) infection caused 887,000 deaths in 2015 and 4.5 million (16.7%) diagnosed with chronic infection in 2016. Similarly, hepatitis C virus (HCV) caused 399,000 deaths with an estimated 71 million diagnosed with chronic infection in 2016. Both these viruses cause chronic infections at 10% in HBV and more than 30% in HCV leading to cirrhosis and hepatocellular carcinoma. Hepatic viruses have evolved mechanisms to avoid their detection from the host innate and adaptive immunity

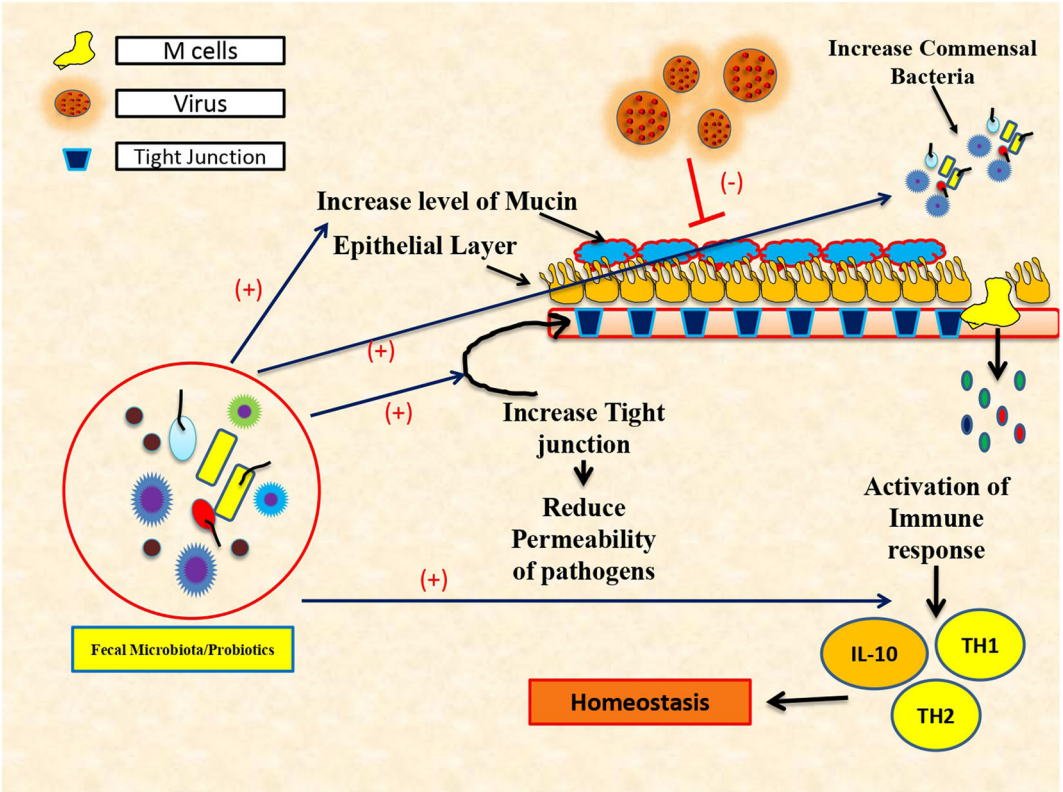

FIGURE 1 | Protective role of fecal microbiota transplantation and use of probiotics in immune restoration.

and characterized as viral escape (Visvanathan et al., 2007). It is observed that chronic hepatitis patients have larger translocation of the intestinal microbiota (Lu et al., 2011; Li et al., 2018).

Bacterial translocation cause intestinal inflammation via dysregulation of immune cell, overgrowth of pathogenic bacteria, as well as dysfunction of the primary barrier (Hill et al., 2010). Xu et al. (2015) also supported the fact that intestinal flora loses homeostasis during dysbiosis, which in fact helps the advancement of hepatitis viral infection (Xu et al., 2015).

Therefore, it is now understood that during chronicity, commensal microbiota have greater impact not only on viral host cell interaction but also on viral replication.

In viral hepatitis, few harmful bacteria like *Escherichia coli*, *Enterobacteriaceae, Enterococcus faecalis*, *and Faecalibacterium prausnitzii* directly alter the profile of good intestinal microbiota with a lower number of intestinal lactic acid species such as *Lactobacillus, Pediococcus, Weissella*, and *Leuconostoc* (Bajaj et al., 2014; Chen et al., 2016). Some of the bacterial species, i.e., *Neisseria, E. coli*, *Enterobacteriaceae, E. faecalis, F. prausnitzii*, and *Gemella*, are also found responsible for the progression of hepatitis B and C virus–related cirrhosis and primary biliary cirrhosis (Chen et al., 2016; Mohamadkhani, 2018). *Candida* is also frequently found in patients with hepatitis B–related cirrhosis (Cui et al., 2013).

Role of Gut Microbiota in Hepatitis B Viral Infection

Dysbiosis of gut microbiota in chronic hepatitis B infection affects disease pathogenesis and causes liver failure in a large proportion. LPS (lipopolysaccharides) from the outer membrane of gram-negative bacteria help in the activation of innate immune response by recognizing TLRs, especially TLR2 and 4. HBV infection leads to progressive decline in butyrate-producing bacteria. However, LPS-producing genera is enriched in HBV infection. In HBV infection, a beneficial bacterium, *Lachnospiraceae*, plays a role in the management of HBV infection via reduction in LPS section and bacterial translocation (Chen et al., 2011; Ren et al., 2019). Studies have shown the role of Faecalibacterium, *Pseudobutyrivibrio, Lachnoclostridium, Ruminoclostridium, Prevotella, Alloprevotella*, and *Phascolarctobacterium* in potential anti-inflammatory SCFA activity, which increases the abundance of butyrate compared to normal subjects (Liu et al., 2019). Lu et al. (2011) have demonstrated that copy numbers of *F. prausnitzii, E. faecalis, Enterobacteriaceae, Bifidobacteria*, and lactic acid bacteria (*Lactobacillus, Pediococcus, Leuconostoc*, and *Weissella*) have marked variation in the intestine of HBV cirrhotic patients. During HBV infection, dysbiosis in the oral microbiota was observed, and yellow tongue coating is suggestive of a reduction in Bacteroidetes but an increase

in Proteobacteria. Zhao et al. (2018) also suggested positive correlation of *Neisseriaceae* with the serum HBV-DNA.

Cirrhotic patients with HBV infection showed a significant decrease in the *Bifidobacteriaceae*/*Enterobacteriaceae* (B/E) ratio (Lu et al., 2011), while Yun et al. observed no difference in the B/E ratio in HBsAg+ with normal or high ALT and in non-cirrhotic HBV carriers (Yun et al., 2019). It means the B/E ratio is disturbed only in cirrhosis. However, other study observed that the *Megasphaera* genus from the Firmicutes phylum was abundant in the HBsAg+ high ALT group than the normal ALT. In patients with normal ALT, butyrate-producing bacteria like *Anaerostipes* are more in feces compared to HBsAg-ve (Yun et al., 2019). It is interesting to note that both *Megasphaera* and *Anaerostipes* produce SCFA as a by-product of lactate fermentation and butyrate. However, butyrate is known as anticarcinogenic and anti-inflammatory, and plays a role in oxidative stress (Hamer et al., 2008). Another study suggests that chronic hepatitis B infected cirrhotic patients exhibit a decrease in *Bifidobacteria* and *Lactobacillus* levels, while significantly increasing *Enterococcus* and *Enterobacteriaceae* levels compared to healthy individuals.

Bacterial translocation is also observed in the development of hepatocellular carcinoma (HCC). Recently, Wang et al. have defined the serum zonulin as an intestinal permeability marker and showed its association with AFP levels in HBV-associated liver cirrhosis and HCC. They are helpful in correlating it with advanced stages of the diseases (Fasano, 2012).

The use of probiotic in HBV-infected patients showed benefit and suggested that probiotic VSL#3 plays an important role in the management of HBV viral infection (Dhiman et al., 2014).

Role of Gut Microbiota in Hepatitis C Viral Infection

Chronic hepatitis C infection is another leading cause of cirrhosis, HCC, and in some cases, liver failure and death. In majority, *Enterobacteriaceae* and *Bacterioidetes* increased in chronic HCV patients, but *Firmicutes* found to be decreased. HCV infection cause marked elevation in LPS, which is suggestive of microbial translocation and inflammation during disease progression (Dolganiuc et al., 2007; Inoue et al., 2018). On the other hand, it was observed that antiviral treatment of HCV with ribavirin (RBV) and immune modulator pegylated interferon (PEG-IFN) has no direct impact on gut dysbiosis. In fact, it increases the production of bile acids, which is important for gut microbiota (Ponziani et al., 2018). Some pathogenic bacteria such as *Enterobacteriaceae*, *Staphylococcus*, and *Enterococcus* decreased the bile acid in HCV-infected cirrhotic patients, which normalized after a direct-acting antiviral treatment. Oral direct-acting antivirals (DAAs) were also found to be helpful in improving gut especially *Lachnospira* and *Dorea* genera, and restored TNFα levels (Pérez-Matute et al., 2019,?).

But after DAA treatment, expression of calprotectin, ZO1, and LPS was found more in HCV patients with cirrhosis. It was also suggested that during HCV infection, *L. acidophilus* and *Bifidobacterium* spp. can act as a supportive supplement with antiviral and antibacterial activities (Dore et al., 2014). Immune response in HCV patients can be stimulated by useful microbiota via activation of CD3+ cells and CD56+ NK cell counts, which were explained by Doskali et al. (2011) and further suggested that good flora increases the cytotoxic effects of NK cells against viral infected cells inhibiting the replication of HCV. Use of probiotics in HCV-infected patients with cirrhosis was significantly beneficial (Preveden et al., 2017).

Another hepatic virus, hepatitis D virus, is a new player and not much is known about it yet. It was also suggested that endotoxemia in HCV and HDV patients seems to be multifactorial, likely depending on impaired phagocytic functions and reduced T-cell-mediated antibacterial activity (Kefalakes and Rehermann, 2019).

MICROBIOTA MODULATES MOLECULAR SIGNALING IN HEPATITIS

LPS is the key component of gram-negative bacteria, i.e., *Enterobacteriaceae*. The active receptor for LPS is CD14/TLR4/MD2 receptor complex on induction, which secretes many pro-inflammatory cytokines including tumor necrosis factor-α, IL-1, IL-6, and chemokines through the NF-κB signaling (Fooladi et al., 2010; Seki and Schnabl, 2012; Bryant et al., 2015) to cause liver injury. In the intestinal tract, LPS downregulates the expression of various tight junction proteins (ZO-1 and closed protein) by increasing the permeability of the intestinal mucosa and enters the blood flow through the portal venous system (Park et al., 2010). In liver, Kupffer cells as specialized macrophages are induced by the LPS-TLR4 pathway for the release of immunosuppressive mediators, such as IL-10, which in turn suppress the release of inflammatory mediators by Kupffer cells (Dixon et al., 2013). In this way, during viral hepatitis, virus specific immune responses are suppressed and ultimately inhibit efficient clearing of bacteria as well as viruses.

In addition to LPS, unmethylated CpG DNA, bacterial DNA/RNA bacterial cell wall also contains teichoic acid, peptidoglycan, and specialized proteins (flagellin). Bacterial DNA/RNA is recognized by TLRs as well as all components of cell-wall-like teichoic acid and peptidoglycan also recognized by TLR2, while TLR5 got activated by flagellin. dsRNA bacteria are recognized by TLR3. ssRNA activates receptors of both TLR7 and TLR8. All these TLRs ultimately stimulate the JAK-STAT pathway. Hepatitis viruses are also recognized by TLRs in the liver or in the intestine and activate downstream signaling pathways (Mencin et al., 2009).

Unmethylated CpG DNAs are found abundantly in the *Lactobacillus* family, i.e., *L. casei, L. plantarum, L. rhamnosus*, and others like *Bifidobacteria,* Proteobacteria, and Bacteroidetes in the intestinal flora of animals. Unmethylated CpG DNA is sensed by TLR9, expressed on various mononuclear cells, and stimulates both innate immune response as well as adaptive immune response (Krieg, 2006; Kauppila et al., 2013). Activation the of CpG-TLR9 pathway stimulates downstream molecules of MyD88 such as IRAK4, TRAF6, and IRAK1, ultimately triggering NF-κB and MAPK signaling pathways. These downstream pathways help in the activation of DCs for the secretion of cytokines and

TABLE 1 | Randomized FMT clinical trials for the treatment of chronic hepatitis B infection.

S.No	Study title	Study type	No. of subjects	Intervention/ Treatment	Status	Phase	Primary outcome measures	Secondary outcome measures	ClinicalTrials.gov Identifier:
1.	Randomized Controlled Trial Comparing the Efficacy and Safety of FMT in Hepatitis B Reactivation Leads to Acute on Chronic Liver Failure. **Location:** Institute of liver and Biliary Sciences New Delhi, Delhi, India	Interventional (Clinical Trial)	64	Drug: Tenofovir Drug: Fecal Microbiota Transplantation (FMT)	Completed	Completed	Transplant free survival. [Time Frame: 3 months]	Reduction in Hepatitis B Virus DNA level $\geq$ 2 log. [Time Frame: 2 weeks] Improvement in MELD (Model for End Stage Liver Disease) score. [Time Frame: 2 weeks]	NCT02689245
2.	Study on Effect of Intestinal Microbiota Transplantation in Chronic Hepatitis B **Location:** Zhongshan Hospital Affiliated to Xiamen University Xiamen, Fujian, China	Interventional (Clinical Trial)	60	Other: intestinal microbiota transplant Drug: Antiviral Agents	Recruiting	N.A.	Change of serum hepatitis B virus e antigen(HBeAg) level [Time Frame: 1, 3, 6 months] Serum hepatitis B virus e antigen(HBeAg) levels is measured in S/CO	Change of serum hepatitis B virus surface antigen(HBsAg) level [Time Frame: 1, 3, 6 months] Serum hepatitis B virus surface antigen(HBsAg) levels is measured in IU/mL. Change of serum anti-hepatitis B virus e antigen(anti-HBe) [Time Frame: 1, 3, 6 months] Appearance of serum anti-hepatitis B virus e antigen(anti-HBe) suggest the ability of body to resistant HBV. Change of serum anti-hepatitis B virus surface antigen(anti-HBs) [Time Frame: 1, 3, 6 months] Appearance of serum anti-hepatitis B virus surface antigen(anti-HBs) suggest the ability of body to resistant HBV. Changes of gut **microbiota** [Time Frame: 1, 3, 6 months] Alpha and Beta diversity of GI **microbiota** by High-throughput sequencing (16S rRNA) on baseline line and 1, 3, 6 months after treatment Relief of constipation [Time Frame: 1, 3, 6 months]; Relief of diarrhea [Time Frame: 1, 3, 6 months]; Relief of abdominal pain [Time Frame: 1, 3, 6 months] The onset and duration of constipation will be assessed by "Evaluation Score Table of Gastrointestinal Symptoms."	NCT03429439

chemokines (Krieg, 2006; Kauppila et al., 2013). Chronic HBV patients have reduced *Lactobacillus* and *Bifidobacteria*. Both are rich in unmethylated CpG DNA levels, ultimately affecting the CpG DNA-TLR9 pathway and immune response on HBV (Lin and Zhang, 2017).

ROLE OF FECAL MICROBIAL TRANSPLANTATION (FMT) IN VIRAL HEPATITIS

FMT mainly involves the insertion of healthy microbiota in the diseased gut. In brief, fecal matter derived from a healthy family member of the patient receiving the same diet as the patient is processed and introduced in the intestinal tract of the patient. These have minimal side effects and proved helpful in reinstating healthy gut flora in the patient. FMT administration can be done using several routes such as oral, nasogastric, nasoduodenal, nasojejunal, endoscopic, rectal, and colonoscopic or midgut transendoscopic enteral tubing (Cui et al., 2015; Tang et al., 2017). For cirrhotic patients with dysbiosis, small bowel route is most affected, while mostly used route is oral delivery. In severe alcoholic hepatitis (SAH), in comparison to steroids, FMT is associated with decreased disease severity and improved survival. Earlier, Wang et al. (2017b) have observed that FMT restored the cognitive function, liver function indexes, and TLR response in carbon tetrachloride (CCl_4)-induced acute hepatitis in rats.

Woodhouse et al. have observed in a PROFIT clinical trial the benefits of fecal microbiota transplantation in the small bowel of cirrhotic patients (Woodhouse et al., 2019). Meiglani et al. (2020) also observed that cirrhotic patients with antibiotic-resistant *Clostridioides difficile* infection (CDI) responded well after FMT treatment. In fact, fecal microbiota of alcohol-resistant mice when given to alcohol-sensitive mice has reduced Bacteroidetes and increased *Actinobacteria* as well as *Firmicutes* and protected steatosis development (Ferrere et al., 2017). Limited studies are published yet on FMT administration in alcohol-related liver disease. However, all these studies showed immense benefit of FMT. Bajaj et al. (2017) observed the recovery of cognitive function and hepatic encephalopathy in patients under clinical trial after administration of FMT. Studies recently published from our center have found better efficiency of FMT in severe alcoholic patients than standard medical treatment (Sarin et al., 2019). There are only a couple of randomized FMT clinical trials for chronic hepatitis B infected patients (**Table 1**).

Recently, groups have addressed how FMT is modulating immunity in gut and liver. Mucosa-associated invariant T (MAIT) cells are found abundant in liver (20% to 50% of intrahepatic T cells), gut, peripheral blood, as well as lungs. Gao et al. have observed that functional MAIT cells were altered in SAH resulting in more bacterial infection in patients. Alteration in circulating MAIT cells is observed with defective antibacterial cytokine/cytotoxic response against the infection (Gao et al., 2018). They believe that FMT administration has a profound effect on the expression of MAIT cells in alcohol-related diseases.

SUMMARY AND CONCLUSION

Gut microbiota has an important role in viral, alcoholic, and metabolic liver diseases. Gut microbiota plays a crucial role in modulating the toll-like receptors, NF-κB signaling, janus kinase/signal transducer and transcription (JAK/STAT) pathway, and CD4+T cell activation. Numerous useful microbiotas like *Ruminoclostridium, Faecalibacterium, Lachnoclostridium, Prevotella, Alloprevotella, Pseudobutyrivibrio, and Phascolarctobacterium* play an important role in potentiating anti-inflammatory short chain fatty acid (SCFA) activity and increased the butyrate abundance, which play a crucial role in the management of various hepatitis-related viral infections. Fecal microbiota transplantation became an attractive and safest mode of treatment for the management of various liver diseases especially in severe alcoholic hepatitis. Despite recent publications, there are still gaps in understanding the role of microbiota in viral hepatitis especially in acute HAV and HEV viral infections. Therefore, there is a need to explore more in these infections.

AUTHOR CONTRIBUTIONS

RS and OB written the review article. NT provide valuable suggestions, corrected, and revised. All authors contributed to the article and approved the submitted version.

REFERENCES

Bajaj, J. S., Heuman, D. M., Hylemon, P. B., Sanyal, A. J., White, M. B., Monteith, P., et al. (2014). The cirrhosis dysbiosis ratio defines changes in the gut microbiome associated with cirrhosis and its complications. *J. Hepatol.* 60, 940–947. doi: 10.1016/j.jhep.2013.12.019

Bajaj, J. S., Kassam, Z., Fagan, A., Gavis, E. A., Liu, E., Cox, I. J., et al. (2017). Fecal microbiota transplant from a rational stool donor improves hepatic encephalopathy: a randomized clinical trial. *Hepatology* 66, 1727–1738. doi: 10.1002/hep.29306

Bryant, C. E., Symmons, M., and Gay, N. J. (2015). Toll-like receptor signalling through macromolecular protein complexes. *Mol. Immunol.* 63, 162–165. doi: 10.1016/j.molimm.2014.06.033

Canny, G. O., and McCormick, B. A. (2008). Bacteria in the intestine, helpful residents or enemies from within? Infection and immunity. *Am. Soc. Microbiol.* 76, 3360–3373. doi: 10.1128/IAI.00187-08

Chen, Y., Ji, F., Guo, J., Shi, D., Fang, D., and Li, L. (2016). Dysbiosis of small intestinal microbiota in liver cirrhosis and its association with etiology. *Sci. Rep.* 6:34055. doi: 10.1038/srep34055

Chen, Y., Yang, F., Lu, H., Wang, B., Chen, Y., Lei, D., et al. (2011). Characterization of fecal microbial communities in patients with liver cirrhosis. *Hepatology* 54, 562–572. doi: 10.1002/hep.24423

Cremer, J., Arnoldini, M., and Hwa, T. (2017). Effect of water flow and chemical environment on microbiota growth and composition in the human colon. *Proc. Natl. Acad. Sci. U.S.A.* 114, 6438–6443. doi: 10.1073/pnas.1619598114

Cui, B., Feng, Q., Wang, H., Wang, M., Peng, Z., Li, P., et al. (2015). Fecal microbiota transplantation through mid-gut for refractory C rohn's disease:

safety, feasibility, and efficacy trial results. *J. Gastroenterol. Hepatol.* 30, 51–58. doi: 10.1111/jgh.12727

Cui, L., Morris, A., and Ghedin, E. (2013). The human mycobiome in health and disease. *Genome Med*. 5:63. doi: 10.1186/gm467

Dhiman, R. K., Rana, B., Agrawal, S., Garg, A., Chopra, M., Thumburu, K. K., et al. (2014). Probiotic VSL\# 3 reduces liver disease severity and hospitalization in patients with cirrhosis: a randomized, controlled trial. *Gastroenterology* 147, 1327–1337. doi: 10.1053/j.gastro.2014.08.031

Dixon, L. J., Barnes, M., Tang, H., Pritchard, M. T., and Nagy, L. E. (2013). Kupffer cells in the liver. *Compr. Physiol*. 3, 785–797. doi: 10.1002/cphy.c120026

Dolganiuc, A., Norkina, O., Kodys, K., Catalano, D., Bakis, G., Marshall, C., et al. (2007). Viral and host factors induce macrophage activation and loss of toll-like receptor tolerance in chronic HCV infection. *Gastroenterology* 133, 1627–1636. doi: 10.1053/j.gastro.2007.08.003

Dore, G., Ward, J., and Thursz, M. (2014). Hepatitis C disease burden and strategies to manage the burden (Guest Editors Mark Thursz, Gregory Dore and John Ward). *J. Viral. Hepat*. 21(Suppl. 1), 1–4. doi: 10.1111/jvh.12253

Doskali, M., Tanaka, Y., Ohira, M., Ishiyama, K., Tashiro, H., Chayama, K., et al. (2011). Possibility of adoptive immunotherapy with peripheral blood-derived $CD3^{-}CD56^{+}$ and $CD3^{+}CD56^{+}$ cells for inducing anti-hepatocellular carcinoma and anti-hepatitis C virus activity. *J. Immunother*. 34, 129–138. doi: 10.1097/CJI.0b013e3182048c4e

Fasano, A. (2012). Intestinal permeability and its regulation by zonulin: diagnostic and therapeutic implications. *Clin. Gastroenterol. Hepatol*. 10, 1096–1100. doi: 10.1016/j.cgh.2012.08.012

Fernández, M. F., Reina-Pérez, I., Astorga, J. M., Rodriguez-Carrillo, A., Plaza-Diaz, J., and Fontana, L. (2018). Breast cancer and its relationship with the microbiota. *Int. J. Environ. Res. Public Health* 15:1747. doi: 10.3390/ijerph15081747

Ferrere, G., Wrzosek, L., Cailleux, F., Turpin, W., Puchois, V., Spatz, M., et al. (2017). Fecal microbiota manipulation prevents dysbiosis and alcohol-induced liver injury in mice. *J. Hepatol*. 66, 806–815. doi: 10.1016/j.jhep.2016.11.008

Fooladi, A. I., Tavakoli, H., and Naderi, A. (2010). Detection of enterotoxigenic *Staphylococcus aureus* isolates in domestic dairy products. *Iran. J. Microbiol*. 2:137.

Gao, B., Ma, J., and Xiang, X. (2018). MAIT cells: a novel therapeutic target for alcoholic liver disease? *Gut* 67, 784–786. doi: 10.1136/gutjnl-2017-315284

Hamer, H. M., Jonkers, D., Venema, K., Vanhoutvin, S., Troost, F., and Brummer, R. J. (2008). The role of butyrate on colonic function. *Aliment. Pharmacol. Ther*. 27, 104–119. doi: 10.1111/j.1365-2036.2007.03562.x

Hill, D. A., Hoffmann, C., Abt, M. C., Du, Y., Kobuley, D., Kirn, T. J., et al. (2010). Metagenomic analyses reveal antibiotic-induced temporal and spatial changes in intestinal microbiota with associated alterations in immune cell homeostasis. *Mucosal. Immunol*. 3, 148–158. doi: 10.1038/mi.2009.132

Hooper, L. V., Xu, J., Falk, P. G., Midtvedt, T., and Gordon, J. I. (1999). A molecular sensor that allows a gut commensal to control its nutrient foundation in a competitive ecosystem. *Proc. Natl. Acad. Sci. U.S.A.* 96, 9833–9838. doi: 10.1073/pnas.96.17.9833

Ichinohe, T., Pang, I. K., Kumamoto, Y., Peaper, D. R., Ho, J. H., Murray, T. S., et al. (2011). Microbiota regulates immune defense against respiratory tract influenza a virus infection. *Proc. Natl. Acad. Sci. U.S.A.* 108, 5354–5359. doi: 10.1073/pnas.1019378108

Inoue, T., Nakayama, J., Moriya, K., Kawaratani, H., Momoda, R., Ito, K., et al. (2018). Gut dysbiosis associated with hepatitis C virus infection. *Clin. Infect. Dis.* 67, 869–877. doi: 10.1093/cid/ciy205

Jiminez, J. A., Uwiera, T. C., Abbott, D. W., Uwiera, R. R., and Inglis, G. D. (2016). Impacts of resistant starch and wheat bran consumption on enteric inflammation in relation to colonic bacterial community structures and short-chain fatty acid concentrations in mice. *Gut Pathog*. 8:67. doi: 10.1186/s13099-016-0149-6

Karst, S. M. (2016). The influence of commensal bacteria on infection with enteric viruses. *Nat. Rev. Microbiol*. 14:197. doi: 10.1038/nrmicro.2015.25

Kauppila, J. H., Karttunen, T. J., Saarnio, J., Nyberg, P., Salo, T., Graves, D. E., et al. (2013). Short DNA sequences and bacterial DNA induce esophageal, gastric, and colorectal cancer cell invasion. *APMIS* 121, 511–522. doi: 10.1111/apm.12016

Kefalakes, H., and Rehermann, B. (2019). Inflammation drives an altered phenotype of mucosal-associated invariant T cells in chronic hepatitis D virus infection. *J. Hepatol*. 71, 237–239. doi: 10.1016/j.jhep.2019.05.024

Khanna, S., and Tosh, P. K. (2014). A clinician's primer on the role of the microbiome in human health and disease. *Mayo Clin. Proc*. 89, 107–114. doi: 10.1016/j.mayocp.2013.10.011

Kreuzer, S., Machnowska, P., Aßmus, J., Sieber, M., Pieper, R., Schmidt, M. F., et al. (2012). Feeding of the probiotic bacterium *Enterococcus faecium* NCIMB 10415 differentially affects shedding of enteric viruses in pigs. *Vet. Res.* 43:58. doi: 10.1186/1297-9716-43-58

Krieg, A. M. (2006). Therapeutic potential of Toll-like receptor 9 activation. *Nat. Rev. Drug Discov*. 5, 471–484. doi: 10.1038/nrd2059

Lee, H., and Ko, G. (2016). Antiviral effect of vitamin A on norovirus infection via modulation of the gut microbiome. *Sci. Rep*. 6:25835. doi: 10.1038/srep25835

Lemon, S. M., Ott, J. J., van Damme, P., and Shouval, D. (2018). Type A viral hepatitis: a summary and update on the molecular virology, epidemiology, pathogenesis and prevention. *J. Hepatol*. 68, 167–184. doi: 10.1016/j.jhep.2017.08.034

Li, D., Yan, P., Abou-Samra, A. B., Chung, R., and Butt, A. (2018). Proton pump inhibitors are associated with accelerated development of cirrhosis, hepatic decompensation and hepatocellular carcinoma in noncirrhotic patients with chronic hepatitis C infection: results from ERCHIVES. *Aliment. Pharmacol. Ther*. 47, 246–258. doi: 10.1111/apt.14391

Li, H., Gao, Z., Zhang, J., Ye, X., Xu, A., Ye, J., et al. (2012). Sodium butyrate stimulates expression of fibroblast growth factor 21 in liver by inhibition of histone deacetylase 3. *Diabetes* 61, 797–806. doi: 10.2337/db11-0846

Lin, L., and Zhang, J. (2017). Role of intestinal microbiota and metabolites on gut homeostasis and human diseases. *BMC Immunol*. 18:12. doi: 10.1186/s12865-016-0187-3

Liu, Q., Li, F., Zhuang, Y., Xu, J., Wang, J., Mao, X., et al. (2019). Alteration in gut microbiota associated with hepatitis B and non-hepatitis virus related hepatocellular carcinoma. *Gut Pathog*. 11:11. doi: 10.1186/s13099-018-0281-6

Lu, H., Wu, Z., Xu, W., Yang, J., Chen, Y., and Li, L. (2011). Intestinal microbiota was assessed in cirrhotic patients with hepatitis B virus infection. *Microb. Ecol*. 61, 693–703. doi: 10.1007/s00248-010-9801-8

Meiglani, A., Alimirah, M., Ramesh, M., and Salgia, R. (2020). Fecal microbiota transplantation for Clostriodioides difficile infection in patients with chronic liver disease. *Int. J. Hepatol*. 2020:1874570. doi: 10.1155/2020/1874570

Mencin, A., Kluwe, J., and Schwabe, R. F. (2009). Toll-like receptors as targets in chronic liver diseases. *Gut* 58, 704–720. doi: 10.1136/gut.2008.156307

Minemura, M., and Shimizu, Y. (2015). Gut microbiota and liver diseases. *World J. Gastroenterol*. 21:1691. doi: 10.3748/wjg.v21.i6.1691

Mohamadkhani, A. (2018). On the potential role of intestinal microbial community in hepatocarcinogenesis in chronic hepatitis B. *Cancer Med*. 7, 3095–3100. doi: 10.1002/cam4.1550

Moratalla, A., Gómez-Hurtado, I., Santacruz, A., Moya, Á., Peiró, G., Zapater, P., et al. (2014). Protective effect of Bifidobacterium pseudocatenulatum CECT 7765 against induced bacterial antigen translocation in experimental cirrhosis. *Liver Int*. 34, 850–8. doi: 10.1111/liv.12380

O'Hara, A. M., and Shanahan, F. (2007). Gut microbiota: mining for therapeutic potential. *Clin. Gastroenterol. Hepatol*. 5, 274–284. doi: 10.1016/j.cgh.2006.12.009

Park, E. J., Thomson, A. B., and Clandinin, M. T. (2010). Protection of intestinal occludin tight junction protein by dietary gangliosides in lipopolysaccharide-induced acute inflammation. *J. Pediatr. Gastroenterol. Nutr*. 50, 321–328. doi: 10.1097/MPG.0b013e3181ae2ba0

Pérez-Matute, P., Íñiguez, M., Villanueva-Millán, M. J., Recio-Fernández, E., and Vázquez, A. M., Sánchez, S. C., et al. (2019). Short-term effects of direct-acting antiviral agents on inflammation and gut microbiota in hepatitis C-infected patients. *Eur. J. Inter. Med*. 67, 47–58. doi: 10.1016/j.ejim.2019.06.005

Ponziani, F. R., Putignani, L., Paroni Sterbini, F., Petito, V., Picca, A., Del Chierico, F., et al. (2018). Influence of hepatitis C virus eradication with direct-acting antivirals on the gut microbiota in patients with cirrhosis. *Aliment. Pharmacol. Ther*. 48, 1301–1311. doi: 10.1111/apt.15004

Preveden, T., Scarpellini, E., Milić N., Luzza, F., and Abenavoli, L. (2017). Gut microbiota changes and chronic hepatitis C virus infection. *Expert Rev. Gastroenterol. Hepatol*. 11, 813–819. doi: 10.1080/17474124.2017.1343663

Raimondi, S., Amaretti, A., Gozzoli, C., Simone, M., Righini, L., Candeliere, F., et al. (2019). Longitudinal survey of fungi in the human gut: ITS profiling, phenotyping and colonization. *Front. Microbiol.* 10:1575. doi: 10.3389/fmicb.2019.01575

Ren, Z., Li, A., Jiang, J., Zhou, L., Yu, Z., Lu, H., et al. (2019). Gut microbiome analysis as a tool towards targeted non-invasive biomarkers for early hepatocellular carcinoma. *Gut* 68, 1014–1023. doi: 10.1136/gutjnl-2017-315084

Rigo-Adrover M del, M., Van Limpt, K., Knipping, K., Garssen, J., Knol, J., Costabile, A., et al. (2018). Preventive effect of a synbiotic combination of galacto-and fructooligosaccharides mixture with Bifidobacterium breve M-16V in a model of multiple rotavirus infections. *Front. Immunol.* 9:1318. doi: 10.3389/fimmu.2018.01318

Sanduzzi Zamparelli, M., Rocco, A., Compare, D., and Nardone, G. (2017). The gut microbiota: A new potential driving force in liver cirrhosis and hepatocellular carcinoma. *United Eur. Gastroenterol. J.* 5, 944–953. doi: 10.1177/2050640617705576

Sarin, S. K., Pande, A., and Schnabl, B. (2019). Microbiome as a therapeutic target in alcohol-related liver disease. *J. Hepatol.* 70, 260–272. doi: 10.1016/j.jhep.2018.10.019

Seki, E., and Schnabl, B. (2012). Role of innate immunity and the microbiota in liver fibrosis: crosstalk between the liver and gut. *J. Physiol.* 590, 447–458. doi: 10.1113/jphysiol.2011.219691

Tang, G., Yin, W., and Liu, W. (2017). Is frozen fecal microbiota transplantation as effective as fresh fecal microbiota transplantation in patients with recurrent or refractory Clostridium difficile infection: a meta-analysis? *Diagn. Microbiol. Infect. Dis.* 88, 322–329. doi: 10.1016/j.diagmicrobio.2017.05.007

Venegas, D. P., Marjorie, K., Landskron, G., González, M. J., Quera, R., Dijkstra, G., et al. (2019). Short chain fatty acids (SCFAs)-mediated gut epithelial and immune regulation and its relevance for inflammatory bowel diseases. *Front. Immunol.* 10:277. doi: 10.3389/fimmu.2019.00277

Visvanathan, K., Skinner, N. A., Thompson, A. J., Riordan, S. M., Sozzi, V., Edwards, R., et al. (2007). Regulation of Toll-like receptor-2 expression in chronic hepatitis B by the precore protein. *Hepatology* 45, 102–110. doi: 10.1002/hep.21482

Wang, J., Wang, Y., Zhang, X., Liu, J., Zhang, Q., Zhao, Y., et al. (2017a). Gut microbial dysbiosis is associated with altered hepatic functions and serum metabolites in chronic hepatitis B patients. *Front. Microbiol.* 8:2222. doi: 10.3389/fmicb.2017.02222

Wang, W.-W., Zhang, Y., Huang, X.-B., You, N., Zheng, L., and Li, J. (2017b). Fecal microbiota transplantation prevents hepatic encephalopathy in rats with carbon tetrachloride-induced acute hepatic dysfunction. *World J. Gastroenterol.* 23:6983. doi: 10.3748/wjg.v23.i38.6983

Woodhouse, C. A., Patel, V. C., Goldenberg, S., Sanchez-Fueyo, A., China, L., O'Brien, A., et al. (2019). PROFIT, a prospective, randomised placebo controlled feasibility trial of faecal microbiota transplantation in cirrhosis: study protocol for a single-blinded trial. *BMJ Open* 9:e023518. doi: 10.1136/bmjopen-2018-023518

Xu, D., Huang, Y., and Wang, J. (2015). Gut microbiota modulate the immune effect against hepatitis B virus infection. *Eur. J. Clin. Microbiol. Infect. Dis.* 34, 2139–2147. doi: 10.1007/s10096-015-2464-0

Yun, Y., Chang, Y., Kim, H. N., Ryu, S., Kwon, M. J., Cho, Y. K., et al. (2019). Alterations of the gut microbiome in chronic hepatitis B virus infection associated with alanine aminotransferase level. *J. Clin. Med.* 8:173. doi: 10.3390/jcm8020173

Zhao, Y., Mao, Y. F., Tang, Y. S., Ni, M. Z., Liu, Q. H., Wang, Y., et al. (2018). Altered oral microbiota in chronic hepatitis B patients with different tongue coatings. *World J. Gastroenterol.* 24:3448. doi: 10.3748/wjg.v24.i30.3448

Zheng, X., Qiu, Y., Zhong, W., Baxter, S., Su, M., Li, Q., et al. (2013). A targeted metabolomic protocol for short-chain fatty acids and branched-chain amino acids. *Metabolomics* 9, 818–827. doi: 10.1007/s11306-013-0500-6

Conflict of Interest: The authors declare that the research was conducted in the absence of any commercial or financial relationships that could be construed as a potential conflict of interest.

Advantages of publishing in Frontiers

OPEN ACCESS
Articles are free to read for greatest visibility and readership

FAST PUBLICATION
Around 90 days from submission to decision

HIGH QUALITY PEER-REVIEW
Rigorous, collaborative, and constructive peer-review

TRANSPARENT PEER-REVIEW
Editors and reviewers acknowledged by name on published articles

Frontiers
Avenue du Tribunal-Fédéral 34
1005 Lausanne | Switzerland

Visit us: www.frontiersin.org
Contact us: frontiersin.org/about/contact

REPRODUCIBILITY OF RESEARCH
Support open data and methods to enhance research reproducibility

DIGITAL PUBLISHING
Articles designed for optimal readership across devices

FOLLOW US
@frontiersin

IMPACT METRICS
Advanced article metrics track visibility across digital media

EXTENSIVE PROMOTION
Marketing and promotion of impactful research

LOOP RESEARCH NETWORK
Our network increases your article's readership